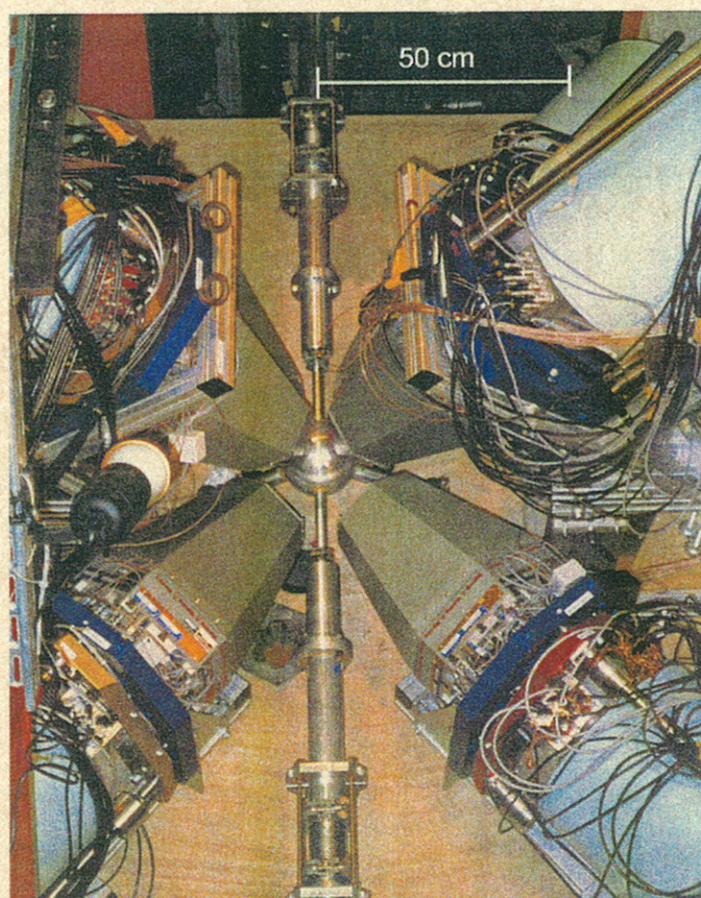


FORSCHUNGSZENTRUM
ROSSENDORF e.V.

FZR
- 130

INSTITUTE OF NUCLEAR
AND HADRONIC PHYSICS



Annual Report 1995



Cover Picture

The front cover displays a top view of an arrangement of six EURO-BALL CLUSTER detectors used in γ -spectroscopic experiments at the MPI Heidelberg. Four CLUSTER detectors are located in a plane and two are tilted out of this plane. In the picture these tilted detectors cover two of the detectors in the plane. In the middle of the picture the beam line and target chamber are seen.

Forschungszentrum Rossendorf e.V.

Postfach 51 01 19 · D-01314 Dresden

Bundesrepublik Deutschland

Telefon (0351) 260 3270

Telefax (0351) 260 3700

E-Mail prade@fz-rossendorf.de

FZR - 130
March 1996

Annual Report 1995

Institute of Nuclear and Hadronic Physics

Editors: F. Döna
H. Prade

Editorial staff: W. Enhardt
K. Möller
J. Mösner
G. Winter
R. Wunsch

Preface

This Annual Report of the Institute of Nuclear and Hadronic Physics (IKH) of the Research Center Rossendorf Inc. (FZR) summarizes the research activities, the results obtained and the progress achieved in 1995.

The research activities continued the experimental and theoretical studies aiming at properties of the nucleonic system and its constituents, the hadrons and their variation under extreme conditions like high excitation, spin, density and temperature. The participation in national and international collaborations and the use of external accelerators and facilities at GSI Darmstadt, Research Center KFA Jülich, JINR Dubna, TH Darmstadt and MPI Heidelberg were of vital importance for the progress achieved.

In nuclear resonance fluorescence experiments at the S-DALINAC the high efficiency of one of the recently completed EUROBALL-CLUSTER detectors was demonstrated. By using this new spectroscopic device the Darmstadt-Cologne-Rossendorf collaboration discovered a very interesting magnetic excitation in ^{196}Pt ; the appearance of this scissor mode was not expected in this soft triaxial nucleus.

In evaluating data obtained within the ALADIN Collaboration at GSI the liquid-gas phase transition has been observed in peripheral heavy ion reactions $\text{Au} + \text{C}$, Al , Cu , Au at projectile energies $E = 600$ and 1000 AMeV. The essential ingredient for obtaining the caloric curves was the determination of the nuclear temperature from the isotopic double ratios $^3\text{He}/^4\text{He}$ to $^6\text{Li}/^7\text{Li}$ which were enabled by the improvements of the TP-MUSIC detector.

The development and the construction of the BARREL configuration for the COSY-TOF spectrometer have obtained a great impact from a new concept developed in cooperation with the Universities at Dresden and Bochum. The first BARREL section will be assembled in Rossendorf during 1996.

The nuclear theory group in Rossendorf has traditionally strong relations to experimental projects. The two examples mentioned below are representative for many common activities:

A new type of nuclear rotation, i.e. the so-called magnetic rotation (MR) was predicted by the nuclear structure theory. In contrast to the common electric rotation which is governed by the rotating deformed density the magnetic rotation is created by some high-spin particles emitting strong M1 radiation. Experimental evidence for MR has been found in Pb isotopes, ^{149}Sm and ^{110}Cd .

In the framework of an effective One-Boson-Exchange model the spectrum for bremsstrahlung produced in nucleon-nucleon collisions in the energy region around 1 GeV was predicted for the first time. This development is relevant for COSY-TOF experiments under way.

The 4π spectrometer FOBOS was completed at the cyclotron U400M in Dubna by the end of 1995. Using an earlier implementation of the FOBOS spectrometer data were taken in the reaction $^{14}\text{N} + ^{197}\text{Au}$ at 53 AMeV to study correlations of the scission, IMF emission and nuclear residues.

A project study for a superconducting 20 MeV electron linac has been worked out in direct cooperation with the infrastructure departments "Experimental Facilities and Information Technology" and "New Accelerators". This machine named ELBE is designed to be a **E**lectron source with high **B**rilliance and low **E**mittance. The scientific program includes not only high resolution nuclear spectroscopy in nuclear resonance fluorescence experiments but aims especially at the development and application of nonconventional photon sources exploiting channeling, parametric X-ray, transition and Smith-Purcell radiation. As another main application of the high brilliance electron beam the construction of a Free Electron Laser for the far infrared region is under consideration.

The ELBE project was evaluated by a Technical Advisory Committee and, after commissioning in the fall of 1995, ELBE is now being designed in detail.

In preparation for the future research with ELBE first experiments using channeling and parametric X-ray radiation were performed in direct cooperation with the radiation physics group at the TH Darmstadt. These contacts are extremely helpful for getting first experience in this direction.

The PET group in the institute achieved a remarkable acceleration in the tomographical reconstruction which is important for the practical application of the dose localisation in the heavy-ion tumor therapy.

These and other accomplishments were made possible by the strong support received from our engineers and technicians and, last but not least, by our doctorands.

Three meetings successfully organized by the IKH in 1995 belong to the highlights in the last year:

In April (10-11) the Annual Meeting of the FOPI collaboration (53 participants), in May (18-19) the EUROBALL-Meeting on ancillary detectors (30 participants) and in July (6-8) the GSI-Theory Meeting (60 participants) took place in Rossendorf or Stolpen.

We are glad to announce that Prof. Eckart Grosse (presently GSI Darmstadt) has got the offer for the position as director of the IKH and professor at the Department of Physics of the Technical University Dresden in September 1995.

All scientific activities of the IKH have benefited from the general support of many institutions. First of all, we gratefully acknowledge the close and fruitful collaboration with our partner institutes in Germany and abroad. This cooperation has been and remains of vital importance for our institute.

Specific projects were financially supported by the Federal Ministry for Education, Science, Research and Technology (BMBF), the German Research Community (DFG), the State Ministry for Science and Art of Saxony (SMWK), the KFA Jülich and the GSI Darmstadt. We express our gratitude to all these institutions as well as to the Executive Board of the Research Center Rossendorf for its promotion of nuclear and hadronic physics in Rossendorf.

Harold Prade

CONTENTS

	PAGE
I Results of Research and Development	1
1 Theoretical Nuclear Physics	3
1.1 Scientific contributions	
$\gamma\gamma$ Correlations in Heavy-Ion Reactions at Intermediate Energies	5
Molecular Dynamics Applied to Fragment Production in Heavy Ion Collisions	6
Directional Effects in Correlations of Intermediate-Mass Fragments Emitted in Central Collisions of Heavy Ions	7
The Reaction $NN \rightarrow NN\gamma$ in the 1 GeV Region within an Effective One-Boson Exchange Model	8
Production of Heavy Particles in Ultra-Relativistic Heavy-Ion Collisions	10
Rho Meson Self-Energy and Dielectron Emission Rate in an Isospin-Asymmetric Pion Medium	11
Analysis of the DLS Data	12
Dilepton Production in a Chemically Equilibrating, Expanding and Hadronizing Quark-Gluon Plasma	13
Rapidity Dependence of Dileptons Produced in High-Energy Heavy-Ion Collisions	14
The Impact of In-Medium Kaon Properties on the K^- Yield in Heavy-Ion Collisions	15
The Role of the Massive Photon Decay Channel for the Neutrino Cooling of Neutron Stars	16
A Hot and Dense Pion System with Fixed Particle Number	17

Study of the Deuteron Break-up Reaction	18
A Quasi-Particle Model of the SU(3) Gluon Plasma	19
Entropy of Hot SU(N) Gauge Theories with Fermions	20
Solitonic Configurations of the SU(2) Nambu & Jona-Lasinio (NJL) Model at Finite Temperature and Density	21
The NJL Soliton in Hot Nuclear Matter	22
Magnetic Rotation	23
How Do Unpaired Nuclei Rotate?	25
Change from Liquid Drop to Quantal Rotation	26
Rotating Nuclear Matter	27
A New Type of Band Crossing at Large Deformation	28
The Trapping Effect Revisited	29
Non-Hermiticity and the Eigenvectors of the Effective Hamiltonian	30
Interference of Resonances and Partial Widths of Collective States	31
Non-Hermiticity and Decay-Rates of Overlapping States	33
Does Resonance Trapping Occur in Real Nuclei?	35
Trapping Effect and Optical Model	36
Shapes and Free Energies of Liquid Sodium Clusters	37
Fission of Metal Clusters	38
Small Fragment Evaporation from Liquid Alkali Clusters	39
A New Optimization Technique for Complex Systems	40

1.2	Abstracts of publication	41
2	<i>Experimental Medium Energy Physics</i>	47
2.1	Scientific contributions	
	An Application of Kinematic Fitting	49
	Measurement on a Prototype Scintillator Module to be used in the COSY-TOF Barrel Hodoscope	51
	Investigations of the Radiation Background in the Detector Laboratory	53
	Beam Profile and Phase Space Measurements of the Beam extracted from COSY	55
	Beam Properties and Beam Focussing near the TOF Target	57
	Test of Transparent Adhesives for Scintillation Detectors	59
	Test of a Scintillating-Fiber Calorimeter for Photons with Energies below 1 GeV	60
	Ratio of Kaon- to Pion-Pair Production as a Signature of Enhanced Strangeness Production	61
	Test Measurements with the ANKE MWC1	63
	Reconstruction of Particle Coordinates with the Wire Chambers at the ANKE-Facility	65
2.2	Abstracts of publication	67
3	<i>Experimental Nuclear Spectroscopy</i>	69
3.1	Scientific contributions	
	Tilted Rotation in Nuclei around $A = 80$	71

Experiments on ^{79}Br and ^{72}Kr with EUROBALL CLUSTER detector arrays at the Max-Planck-Institut für Kernphysik in Heidelberg	73
Resolution-enhanced Spectroscopy of High-Spin States in ^{81}Y by Kinematic Doppler-Shift Correction	75
Photon Scattering Experiment on ^{89}Y	77
Spin-Flip Transitions in ^{89}Y	78
Search for Smooth Band Termination in ^{109}Sn	79
Dipole Excitations in ^{126}Te and ^{130}Te	81
Dipole Excitations in ^{154}Sm around 6 MeV observed with an EUROBALL CLUSTER Detector	82
3.2 Abstracts of publications	84
4 <i>Experimental Heavy Ion Physics</i>	87
4.1 Scientific contributions	
Two Modes of IMF Emission Accompanying Fission in the Reaction ^7Li (43 AMeV) + ^{232}Th	89
Fragment Masses and Total Kinetic Energies in Two-Body Decays of Hot Heavy Nuclei Produced in the Reaction ^{14}N (34 AMeV) + ^{197}Au	91
Pre- and Post-Scission Components of Light Charged Particles Accompanying Fission in the Reaction ^{14}N (34 AMeV) + ^{197}Au	93
Study of the Reaction ^{14}N (53 AMeV) + ^{197}Au by Simultaneous Registration of Charged Products from Protons up to Evaporation Residues with the FOBOS Array	95
Combined Dynamical Statistical Model Calculations for Hot Fissioning Systems Studied at the 4π -Array FOBOS	97

Spontaneous Fission of ^{252}Cf Examined at the FOBOS Spectrometer	99
Phase Space Distributions of Charged Particles from Central Collisions of Au+Au between 250 and 1050 MeV per nucleon	101
Energy Equilibration in Central Au on Au Collisions in the Projectile Energy Range from 150 AMeV to 1050 AMeV	103
Charged Particle Distributions in the Reaction Au + Au at 150 - 1050 AMeV	105
Bounce Off and Squeeze Out of Charged Particles in the Reaction Au + Au at 1050 MeV	106
Nuclear Temperatures from Isotopic Ratios in Proton-Nucleus Interactions	108
Systematic Study of Emission Temperatures in Projectile Fragmentation	110
4.2 Abstracts of publications	112
5 <i>Positron Emission Tomography and Radiation Physics</i>	119
5.1 Scientific contributions	
The Installation of a PET-Scanner for In-Situ Dose Localization at the Heavy Ion Therapy at GSI Darmstadt	121
The Determination of the Bragg Peak Position from β^+ -Emitters Generated by Nuclear Fragmentation for the Treatment Plan Verification at Heavy Ion Tumour Therapy	122
Parallelization of an Iterative Reconstruction Algorithm for Positron Emission Tomography	124
Modifications of an Iterative Reconstruction Algorithm for a Spherical Symmetric PET-Scanner	125
Detector Investigations for Non-Invasive PET Input Function Measurement	126

Experimental Determination of the Linewidth of Parametric X-Ray Radiation at Electron Energies below 10 MeV	127
Comparison of Channeling Radiation and Parametric X-Ray Radiation Intensities for Diamond Crystals	129
6 <i>Technical and Methodic Developments</i>	131
6.1 Scientific contributions	
Status of the Beam Transport System for ELBE	133
EuroSiB - A 4π Silicon Ball for Detection of Light Charged Particles Inside the γ -Spectrometer EUROBALL	135
Beam Test of Si Detectors and Electronics for EuroSiB	137
A Simple Method to Test the Performance of Si Detectors for Particle Identification Based on PSD	139
A Method to Localize and Characterize Resistivity Fluctuations in Large-Area Si Detectors	141
Activities of the Detector Laboratory	143
Status of the 2 nd Multiwire Proportional Chamber MWPC2 for the ANKE-Facility	144
Apparatus for an Investigation of Long Scintillator Strips through Use of Cosmic Rays	145
A LED-Based Monitoring System for Scintillation and Cerenkov Counters at ANKE	147
Commissioning of three EUROBALL CLUSTER Detectors	149
Analysis and Calibration of the Response of the FOBOS CsI(Tl) Scintillator Shell for Light Charged Particles	150
Installation of RADWARE, Programs for the Analysis of High-Spin Spectroscopy Experiments	152

6.2	Abstracts of publications	153
II	Publications and Talks	155
1	Publications	157
2	Conference Contributions and Research Reports	167
3	Lectures and Seminars	187
4	Talks of Visitors	199
III	Personnel	205

I Results of Research and Development

Explanation of special symbols:

The following letters indicated in brackets in the following text and used as appendix in the title of the scientific contributions do express our grateful acknowledgement to the funding, sponsoring or grants provided by several institutions.

Research projects were funded by the Federal Ministry of Education, Science, Research and Technology BMBF (B), by the German Research Community DFG (D), by the GSI Darmstadt (G), by the KFA Jülich (K), were sponsored by the German Academic Exchange Service DAAD (A) or within Scientific agreements with eastern European countries (W). Several activities were funded by EC contracts (E) or INTAS contracts (I) or by the Landau-Heisenberg programme (L). All other support by special contracts or grants is indicated by (S).

1 Theoretical Nuclear Physics

$\gamma\gamma$ Correlations in Heavy-Ion Reactions at Intermediate Energies^B

H.W. BARZ¹, B. KÄMPFER¹, W. BAUER³, AND GY. WOLF³

Recently reported measurements of hard photon correlations in the reactions ^{36}Ar on ^{27}Al at 95 A·MeV [1], ^{86}Kr on $^{\text{nat}}\text{Ni}$ at 60 A·MeV, and ^{181}Ta on ^{197}Au at 39.5 A·MeV [2] are analyzed. A Boltzmann-Ühling-Uhlenbeck transport model is used to describe the photon production by individual nucleon-nucleon collisions. In the lighter systems (Fig. 1) we find the best agreement with data when taking into account only photons from first-chance collisions of nucleons or photons produced during the passage of the nuclei. However, the model predicts also a considerable late-time emission of photons which leads to a depletion of the calculated correlation function. The accuracy of the present data does not allow firm conclusions on the reliability of this late time evolution. Our BUU investigations do not support a recently reported interference pattern in the heavy Ta + Au system (Fig. 2). Only a schematic two-source model [3] for very particular parameters is able to describe such oscillations.

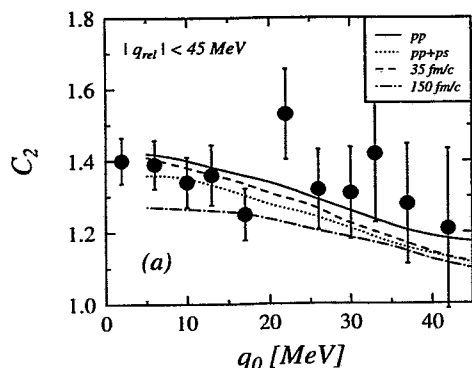


Fig. 1 The correlation function C_2 as function of the relative energy q_0 for relative momenta $|\vec{q}| < 45$ MeV in the reaction $^{36}\text{Ar} + ^{27}\text{Al}$ at 95 A·MeV. The curves are calculated using photons from primary-primary (pp), primary-primary + primary-secondary (pp+ps) nucleon-nucleon collisions and for two different freeze-out times. Experimental data (symbols) from [1].

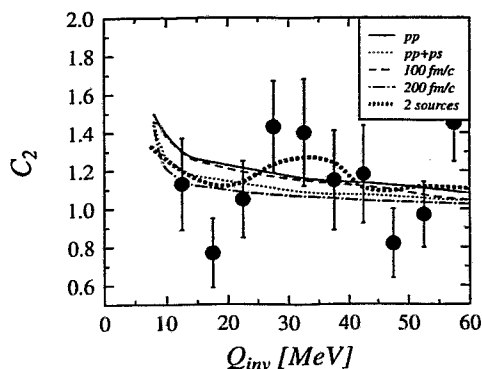


Fig. 2 The same as in Fig. 1 but now for the correlation function C_2 as function of $Q_{\text{inv}} = \sqrt{q_0^2 - \vec{q}^2}$ for the reaction $^{181}\text{Ta} + ^{197}\text{Au}$ at 39.5 A·MeV. Data is from [2]. The oscillatory heavy dotted curve (2 sources) depicts the result of a schematic two-source model for parameters described in [3].

¹ Institut für Theoretische Physik, TU Dresden and Institut für Kern- und Hadronenphysik, FZR

² MSU Michigan, East Lansing, USA

³ KFKI Budapest, Hungary

References

- [1] A. Badalà et al., Phys. Rev. Lett. 74 (1995) 4779
- [2] F.M. Marqués et al., Phys. Rev. Lett. 73 (1994) 34
- [3] H.W. Barz, B. Kämpfer, Gy. Wolf, W. Bauer, FZR-111 (1995), Phys. Rev. C (1996) in print

Molecular Dynamics Applied to Fragment Production in Heavy Ion Collisions

H.W. BARZ¹, J.P. BONDORF², D. IDIER² AND I.N. MISHUSTIN^{2,3}

To describe heavy-ion collisions at intermediate energies a molecular dynamical model has been developed on the basis of the Boltzmann-Ühling-Uhlenbeck approach using the algorithm of pseudo-particles [1]. Each nucleon is represented by a distribution function $f_i(\mathbf{r}, \mathbf{p}) = g(\chi, \mathbf{r} - \mathbf{r}_i)g(\phi, \mathbf{p} - \mathbf{p}_i)$ using Gaussian distribution functions $g(\Delta, \mathbf{x})$ of width Δ . Their motion is derived from an effective Hamiltonian

$$H = \sum_{k=1}^A \left[\frac{\mathbf{p}_k^2}{2m} + a\rho(\mathbf{r}_k) + b\rho(\mathbf{r}_k)^{1+\gamma} + c\Delta\rho(\mathbf{r}_k) + d \sum_{i=1}^A (\mathbf{p}_i - \mathbf{p}_k)^2 g(\chi, \mathbf{r}_i - \mathbf{r}_k) \right]. \quad (1)$$

as a function of the density ρ . The coefficients a, b, c, d, γ can be expressed through conventional Skyrme parameters. In addition two-particle collisions are included obeying the Pauli principle by excluding scatterings into the occupied regions of the phase space. Within this model we have studied the formation of fragments for various bombarding energies. In Fig.1 the number of produced intermediate mass fragments (IMFs) is plotted as a function of the total charge multiplicity for the reaction of Kr on Au at energies ranging from 55 MeV to 400 MeV. The characteristic rise and fall of multifragmentation with increasing energy is reproduced. However, at energies around 50 MeV the production is clearly underestimated while at larger energies satisfactory agreement is reached. The results have not changed essentially when different sets of parameters for Skyrme forces and in-medium cross sections were used.

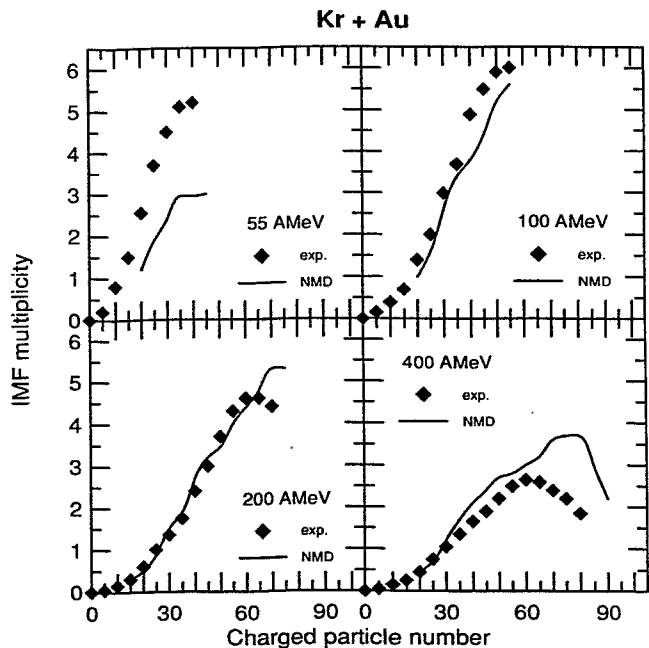


Fig. 1. Correlation between averaged IMF multiplicities and charged particle multiplicities. Full squares indicate the data [2] while lines represent the results of the calculations.

¹ Institut für Theoretische Physik, TU Dresden and Institut für Kern- und Hadronenphysik, FZR

² The Niels Bohr Institute, Copenhagen, Denmark

³ The Kurchatov Institute, Russian Scientific Center, Moscow, Russia

References

- [1] D. Idier, M. Farine, B. Remaud and F. Seville, Ann. Phys. Fr. **19** (1994) 159
- [2] G.F. Peaslee et al., Phys. Rev. **C51** (1994) R2271

Directional Effects in Correlations of Intermediate-Mass Fragments Emitted in Central Collisions of Heavy Ions^B

B. KÄMPFER¹ AND R. KOTTE

Our recent studies of velocity correlations of intermediate-mass fragments (IMFs) [1, 2] are aimed to get information on the space-time extent of the IMF emitting source in central collisions of gold nuclei at beam energies of 100 - 400 A·MeV. The source parameters extracted in [1, 2] from the correlations are based on a N-body Coulomb trajectory model with sudden freeze-out of a spherical source. Theoretical studies [3] however indicate that the source in non-perfect central collisions might be strongly prolate and tilted. To catch such non-isotropic effects we have extended our model to a non-spherical source.

Actually we employ as freeze-out configuration a cylinder with radius $R_{\perp} = 10$ fm and length 20 fm. Also the initial velocity distribution of IMFs with charges $Z \geq 3$ is assumed to be anisotropic with averaged collective flow energies per nucleon $E_{x,y,z} = (2,2,8)$ MeV, superimposed on a random thermal distribution [2]. This source is tilted by 50° relative to the beam axis. The resulting acceptance-filtered azimuthal distribution $dN/d\phi$, the azimuthal correlation function $1 + R(\phi_1 - \phi_2)$, and the correlation function $1 + R(v_{red})$ are displayed in Fig. 1 (for more details see [2]). One observes a satisfactory agreement with the data, which are selected according to the centrality criterion ERAT5 [1].

We tried also to elucidate whether one can determine the different spatial source extensions of the non-spherical break-up configuration when viewing the expanding source from different orientations. Similar to simulations of the Michigan group we find only very tiny differences after passing our simulations through the acceptance filter. In conclusion, it seems hardly possible to observe such directional anisotropies of the source via the Coulomb dominated velocity correlations of IMFs.

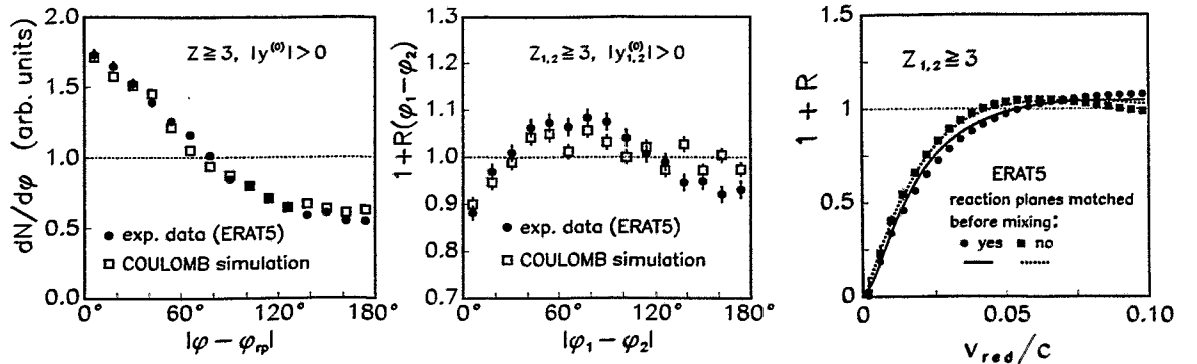


Fig. 1 Azimuthal IMF distribution (left panel), azimuthal correlation (middle panel), and velocity correlation (right panel, $v_{red} = v_{12}/\sqrt{Z_1 + Z_2}$) in our Coulomb model with source parameters described in the text in comparison with data [2] Au(150 A MeV) + Au.

¹ Institut für Theoretische Physik, TU Dresden and Institut für Kern- und Hadronenphysik, FZR

References

- [1] B. Kämpfer, R. Kotte, J. Mösner, W. Neubert, D. Wohlfarth, et al. (FOPI), Phys. Rev. C 48 (1993) 955
- [2] R. Kotte, B. Kämpfer, J. Mösner, W. Neubert, D. Wohlfarth, et al. (FOPI), Phys. Rev. C 51 (1995) 2688
- [3] B. Heide, H.W. Barz, Nucl. Phys. A 588 (1995) 918

The Reaction $NN \rightarrow NN\gamma$ in the 1 GeV Region within an Effective One-Boson Exchange Model^B

A.I. TITOV¹, B. KÄMPFER², B.L. REZNIK³, AND V. SHKLYAR¹

Within an effective one-boson exchange parametrization of the T matrix of NN interactions we calculate cross sections for the reactions $pp \rightarrow pp\gamma$ and $pn \rightarrow pn\gamma$ for proton incidence energies in the order of 1 GeV. Besides bremsstrahlung processes we consider photons from Δ decays and contributions from the $\eta \rightarrow \gamma\gamma$ process, where the η is excited via the N_{1535} resonance. At beam energies above 700 MeV the Δ decay channel dominates for large photon energies, while above the η -threshold the η -decay photons show up in a narrow window. The low energy photons stem from pure bremsstrahlung processes. Examples of our results [1] are displayed in Fig. 1. These estimates should be considered as predictions for forthcoming measurements with the time-of-flight detector at COSY. The present calculations are based on the Feynman diagrams shown in Fig. 2.

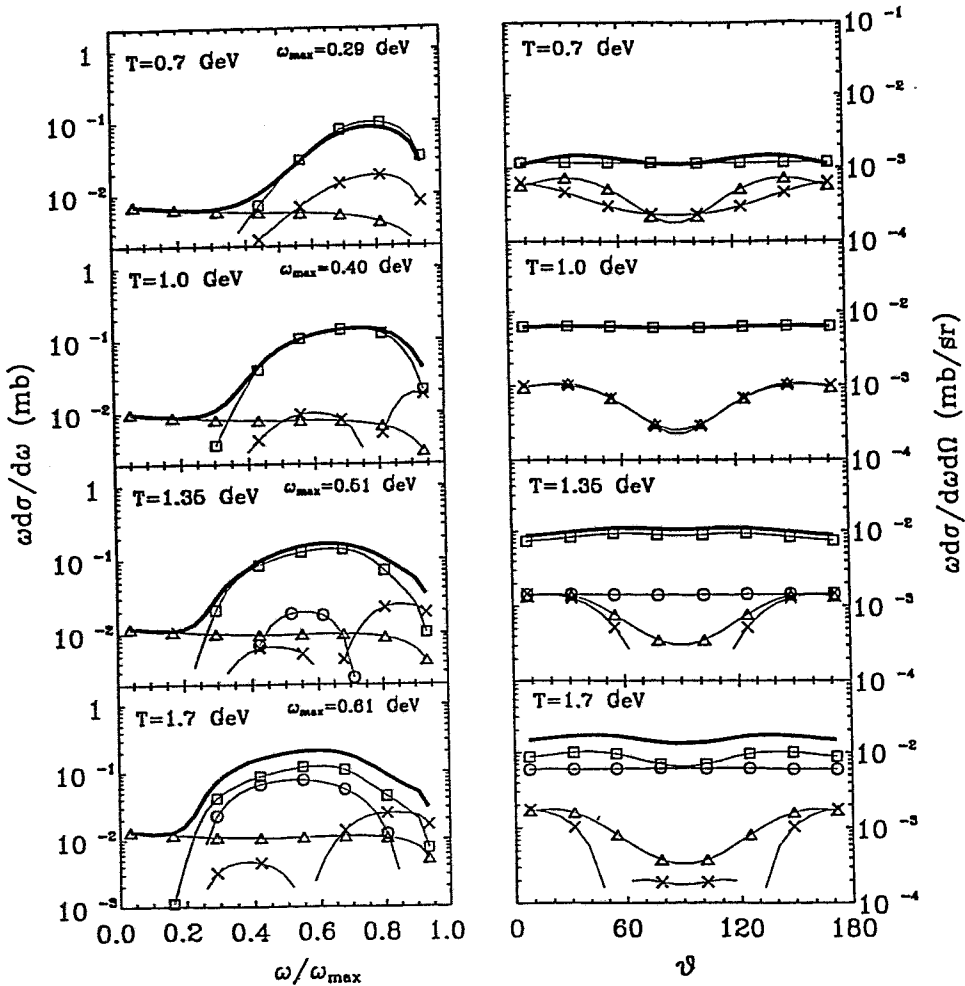


Fig. 1 The photon cross sections $\omega d\sigma/d\omega$ (left panel) and $\omega d\sigma/d\omega d\Omega$ (right panel) for the reaction $pp \rightarrow pp\gamma$ at several beam energies. The photon energy ω and solid angle Ω refer to the NN center-of-mass system (triangles: bremsstrahlung, squares: Δ decay, circles: η decays, crosses: interference contributions, heavy full lines: total cross section).

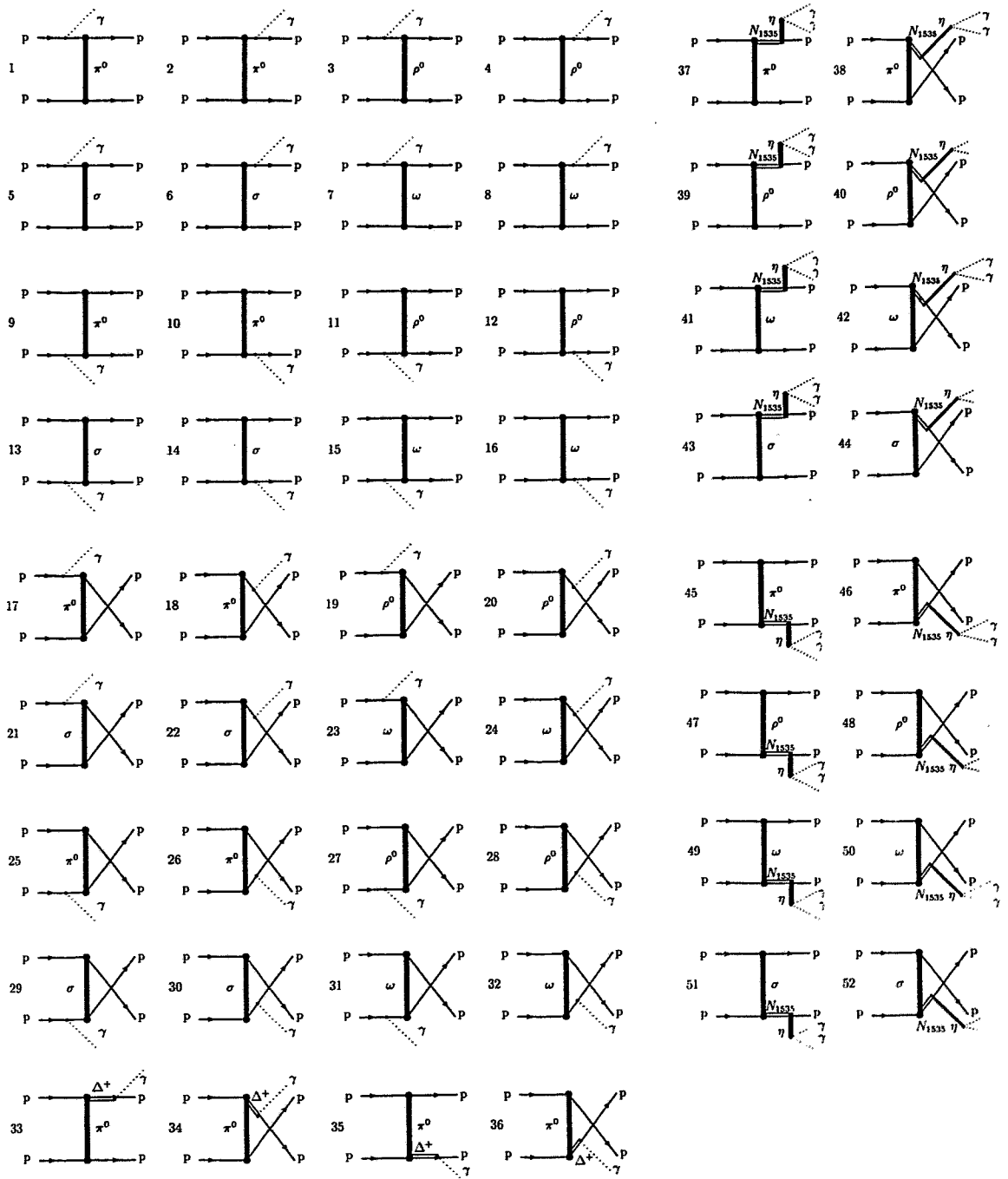


Fig. 2 The Feynman diagrams for the $NN \rightarrow NN\gamma$ reactions. Strong nucleon-nucleon-meson vertices are dressed by form factors which preserve gauge invariance. Electromagnetic $NN\gamma$ vertices neglect the magnetic part. Interferences are exactly regarded.

¹ Bogoliubov Institute of Theoretical Physics, JINR Dubna, Russia

² Institut für Theoretische Physik, TU Dresden and Institut für Kern- und Hadronenphysik, FZR

³ Far Eastern University, Vladivostok, Russia

References

- [1] A.I. Titov, B. Kämpfer, B.L. Reznik, V. Shklyar, FZR-118 (1995), Phys. Lett. B (1996) in print

Production of Heavy Particles in Ultra-Relativistic Heavy-Ion Collisions^B

M.W. BEINKER¹, B. KÄMPFER², AND G. SOFF¹

Hadronic and heavy-ion collisions at ultra-relativistic energies can be considered as superposition of parton-parton collisions. If the center-of-mass (c.m.) energy of these elementary partonic collisions is sufficiently large, also heavy particles, like the very heavy quarks or the conjectured supersymmetric particles, might be produced. Here we address the question, whether there are significant nuclear effects when comparing the parton time evolution in hadronic and central heavy-ion collisions. For this purpose we employ the perturbative QCD-based parton cascade model of Klaus Geiger [1].

In Fig. 1 the results of simulation runs of central proton-proton, $^{16}\text{O} - ^{16}\text{O}$, $^{56}\text{S} - ^{56}\text{S}$, and $^{197}\text{Au} - ^{197}\text{Au}$ collisions are displayed at c.m. energy $\sqrt{s} = 0.2$ and 1 ATeV. We display the number of parton collisions per elementary partonic c.m. energy $\sqrt{\hat{s}}$. The distributions are normalized to 1. Fig. 1 shows that for $\sqrt{s} = 0.2$ ATeV the slopes of the distributions are roughly unaffected by the size of the colliding systems; the only remarkable fact is the rather extended tail of the distribution for the gold-gold collisions. At $\sqrt{s} = 1$ ATeV, however, the slope of the distribution for the gold system is much larger, and the distribution leaks out to rather high values of $\sqrt{\hat{s}}$. This gives rise to the hope that at sufficiently high bombarding energies also very heavy elementary particles can be produced in central collisions of heavy ions, since the threshold energy can be reached due to copious parton rescatterings. Presently we are implementing the cross sections for the production of supersymmetric particles.

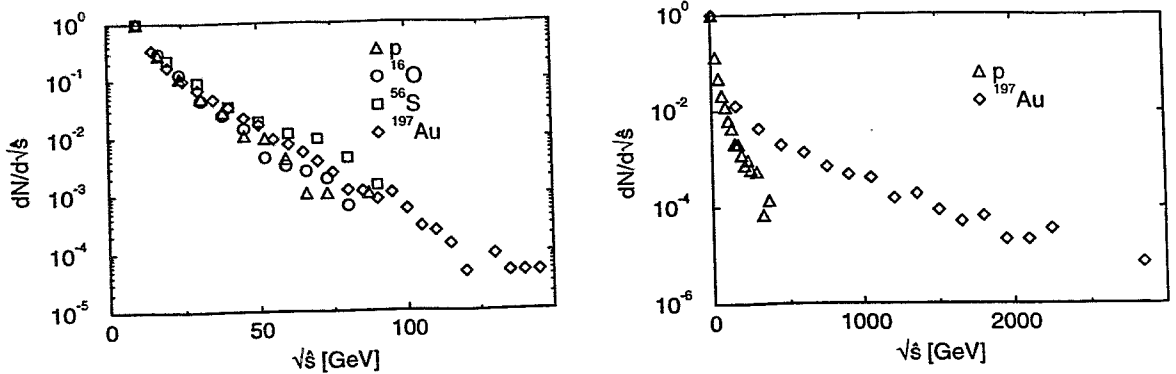


Fig. 1 The distribution $dN_{coll}(\sqrt{\hat{s}})/d\sqrt{\hat{s}}$ in the center-of-mass system of various colliding systems as indicated at c.m. energies 0.2 ATeV (left panel) and 1 ATeV (right panel).

¹ Institut für Theoretische Physik, TU Dresden

² Institut für Theoretische Physik, TU Dresden and Institut für Kern- und Hadronenphysik, FZR

References

- [1] K. Geiger, Phys. Rep. 258 (1995) 237

Rho Meson Self-Energy and Dielectron Emission Rate in an Isospin-Asymmetric Pion Medium^B

A.I. TITOV¹, T.I. GUMALOV¹, AND B. KÄMPFER²

The ρ meson self-energy in an isospin asymmetric pion gas at finite temperature and charged-pion chemical potential is evaluated [1]. We utilize a conventional effective π - ρ Lagrangian and the functional integral representation of the partition function in the second order in the $\rho\pi\pi$ coupling constant. We analyze the ρ meson polarization operator as function of the invariant mass M and spatial momentum $|\mathbf{p}|$ of the ρ meson. The pole positions and the values of the imaginary parts of the self-energy for different polarization states have different functional dependencies on M and $|\mathbf{p}|$. The corresponding dielectron rate (calculated from the imaginary part of the ρ meson propagator) shows a distinctive asymmetry when the relative momentum $\mathbf{t} = \mathbf{p}_+ - \mathbf{p}_-$ is perpendicular or parallel to the total momentum $\mathbf{p} = \mathbf{p}_+ + \mathbf{p}_-$ where \mathbf{p}_\pm are the e^\pm momenta of the electron pair.

To quantify this effect we define the asymmetry as $A = (W_L - W_T)/(W_L + W_T)$, where $W_{L,T}$ are related to the in-medium ρ propagator via $W_L = -\text{Im} F / [(M^2 - m_\rho^2 - \text{Re} F)^2 + (\text{Im} F)^2]$, $W_T = -\text{Im} G / [(M^2 - m_\rho^2 - \text{Re} G)^2 + (\text{Im} G)^2]$; here M and m_ρ denote the dilepton mass and the ρ mass, and F and G are the complex valued longitudinal (L) and transverse (T) parts of the in-medium ρ propagator $D^{\mu\nu} = -P_L^{\mu\nu} / [p^2 - m_\rho^2 - F] - P_T^{\mu\nu} / [p^2 - m_\rho^2 - G]$, with $P_{L,T}^{\mu\nu}$ as the corresponding projectors [1]. In vacuum, the asymmetry A vanishes.

An example of the asymmetry A is displayed in Fig. 1. One observes that a large isospin asymmetry, caused by a large charged-pion chemical potential μ_Q , enhances the dilepton asymmetry (1). We hope that forthcoming precision measurements with HADES at GSI Darmstadt can identify such a general in-medium effect of the ρ meson in excited nuclear matter. However, before firm quantitative predictions can be made the baryonic degree of freedom must be included.

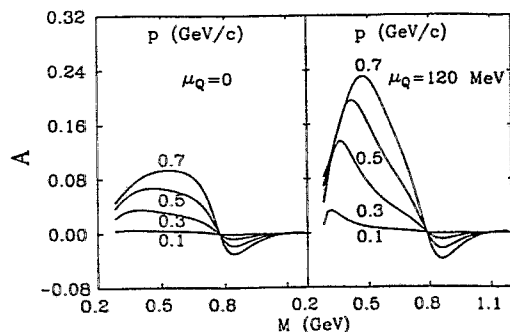


Fig. 1 The asymmetry A as function of the dilepton invariant mass M for several values of the ρ meson momentum $|\mathbf{p}|$ at a medium temperature $T = 150$ MeV and for the pion chemical potential $\mu_Q = 0$ (left panel) and 120 MeV (right panel).

¹ Bogoliubov Institute of Theoretical Physics, JINR Dubna, Russia

¹ Institut für Theoretische Physik, TU Dresden and Institut für Kern- und Hadronenphysik, FZR

References

- [1] T.I. Gulamov, A.I. Titov, B. Kämpfer, FZR-90 (1995), FZR-113 (1995)
Phys. Rev. D (1996) in print, Phys. Lett. B (1996) in print

Analysis of the DLS Data^B

A.I. TITOV¹, B. KÄMPFER², AND E.L. BRATKOVSKAYA¹

The di-electron measurements in pp and pD reactions at 1 - 5 GeV with the dilepton spectrometer (DLS) [1] are analyzed by several groups (cf. [2, 3] for references). Satisfactory descriptions of the data [1] are achieved in different models. Our model [2] is based on an improved soft-photon approximation for the bremsstrahlung contribution, a correct description of the Δ excitation with subsequent Dalitz decay, and an effective description of the η excitation with subsequent Dalitz decay. These ingredients (with experimental filter) allow for a good reproduction of the DLS mass spectra [1].

However, we would like to stress that there are observables which are not so perfectly described. Figs. 1 and 2 display the ratio of the di-electron production cross sections in pD to pp reactions as function of invariant mass M or beam energy (E), respectively. While the ratio $R(M) = (d\sigma^{pD}/dM)/(d\sigma^{pp}/dM)$ at several beam energies is reasonably well reproduced (Fig. 1), the ratio of integrated cross sections $R(E) = (\int_{0.1\text{GeV}}^{M_{max}} dM d\sigma^{pD}/dM)/(\int_{0.1\text{GeV}}^{M_{max}} dM d\sigma^{pp}/dM)$ (here M_{max} is the kinematically allowed maximum invariant mass) in Fig. 2 seems to be underestimated. In our model the η decay channel plays a crucial role for obtaining the enhancement of the ratio \tilde{R} in the region of $E \approx 1.2$ GeV. In another model [3] this subtle beam energy dependence of the ratio R is ascribed to an interference of the bremsstrahlung processes with Δ excitations processes. These differences seem to point to some uncertainties in understanding the relevant di-electron sources in elementary processes, which need clarification before one can safely describe forthcoming precision measurements with HADES.

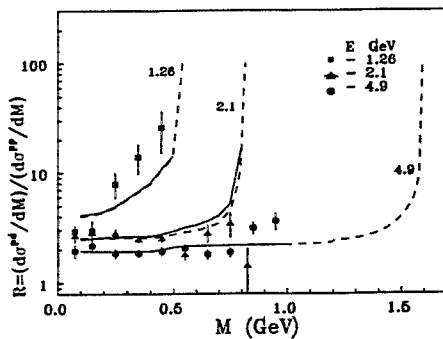


Fig. 1 The ratio $R(M)$ at various beam energies. Data from [1]; dashed (solid) lines depict our results with (without) DLS filter.

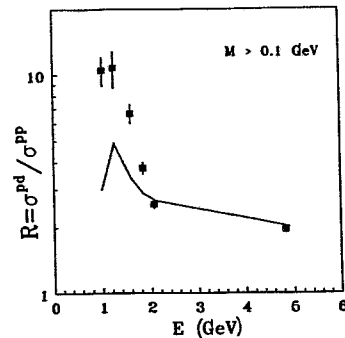


Fig. 2 The ratio $R(E)$. Data from [1]; the solid line depicts our results with DLS filter and seems to point to some deficits of our model.

¹ Bogoliubov Institute of Theoretical Physics, JINR Dubna, Russia

² Institut für Theoretische Physik, TU Dresden and Institut für Kern- und Hadronenphysik, FZR

References

- [1] W.K. Wilson et al., Phys. Lett. B 316 (1994) 245
- [2] A.I. Titov, B. Kämpfer, E.L. Bratkovskaya, Phys. Rev. C 51 (1995) 227
- [3] M. Schäfer et al., Nucl. Phys. A 575 (1994) 429

Dilepton Production in a Chemically Equilibrating, Expanding and Hadronizing Quark-Gluon Plasma^B

B. KÄMPFER¹, O.P. PAVLENKO², A. PESHIER, AND G. SOFF³

Dilepton production is considered within a complete dynamical framework for thermalized matter assumed to be formed in ultra-relativistic heavy-ion collisions. Our model [1] includes (i) chemical equilibration processes in the initially gluon-enriched plasma, (ii) longitudinal and transverse expansion, and (iii) the hadronization. Besides the electromagnetic quark - antiquark annihilation process we also take into account the lowest-order QCD processes for calculating the dilepton rate in the deconfined phase, while in the hadronic stage we employ a parametrization of the effective form factor.

We find that, due to the transverse expansion of the matter, the dilepton yield from the hadron gas is strongly reduced and, therefore, the deconfined matter gives the dominant contribution for initial conditions expected at RHIC. This provides the basis for the M_{\perp} -scaling restoration of the dilepton spectra from thermalized matter.

Fig. 1 shows an example of the total dilepton yield (invariant mass spectrum) for different initial fugacities of quarks (q) and gluons (g) but the same initial temperature of $T_0 = 550$ MeV at initial time of the thermalized era $\tau_0 = 0.32$ fm/c. The chemical evolution employs up-scaled thermally averaged reaction rates so that at confinement temperature of $T_c = 160$ MeV both the gluon and the u,d quark phase spaces are saturated.

In Fig. 2 the transverse momentum spectrum at fixed transverse dilepton mass $M_{\perp} = 2.6$ GeV is displayed. Even if the system is initially strongly undersaturated, the basic electromagnetic annihilation process $q\bar{q} \rightarrow \gamma^* \rightarrow l\bar{l}$ is seen to exceed the QCD contributions from the Compton-like process $qg \rightarrow q\gamma^* \rightarrow q\bar{l}l$ and the annihilation process $q\bar{q} \rightarrow g\gamma^* \rightarrow g\bar{l}l$. The QCD rates are regularized by a thermal mass [1].

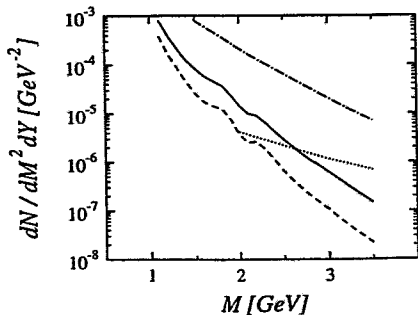


Fig. 1 The dilepton spectrum for various initial fugacities: $\lambda_g = 1$, $\lambda_q = 1$ (dot-dashed line), $\lambda_g = 0.5$, $\lambda_q = 0.1$ (solid line), $\lambda_g = 0.25$, $\lambda_q = 0.05$ (solid line). The dotted line depicts the Drell-Yan background (Duke-Owens structure functions, set 1.1, K factor 2)

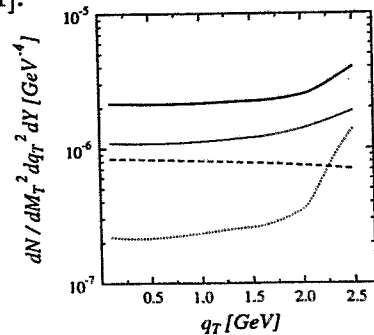


Fig. 2 The different contributions to the transverse momentum dilepton spectrum with initial fugacities $\lambda_g = 0.5$, $\lambda_q = 0.1$ (thin line: electromagnetic annihilation process, dashed line: QCD annihilation, dotted line: QCD Compton process, heavy full line: sum of all contributions).

¹ Institut für Theoretische Physik, TU Dresden and Institut für Kern- und Hadronenphysik, FZR

² Institute for Theoretical Physics, Kiev, Ukraine

³ Institut für Theoretische Physik, TU Dresden

References

- [1] B. Kämpfer, O.P. Pavlenko, A. Peshier, G. Soff, Phys. Rev. C 52 (1995) 2704

Rapidity Dependence of Dileptons Produced in High-Energy Heavy-Ion Collisions^B

B. KÄMPFER¹, O.P. PAVLENKO², M.I. GORENSTEIN, A. PESHIER, AND G. SOFF³

In a recent study [1] we investigated the rapidity dependence of thermal dileptons resulting from hadronizing quark-gluon matter with finite baryon charge. The idea behind such an investigation is to explore more dependencies of the dileptons as direct messengers from strongly interacting matter. Besides the usual invariant mass (M) spectra we proclaimed the need for measuring the transverse momentum spectrum as well to get information on the early parton distribution [2]. Here we consider the rapidity (Y) dependence caused by realistic meson and baryon rapidity distributions.

Fig. 1 displays the thermal mass spectrum of dileptons $dN_{\bar{l}l}/dM^2 dY$ at various rapidities for different assumptions on the beginning of the thermalized era. One clearly observes different slopes and absolute yields in different rapidity bins.

There is the longstanding problem of disentangling thermal dileptons from Drell-Yan pairs. Following an earlier ansatz [3] we here define a correlation function $K(Y) = A^{2/3}(dN_{\bar{l}l}/dM^2 dY)(dN_{\pi}/dY)^{-2}$, which is displayed in Fig. 2. The crucial point is the different dependence of thermal dilepton yield and Drell-Yan yield on the pion rapidity density dN_{π}/dY . The superposition of both sources however results in a rather structureless curve. The origin of this behavior lies in the different freeze-out rapidity distributions of mesons and baryons, which we extrapolate back with our dynamical model [1].

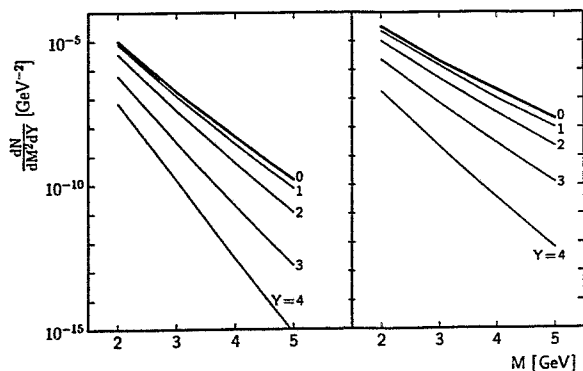


Fig. 1 The thermal mass spectrum of dileptons at various rapidities (left/right panel: initial time of the thermalized era 1.0/0.25 fm/c).

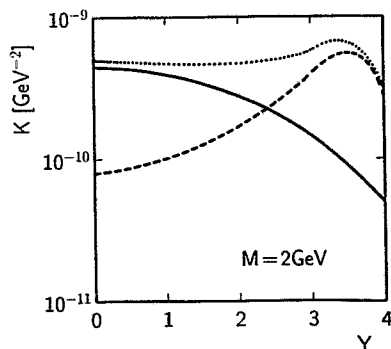


Fig. 2 The correlation function $K(Y)$ for invariant dilepton mass $M = 2$ GeV; dotted curve: sum of Drell-Yan background (dashed line) and thermal yield (heavy full curve).

¹ Institut für Theoretische Physik, TU Dresden and Institut für Kern- und Hadronenphysik, FZR

² Institute for Theoretical Physics, Kiev, Ukraine

³ Institut für Theoretische Physik, TU Dresden

References

- [1] B. Kämpfer, O.P. Pavlenko, M.I. Gorenstein, A. Peshier, G. Soff, Z. Phys. A 353 (1995) 71
- [2] B. Kämpfer, O.P. Pavlenko, Phys. Rev. C 49 (1994) 2616
- [3] B. Kämpfer, M.I. Gorenstein, O.P. Pavlenko, Z. Phys. C 45 (1990) 491

The Impact of In-Medium Kaon Properties on the K^- Yield in Heavy-Ion Collisions^B

E.E. KOLOMEITSEV, D.N. VOSKRESENSKY¹, AND B. KÄMPFER²

Recently we have derived a description of the kaon properties in nuclear matter, which includes both the s-wave $KKNN$ interaction and the p-wave $KN\Lambda$ interaction [1]. The latter one causes the appearance of an additional branch in the spectra of K^- , \bar{K}^0 mesons. The presence of this branch increases the population of the in-medium kaon excitations by a factor 2-3. Here we explore possible consequences of these new excitations. Basing on the fireball model [2] we consider the strange particle production in heavy-ion collisions. At beam energies < 2 AGeV the strangeness production occurs mainly in the hot initial stage of nuclear collisions. The particles of distinct strangeness interact differently with the nuclear environment: $K^{+,0}$ mesons can escape from the fireball at a somewhat earlier stage of the collision, whereas the negatively strange particles K^- , \bar{K}^0 , Λ , Σ might be confined up to break-up. The strangeness accumulated during the short initial stage is redistributed during the longer fireball expansion among the strange particle states available in the medium. In the model of a prompt fireball break-up we have calculated the K^- cross section. The strangeness chemical potential is adjusted by the number of observed K^+ mesons. The results agree with experimental data (Fig. 1).

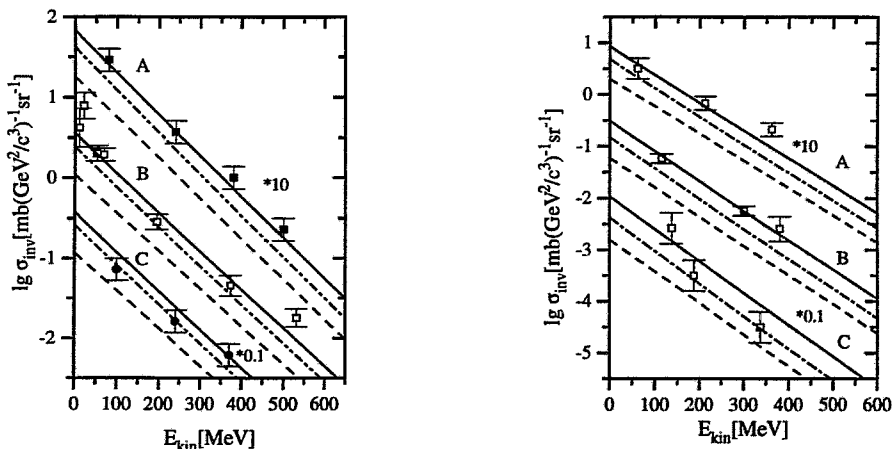


Fig. 1 The invariant differential cross section of K^- production (solid lines). Dashed curves are calculated with the free kaon spectrum, whereas dash-dotted curves include only the s-wave KN -interaction. In the right panel the curves labelled by A are depicted for $Ni + Ni$ at 1.85 AGeV, B for $Si + Si$ at 2.1 AGeV, and C for $Ne + Ne$ at 2.1 AGeV. In the left panel the curves correspond to $Si + Si$ collisions at beam energies 1.65 AGeV (A), 1.4 AGeV (B) and 1.16 AGeV (C) (for details cf. [3]).

¹ MEPhI, Moscow, Russia and GSI, Darmstadt

² Institut für Theoretische Physik, TU Dresden and Institut für Kern- und Hadronenphysik, FZR

References

- [1] E.E. Kolomeitsev, D.N. Voskresensky, B. Kämpfer, Nucl. Phys. A 588 (1995) 889
- [2] D.N. Voskresensky, Nucl. Phys. A555 (1993) 293
- [3] E.E. Kolomeitsev, D.N. Voskresensky, B. Kämpfer, FZR-91 (1995) Int. J. Mod. Phys. (1996) in print

The Role of the Massive Photon Decay Channel for the Neutrino Cooling of Neutron Stars^B

D.N. VOSKRESENSKY¹, E.E. KOLOMEITSEV, B. KÄMPFER²

A new mechanism of rapid neutron star cooling is suggested [1], that might be operative in the region of proton pairing. In a superconducting medium the photons acquire an effective in-medium mass due to the Higgs-Meissner effect $m_\gamma(T, \rho) = 1.4 \frac{\rho}{\rho_0} \sqrt{\frac{m_p}{m_p^*(\rho)} \frac{(T_{c,p} - T)}{T_{c,p}}}$ MeV, where $T_{c,p}$ is the critical temperature of proton pairing and m_p (m_p^*) stands for the free (in-medium) proton mass. We calculate the emissivity of the massive photon decay processes to neutrino-anti-neutrino pairs via electron-electron-hole and proton-proton-hole states. The ratio of the obtained emissivity to the emissivity of the modified Urca processes [2] yields

$$R_{FM} \approx 1.5 \cdot 10^4 T_9^{13/2} e^{\frac{\Delta_n + \Delta_p - m_\gamma}{T}} \left(\frac{m_\gamma}{\text{MeV}} \right)^{7/2} \left(1 + \frac{3 T}{2 m_\gamma} \right) \left(\frac{\rho}{\rho_0} \right)^2 \left(\frac{m_n^3 m_p}{m_n^* m_p^*} \right),$$

where $\Delta_{n,p}$ corresponds to the neutron and proton gaps. The lower temperature limit, at which the process $\gamma \rightarrow \nu\bar{\nu}$ is still operative, is determined by a comparison with the photon emissivity from the neutron star surface

$$R_\gamma \approx 1.2 \cdot 10^9 T_9^{-0.7} e^{-\frac{m_\gamma}{T}} \left(\frac{m_\gamma}{\text{MeV}} \right)^{7/2} \left(1 + \frac{3 T}{2 m_\gamma} \right) \left(\frac{\rho}{\rho_0} \right)^{8/3},$$

where the quantity T_9 stands for the temperature measured in 10^9 K. The ratios R_{FM} and R_γ are plotted in Fig. 1 as function of the temperature at nucleon density $\rho = \rho_0$ for two sets of the parameters $T_{c,p}$ and $\Delta_{n,p}$ from [3]. We see that our new process is operative in the temperature range $1 \cdot 10^9 \text{ K} < T < (4 - 8) \cdot 10^9 \text{ K}$.

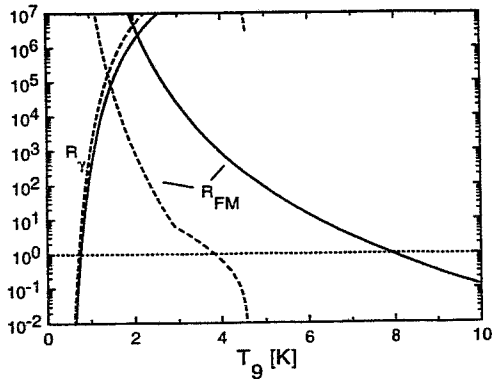


Fig. 1 The temperature dependence of the ratios R_{FM} and R_γ , at nucleon density $\rho = \rho_0$. The solid curves correspond to the parameter choice of ref. [2], whereas the dashed curves depict results with parameters of ref. [3]

¹ MEPhI, Moscow, Russia and GSI, Darmstadt

² Institut für Theoretische Physik, TU Dresden and Institut für Kern- und Hadronenphysik, FZR

References

- [1] D.N. Voskresensky, E.E. Kolomeitsev, B. Kämpfer, FZR-117 (1995)
- [2] B. Friman, O.V. Maxwell, Ap. J. 232 (1979) 541
- [3] T. Takatsuka, Prog. Theor. Phys. 48 (1972) 1517
D. Pines, M.A. Alpar, Nature 316 (1985) 27

A Hot and Dense Pion System with Fixed Particle Number^B

E.E. KOLOMEITSEV, D.N. VOSKRESENSKY¹, AND B. KÄMPFER²

A dense and hot system of strongly interacting pions with a dynamically fixed number of particles is investigated with respect to applications to ultra-relativistic heavy-ion collisions. The Lagrangian for such a system is derived from the chiral Weinberg Lagrangian for pion-pion interaction. Polarization operators of pions in the gas phase with an initially arbitrary isotopic composition are calculated within the Hartree approximation. Expressions for the effective in-medium pion gaps are obtained. They are shown to depend essentially on the isotopic composition of the system and to differ substantially from those for a pion gas in chemical equilibrium (see Fig. 1).

The rates of the pion rescattering and absorption reactions are calculated. The found strong suppression of the absorption processes supports our assumption of the lack of chemical equilibrium in pion-dominated systems which might be created in the central region in ultra-relativistic heavy-ion collisions. The validity of Hartree's approximation is verified by evaluation of high-order graphs. Thermodynamical characteristics of an interacting pion gas are calculated. The critical temperature of Bose condensation via a second-order phase transition is determined. Since the effective pion gaps are larger than the bare pion mass, the critical temperature is less than that for an ideal pion gas. Possible condensate instabilities of a superdense pion gas are currently considered.

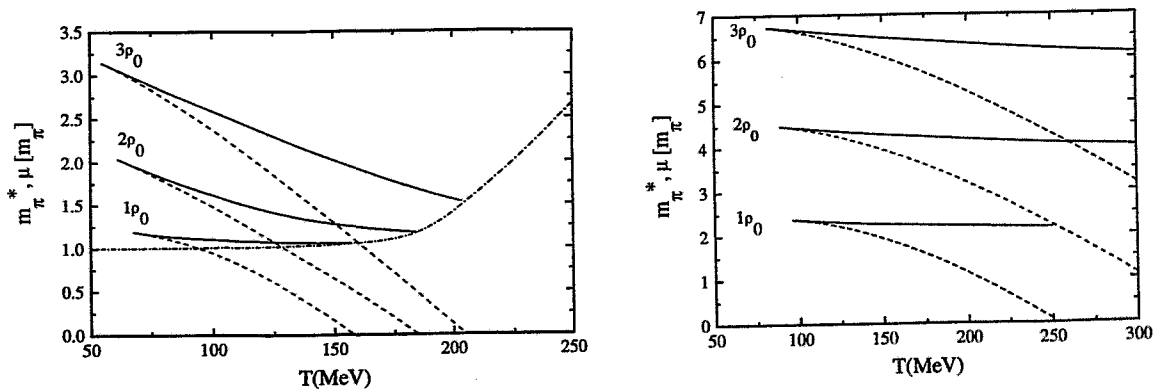


Fig. 1 The temperature dependence of the in-medium pion mass m_{π}^* (solid lines) and the chemical potential μ (dashed lines) for the isospin-symmetric pion gas (left panel) and a gas of π^- mesons (right panel) at various densities. The dashed-dotted line on the left panel corresponds to the calculation of the effective pion mass for a non-fixed number of pions with chemical potential $\mu = 0$ [1].

¹ *MEPhI, Moscow, Russia and GSI, Darmstadt*

² *Institut für Theoretische Physik, TU Dresden and Institut für Kern- und Hadronenphysik, FZR*

References

- [1] G.G. Bunatian, B. Kämpfer, FZR-28 (1993), unpublished

Study of the Deuteron Break-up Reaction^B

L.P. KAPTARI¹, A.YU. UMNIKOV¹, F.C. KAHANNA², AND B. KÄMPFER³

In a recent note [1] we have reported a calculation of the tensor analyzing power T_{20} in deuteron break-up reactions $Dp \rightarrow p'X$ in the impulse approximation. Our approach is based on the Bethe-Salpeter (BS) formalism with a realistic meson exchange potential. While one can reasonably well reproduce the differential cross section $E d\sigma/d^3p'$ as function of the final proton momentum p' in the deuteron's rest frame (except a shoulder at $p' = 0.35 - 0.45$ GeV in the experimental data), the quantity T_{20} in all calculations (ours, or calculations using the non-relativistic (NR) Bonn potential, or implementing a minimal relativization procedure by replacing the appropriate variables in the Bonn or Paris deuteron wave functions by light cone (LC) variables) seem to fail the experimental data at $p' > 0.3$ GeV. Particular disappointing is the fact that the data strictly indicate $T_{20} < 0$, while the calculations result in $T_{20} > 0$ for sufficiently large values of p' .

We have now supplemented [2] our previous calculations [1] by an estimate of the polarization transfer $\kappa = (d\sigma(\uparrow\uparrow) - d\sigma(\uparrow\downarrow))/d\sigma_{unpol}$, where $\uparrow\uparrow$ and $\uparrow\downarrow$ mean the orientation of the deuteron spin and the final proton spin. This polarization transfer is displayed in Fig. 1. The agreement of our model within the Bethe-Salpeter formalism with the data is quite acceptable, but in the region of $p' \approx 0.2$ GeV there seems to appear a slight overestimate of the data.

We now plan to apply our model to the special momentum range and acceptance regions of the experiment # 20 at the 0° facility with internal targets at COSY. Since this envisaged experiment is performed under semi-exclusive conditions, in contrast to previous inclusive measurements, one can hope to get more conclusive data.

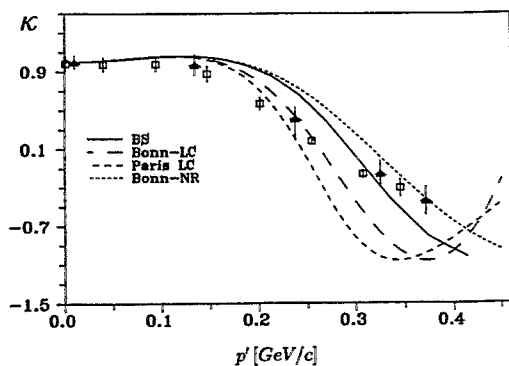


Fig. 1 The polarization transfer κ as function of the final proton momentum p' in the deuteron's rest frame. The references of the experimental data (symbols) are quoted in [2].

¹ Bogoliubov Institute of Theoretical Physics, JINR Dubna, Russia

² TRIUMF, Vancouver, Canada

³ Institut für Theoretische Physik, TU Dresden and Institut für Kern- und Hadronenphysik, FZR

References

- [1] L.P. Kaptari, A.Yu. Umnikov, F.C. Kahanna, B. Kämpfer, FZR-64 (1994)
- [2] L.P. Kaptari, A.Yu. Umnikov, F.C. Kahanna, B. Kämpfer, Phys. Lett. B 351 (1995) 400

A Quasi-Particle Model of the SU(3) Gluon Plasma^B

A. PESHIER, B. KÄMPFER¹, O.P. PAVLENKO², AND G. SOFF³

Recently, the thermodynamics of the SU(3) gluon plasma has been calculated on sufficiently large lattices which allow for a safe continuum extrapolation [1]. We follow here an earlier attempt [2] and describe this new lattice data [1] by a quasi-particle model of non-interacting quasi-gluons with an effective thermal mass. A system of quasi-particles with the temperature dependent dispersion relation $\omega^2 = k^2 + m^2(T)$ is described by the effective Hamiltonian $H_{eff} = d \sum_{\vec{k}} \omega(\vec{k}, T) n_{\vec{k}} + E_0(T)$ with the number operator $n_{\vec{k}}$ of d -fold degenerate particles of momentum \vec{k} . $E_0(T)$ is the ground state energy. In the limit of infinite volume V one obtains for the pressure and the energy density of the quasi-particle system the well-known ideal gas expressions up to a temperature dependent ground state contribution $B(T) \stackrel{V \rightarrow \infty}{=} E_0(T)/V$, $p(T) = p_{id}(T, m(T)) - B(T)$, $e(T) = e_{id}(T, m(T)) + B(T)$. From the requirement of thermodynamical self-consistency $s = \partial p / \partial T \stackrel{!}{=} (e + p)/T$ one gets $B(T) = B_0 - \frac{d}{4\pi^2} \int_{T_0}^T d\tau \frac{dm^2(\tau)}{d\tau} \int_0^\infty dk f(k, T) k^2 / \omega(k, \tau)$, where $f(k, T) = [e^{\omega(k, T)/T} \pm 1]^{-1}$ denotes the thermal distribution function.

To determine the functional dependence of the effective thermal mass $m(T)$ for the hot SU(3) theory we consider the dispersion of excitations. in the perturbative regime with coupling $g \ll 1$. To leading order only the transverse modes with large-momentum $k \gg gT$ and with the approximate dispersion relation $\omega^2 = k^2 + \frac{3}{2} \omega_0^2$ are relevant. With the gauge invariant plasma frequency $\omega_0^2 = \frac{1}{3} g^2 T^2$ and a factor $\frac{1}{2}$ for partitioning the self-energy between two interaction partners we find $m^2(T) = \frac{1}{4} g^2(T) T^2$. In accordance with perturbative QCD we choose the coupling $g^2(T) = \frac{16\pi^2}{11 \ln(\lambda T / T_c + T_s / T_c)^2}$ with the scaling parameter λ and T_s/T_c as a phenomenological regularization.

As shown in Fig. 1, our model reproduces the continuum-extrapolated data [1] perfectly. The function $B(T)$ changes its sign at $2T_c$. This might be considered as a hint to a complicated non-perturbative vacuum structure.

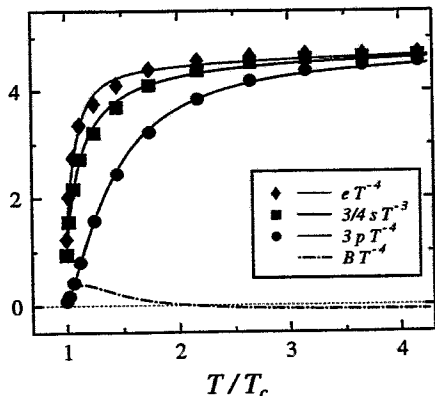


Fig. 1 Comparison of our model (thin lines) with continuum-extrapolated lattice data (symbols, from [1]) of scaled energy density, pressure and entropy density. The dash-dotted curve depicts the function $B(T)/T^4$. The fit parameters are $\lambda = 2.14$, $T_s/T_c = -1.04$, $B_0 = 0.16 T_0^4$ [3].

¹ Institut für Theoretische Physik, TU Dresden and Institut für Kern- und Hadronenphysik, FZR

² Institute for Theoretical Physics, Kiev, Ukraine

³ Institut für Theoretische Physik, TU Dresden

References

- [1] G. Boyd et al., Phys. Rev. Lett. 75 (1995) 4169
- [2] A. Peshier, B. Kämpfer, O.P. Pavlenko, G. Soff, Phys. Lett. B 337 (1994) 235
- [3] A. Peshier, B. Kämpfer, O.P. Pavlenko, G. Soff, FZR-106 (1995)

Entropy of Hot SU(N) Gauge Theories with Fermions^B

A. PESHIER, B. KÄMPFER¹, AND G. SOFF²

The entropy plays a central role in the quasi-particle description of strongly interacting systems. While for the energy density the ground state energy has to be taken into account, the entropy is only sensitive to the dispersion relation of the quasi-particles [1]. Within QCD, the gluon polarization and the quark self-energy determine the dispersive behavior of gluons and quarks in a hot plasma; they are known in the weak coupling regime ($g \ll 1$) in the 1-loop approximation. For large momenta $k \geq gT$ it turns out that the transverse gluon and quark excitations are damped only at higher order in the coupling g and can be interpreted as quasi-particles, whereas large- k longitudinal modes are overdamped and do not propagate. The main contributions to thermodynamical quantities come from quasi-particles with momentum $k \sim T$. In that region the dispersion relation for transverse gluons and quarks with N_f flavors can be approximated [2] by $\omega_{g,q}^2 = k^2 + m_{g,q}^2$, where

$$m_g^2 = \frac{3}{2} \omega_{pl}^2 = \frac{3}{2} \frac{1}{9} \left(N + \frac{1}{2} N_f \right) g^2 T^2, \quad m_q^2 = 2\omega_0^2 = 2 \frac{N^2 - 1}{16N} g^2 T^2. \quad (1)$$

Gluons in the momentum space sphere $k < gT$ contribute only to order $k^3 [e^{\omega/T} - 1]^{-1} \omega \sim g^3 T^4$ to the energy density, for instance. Thus, the above transverse gluon and quark dispersion relation can be applied in the whole phase space and also the longitudinal modes can be neglected when calculating thermodynamic quantities up to order g^2 .

Expanding the entropy of an ideal Boson or Fermion gas with degeneracy d in powers of the mass m ,

$$s_B^{id} = s_{SB} \left[1 - \frac{15}{8\pi^2} \left(\frac{m}{T} \right)^2 + \frac{15}{8\pi^3} \left(\frac{m}{T} \right)^3 + \dots \right], \quad s_F^{id} = s_{SB} \left[\frac{7}{8} - \frac{15}{16\pi^2} \left(\frac{m}{T} \right)^2 + \dots \right] \quad (2)$$

with $s_{SB} := d \frac{4\pi^2}{90} T^3$, and inserting the effective gluon and quark masses (1) we obtain an expansion in powers of g for the entropy of the system of $2 \cdot (N^2 - 1)$ (transverse) quasi-gluons and $2_{1\uparrow} \cdot 2_{q\bar{q}} \cdot N \cdot N_f$ quasi-quarks

$$s_{gg} = \frac{4\pi^2}{90} T^3 \left[2(N^2 - 1) + \frac{7}{8} 4NN_f - \frac{5}{8\pi^2} (N^2 - 1) \left(N + \frac{5}{4} N_f \right) + \dots \right]. \quad (3)$$

This agrees with the result [3] obtained from the perturbative calculation of the thermodynamical potential p_{gg}^{pQCD} and $s = \partial p / \partial T$.

Though it is not straightforward to get the next order of the expansion due to the complicated dispersion relations of hot QCD we can apply the same consideration to the simpler φ^4 model. Relying on the resummed effective mass $m_\varphi^2 = g^2 T^2 (1 - \frac{3}{\pi} g + \dots)$ and s_B^{id} expanded up to the 'non-analytic' m_φ^3 term we find the next-to-next-to-leading order entropy of the φ^4 -model

$$s_\varphi = \frac{4\pi^2}{90} T^3 \left[1 - \frac{15}{8\pi^2} g^2 + \frac{15}{2\pi^3} g^3 + \dots \right] \quad (4)$$

in agreement with calculations based on the partition function [3].

¹ Institut für Theoretische Physik, TU Dresden and Institut für Kern- und Hadronenphysik, FZR

² Institut für Theoretische Physik, TU Dresden

References

- [1] M.I. Gorenstein, S.N. Yang, Phys. Rev. D 52 (1995) 5206
- [2] H.A. Weldon, Phys. Rev. D26 (1982) 1394, 2789
- [3] J.I. Kapusta, Finite Temperature Field Theory, Cambridge University Press (1989)

Solitonic Configurations of the SU(2) Nambu & Jona-Lasinio (NJL) Model at Finite Temperature and Density^B

M. SCHLEIF AND R. WÜNSCH

We have studied nucleonic properties in nuclear matter using the solitonic picture of the NJL model [1]. The medium is modeled as a gas of constituent quarks acting on the soliton as a heat and particle bath [2]. The soliton constitutes a localized deviation from the homogeneous medium. In static mean-field approximation (MFA), the quarks move in time-independent classical mesonic background fields obtained by minimizing the grand canonical potential Ω_{MFA} . The quark part of Ω_{MFA} consists of a term which does not explicitly depend on temperature T_m and chemical potential μ_m of the medium. It results from virtual quark-antiquark fluctuations in the vacuum configuration and describes excitations (polarization) of the Dirac sea. This term diverges and we have it regularized within Schwinger's proper-time scheme. A second term (medium part) comes from real quarks and antiquarks due to the finite values of T_m and μ_m . One particular level (valence level) with the lowest positive energy is considered separately. Usually it gives the main contribution to the grand canonical potential and to quark observables as well. On the basis of this decomposition one can define sea, medium and valence contributions to an observable of the soliton.

Fig. 1 shows the baryonic particle density for two self-consistently determined soliton configurations at $T_m = 50$ MeV for two different medium densities. The valence part (*val*) gives the main contribution to the solitonic distribution. Both the Dirac sea (*sea*) and the medium (*med*) contributions are polarized, *i. e.* they deviate from the configuration without the additional soliton. The picture illustrates the beginning of a delocalization of the soliton with increasing medium density. The mean radius $r_{\frac{1}{2}}$ of the soliton, defined as that radius where the particle density has dropped to half of its maximum value, is 15% larger at normal nuclear density (right figure) than at half normal density (left figure). This is a possible explanation for the expected swelling of nucleons in nuclear matter. The calculations show also a decreasing of the internal energy of the soliton with increasing density. This is in qualitative agreement with QCD sum rules.

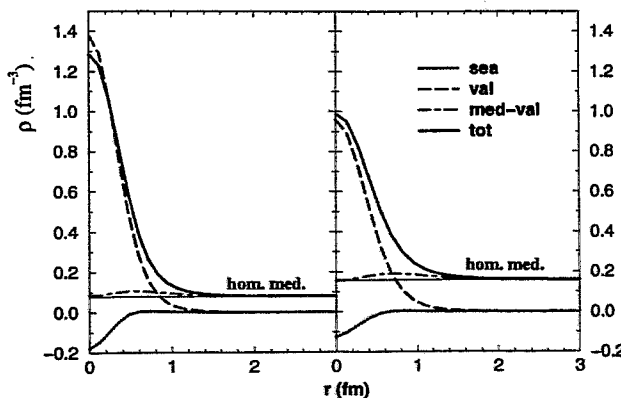


Fig. 1 Baryonic particle density in dependence on the distance from the center of the soliton at temperature $T = 50$ MeV for two different densities ρ_m of the surrounding matter.

Left figure: $\rho_m = 0.08 \text{ fm}^{-3}$,
right figure: $\rho_m = 0.16 \text{ fm}^{-3}$ (normal nuclear matter density).

References

- [1] Th. Meißner, A. Blotz, E. Ruiz Arriola and K. Goeke, RUB-TPII-42/93; *hep-ph/9401216*; to be published in *Rep. Prog. Theor. Physics* (1996)
- [2] M. Schleif and R. Wünsch, this annual report

The NJL Soliton in Hot Nuclear Matter^B

R. WÜNSCH AND M. SCHLEIF

It has been shown (see e. g. ref. [1]) that the effective action of the semibosonized Nambu & Jona-Lasinio (NJL) model is capable of describing the fundamental transformation which undergoes strongly interacting matter at large temperature (T_m) and/or density (ϱ_m). Describing nuclear matter as a homogeneous gas consisting of free quarks moving in a mesonic background field one can investigate both mesonic and quark degrees of freedom. The calculated dependence of meson and constituent quark masses on T_m and ϱ_m is in principle in agreement with the expected behavior.

In this picture the quarks occupy a continuous spectrum with a gap for energies $-M^* \leq E \leq +M^*$, where M^* is the constituent quark mass. The occupation probability of the various quark levels is given by the Fermi-Dirac distribution. The gap decreases with increasing temperature and density and vanishes at the critical values of T_m and ϱ_m nearly. Although neglecting the confinement of quarks completely the quark gas gives a reasonable description of hadronic matter even far below the critical point.

On the other hand isolated baryons at $T_m=0$ have successfully been modeled by spatially restricted field configurations (solitons) (see e. g. ref. [2]). In this picture the nucleon is described by a completely occupied Dirac sea and 3 additional valence quarks at the lowest level with positive energy.

In order to describe a nucleon in nuclear matter we combine the soliton picture with the constituent quark gas model. We evaluate the effective NJL action at finite values of temperature and chemical potential and look for solitonic configurations and their properties. Such a combination of a microscopic and a thermodynamic approach suffers naturally from inconsistencies. For instance it is impossible simultaneously to ensure the medium density ϱ_m at large separations from the soliton and the baryon number $B = 1$ for the soliton itself. We have tested several methods to reconcile the inconsistencies by modifying the assumptions concerning the thermal equilibrium between the quarks.

Thermal equilibrium between all the quarks is a prerequisite of the quark gas model. The clustering of quarks in hadronic matter affects the equilibrium. On the one hand the soliton is made of sea quarks, which are unbound and hence in close contact with the quarks of the nucleons in the medium. On the other hand the soliton contains valence quarks, which are confined by the meson field and, at not too high density, well separated from the valence quarks of the neighboring soliton. While it seems to be reasonable to use the thermal occupation numbers for the sea quarks the probability of quarks on the valence level is not necessarily determined by thermodynamics.

We have tested several methods of assigning occupation numbers to the various quark levels and studied their behavior during the self-consistent determination of solitonic meson and quark fields. Baryonic density distribution and root mean-square radii have been calculated. To determine the energy contribution of the unphysical center-of-mass motion of the soliton and the mass splitting between nucleon and Δ isobar we have extended the pushing and cranking procedures to finite temperature and density.

References

- [1] T. Hatsuda and T. Kunihiro, Phys. Rep. **247** (1994) 221
- [2] Th. Meißner, W. Ruiz Arriola, A. Blotz and K. Goeke, to be published in Rep. Prog. Theor. Physics (1996)

Magnetic Rotation^B

S. FRAUENDORF

Rotational bands appear if the nucleus is deformed and long regular sequences are an indication of a substantial deformation. This is a familiar concept of nuclear physics. From the theoretical point of view, one may say that the deformation permits to specify the orientation of the nucleus in the plane perpendicular to the total angular momentum \vec{J} . Once there exists such orientation angle, the system may change it, i. e. rotate. Quantized states of this motion will form a rotational band. The deformed charge distribution that goes round emits electric quadrupole radiation, the quanta of which connect the states of a band. The left part of fig. 1 summarizes this familiar picture of nuclear rotation. However, there is another possibility to specify the orientation, which is illustrated in the right part of the figure. If e. g. the angular momentum vectors of some high j proton particles and some high j neutron holes include a large angle, there is a transversal magnetic dipole moment, which specifies the orientation. Again, rotation is possible and manifests itself as a band. Now it is the magnetic dipole that goes round and emits magnetic dipole radiation, the quanta of which connect the states of the band. Such situation may also occur in nuclei with very small deformation, which are not expected to show rotational bands, because the interaction between protons and neutron holes favors an angle of 90° between their vectors \vec{j} . Since this kind of rotation is very different from the familiar nuclear rotation (A magnetic dipole goes round instead of an electric quadrupole.) it seems appropriate to call it *magnetic rotation* (MR), in contrast to the familiar case, for which in this context the name *electric rotation* (ER) suggests itself. MR manifests itself as a regular rotational band with strong $M1$ transitions connecting the levels and very weak or no $E2$ crossover transitions.

There is also a difference between the two types of rotation in the way the angular

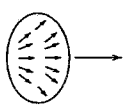
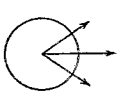

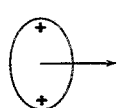
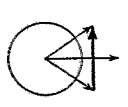
$\Delta I = 2$ ordinary bands	Characteristic of rotational bands	$\Delta I = 1$ shears bands
	regular $E_2 \propto I$	
gradual alignment of many short vectors		gradual alignment of few long vectors
E2	enhanced transitions	M1
	possibly to define the orientation (with respect to the a. m. vector)	
electric quadrupole mass distribution	large, collective isotropy broken "inertia" $J^{(2)} = \Delta I / \Delta E$	magnetic dipole current distribution
classic and quantal		quantal
electric	rotation	magnetic

Fig. 1 The relation between electric and magnetic rotation [1].

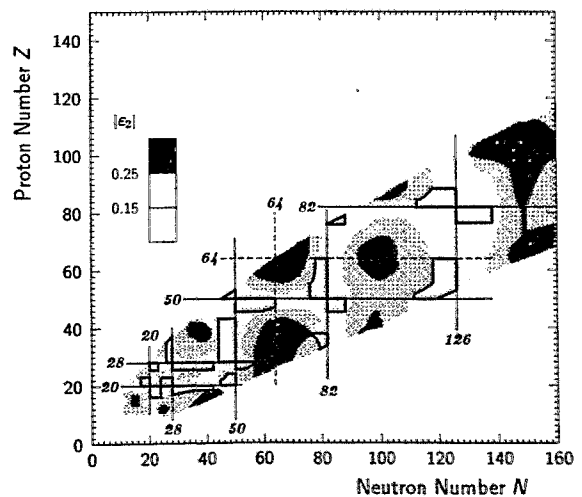


Fig. 2 Appearance of magnetic rotation [1]. The predicted regions are enclosed by the heavy lines.

momentum is built up. In the case of ER many particles participate, each contributing a small amount of angular momentum. In the case of MR a few high j orbitals generate the angular momentum. If the vectors \vec{j} of the latter are long enough they may gradually align, resulting in a regular band that will terminate (if not crossed by another band before).

MR is expected in weakly deformed nuclei, when high j particles of one kind are combined with high j holes of the other kind of nucleons. Then, the vectors \vec{j} point away from \vec{J} , specifying the orientation and they combine to a large dipole moment. To observe regular bands with many transitions the vectors \vec{j} of the particles and holes should gradually align with \vec{J} . This situation occurs when the vectors \vec{j} of at least two high j particles (and two holes) couple to maximal angular momentum. Such a stretched coupling is particularly favorable for two particles with different j because the interaction energy is large. This is not the case for two particles from the same j shell. Then regular rotational bands only appear if the core of the nucleus is soft enough such that the high j particles may induce a slight deformation that keeps the particles from the same j shell in stretched coupling. Fig. 2 gives a survey where MR can be expected. The regions delineated correspond to MR appearing at the yrast line and at moderate angular momentum (band heads at $10-20\hbar$). Some excitation energy or higher spin can bring suitable high j orbitals into reach and trigger MR.

In collaboration with experimental groups, examples for MR in several of the predicted regions are being studied by means of the Tilted Axis Cranking approach [2]. The region $Z > 80$ and $N < 126$ contains the "Shears Bands" of the Pb - isotopes, known for some time. The pair of $h_{9/2}, i_{13/2}$ protons in stretched coupling and 1,2 or 3 $i_{13/2}$ neutron holes in stretched coupling form "two blades of a pair of shears" that gradually close along the band [2]. A slight oblate deformation ($\epsilon < 0.1$) is necessary to keep the $i_{13/2}$ neutron holes in stretched coupling. The study of the region in collaboration with the Universität Bonn has been continued with ^{193}Pb [3]. In the region $Z > 50$ and $N < 64$ a MR band basing on the combination $\pi h_{11/2}^2, \nu h_{11/2}$ has been observed in ^{149}Sm (GASP) and is studied [4]. An example for MR in the region $Z < 48$ and $N > 50$ is ^{110}Cd [1,5], where the configuration is a combination of two $g_{9/2}$ proton holes with two $h_{11/2}$ quasi neutrons and additionally two normal parity quasi neutrons excited. The normal parity neutrons contribute noticeably to the angular momentum by aligning with \vec{J} . Such a triple of vectors is an example for MR, which is somewhat more complex than the shears bands. ^{105}Sn (GASP) has a MR band of similar structure with one $h_{11/2}$ quasi neutron less [6].

References

- [1] S. Frauendorf, Phys. Rev. Lett. , to be published; Proc. of Workshop on GAMMA Sphere Physics, LBNL Berkeley, Dec. 1995, World Science Pub., in print
- [2] S. Frauendorf, Nucl. Phys. A **557** 469c, (1993)
- [3] G. Baldsiefen, S. Frauendorf *et al.*, Nucl. Phys. , submitted
- [4] F. Brandolini, S. Frauendorf *et al.*, in preparation
- [5] S. Juutinen *et al.*, Nucl. Phys. A **573**, 306 (1994)
- [6] G. DeAngelis, S. Frauendorf *et al.*, in preparation

How Do Unpaired Nuclei Rotate?

S. FRAUENDORF

The moments of inertia of normally deformed nuclei at low spin are substantially smaller than the rigid body value. The reduction is attributed to the pair correlations. Accordingly, it is expected that along with the reduction of the pairing the moment of inertia will approach the rigid body value at high spin. Rotational bands built on multi quasiparticle high K bands should be close to this limit, because the excitation of the quasi particles blocks the pairing. Fig. 1 shows the angular momentum $J(\omega)$ as function of the rotational frequency, and its slope, the $\mathcal{J}^{(2)}$ moment of inertia, for 8 and 9 quasi particle bands in $^{178,179}\text{W}$. The experimental curves distinctly differ from the limit of strong coupling and rigid rotation. Fig. 1 also shows a Tilted Axis Cranking (TAC) calculation [2], which assumes zero pairing. The main features of the experimental curves are reproduced, i. e. the deviations from rigid rotation are not a consequence of pairing.

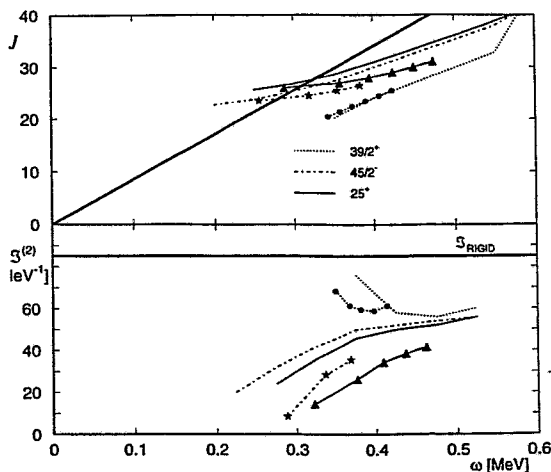


Fig. 1 Angular momenta and moments of inertia of high K bands in $^{178,179}\text{W}$. The TAC calculation assumes zero pairing and the ground state deformation $\epsilon = 0.23$. The experimental curves contain the data points [2,3] as symbols. The limit of strong coupling and rigid rotation is indicated by the heavy lines.

In the strong coupling limit J would be equal to $\omega \mathcal{J}^{(2)}$ corresponding to the straight line intercepting the origin in the upper panel of fig. 1. The configuration $39/2^+$ is an example. All other bands contain an $h_{9/2}$ proton, which aligns with the 1 - axis (perpendicular to the symmetry axis 3) immediately at the band head. The frequency is lower than for strong coupling, because of the alignment of the $h_{9/2}$ proton. The frequency reduction near the band head becomes quite substantial because of the tilted geometry.

For high ω the low value of $\mathcal{J}^{(2)}$ reflects the gross shell structure. The moments of inertia of unpaired nuclei take the rigid body value *only if averaged over a whole shell*. In the lower part of the shell, the concentration of orbitals weakly bound to the deformed potential makes angular momentum easily accessible, corresponding to a large moment of inertia. Vice versa, the concentration of strongly bound orbitals in the higher part of the shell results in a small moment of inertia, as for $^{178,179}\text{W}$.

The material is to be published in ref. [1].

References

- [1] S. Frauendorf, Phys. Lett., to be published
- [2] S. Frauendorf, Nucl. Phys. A **557** 469c, (1993)
- [3] C. S. Purrey *et al*, Phys. Rev. Lett. **75**, 406, (1995)
- [4] P. M. Walker *et al*, Nucl. Phys. A **568** 397, (1994)

Change from Liquid Drop to Quantal Rotation

S. ASZATOLES¹, S. FRAUENDORF, I. Y. LEE¹, M. A. DELEPLANQUE¹
AND F. S. STEPHENS¹

High angular momentum exposes the coarse quantal structure underlying nuclear rotation. The traditional concept of collective rotation considers the nucleus as a droplet of liquid whose surface rotates in space. This classical motion is quantized. The main trends of rotational bands in well deformed nuclei at low angular momentum are accounted for by this picture. For high angular momentum the mesoscopic nature of the nucleus becomes prominent. Rotation appears there as the correlated motion of a relatively small number of nucleons that move on quantized orbitals. It strongly deviates from the rotation of a liquid drop as well as from the rigid rotation of molecules.

Studies of a sequence of the rotational over a large number of neutron numbers permit to distinguish between liquid drop and quantum body rotation. For long chains of nuclei the measurements of rotational bands in neutron rich nuclei is necessary. The detection of γ rays following a deep inelastic reaction by means of GAMMA sphere allows to measure the yrast bands in ^{174,175,176,177,178}Yb up to spins between 12 and 18 \hbar .

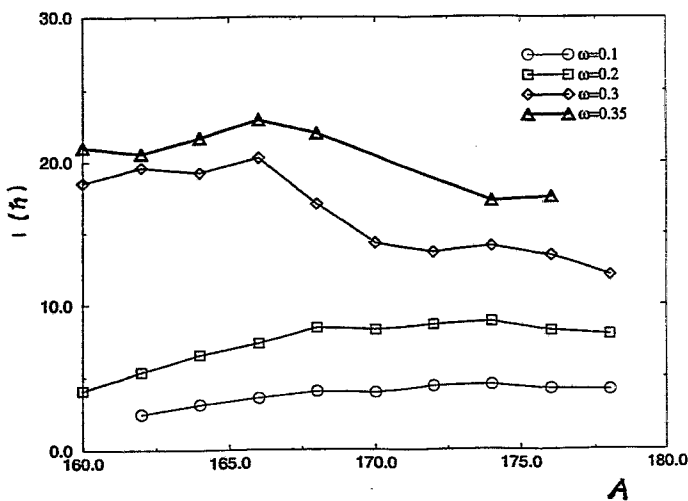


Fig. 1 Angular momentum I at a given rotational frequency ω for the even Yb isotopes.

At low frequency the moment of inertia \mathcal{J} shows the well known liquid drop behavior. It is proportional to the square of the deformation parameter, which is about constant above $A = 168$ and decreases towards 160, the boundary of the deformed region. For large frequency the angular momentum is large for small A and small for large A , contrary to the classical picture. The underlying shell structure becomes visible at high frequency. In the lower part of the shell, the concentration of orbitals weakly bound to the deformed potential makes angular momentum easily accessible, whereas the concentration of strongly bound orbitals in the higher part of the shell has the opposite consequence. At low frequency the presence of pair correlation efficiently suppresses the shell structure, resulting in the liquid drop like rotation. Cranking calculations to substantiate this picture are being carried out.

¹ Nuclear Science Division, Lawrence Berkeley National Laboratory, Berkeley Ca 94720, USA

Rotating Nuclear Matter

S. FRAUENDORF AND K. NEERGÅRD¹

We have studied [1] an infinite large system of interacting nucleons in the rotating frame of reference by the time-dependent Hartree-Fock theory. Stable homogeneous solutions to the time-dependent Hartree-Fock equations were obtained by omitting from the energy functional the electrostatic two-proton interaction and the centrifugal single-nucleon potential. The resulting system, which we call 'rotating nuclear matter', represents the interior of a rotating nucleus. For the effective Hartree-Fock two-nucleon interaction the Sprung-Banerjee force [2] was adopted.

The limit where the rotational frequency ω is much smaller than the Fermi kinetic energy ϵ_F was studied in detail. The terms linear in ω describe a distribution of spin density with a monopole and a quadrupole term at the surface of a local Fermi sphere. The quadrupole term gives rise to a tilting of the spin density vector in some points of the Fermi surface. In the case of rotating symmetric nuclear matter at normal density the monopole spin density is almost equal to its non-interacting value as a result of practically equally large relative enhancements of the spin cranking term by the spin-orbit interaction and the kinetic energy restoring force by the central and tensor interactions. The ratio of the monopole spin density to its non-interacting value has a minimum at lower densities and increases towards higher densities. The quadrupole spin density is produced by the interaction of the nucleonic spin partly with the curl of the rigid rotational momentum distribution via the spin-orbit force and partly with the monopole spin density via the tensor force.

The volume contribution of the spin to the moment of inertia is proportional to A , amounting to to 3.1 % of the rigid body value for $A = 100$. Two surface contributions to the moment of inertia are also proportional to A . Due to canceling out of these three contributions the total correction to the moment of inertia proportional to A vanishes within the accuracy of the calculation.

The single particle Routhian of a finite rotating nucleus was studied. It is obtained from the ordinary shell model single-nucleon Hamiltonian by adding the centrifugal field and subtracting from the momentum that of a free nucleon following the rigid rotation. This differs from the common practice to just add a cranking term to the nonrotating Hamiltonian. The additional terms arising form an orbital cranking field enhanced by the ratio of the bare and effective nucleonic mass, and a residual centrifugal potential. The second correction term is a momentum dependent modified spin cranking field with a monopole plus quadrupole dependence on the direction of the momentum relative to that of a free nucleon following the rigid rotation. At the Fermi surface of symmetric nuclear matter at normal density the monopole spin cranking field is enhanced by practically the same factor as the orbital cranking field.

High spin spectroscopy of normally and superdeformed nuclei can study these time-odd terms of the rotating mean field and provide information about time-odd components of the effective nucleon-nucleon interaction, not accessible so far.

¹ *Næstved Gymnasium og HF Nygårdsvvej 43, DK-4700 Næstved, Denmark*

References

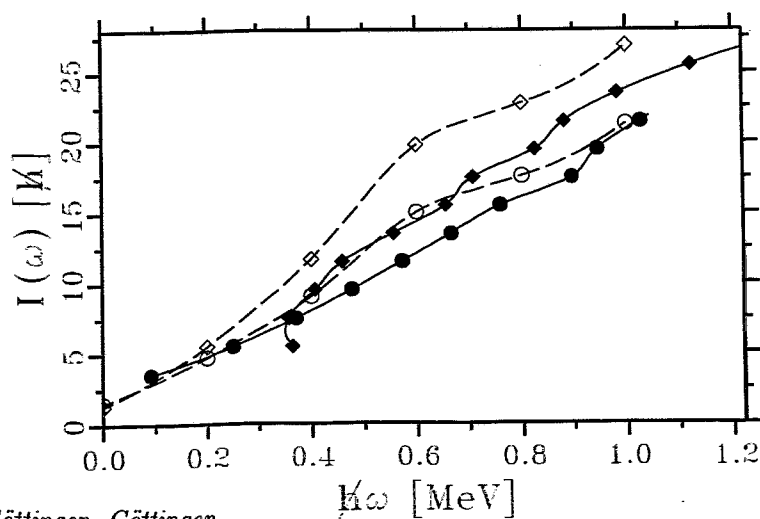
- [1] S. Frauendorf and K. Neergård, *Z. Phys. A* (1996), in print
- [2] D. W. L. Sprung and P. K. Banerjee, *Nucl. Phys. A* **168**, 273 (1971)

A New Type of Band Crossing at Large Deformation^{B,S}

F. DÖNAU, A. HARDER¹ AND K. P. LIEB³

The positive parity, favoured yrast and yrare rotational bands in ⁷⁷Rb were recently measured with the EUROGAM I spectrometer. In the extensive experiment one was able to follow both bands over a large spin range below and above the band crossing. In addition, the *E2* strength of many in-band and inter-band transitions were measured. Comparing the deduced moments of inertia and transition quadrupole moments Q_t the unusual behaviour of those band structures shows up: A more deformed band structure is crossed by a less deformed one and, since the yrare band starts at the extremely low spin value $I = 9/2$, the conventional band crossing mechanism of two aligning high- j quasiparticles is excluded. The latter feature gets apparent in Fig.1 by extrapolating the spin function $I(\omega)$ to the ordinate intersection at $\hbar\omega = 0$ resulting in our case in a very low value of the particle alignment i . The strikingly new properties (band energies, Q_t values) were investigated within the framework of the Nilsson-Strutinsky approach [1]. Potential energy surfaces $E_\omega(\epsilon, \gamma)$ for a sequence of rotational frequencies $\hbar\omega$ were calculated in order to find the equilibrium shapes of those bands. The use of diabatic tracing of configurations was an indispensable ingredient of these calculations. We found that the unexpected features of these bands are related to the particular structure of the Fermi level at neutron number $N=40$ above the $N=38$ shell gap in the deformed potential. In the interesting deformation region near $\epsilon \approx 0.32$ the Fermi level is formed from the neutron orbitals $[301\ 3/2]$ and $[422\ 5/2]$ each of which driving to a different deformation. Hence, the corresponding occupation change of the valence neutron pair in ⁷⁷Rb is responsible for two different equilibrium configurations. Following diabatically their frequency dependence one obtains qualitatively the unusual alignment and transition properties seen within the experiment. Up to $\hbar\omega = 0.6$ MeV both bands have a nearly axial shape with a decreasing ϵ deformation starting at large values $\epsilon=0.34$ and $\epsilon=0.31$, correspondingly. At higher frequency the lower deformed yrast band changes to a triaxial shape close to $\gamma = 30^\circ$. This is the first observation of such a type of band crossing.

Fig. 1
Spin I as a function of the rotational frequency $\hbar\omega$.
Solid curves: Experiment
Dashed curves: Calculation



¹ II. Phys. Institut der Universität Göttingen, Göttingen

References

- [1] R. Bengtsson *et al.*, Phys. Lett. B **57**, 301 (1975)

The Trapping Effect Revisited^{D,W}

T. GORIN, S. DROŹDŹ¹, J. OKOŁOWICZ¹ AND I. ROTTER²

We investigate the influence of spectral correlations on the trapping mechanism within two models: the continuum shell model (CSM) [3] and the statistical model (StM) [1,2].

a) In the StM a Hermitean random matrix is coupled to the continuum via a random vector: $H = H_{\text{QQ}} - iVV^\dagger$. We investigate two cases, where H_{QQ} is chosen either from the Gaussian orthogonal ensemble (GOE) or the ensemble of diagonal matrices, with equidistributed elements, the Poissonian ensemble (PE). For the GOE it is shown in [1] that the joint probability distribution of all resonances, except the broadest, is equal for small and large coupling strengths.

The coupling strength is defined as the summed width of all resonances. It is given by $2\|V\|^2$. Defining it in appropriate units, we get a dimensionless number $\kappa = \frac{2\langle\Gamma\rangle}{D}$ for which the following relations hold [2]: $\kappa < 1 : \kappa_{\text{fine}} \approx \kappa$ and $\kappa > 1 : \kappa_{\text{fine}} \approx \kappa^{-1}$. $\langle\Gamma\rangle$ is the average width of all resonances, D the mean level-spacing, $\langle\Gamma\rangle_{\text{fine}}$ the average width of all, except the broadest resonance and $\kappa_{\text{fine}} = \frac{2\langle\Gamma\rangle_{\text{fine}}}{D}$. Fig. 1 shows the accuracy of the above stated relations in the GOE case. For the PE we get considerable deviations due to the different shapes of the level densities (semi-circle law for GOE and equidistribution for PE).

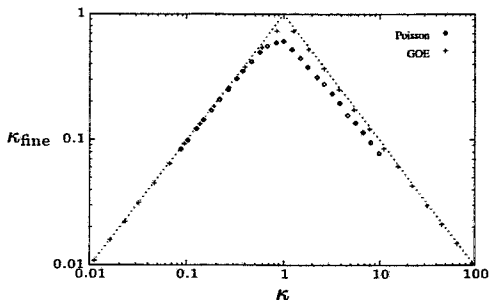


Fig. 1 Ratio κ_{fine} within the StM for the GOE and the Poissonian ensemble.

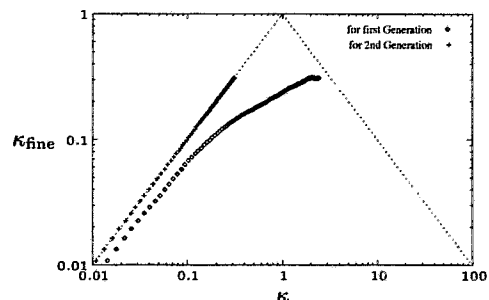


Fig. 2 Ratio κ_{fine} within the CSM. The crosses are obtained having discarded the broadest mode.

b) In the CSM, this part of the Hamiltonian, which describes the coupling to the continuum, is explicitly energy dependent and the broadest resonance is shifted far apart from the remaining ones. A second resonance can grow up, take the vacant position and trap the others (the second generation) [3]. In order to demonstrate this mechanism, we plot κ_{fine} versus κ twice, first taking into account all resonances, then we discard the broadest and repeat the procedure again. The result is shown in Fig. 2. As the second broadest resonance does not get such a large shift, the obtained curve follows exactly the predictions within the StM. It only does not reach the critical region $\kappa \approx 1$.

¹ Institute of Nuclear Physics, Kraków, Poland

² Institut für Theoretische Physik, TU Dresden and Institut für Kern- und Hadronenphysik, FZR

References

- [1] V. V. Sokolov and V. G. Zelevinski, Nucl. Phys. A **504** 562 (1989)
- [2] F.-M. Dittes, H. L. Harnay and I. Rotter, Phys. Lett. A **153**, 8 451 (1991)
- [3] W. Iskra, M. Müller and I. Rotter, J. Phys. G **19**, 2045 (1993); G **20**, 775 (1994)

Non-Hermiticity and the Eigenvectors of the Effective Hamiltonian^{A,D}

T. GORIN, E. PERSSON AND I. ROTTER¹

In the statistical model, the particle decay of a compound nucleus is described by a non-hermitean effective Hamiltonian, $H_{QQ}^{eff} = H_{GOE} + i\alpha\pi VV^\dagger$ [1]. Here, the Q denotes that H_{QQ}^{eff} operates only in the closed Q -subspace of the compound nucleus. Through the coupling vector V , describing the coupling of the states to the decay channels, H_{QQ}^{eff} is influenced by the continuum of decay channels. H_{GOE} is the Hamilton operator for the closed system without contribution from the continuum. $Rank(H_{GOE}) = N$ whereas $rank(VV^\dagger) = K$, where K is the number of open channels and N the number of states. H_{GOE} is drawn from the Gaussian orthogonal ensemble and V is a real random vector. The eigenvalues of H_{QQ}^{eff} determine the energy and the width of the resonance states. Its eigenfunctions give the wavefunctions of the compound nucleus states. Our calculations are performed by increasing α , which means increasing the degree of overlapping $\bar{\Gamma}/D$.

The effective Hamiltonian is complex, but has the symmetry $H_{QQ}^{eff} = (H_{QQ}^{eff})^T$. It follows that $\langle \tilde{\Phi}_{R'}^* | \tilde{\Phi}_R \rangle = \delta_{RR'}$ where $\tilde{\Phi}_R$ are the eigenfunctions of the effective Hamiltonian. However, $\langle \tilde{\Phi}_{R'} | \tilde{\Phi}_R \rangle$ is in general a complex number. Fig. 1 shows $|\langle \tilde{\Phi}_{R'} | \tilde{\Phi}_R \rangle|$ for $N = 70$ and $K = 2$ for all the 70 states with respect to all states. H_{QQ}^{eff} is chosen to be in the critical

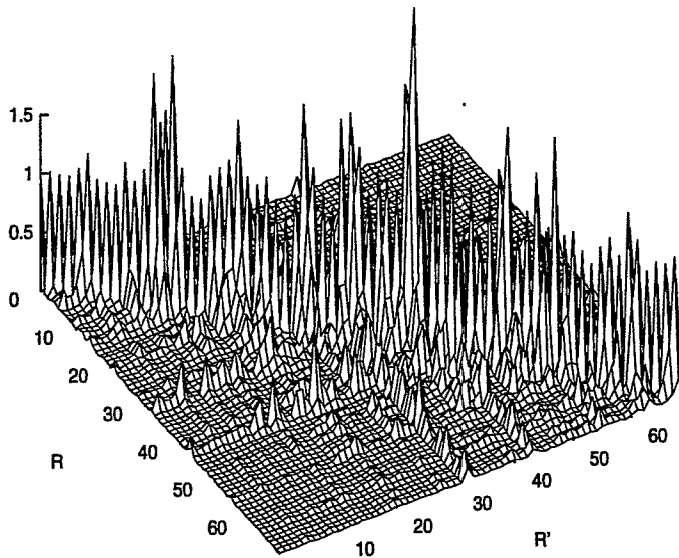


Fig. 1 $|\langle \tilde{\Phi}_{R'} | \tilde{\Phi}_R \rangle|$ for $N=70$ and $K=2$.

region, where the degree of overlapping is $\bar{\Gamma}/D \approx K$. In this region a reorganisation of the eigenvalues takes place, giving most of the available width to K states (trapping effect). This reorganisation is reflected in the $|\langle \tilde{\Phi}_{R'} | \tilde{\Phi}_R \rangle|$ (Fig.1), which are often non-zero for $R' \neq R$ and larger than one for $R' = R$. Below the critical region, the first hermitean part of the effective Hamiltonian is important. Here $\langle \tilde{\Phi}_{R'} | \tilde{\Phi}_R \rangle \approx \delta_{RR'}$. The same also holds far above the critical region.

¹ Institut für Theoretische Physik, TU Dresden, and Institut für Kern- und Hadronenphysik, FZR

References

- [1] V. V. Sokolov, V. G. Zelevinsky, Nucl. Phys. A, **504**(1989)569

Interference of Resonances and Partial Widths of Collective States^D

V.V. SOKOLOV¹ AND I. ROTTER²

In spite of much efforts, the nature of giant resonances (GR) is only partly understood nowadays. It is generally accepted that they mainly consist of coherent superpositions of many $1p - 1h$ configurations which are correlated by the residual interaction and are embedded in the energy continuum of decay channels. But their microscopic structure still needs further investigation. The partial widths of direct particle decay of GRs carry a detailed information of this structure. They became therefore a useful tool for a careful study [1] of collective modes of nuclear motion.

A collective mode being shifted in energy from the domain of its parental single-particle states is usually considered as an isolated resonance damped by coupling to complicated incoherent states, e.g. [2]. However, this shift is, as a rule, of the order of magnitude of the total escape width. Therefore, the collective mode noticeably interferes with other states of $1p - 1h$ nature which are almost unshifted and carry only a small degree of collectivity. The total and partial proton escape widths of isobaric analog (IAR) as well as Gamov-Teller (GTR) resonances in ^{208}Bi are calculated in the framework of the same theoretical scheme in the ref.[3]. The results, being quite satisfactory for the narrow IAR, feign appreciable loss of unitarity in the case of the much broader GTR: the sum of calculated partial widths turned out to be 30% larger than the total width of the collective state. This points to the fact that the GTR cannot be considered as being perfectly isolated. By incorporating damping effects [4] giving rise to a spreading width of the collective mode the problem is only screened but not solved. The correct consideration of the external mixing of resonances is necessary [5,6] to insure unitarity.

In [7], a simple schematic model for a collective state embedded in continuum has been worked out. Internal and external mixings of the parental single-particle states are treated on equal footing. We extend the single-channel consideration of ref. [7] to the case of an arbitrary number of decay channels in order to demonstrate the influence of interference between collective and non-collective modes on the decay pattern. The effective model Hamiltonian

$$\mathcal{H} = H_0 + DD^T - \frac{i}{2}AA^T \quad (1)$$

consists of three parts: H_0 describes N unperturbed discrete states of $1p - 1h$ nature, DD^T is the internal residual interaction of multipole-multipole type and AA^T describes the coupling of the states via k common decay channels. The column D is an N -dimensional vector of multipole matrix elements while the $N \times k$ -matrix A is formed by k vectors \mathbf{A}^c of transition amplitudes between N unperturbed discrete states and the channel c . Due to the two interactions, the Hamiltonian (1) provides two different types of collectivity, internal and external. The latter is called "width collectivisation" in [6].

The complex eigenvalues of the nonhermitian matrix \mathcal{H} are the roots of the secular equation

$$\Lambda(\mathcal{E}) \equiv 1 - D^T \frac{1}{\mathcal{E} - \mathcal{H}_0} D =$$

$$1 - D^T \frac{1}{\mathcal{E} - H_0} D - \frac{i}{2} D^T \frac{1}{\mathcal{E} - H_0} A \left[1 + \frac{i}{2} A^T \frac{1}{\mathcal{E} - H_0} A \right]^{-1} A^T \frac{1}{\mathcal{E} - H_0} D = 0 \quad , \quad (2)$$

where $\mathcal{H}_0 \equiv \mathcal{H} - DD^T$. They give the full set of energies and widths of all interfering resonances. One of these resonances corresponds to the collective mode while the internal collectivity of the other resonances is small.

The hermitian R -matrix of our model can be explicitly found as

$$\hat{R}(E) = A^T \frac{1}{E - H_0} A + A^T \frac{1}{E - H_0} D \left[1 - D^T \frac{1}{E - H_0} D \right]^{-1} D^T \frac{1}{E - H_0} A \quad . \quad (3)$$

The collision matrix containing all interference effects looks like

$$\hat{T}(E) = \frac{\hat{R}(E)}{1 + \frac{i}{2} \hat{R}(E)} \quad . \quad (4)$$

This form of the collision matrix provides unitarity.

There are two parameters of the model, $\lambda \equiv D^T D = \mathbf{D}^2$ and $\gamma \equiv \frac{1}{k} \text{tr} A^T A = \langle [A^c]^2 \rangle$, the total energy shift and the average total partial width of resonances, characterizing internal and external collectivity respectively. Only if internal collectivity appreciably prevails, $\lambda \gg \gamma$, the general formula (4) simplifies to

$$\hat{T}(E) = \frac{A_D A_D^T / \mathbf{D}^2}{E - E_{coll} + \frac{i}{2} A_D^T A_D / \mathbf{D}^2} \quad . \quad (5)$$

Here E_{coll} stands for the position of the collective mode and the column vector $A_D \equiv A^T D$ consists of the scalar products ($A^c \mathbf{D}$) in N -dimensional space of $1p - 1h$ states. This expression has standard many channel Breit-Wigner form valid for an isolated resonance. Generally, eq. (4) together with (3) shows a more complicated energy behaviour of the cross sections in the region of the collective resonance because of the influence of other resonances. We analyse the coherent interference of resonances in detail for the case when both parameters of collectivity are comparable, $\lambda \sim \gamma$.

¹ *Budker Institute of Nuclear Physics, Novosibirsk, Russia*

² *Institut für Theoretische Physik, TU Dresden and Institut für Kern- und Hadronenphysik, FZR*

References

- [1] C.Gaarde et al., Phys. Rev. Lett. **46** (1981) 902.
- [2] S.E. Muraviev and M.H. Urin, Nucl. Phys. **A569** (1994) 267c.
- [3] Nguyen Van Giai et al., Phys. Lett. **B233** (1989) 1.
- [4] G. Colo et al. Nucl. Phys. **A577** (1994) 73c.;
T. Udagawa et al. Nucl. Phys. **A577** (1994) 67c.
- [5] P. Kleinwächter and I. Rotter, J. Phys. G: Nucl. Phys. **12** (1986) 821.
- [6] V.V. Sokolov and V.G. Zelevinsky, Nucl. Phys. **A504** (1989) 562.
- [7] V.V. Sokolov and V.G. Zelevinsky, Fizika **22** (1990) 303.

Non-Hermiticity and Decay-Rates of Overlapping States^{A,D}

E. PERSSON, T. GORIN AND I. ROTTER¹

Decaying states can be described as eigenstates of an effective Hamiltonian, $H_{QQ}^{eff} = QHQ + QVP \cdot G_P^{(+)} \cdot PVQ$ [1]. Q projects onto the closed system and P onto the continuum of decay channels. $G_P^{(+)}$ is the propagator in the P-subspace, H the complete Hamiltonian and V the residual interaction. The eigenvalues, $E_R - \frac{i}{2}\Gamma_R$, of H_{QQ}^{eff} give the energy and the lifetime of the resonance states while its eigenfunctions, $\tilde{\Phi}_R$, determine their wavefunctions.

In the following we do the investigations in a simplified model where QHQ is drawn from the Gaussian orthogonal ensemble. The energy dependence of the coupling matrix elements is not taken into account, which let us write $H_{QQ}^{eff} = H_{GOE} + i\alpha\pi VV^\dagger$ [2]. Overlapping resonances cannot be excited separately, and thus must be described by $|\phi(t)\rangle = \sum_R a_R(t) |\tilde{\Phi}_R\rangle$. The $a_R(0)$ are chosen as the overlap between a high-resolution beam and isolated Breit-Wigner shaped resonances. The time development follows from $i\hbar \frac{\partial}{\partial t} |\phi(t)\rangle = H_{QQ}^{eff} |\phi(t)\rangle$. Also, the $\tilde{\Phi}_R$ are not orthogonal, $\langle \tilde{\Phi}_{R'} | \tilde{\Phi}_R \rangle \neq \delta_{RR'}$. It follows for the survival probability

$$\begin{aligned} \langle \phi(t) | \phi(t) \rangle &= \sum_R |a_R(0)|^2 e^{-\frac{1}{\hbar} \Gamma_R t} \langle \tilde{\Phi}_R | \tilde{\Phi}_R \rangle \\ &+ 2 \sum_{R < R'} e^{-\frac{1}{2\hbar} (\Gamma_R + \Gamma_{R'}) t} \Re [a_R(0) a_{R'}(0)^* e^{-\frac{i}{\hbar} (E_R - E_{R'}) t} \langle \tilde{\Phi}_{R'} | \tilde{\Phi}_R \rangle]. \quad (1) \end{aligned}$$

The decay rate k^{eff} of the state is defined by $k^{eff}(t) = -\frac{\partial}{\partial t} \ln \langle \phi(t) | \phi(t) \rangle$ [3].

To study the gross time dependence of k^{eff} we also define $k_{gr}^{eff} = -\frac{\partial}{\partial t} \ln B(t)$ where B is the first, single sum in eq. (1).

In fig.1, the behaviour of $k^{eff}(t)$ is illustrated for a model system of two states with different widths. The beam excites the narrow state. $k^{eff}(t)$ is calculated for three cases, a) $\bar{\Gamma}/D = 0.1$, b) $\bar{\Gamma}/D = 1.2$ and c) $\bar{\Gamma}/D = 4.1$. $\bar{\Gamma}$ is the mean width and D is the average level distance. The thick lines show k_{gr}^{eff} and the thin ones k^{eff} . In a) k_{gr}^{eff} equals Γ for the narrower state and one can see the effects of the interference term. The second curve (b) shows that k_{gr}^{eff} is in general not constant and that k^{eff} can be very different from k_{gr}^{eff} . In c) $k_{gr}^{eff}(t)$ goes from a value governed by the short-lived resonance at short time-scales to a constant value governed by the long-lived resonance at long time-scales.

In fig.2, $k^{eff}(t)$ is calculated for a system of 70 states and two channels for $\bar{\Gamma}/D = 6.0$. An isolated, trapped state is excited, but apart from the two broad states, also its trapped neighbours get a non-negligible $|a_R(0)|^2$. For $k^{eff}(t)$ (thin line) one can see a complicated interference picture. $k_{gr}^{eff}(t)$ (thick line) shows a transition time, from an interval, where one trapped state is important, to another interval, where a narrower state is important.

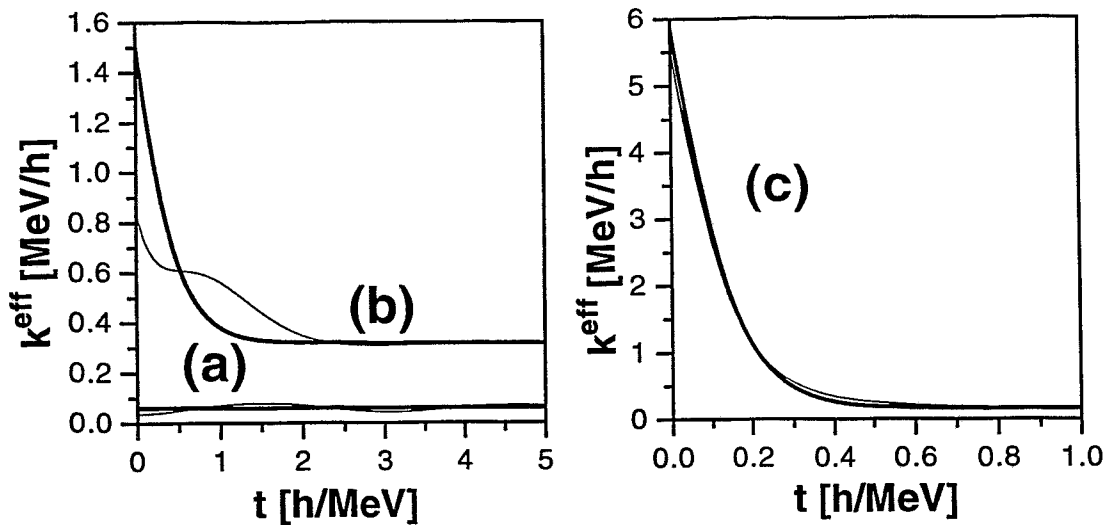


Fig. 1 k_{gr}^{eff} (thick line) and $k^{eff}(t)$ (thin line) for a system of two resonances. $\bar{\Gamma}/D = 0.1$ (a), $\bar{\Gamma}/D = 1.2$ (b) and $\bar{\Gamma}/D = 4.1$ (c).

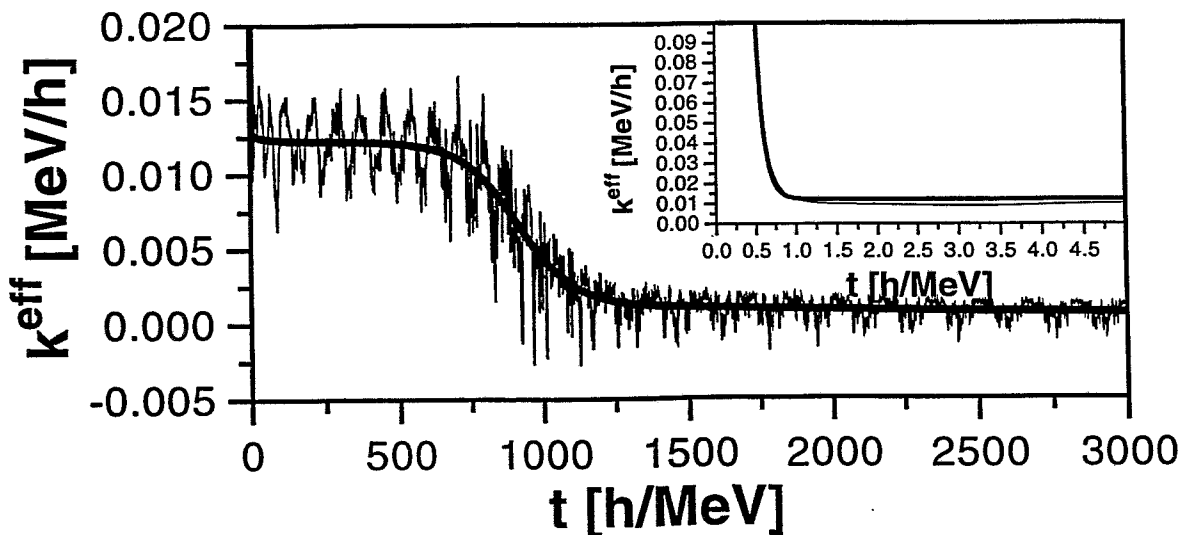


Fig. 2 k_{gr}^{eff} (thick line) and $k^{eff}(t)$ (thin line) for a system of 70 resonances.

¹ Institut für Theoretische Physik, TU Dresden, and Institut für Kern- und Hadronenphysik, FZR

References

- [1] I. Rotter Rep. Prog. Phys. 54(1991)632
- [2] V. V. Sokolov, V. G. Zelevinsky, Nucl. Phys. A, 504(1989)569
- [3] U. Peskin, H. Reisler, W. H. Miller, J. Chem. Phys 101(1994)9672

Does Resonance Trapping Occur in Real Nuclei?^W

V.E. BUNAKOV¹ AND I. ROTTER²

The interesting phenomenon of "trapping" occurring in a system of resonance states interacting with each other via the continuum has been studied now for more than a decade. However the question whether this phenomenon is typical for real nuclear systems needs further study.

We start investigating this question in case of resonance states for medium and heavy nuclei where the statistical approach has proved its validity. Here, the residual interaction together with the real part of the resonance coupling via the continuum is supposed to create a Gaussian orthogonal ensemble (described by H). The energy dependence is neglected. The Hamiltonian then reads $H^{eff} = H - i\pi VV^+$ where V is the coupling vector containing the coupling between discrete states and continuum.

As a starting point we use the results of [1], where it was shown analytically that in the one-channel case the onset of trapping occurs when the ratio of average resonance widths $\langle \Gamma \rangle$ to average resonance spacing D reaches the critical value $2/\pi$. In order to apply this criterion to the realistic nuclear case we have first to generalize the approach of [1] for the case of K channels whose partial widths $\langle \Gamma^n \rangle$ contribute approximately equally to the total resonance width $\langle \Gamma_{tot} \rangle \approx K \langle \Gamma^n \rangle$. We show that the above critical condition in this case can be generalized to

$$\frac{\langle \Gamma^n \rangle}{D} = \frac{2N}{(N-K)\pi} \approx 1. \quad (1)$$

Here N is the number of coupled resonances ($N \gg K$).

Further on we apply the methods of Mahaux-Weidenmüller's theory [2] together with R-matrix approach in order to get the analytic estimate for nucleon channels:

$$\frac{\langle \Gamma \rangle}{D} \approx \frac{4W(E)\Gamma_0(E)}{D_0^2}. \quad (2)$$

Here $W(E)$ is the imaginary part of the optical model potential, while $\Gamma_0(E)$ and D_0 are the single-particle resonance width and spacing, correspondingly. Combining eqs.(1) and (2) with the dependences of W , Γ_0 and D_0 on neutron energy E and atomic number A , we obtain an expression for the value E_{crit} which defines the onset of trapping phenomena in each region of target nuclei A . The greatest ambiguity in numerical estimates of E_{crit} comes from the lack of precise information on the E -dependence of Γ_0 . The most conservative estimates can be obtained for s-wave neutrons whose Γ_0 has the slowest increase with E . Those conservative estimates show, for example, that for $A \approx 150$ resonance trapping starts at $E_{crit} \approx 30$ MeV.

This demonstrates that resonance trapping might be not an exotic phenomena but a rather frequent case in nuclear reactions at reasonably low energies.

¹ Petersburg Nuclear Physics Institute, St. Petersburg, Russia

² Institut für Theoretische Physik, TU Dresden, and Institut für Kern- und Hadronenphysik, FZR

References

- [1] F.M.Dittes, H.Harney, I.Rotter, Phys.Lett. A153(1991)451
- [2] C.Mahaux, H.Weidenmüller, "Shell-Model Approach to Nuclear Reactions", North-Holland, Amsterdam, 1969

Trapping Effect and Optical Model

I. ROTTER¹

In [1] it is claimed that the optical model breaks down at high level density. This statement is in contradiction to the experience, at least in nuclear physics, where the optical model is used quite successfully for a long time for the description of data at high level density. It is necessary therefore to investigate this question once more.

Due to the trapping effect, different time scales are formed at high level density [2]. It holds

$$\sum_{R=1}^K \tilde{\Gamma}_R \gg \sum_{R=K+1}^N \tilde{\Gamma}_R \quad (1)$$

where N is the number of resonance states, K is the number of open decay channels and the first K states are those with the largest widths. This relation is proven numerically as well as analytically for different systems (for references see [3]).

As a consequence of the relation (1), the definition of an "average width" at high level density by $\frac{1}{N} \sum_{R=1}^N \tilde{\Gamma}_R$ is meaningless. According to (1), only

$$\tilde{\Gamma}_{av} = \frac{1}{N-K} \sum_{R=K+1}^N \tilde{\Gamma}_R \quad (2)$$

for the long-lived states has a physical meaning. These $\tilde{\Gamma}_{av}$ are considered in the optical model. Further, an average decay rate in the long-time scale can be defined by

$$k_{av}^{eff} = \frac{\tilde{\Gamma}_{av}}{\hbar} \quad (3)$$

with the average width $\tilde{\Gamma}_{av}$ of the long-lived states given by (2). Due to eq. (1), the k_{av}^{eff} at large times saturate as a function of $\bar{\Gamma} = \frac{1}{N} \sum_{R=1}^N \tilde{\Gamma}_R$. The saturation starts in the critical region of level density where trapping of resonance states gets important.

Such a saturation of the decay rate at high level density is observed also in [1]. In full agreement with the discussion above, it is considered to be caused by the trapping effect. However, the saturation of the decay rates is interpreted by the authors as a "breakdown" of the optical model which takes place at high level density where the resonance states overlap. This conclusion rests on the interpretation of $\bar{\Gamma} = \frac{1}{N} \sum_{R=1}^N \tilde{\Gamma}_R$ as an "average width". As shown above, the value $\bar{\Gamma}$ is, at high level density, quite different from the average width $\tilde{\Gamma}_{av}$, eq. (2), of the long-lived states.

Summarizing the results we state the following: The optical model does *not* break down at high level density due to the trapping effect. It rather finds justification by this effect. Nevertheless, it is difficult to determine the partial widths and widths from the cross section at high level density [3] because it is an interference picture to which many resonances contribute. The average lifetime of the narrow resonances should be determined therefore by direct time measurements.

¹ *Institut für Theoretische Physik, TU Dresden and Institut für Kern- und Hadronenphysik, FZR*

References

- [1] U. Peskin, H. Reisler and W.H. Miller, J. Chem. Phys. 101, 9672 (1994)
- [2] I. Rotter, Rep. Prog. Phys. 54, 635 (1991)
- [3] M. Müller, F.-M. Dittes, W. Iskra and I. Rotter, Phys. Rev. E 52, 5961 (1995)

Shapes and Free Energies of Liquid Sodium Clusters¹

S. FRAUENDORF AND V.V.PASHKEVICH¹

The shell correction method introduced in ref. [1] is used to calculate the free energy and shapes of alkali atom clusters at finite temperature T . The free energy F is obtained as the sum

$$F = F_{LD} + \delta F.$$

Here, F_{LD} is the free energy of a classical drop of liquid Na with the experimental bulk values of the specific free energy and the surface tension. The shell correction δF is calculated from the free energy of the valence electrons in the average potential generated by them and the positive ions. A new method is proposed that permits to calculate very efficiently the *canonical* partition function of N electrons in the potential. It is combined with a new averaging procedure that eliminates the smooth part of the *canonical* free energy of the valence electrons. Equilibrium shapes for $T = 0, 0.04$ and 0.06eV are determined by minimizing $F(T, \alpha, \alpha_\mu)$, $\mu = 3, 4, 5, 6$ simultaneously with respect to the five deformation parameters (α, α_μ) .

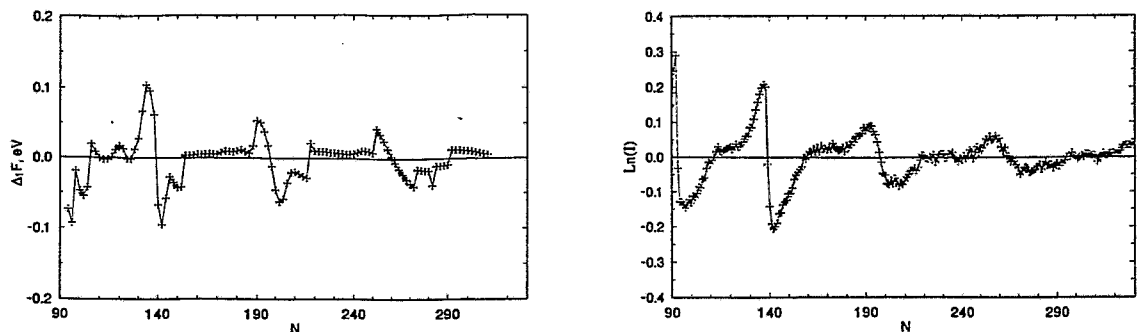


Fig. 1 Differences of the free energies (left panel) and logarithm of the relative experimental intensities (right panel) as determined in ref. [2] for Na clusters in the mass range $90 \leq N \leq 310$. The quantity $\Delta_1 F(N) = (F_{SH}(T, N-2) - F_{SH}(T, N))/2$ is displayed for $T = 0.06 \text{ eV}$.

The shapes of the curves $\Delta_1 F_{SH}(T = 0.06\text{eV}, N)$ and $\ln(I_{rel})$, where I_{rel} are the experimental cluster abundances relative to a smooth background, are remarkably similar. The magic numbers correspond to the intersections of the downsloping parts of $\Delta_1 F_{SH}$ with the zero line. These zeros agree well with the zeros of $\ln(I_{rel})$. The function $\Delta_1 F_{SH}$ has a horizontal section in the middle of each shell, which is a consequence of the deformation. Flat sections in the middle of the shells are clearly visible in the experimental curves $\ln(I_{rel})$. They present evidence for the existence of cluster deformation, which according to the calculation survives at the experimental temperature of about 700 K (0.06 eV).

¹ LTP JINR, Dubna, Russian Federation

References

- [1] S. Frauendorf and V.V.Pashkevich, Surface Review and Letters, in print; Proc. NATO Adv. Study Inst., 6th Course, Erice, Sicily, 1995, Kluvers, in print
- [2] F. Chandezon *et al.*, Phys. Rev. Lett., to be published

Fission of Metal Clusters^E

U. NÄHER¹, S. BJØRNHOLM², S. FRAUENDORF, F. GARCÍAS³ AND C. GUET⁴

Experimental results on the fission of doubly and other multiply charged metal cluster are reviewed and examined in the light of what is known about nuclear fission and alpha emission. A simple model, where the fission barrier is approximated as two charged spheres in near-contact, at a mutual distance given by the balance between Coulomb repulsion and attractive polarization effects, is used for comparison with the experiments. The barriers are estimated for different mass- and charge splits and are compared to the activation energy for the competing evaporation process. From the model as well as in the experiment one finds a strong preference for singly charged trimers (with two electrons) in the "fission" channel, but also fragments with the higher magic electron numbers 8 and 20 may occur with enhanced abundance. In addition there is a pronounced odd-even effect.

In most of the experiments that have been carried out so far fission occurs as the termination of a chain of evaporations of neutral atoms. This limits the observations to a range where the surface energy dominates over the Coulomb energy of the fissioning cluster, explaining the tendency for asymmetric fission and justifying the two-sphere barrier approximation.

Conditions favouring symmetric fission and other fission modes specific to highly charged metal drops are discussed, and experimental approaches are suggested.

The material is to appear as a review article in ref. [1]. Submission is planned for 1996.

¹ Siemens AG, Otto-Hahn-Ring 6, D-81739 München, Germany

² The Niels Bohr Institute, University of Copenhagen, Blegdamsvej 17, DK-2100 Copenhagen Ø, Denmark

³ Departament de Física, Universitat de les Illes Balears, E-07071 Palma de Mallorca, Spain

⁴ Département de Recherche Fondamentale sur la Matière Condensée. Service des Ions, Atomes et Agrégats, CEA, Grenoble, 17 Rue des Martyrs. F-38054 Grenoble Cedex 9, France

References

- [1] Phys. Rep. , to be published

Small Fragment Evaporation from Liquid Alkali Clusters^E

S. FRAUENDORF

The evaporation of mono -, di - and trimers from hot alkali clusters can be considered as a statistical process. The evaporation rate can be estimated using the principle of detailed balance which Weiskopf [1] applied to the evaporation of neutrons from nuclei. The quantities entering the rate expression are the absorption cross section and the ratio of the level densities of the transitional state and the mother cluster.

A new method to calculate the rates has been suggested, which expresses the level density in terms of the cluster entropy, which is the derivative of the free energy of the cluster,

$$F_{LD} = fN + r_S^2 N^{2/3} \sigma S(\alpha, \alpha_\mu), \quad (1)$$

where N is the number of atoms. The first, "volume" term is determined by the specific free energy f . The second, "surface" term is the product of the surface tension σ and the surface area. The function $S(\alpha, \alpha_\mu)$ is the area of the surface enclosing the unit sphere, which depends on the deformation parameters $\alpha, \alpha_3, \alpha_4, \dots$. The parameters f, r_S, σ are taken as the bulk values, which are well known as functions of the temperature. By extrapolating from the bulk down to clusters as small as 20 atoms, one does not need a model for the motion of the metal ions, which are still in a very crude stage. By means of the Shell Correction Method [2] one may easily include the shell structure of the valence electrons into the expression for F .

Eq. (1) has been used to calculate the rates for evaporation of monomers [3]. In this case the transition state simply corresponds to a separated atom and the inverse cross section is the geometric one. Differences of several orders of magnitude have been found in comparison with previous calculations using oscillator estimates of the level density. Such models give a specific heat of 3, which is significantly below the experimental values for liquid metals.

For dimer evaporation the level density due to the excitation of the molecule must be taken into account. The rotation contributes significantly to the free energy and the vibrational contribution is non negligible. The molecular free energy can accurately be obtained from the measured free energies of the alkali gases. The combination of the rate expressions for the mono- and dimers permits to reanalyze the experiments of LASER induced evaporation. Such an investigation is planned in the framework of the EC network on Large Metal Clusters.

The evaporation of trimer ions from multiply charged clusters is complicated by the fact that the transition state is on the top of the Coulomb barrier. Thus, this process is analog to the α particle emission from nuclei. However, the barrier is much lower because of the mutual charge polarization of the cluster and the trimer. A model has been suggested that combines the image charge method of electrostatics with a standard quantum chemical model for the potential between molecules, which permits to take into account the increased dipole polarizability of small clusters. Interpretation of experiments of the monomer - trimer evaporation competition are planned.

References

- [1] V. Weiskopf, Phys. Rev. **52**, 295 (1937)
- [2] S. Frauendorf, V. V. Pashkevich, this annual report
- [3] S. Frauendorf, Z. Phys. **D 35**, 191 (1995)

A New Optimization Technique for Complex Systems

F.-M. DITTES

The description of complex systems with many competing requirements generically leads to multi-peaked or “rugged” functions: the energy, cost or fitness landscape (over the space of all possible configurations of the system) is characterized by a complicated structure with many local optima. In a physical context typical examples are the energy functions of many-body systems with a high amount of frustration: glasses, antiferromagnetics and many random systems. In a broader setting rugged landscapes describe, e. g., the fitness of biological individuals (as a function of the pheno- or genotype), the “payoff” of economical or social actions (as a function of the sequence of possible decisions) or the cost or time required to achieve a certain aim.

On the formal level, multi-peaked functions arise in any many-parametric problem, e. g., in the fitting of experimental data within a certain class of trial functions or in the determination of ground state energies within a variational ansatz. Finding the global optimum of such functions is a highly non-trivial problem since fulfilling one requirement often leads to an increase in the mismatch of others. In the notion of energy or fitness landscapes such situations correspond to local optima, i. e., to situations from which no way out by changing a single degree of freedom is possible.

Various strategies have been proposed to tackle this problem, adopting ideas from different areas of science. Most prominent examples are simulated annealing (based on the thermodynamically motivated Metropolis algorithm) and evolutionary or genetic algorithms imitating adaptive processes in biological systems.

In the present work an alternative approach is proposed based on the assumption that an optimal (or near-optimal) solution to complex problems can be found by an interplay of *individual* interests, synchronized by group and system regulations. In order to implement this assumption into a Monte Carlo optimization algorithm, the function to be optimized – e. g., the many-body energy functional – has to be represented as a sum of single-particle terms (“dressed” by interaction contributions), and a *simultaneous* optimization of these single-particle energy functions has to be performed.

The proposed algorithm has been tested on different examples of the spin glass type and on travelling salesman problems with up to 1000 discrete variables [1] as well as on problems with 50 – 100 continuous degrees of freedom. Even without adjusting it to the details of the specific problem, it turns out to work in an efficient and robust way, often performing better than previously used techniques – especially for hard problems with an extremely rugged landscape structure.

References

- [1] F.-M. Dittes, Preprint FZR-92, October 1995

Shears bands in ^{201}Pb and ^{202}Pb
(Nucl. Phys. A 592 (1995) 365)

Baldsiefen, G., P. Maagh, H. Hübel, W. Korten, S. Chmel, M. Neffgen, W. Pohler, H. Grawe, K.H. Maier, K. Spohr, R. Schubart, S. Frauendorf, H.J. Maier

Abstract: High-spin states in ^{201}Pb and ^{202}Pb have been investigated using in-beam γ -ray spectroscopic techniques. Seven regular sequences of enhanced dipole transitions, with weak E2 crossovers in some cases, have been found, one of which is firmly connected to low-lying levels in ^{201}Pb . These bands are interpreted to be built on high-spin proton-particle neutron-hole excitations. Tilted-axis cranking calculations show that the angular momentum along the bands is predominantly generated by a continuous and simultaneous reorientation of the proton and neutron spins into the direction of the total angular momentum (shears effect)

Low-spin termination of the superdeformed band in ^{135}Nd
(Phys. Rev. C 52 (1995) R2302)

Deleplanque, M.A., S. Frauendorf, R.M. Clark, R.M. Diamond, F.S. Stephens, J.A. Becker, M.J. Brinkman, B. Cederwall, P. Fallon, L.P. Farris, E.A. Henry, H. Hubel, J.R. Hughes, W. Korten, I.Y. Lee, A.O. Macchiavelli, M.A. Stoyer, P. Willsau, J.E. Draper, C. Duyar, E. Rubel

Abstract: The decay of the superdeformed (SD) band in ^{135}Nd was studied with the early implementation of gamma-sphere. The results suggest that the SD band "terminates" at spin 25/2. This termination is explained by a change of the SD minimum toward a triaxial lower deformation. Ultimate cranked calculations with the $i_{13/2}$ orbital occupied relate this change to a shift of a proton and neutron pair out of deformation-driving Nilsson orbitals. This is a completely new and unexpected mechanism for the decay of SD bands.

Tilted four-quasiparticle bands in even-even Xe- and Ba- nuclei
(Nucl. Phys. A 584 (1995) 241)

Döna, F., S. Frauendorf, O. Vogel, A. Gelberg, P. von Brentano

Abstract: Rotational band structures with distinct properties found in several even-even Xe and Ba nuclei are investigated by means of the conventional cranked shell model and by the newly developed tilted axis cranking model. Analyzing the band energies and electromagnetic branching ratios a nearly oblate configuration ($\pi h_{11/2} d_{5/2}$)($\nu h^2_{11/2}$) with a tilted i.e. non-principal axis spin orientation is found to give a fair description of the experimental features.

Evaporation rates for liquid clusters
(Z. Phys. D 35 (1995) 191)

Frauendorf, S.

Abstract: An expression for the evaporation rate of neutral atoms from a hot liquid cluster is suggested. It combines Weisskopf's statistical model with a level density that is derived from the experimentally known free energy of a macroscopic droplet of the cluster material. For the case of sodium clusters, it is compared with the rate based on the level density of a system of oscillators. For the same internal energy the latter gives substantially larger evaporation rates, whereas for equal temperature the increase is moderate. For large clusters the electronic contribution to the entropy can no longer be neglected.

Collective effects and multifragmentation in heavy-ion collisions at intermediate energies within a hybrid model
(Nucl. Phys. A 588 (1995) 918)

Heide, B., H.W. Barz

Abstract: Central and semi-central Au + Au collisions at 150 and 250 A MeV are investigated in the framework of a hybrid model with dynamical and statistical components. Starting from the BUU approach an ansatz for the Wigner function is made which describes thermal and collective motion of the nucleons and models the transition from the one-source to the two-source behavior. Anisotropic flow energies and temperatures as well as angular momenta are extracted. Nucleonic flow and pre-equilibrium emission reduce considerably the excitation energy of the matter. The cluster formation is described by the Copenhagen multifragmentation model. Charge spectra, energy spectra and two-particle correlations of the fragments are reproduced. Agreement with experiment can be improved by assuming a reduced transverse flow.

Radial pattern of nuclear decay processes
(Phys. Rev.C 51 (1995) 1842)

Iskra, W., M. Müller, I. Rotter

Abstract: At high level density of nuclear states, a separation of different time scales is observed (trapping effect). We calculate the radial profile of partial widths in the framework of the continuum shell model for some 1^- resonances with $2p-2h$ nuclear structure in ^{16}O as a function of the coupling strength to the continuum. A correlation between the lifetime of a nuclear state and the radial profile of the corresponding decay process is observed. We conclude from our numerical results that the trapping effect creates structures in space and time characterized by a small radial extension and a short lifetime.

Dilepton production a chemically equilibrating, expanding and hadronizing quark-gluon plasma

(Phys. Rev. C 52 (1995) 2704)

Kämpfer, B., O.P. Pavlenko, A. Peshier, G. Soff

Abstract: Dilepton production is considered within a complete dynamical framework for thermalized matter assumed to be formed in ultrarelativistic heavy-ion collisions. Our model includes (i) chemical equilibration processes in the initially gluon enriched plasma, (ii) longitudinal as well as transverse expansion, and (iii) the hadronization through a mixed phase. Besides the basic electromagnetic quark-antiquark annihilation process we also take into account the QCD Compton-like and annihilation processes for calculating the dilepton rate in the deconfined phase, while in the hadronic stage we employ a parametrization of the effective form factor which is based on the complete set of meson decays and reactions. We find that, due to the transverse expansion of the matter, the dilepton yield from the hadron gas is strongly reduced and, therefore, the deconfined matter gives the dominant contribution in case of initial conditions which are expected to be achieved at RHIC. This provides the basis for the M_{\perp} scaling restoration of the dilepton spectra from thermalized matter.

Rapidity dependence of thermal dileptons resulting from hadronizing quark-gluon matter with finite baryon charge

(Z. Phys. A 353 (1995) 71)

Kämpfer, B., O.P. Pavlenko, M.I. Gorenstein, A. Peshier, G. Soff

Abstract: The influence of a non-vanishing baryon charge on the rapidity distribution of dileptons produced in ultra-relativistic heavy-ion collisions is studied. We employ a frozen motion model with scaling invariant expansion of the hadronizing quark-gluon plasma as well as a realistic rapidity distribution of secondary particles (i.e., pions and baryons) expected for RHIC energies. We demonstrate a sizeable suppression of the thermal dilepton yield at large rapidities due to the finite baryon density. This affects the most favorable rapidity window for using dileptons for the diagnostic of the quark-gluon plasma and the early temperature distribution of the hot reaction zone. To discriminate the thermal dileptons from Drell-Yan background we propose to utilize the dilepton yield scaled suitably by the pion multiplicity as function of rapidity.

The tensor analyzing power T_{20} in deuteron break-up reactions within the Bethe-Salpeter formalism

(Phys. Lett. B 351 (1995) 400)

Kaptari, L.P., A.Yu. Umnikov, F.C. Khanna, B. Kämpfer

Abstract: The tensor analyzing power T_{20} and the polarization transfer κ in the deuteron break-up reaction $Dp \rightarrow pX$ are calculated within a relativistic approach based on the Bethe-Salpeter equation with a realistic meson-exchange potential. Our results on T_{20} , κ and the cross section are compared with experimental data and non-relativistic calculations and with the outcome of a relativization procedure of the deuteron wave function.

Kaon polarization in nuclear matter
(Nucl. Phys. A 588 (1995) 889)

Kolomeitsev, E.E., D.N. Voskresensky, B. Kämpfer

Abstract: The kaon-nucleon interaction in nuclear matter is considered by taking into account tree graphs, p-wave interaction, pionic intermediate states, kaon fluctuations and some residual interaction. The latter one is constrained by Adler's consistency condition. K^- , K^+ , K^0 , \bar{K}^0 polarization operators are calculated in cold nuclear matter with arbitrary isotopic composition. An extra s-wave repulsion is found, which probably shifts the critical point of a K^- condensation with vanishing kaon momentum to large nucleon densities. Oppositely, an extra p-wave attraction is obtained, which may lead to a K^- condensation at vanishing temperatures and densities $p \geq p_c \sim (4-6)p_0$. The spectrum of the kaonic excitations in nuclear matter is analyzed and a new low-lying branch in the K^- (and also \bar{K}^0) spectrum is found. Its presence may lead to interesting observable consequences, such as the enhancement of the K^- yields in heavy-ion reactions. At $p \geq p_c$ the frequency of this low-lying branch becomes negative at non-vanishing momentum; that signals the onset of a new type inhomogeneous K^- condensation. The K^- condensate energy is calculated in the approximation of a small KK coupling constant. Accordingly, neutron star matter may undergo a first-order phase transition to proton matter with K^- condensate at $p > p_c$ due to p-wave interaction. The temperature dependence of the most important terms of the K^- polarization operator is discussed. In a rather wide temperature region $0 < T < 1/2m_\pi$ a growing temperature enlarges the $K^- N$ attraction and promotes the kaon condensation. The possibility of p-wave \bar{K}^0 condensation is also considered. The question is qualitatively discussed whether proton matter with K^- condensate or neutron matter with \bar{K}^0 condensate is energetically more favorable.

"Shears bands" in Pb nuclei - a new nuclear structure effect
(Physica Scripta T56 (1995) 44)

Korten, W., G. Baldsiefen, M. Neffgen, H. Hübel, S. Chmel, W. Pohler, U.J. van Severen, P. Willsau, S. Frauendorf, J. Meng, H. Grawe, J. Heese, H. Kluge, K.H. Maier, R. Schubart, K. Spohr:

Abstract: In nuclei in the mass region around $A = 190-200$ a large number of regular dipole sequences have recently been found. In these bands the gain in angular momentum may not be created by collective rotation as is usual for more deformed nuclei, but stems from aligning the proton and neutron spins in the direction of the total spin axis. Calculations within the framework of the tilted axis cranking model reproduce the available experimental data and support the alignment picture.

Study of high-spin states in $^{181,182}\text{Os}$
(Nucl. Phys. A 587 (1995) 111)

Kutsarova, T., R.M. Lieder, H. Schnare, G. Hebbinghaus, D. Balabanski, W. Gast, A. Krämer-Flecken, M.A. Bentley, P. Fallon, D. Howe, A.R. Mokhtar, J.F. Sharpey-Schafer, P. Walker, P. Chowdhury, B. Fabricius, G. Sletten, S. Frauendorf

Abstract: High-spin states in the nuclei $^{181,182}\text{Os}$ have been populated in the $^{150}\text{Nd}(^{36}\text{S},\text{xn})$ reaction and studied with the ESSA30 array. The nucleus ^{181}Os has also been studied at the NBI tandem accelerator using the $^{167}\text{Er}(^{18}\text{O},4\text{n})$ reaction. The previously known bands in both nuclei have been extended to higher spins and two new side bands have been found in ^{181}Os . In the latter nucleus the ground state has been established to have $I^\pi = 1/2^-$. The extraction of the ratios of reduced transition probabilities $B(\text{M1})/B(\text{E2})$ from branching and E2/M1 mixing ratios permitted configuration assignments for most of the bands in both nuclei. The analysis has been carried out within the semiclassical vector model for M1 radiation. The positive-parity yrare sequences in ^{182}Os and the band based on the $I^\pi = K^\pi = 23/2^-$ state in ^{181}Os have been interpreted as t-bands arising from a rotation about a tilted axis. The alignment behaviour and the crossing frequencies are for most of the bands consistent with predictions of the cranked shell model.

Level repulsion in the complex plane
(Phys. Rev. E 52 (1995) 5961)

Müller, M., F.-M. Dittes, W. Iskra, I. Rotter

Abstract: We consider the spectral properties of a model quantum system describing the coupling of bound states to a number of decay channels. We describe the separation of a few modes from the set of all resonances during the transition from low to high coupling strength between bound and continuum states (*trapping effect*) leading at high coupling to the formation of two time scales in terms of the life times of the resonance states. In particular, we give a detailed analysis of the critical region where the system finds its new resonance structure. Eigenvalues, eigenfunctions and their degree of mixing in relation to the corresponding wavefunctions of the closed system as well as cross sections are studied analytically and numerically for the cases of two and four resonances. For a multi-resonance case the dependence of these quantities on the spectrum of the underlying closed system is studied. We find that the global reorganization of the spectrum in the high coupling regime can be traced back to local redistributions acting on an energy scale comparable to the widths of the interfering resonances.

Triaxial shapes of sodium clusters
(Z. Phys. D 34 (1995) 125)

Reimann, S.M., S. Frauendorf, M. Brack

Abstract: A modified Nilsson-Clemenger model is combined with Strutinsky's shell correction method. For spherical clusters, the model potential is fitted to the single-particle spectra obtained from selfconsistent Kohn-Sham calculations. The deformation energy surfaces of sodium clusters with sizes of up to $N = 270$ atoms are calculated for a combination of triaxial, quadrupole and hexadecapole deformations. The ground state shapes and energies are determined by simultaneous minimization with respect to the three shape parameters. A significant fraction of the clusters is predicted to be triaxial. The deviations from the axial shape do not generate any systematic odd-even staggering of the binding energies.

Resonance phenomena at high level density
(J. Phys. A 28 (1995) 2963)

Sobeslavsky, E., F.-M. Dittes and I. Rotter

Abstract: We investigate the behaviour of resonances as a function of the coupling strength between bound and unbound states on the basis of a simple S -matrix model. Resonance energies and widths are calculated for well isolated, overlapping and strongly overlapping resonance states. The formation of shorter and longer time scales (trapping effect) is traced. We illustrate that the cross section results from an interference of all resonance states in spite of the fact that their lifetimes may be very different.

Dielectron production in proton-proton and proton-deuteron collisions at 1-2 GeV
(Phys. Rev. C51 (1995) 227)

Titov, A.I., B. Kämpfer and E.L. Bratkovskaya

Abstract: Estimates of elementary cross sections for dielectron production in pN and pd reactions are presented. Throughout, we use the vector dominance model for all hadron-hadron-photon vertices. The Δ , η Dalitz decays and bremsstrahlung appear as dominant sources of dielectrons. We show that the recently observed strong enhancement of 2 of the ratio of dielectron production from pd to pp collision at low energy $E \sim 1.0$ - 1.3 GeV may be understood by a different threshold behaviour of eta production in proton-proton and proton-neutron collisions. Relying on a realistic deuteron wave function we estimate the energy dependence of the ratio and find qualitative agreement with new experimental results.

2 Experimental Medium Energy Physics

An Application of Kinematic Fitting^{B,K}

A. SCHÜLKE, H. FREIESLEBEN¹ AND K. MÖLLER²

At the COSY-TOF spectrometer [1] the scattering angles and the time-of-flight of charged particles are measured. In spring 1994 a first TOF-experiment has been carried out [2] using a 455-MeV proton beam impinging on a liquid-hydrogen target. For the extraction of three-body reactions ($pp\pi^0$, $pn\pi^+$) the complete reconstruction of the velocity vectors and a hypothesis for the particle masses are necessary to uniquely determine the nature of the neutral particle, i.e. the four-momentum-vectors of the measured particles are inferred from a certain particle-hypothesis. The missing mass analysis has shown that the $pn\pi^+$ -reaction can clearly be extracted. In order to separate the reaction channels, $p\pi^+n$ or π^+pn , the method of kinematic fitting [3] is utilized. The momentum components, the variables to be fitted, are modified according to their error range such that the new values fulfill the reaction hypothesis best. Energy and momentum conservation are the kinematical constraints. The method consists in a least squares fitting procedure which incorporates constraints among the variables by the use of Lagrangian multipliers. In the case where the errors of the measured values are correlated one can construct the quantity

$$S = (\vec{\varrho} - \vec{\varrho}_0)^T \cdot \hat{G}^{-1} \cdot (\vec{\varrho} - \vec{\varrho}_0) + 2 \cdot \vec{\Lambda}^T \cdot \vec{f}(\vec{\varrho}, \vec{\xi}),$$

where $\vec{\varrho}$ is the vector of measured values, $\vec{\xi}$ that of unmeasured ones, \hat{G}^{-1} is the inverse matrix of correlated errors. One has to find S_{min} by varying the components of $\vec{\varrho}$. To solve this problem the constraints $\vec{f}(\vec{\varrho}, \vec{\xi})$, which connect the components of $\vec{\varrho}$ and $\vec{\xi}$, are linearized. The vector $\vec{\Lambda}$ contains the Lagrangian multipliers. All possible configurations of momentum vectors of the outgoing particles are considered. Then, from this infinite number of possible sets, the one closest to the observed set (in the least square sense) is chosen. A detailed derivation of the fitting procedure and its application for the TOF spectrometer data can be found in [4].

Here χ_{norm}^2 is calculated as

$$\chi_{norm}^2 = \frac{1}{n-1} (\vec{\varrho} - \vec{\varrho}_0)^T \cdot \hat{G}^{-1} \cdot (\vec{\varrho} - \vec{\varrho}_0),$$

where n is the number of degrees of freedom of the fit and χ_{norm}^2 is determined for both hypotheses. In fig. 1 the χ_{norm}^2 -distributions versus the reconstructed mass of the unmeasured particle are shown.

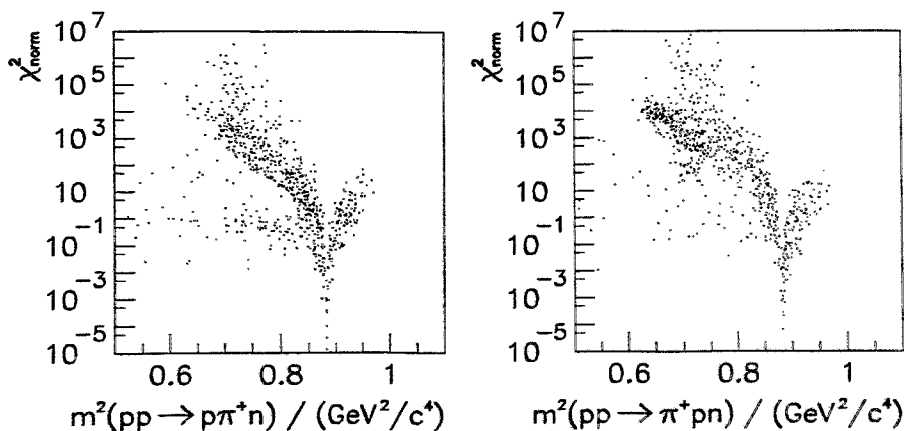


Fig. 1 χ_{norm}^2 -distribution versus missing mass for the hypothesis $pp \rightarrow p\pi^+n$ (left) and $pp \rightarrow \pi^+pn$ (right)

In case of a correct hypothesis the value of χ_{norm}^2 is in the range $\chi_{norm}^2 \leq 1$. This normalized condition is the criterion for the assignment of a certain reaction to a given event.

Fig. 2 represents the reconstructed missing mass spectra without cut (left) and with a cut on $\chi_{norm}^2 \leq 1$ (right) in the chosen reaction channel $pp \rightarrow p\pi^+n$. The calculation shows that about 95% of events are unambiguously assigned if a cut on $\chi_{norm}^2 \leq 0.1$ is applied.

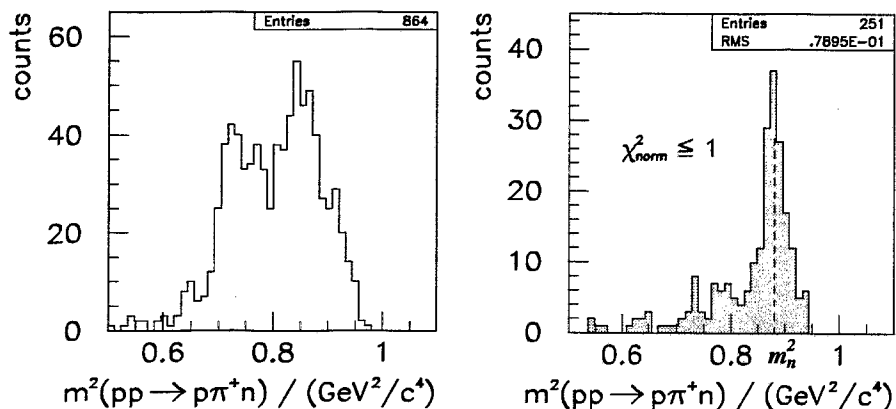


Fig. 2 Missing mass spectrum for the hypothesis $pp \rightarrow p\pi^+n$ without (left) and with cut (right) on $\chi_{norm}^2 \leq 1$

¹ Institut für Kern- und Teilchenphysik, TU Dresden

² Institut für Kern- und Teilchenphysik, TU Dresden and Institut für Kern- und Hadronenphysik, FZR

References

- [1] COSY proposal #9, 1990
- [2] A. Schülke et al., Annual Report 1994, KFA Jülich, Jül-3035 (1995) 13
- [3] L. Lyons, *Statistics for nuclear and particle physicists*, Cambridge 1989
- [4] A. Schülke, doctoral thesis, FZR-120 (1995)

Measurement on a Prototype Scintillator Module to be used in the COSY-TOF Barrel Hodoscope^B

P. MICHEL, K. MÖLLER¹, A. SCHAMLOTT AND A. SCHÜLKE
FOR THE COSY-TOF COLLABORATION

Recently a test facility was developed [1, 2] to investigate the possibility of building the COSY-TOF barrel hodoscope on the basis of an one-layer scintillator configuration with two-sided PM read-out. In the present paper a short account is given on results of measurements performed with the help of this test facility. Details on the measuring procedure are described in Ref. [2].

In a first step of the test program the efficiency of scintillator-light guide coupling was investigated for different coupling configurations. Resulting attenuation lengths and light output are shown in Fig. 1. Here, as expected, the light output increases with the quality of the coupling being improved. As concerns the attenuation length so it is not a mere intrinsic property of the scintillator bar but is strongly influenced by the coupling to the PM as well.

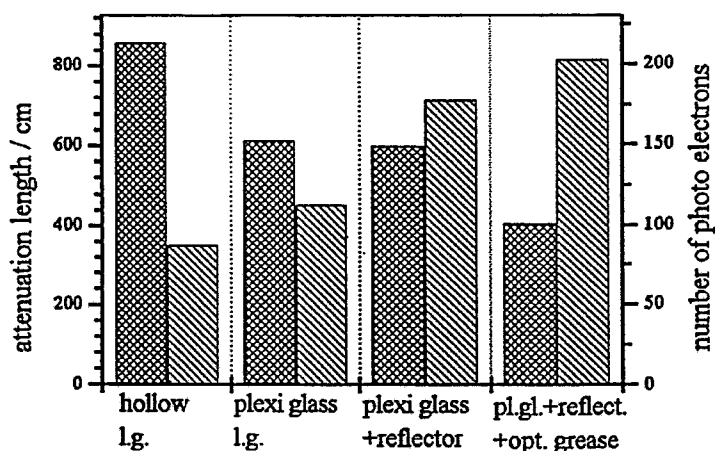


Fig. 1 Attenuation lengths and light output for four different light guide systems

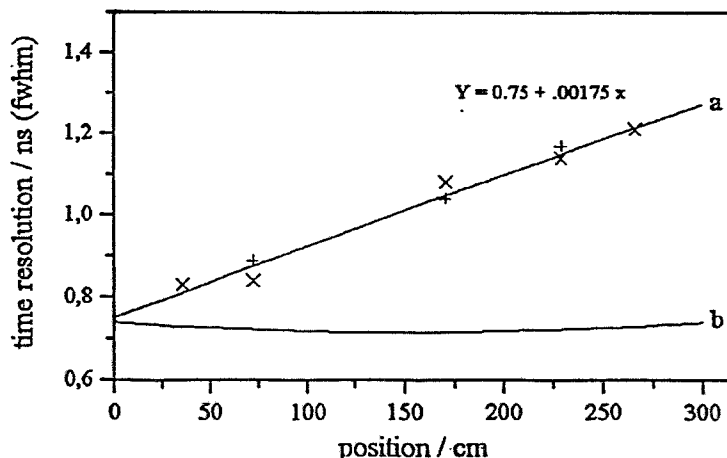


Fig. 2 Time resolution of the prototype scintillator module (NE110A)

A remarkable feature of the results shown in Fig.1 is the fact that the attenuation length decreases with the light output increasing. This seemingly contradictory result can be explained by the fact that the different coupling conditions act as different "angular filters" with respect to the angular spectrum of the photons emerging from the scintillator bar. In a next step of the measuring program the time resolution of the prototype scintillator module was determined for the best coupling configuration case (right-most column in Fig. 1).

In Fig. 2 (line a) the resulting time resolution is presented for light read-out at the left end (s.Fig. 1 in Ref.[2]) of the scintillator bar. By symmetry arguments the same situation is observed at the other end of the scintillator bar (not directly measured in the present case). The relevant time of flight information T for two-sided scintillator read out is obtained by $T = (T_l + T_r)/2 - L/2v_D$, where T_l and T_r denote the time of flight values measured at the left and the right side respectively of the scintillator bar with respect to a common time reference unit (start detector or master scintillator in the present case). The quantities L and v_D describe the length of the scintillator bar and the drift velocity respectively.

The time-of-flight resolution σ_T for two-sided read out is given by $\sigma_T^2 = (1/4) (\sigma_{T_l}^2 + \sigma_{T_r}^2)$. The value σ_T (multiplied by 2.35) is plotted in Fig. 2, line b. It should be noticed that $\sigma_T < \sigma_{T_l}, \sigma_{T_r}$ and that the time-of-flight resolution is nearly position independent. Another important property to be measured is the spatial resolution of the prototype

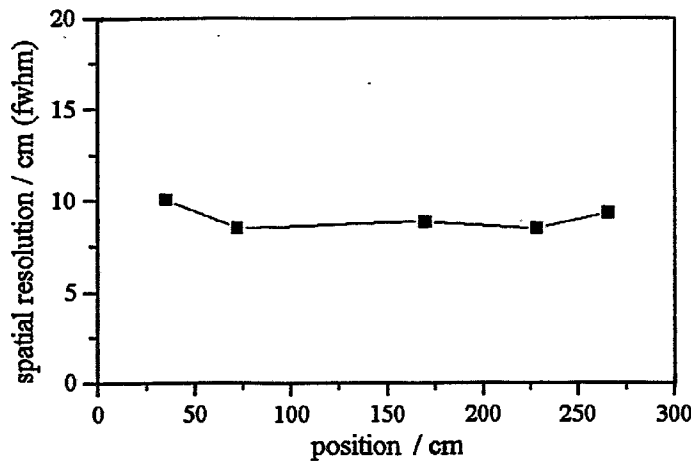


Fig. 3 Spatial resolution of the tested scintillator module

scintillator module. The point x of particle impact is determined by measuring photon drift time differences at both ends of the scintillator bar. Then the position x is given by $x = L/2 - (v_D/2) \cdot (T_r - T_l)$ and the position resolution σ_x by $\sigma_x^2 = (v_D/2)^2 (\sigma_{T_l}^2 + \sigma_{T_r}^2)$. The measured spatial resolution is shown in Fig. 3.

¹ Institut für Kern- und Teilchenphysik, TU Dresden and Institut für Kern- und Hadronenphysik, FZR

References

- [1] P. Michel et al., Annual Report 1994, KFA Jülich, Jül-3035 (1995) 11
- [2] P. Michel et al., this Annual Report

Investigations of the Radiation Background in the Detector Laboratory^B

P. MICHEL, K. MÖLLER¹, A. SCHAMLOTT AND W. SCHULZE
FOR THE COSY-TOF COLLABORATION

Cosmic rays were used for the investigation of the 2-sided read-out of long scintillator strips for the COSY-TOF spectrometer [1]. The background load of the strip was tested to prove that the background counting rate measured with the strip may be understood as γ -radiation from the environment.

The single rate of cosmic myons amounts to 40 s^{-1} for a scintillator strip of $300 \times 10 \times 1.5 \text{ cm}^3$. On the other hand a single rate of 600 s^{-1} was measured with a discriminator threshold of approximately 6 % of the minimum ionizing particle peak. This counting rate can not be interpreted by the cosmic rays. It is caused by the natural radiation background.

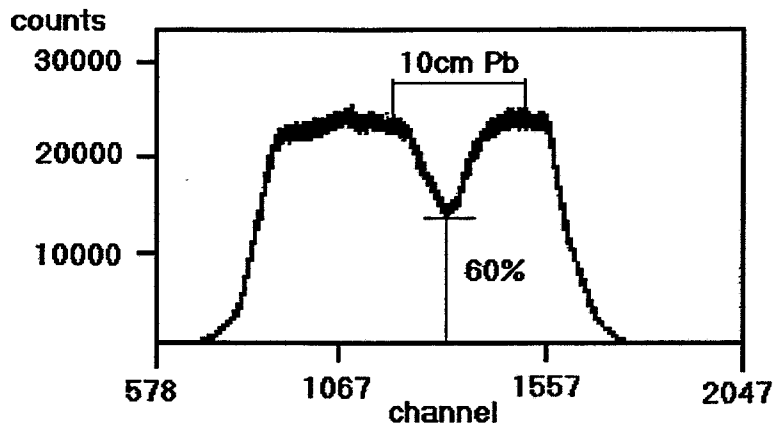


Fig. 1 TDC-spectrum of the long scintillator strip with the effect of 10 cm Pb-plates

For a more detailed analysis of the radiation background a region in the middle of the scintillator strip with a length of about 20 cm was covered with 10 cm thick bricks of lead. The effect of shielding is clearly perceptible (Fig. 1). The background intensity however is reduced to only 60 %.

Several reasons exist for this result [2]:

- incomplete shielding of external γ -radiation (gaps, thickness of shielding)
- contamination of the scintillator and shielding material
- ^{222}Rn and its daughters, included in the shielding material
- cosmic myons
- activity induced by cosmic rays in the scintillator and shielding material, for instance ($n, n'\gamma$) reactions on Pb

A better suppression of the γ -background is not primarily obtaining by an increasing thickness of the lead shielding, but contrary by the selection of low radiation level kinds of lead and combinations of different materials (for instance a copper layer inside the lead shielding) [3].

With the help of a Ge-detector GMX 10180-P and the spectrum analyzer CICERO the radiation background of the detector laboratory was investigated. The measured

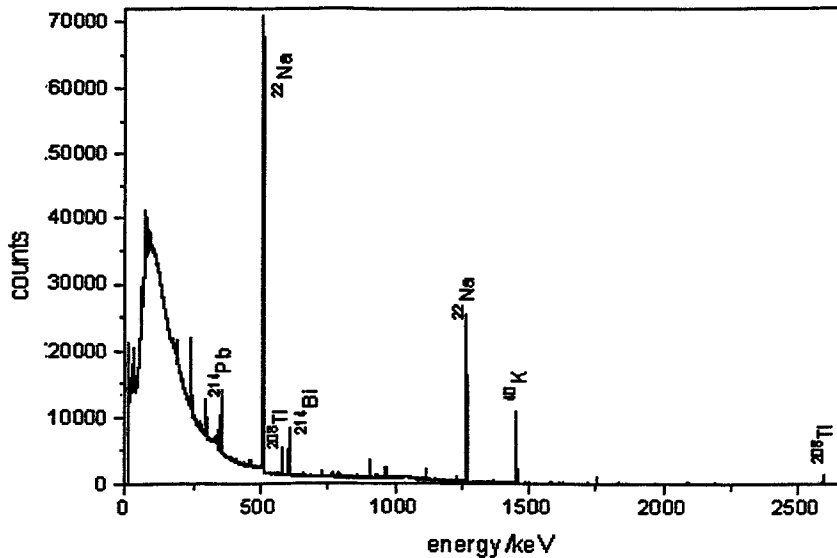


Fig. 2 γ -background-spectrum(detector laboratory), measuring time 10^5 sec

γ -spectrum is shown in Fig. 2. Besides peaks due to ^{214}Pb (351.91 keV), ^{208}Tl (583.19 keV, 2614.53 keV) and ^{40}K (1460.75 keV) two pronounced ^{22}Na lines are observed. These lines originate from a neighbouring experiment using a ^{22}Na -source with an activity of 5 MBq. The presence of the ^{22}Na -source leads to an increase in the single rate on the scintillator strip by 200 s^{-1} .

The volume of the Ge-detector amounts to 100 cm^3 and the γ -efficiency is about 20 %. The spectrum yields a counting rate of 200 s^{-1} in an energy range from 5 keV to 2700 keV. At the same γ -efficiency the counting rate of the scintillator strip ($V = 4500\text{ cm}^3$) would be $1 \times 10^4\text{ s}^{-1}$.

This counting rate corresponds to a counting rate of 2500 s^{-1} at an assumed γ -efficiency of the scintillator material of 5 %. This value is greater than the measured counting rate of the strip by a factor of nearly three. An exact quantitative correspondence was not expected because of the different thresholds of the two measuring arrangements.

A possibility of reducing the high single rate of the scintillator strip consists in a detector arrangement with two scintillator strips placed one above the other. Forming the coincidence from the signals of the left side of one strip and the right side from the other one a counting rate of 60 s^{-1} results. This rate is comparable with the amount of the primary component of cosmic myons. With this arrangement a very good suppression of the background is obtained with the drawback that, however, the energy threshold of the detector is increased.

¹ *Institut für Kern- und Teilchenphysik, TU Dresden and Institut für Kern- und Hadronenphysik, FZR*

References

- [1] P. Michel et al., this Annual Report
- [2] G. Heusser, Nucl. Instr. and Meth. in Physics Research **B17** (1986) 418
- [3] J. Verplancke, Nucl. Instr. and Meth. in Physics Research **A312** (1992) 174

Beam Profile and Phase Space Measurements of the Beam extracted from COSY^B

A. HASSAN¹, P. JAHN², R. MAIER², B. NAUMANN, D. PRASUHN², M. ROGGE² AND R. TÖLLE²

The method of phase space measurement by imaging with a quadrupole is now well established at COSY. In the first section of the COSY extraction beamline [1] it allows to measure the beam intensity distribution. The results of the measurements at three different beam momenta p during the last run at the COSY-TOF-Spectrometer are given in Fig. 1.

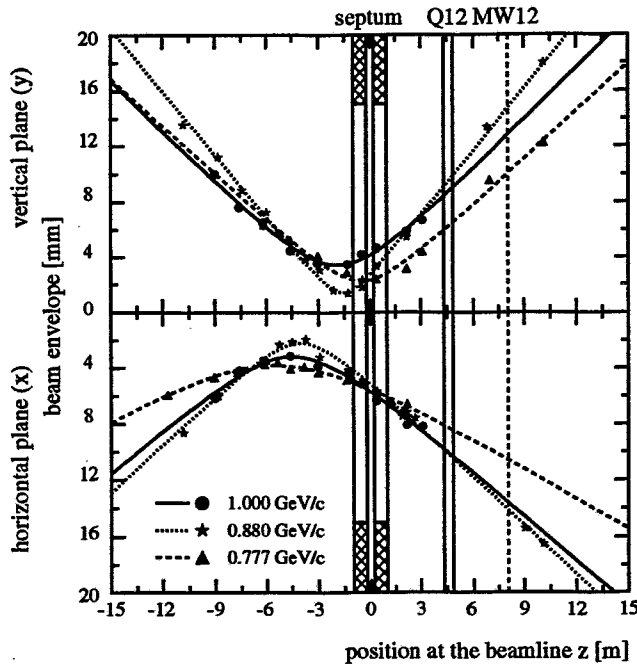


Fig. 1 Beam envelope of the beam extracted from COSY at 1.000, 0.880 and 0.777 GeV/c. Magnetic septum, quadrupole Q12 and the Multi Wire Chamber MW12 are indicated.

From these curves four parameters are derived for both planes (Tab. 1), as are i) the position of the minimum beam extension z_{waist} , ii) the beam radii x_{waist} , y_{waist} , iii) the extension of the beam in the angle coordinate x'_{waist} , y'_{waist} and iii) the emittances $\epsilon_x = \pi \cdot x_{\text{waist}} \cdot x'_{\text{waist}}$ and ϵ_y [1].

Table 1 Results of phase space measurements

p	horizontal plane x				vertical plane y			
	z_{waist}	x_{waist}	x'_{waist}	ϵ_x	z_{waist}	y_{waist}	y'_{waist}	ϵ_y
[GeV/c]	[m]	[mm]	[mrad]	$[\pi \cdot \text{mm} \cdot \text{mrad}]$	[m]	[mm]	[mrad]	$[\pi \cdot \text{mm} \cdot \text{mrad}]$
1.000	-4.48	3.16	1.06	3.43	-1.86	3.43	1.24	4.26
0.880	-4.01	2.22	1.16	2.57	-1.56	1.39	1.52	2.12
0.777	-5.49	3.80	0.73	2.77	-0.45	2.27	1.15	2.60

The values for x'_{waist} and y'_{waist} can be measured directly by adjusting the focal plane of the quadrupole lens to the MW12. This agrees with the data from Fig. 1 to within 10%.

These values reflect a considerable improvement in COSY beam quality during the last year. Now the phase space of the uncooled external COSY beam approaches the values, which can be transported through the beam line to the experimental areas. All results are obtained in the thin lens approximation. Two corrections, each of them in the order of a few percent in the quadrupole currents I have been introduced :

- i) the calculations have been adapted to thick lenses and
- ii) saturation effects in the quadrupoles are included.

According to field measurements for the quadrupoles used, the saturation can be described by

$$B[\text{kG}] = 0.03775 \cdot I \cdot (1 - 0.2 \cdot 10^{-6} \cdot I^2 + 0.1 \cdot 10^{-11} \cdot I^4 + 1.94 \cdot 10^{-15} \cdot I^6),$$

where the current I is measured in Ampere.

Some technical changes in the first part of the extraction beam line have been performed and additional calibration data have been gathered. The steerer SH10 is replaced by a stronger one with a calibration constant of 0.677 mrad/A for $p = 1 \text{ GeV}/c$. The electrostatic septum has a calculated calibration constant of 8.5 mrad/kV for an electrode gap of 17 mm. The effect on the position of the beam at the entrance of the electrostatic septum was measured to be $dx/dU = 0.304 \text{ mm}/\text{kV}$ and is somewhat dependent on the working conditions of COSY. An error in a commercial program for evaluation of the half width of the beam profile (a factor 1.4) was found. All values given here are corrected values.

The imaging method is applicable to measure the intensity distribution at some points of interest along the beam line. As an example the beam position and intensity distribution at the entrance aperture of the magnetic septum is shown in Fig. 2.

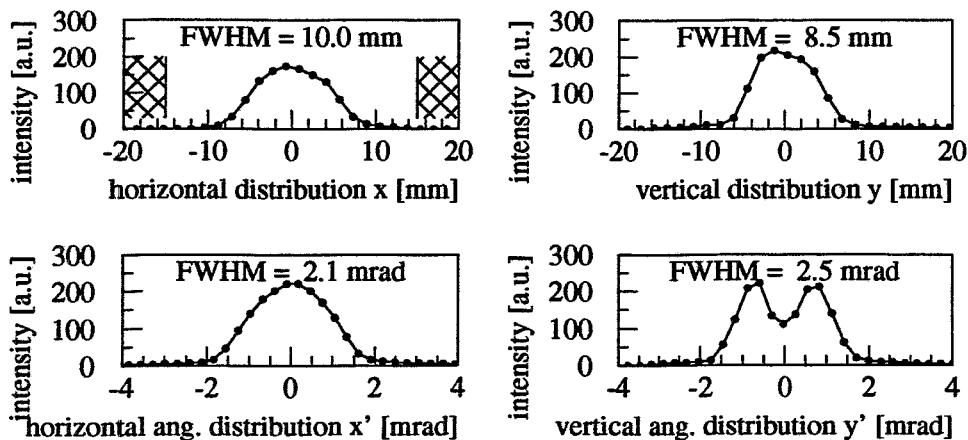


Fig. 2 Intensity distribution of the beam extracted from COSY at the entrance of the magnetic septum. The limits of the aperture were determined by changing the voltage on the electrostatic septum until the beam profile is partially cut by the aperture. Upper part: spatial distribution at 1.0 GeV/c; lower part: angular distribution at 1.0 GeV/c.

¹ Atomic Energy Agency, NRC, Cairo, Egypt

² Institut für Kernphysik KFA Jülich, Germany

References

- [1] P. Jahn et al., Annual Report 1994, FZR, FZR-78 (1995) 43

Beam Properties and Beam Focussing near the TOF Target^B

A.HASSAN¹, P.JAHN², R.KLEIN², B.NAUMANN, M.ROGGE², M.STEINKE³ AND R.TÖLLE².

The ion optical properties and the beam transport possibilities in the last part of the TOF beam line [1] had been investigated. In section IV of the TOF beam line exists a region with a reduced aperture ($R = 30 \text{ mm}$) between the vertically deflecting dipoles BE34 and BE35 due to the actual gap widths. Extensive calculations were done assuming a waist to waist transfer, starting at different positions upstream the aperture and producing a small beam spot at the target. In addition, the optical settings should be optimized with respect to maximum beam emittances ϵ_x and ϵ_y to pass through the aperture for a chosen waist position. The main results of the calculations are :

- i) the beam extensions at the starting waist amount to $x_{\text{waist}} = y_{\text{waist}} = 30/\sqrt{2} = 21.2 \text{ mm}$ independently from the waist position;
- ii) the angle extensions are $x'_{\text{waist}} = y'_{\text{waist}} = R/(L \cdot \sqrt{2}) = x_{\text{waist}}/L$, where L is the distance between the starting waist and the aperture;
- iii) the beam emittances amount to $\epsilon_x = \epsilon_y = \epsilon_{\text{max}} = R^2/(2 \cdot L)$.

Calculations with the program TRANSPORT [2] give the field strength B in the last four quadrupoles Q35 to Q38 . The results are shown in Fig. 1.

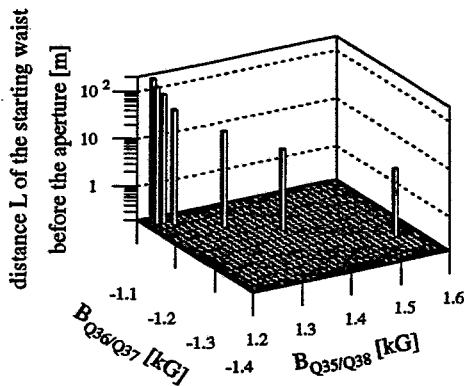


Fig. 1 Field strength B setting in the last four quadrupoles in front of TOF to get a focus (waist) on the target. Q35 and Q38 are coupled to a one power supply as Q36 and Q37 to another.

Calculations assume a waist on the target 2.5 m behind the quadrupole Q38. In linear approximation the quadrupole current I_Q is

$$I_Q[\text{A}] = 26.6 \cdot B_Q[\text{kG}] \cdot p,$$

where p is the momentum of the protons in $[\text{GeV}/c]$.

During the last TOF experiment the currents in the final quadrupoles were chosen according to these calculations for a beam spot on the target of $r = 0.6 \text{ mm}$. Then the beam line before the waist was set experimentally to fit the starting conditions for the entrance waist. The halo normally hits the walls of the gap in the vertical dipoles. In order to reduce the halo near the TOF the beam was successfully limited in emittance within two upstream dipoles far away from the target. The geometrical situation near the target is shown in Fig. 2.

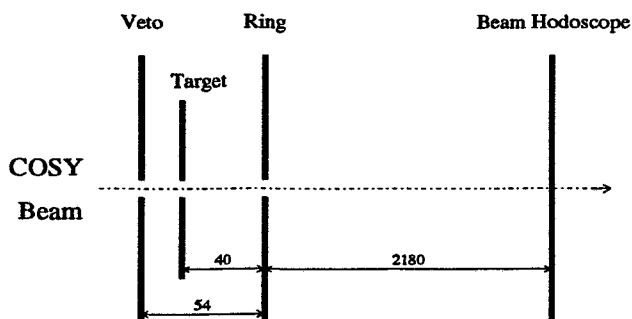


Fig. 2 Arrangement of the detectors near the target region

Some properties of the beam in the target region can be seen in Fig. 3. The ratio of the beam intensity on the veto detector $R_v = I_v/I$ and the ring detector $R_r = I_r/I$ are given, where I is the total intensity in the beam measured with a hodoscope. The vertical beam position y is shifted across the detectors by a vertical steerer. A beam extension on target $r = \text{FWHM}/2 = 0.8$ mm is deduced. 87% of the beam passes through the holes of $r_v = 1$ mm and $r_r = 1.2$ mm and 93% passes through the ring detector. The center of the veto counter is shifted relative to the ring counter by 0.2 mm. The structure of the remaining halo is demonstrated in Fig. 4. A fine adjustment for minimum halo shows, that a precision of the quadrupole currents near 10^{-4} is necessary.

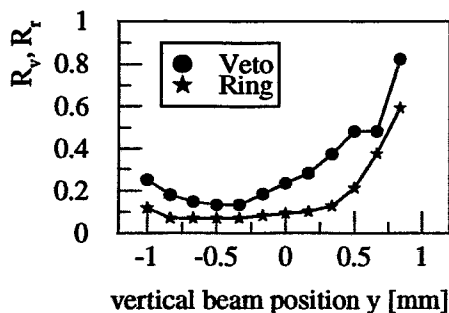


Fig. 3 Ratio of the beam intensity on the veto detector

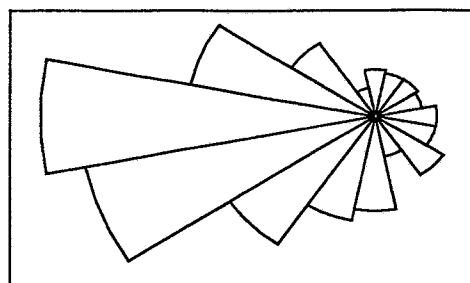


Fig. 4 Intensity distribution of the halo on the ring detector in polar presentation at 0.88 GeV/c corresponding to the sectors of the ring detector.

The adjustment of detectors, target, viewers etc. by two optical telescopes to better than 0.5 mm has made the focussing of the beam much easier. The sensibility to steering in the quadrupoles is reduced considerably. A viewer of $\text{Al}_2\text{O}_3(\text{Cr})$ was used for the adjustment of the beam. In vacuum it was applicable for beam intensities down to 10^6 protons/(sec · mm²).

¹ Atomic Energy Agency, NRC, Cairo, Egypt

² Institut für Kernphysik KFA Jülich

³ Institut für Experimentalphysik I, Ruhr-Universität Bochum

References

- [1] Annual Report 1994, KFA Jülich, Jül-3035 (1995) 18
- [2] K.L. Brown et al., TRANSPORT Manual, Geneva, CERN 80-04 (1980)

Test of Transparent Adhesives for Scintillation Detectors^B

P. MICHEL, K.-H. HERMANN, K. MÖLLER, J. MÖSNER AND A. SCHAMLOTT

In order to couple scintillators or light guides with phototubes often adhesives (e.g. Röhm, Agryfix 190; Devcon, 5-min-Epoxy; Delo, Delo-CA) are used which are more or less inflexible. In case of large temperature changes of the order of 20° C this can result in a break-off due to thermal expansion. Therefore, we systematically tested some *flexible* adhesives with respect to their performance in glueing phototubes onto various light guides, their behaviour at temperature changes and their long-time stability when exposed to vacuum and atmospheric pressure. All the used products (Henkel-Sista, Rhone Poulence-Elch glasklar and Bicon-BC 636) were silicone adhesives.

Fig. 1 shows a sketch of the setup used for determination of transparency of the adhesives. In order to measure the light attenuation length λ of the adhesives, sandwiches have been prepared consisting of layers of adhesives of different thickness between plates of 1.5 mm perspex. They have been placed between a radioactive source (^{241}Am) on 3*3*3 mm³ NE 110 scintillator and a XP 2020 phototube. The results of this measurement are shown in fig. 2. The measured values are 23.2, 8.6 and 5.5 mm for Elch, BC and Sista, respectively. The times needed for a thorough harding are nearly the same for the three adhesives and amount to about 24 h.

In case of the Sista adhesive we found that λ decreases to 3.8 mm after 4 weeks due to the influence of the air. For the Elch adhesive we observed a *constant* λ after 18 months in air, but using it in vacuum it acquires a yellow-brown tint. The BC adhesive turned out to be stable under both conditions.

Furthermore, the mechanical stability of 1"-phototubes glued on perspex was tested. We compared probes of Elch and Delo-CA under temperature changes of $\pm 20^\circ\text{C}$. Whereas the Delo-CA probes broke-off the Elch ones did not show any changes. Additionally, the Elch probes have been stressed by a torque of 0.5 Nm parallel to the glued area over 4 months with the result that no changes could be observed neither optically nor mechanically.

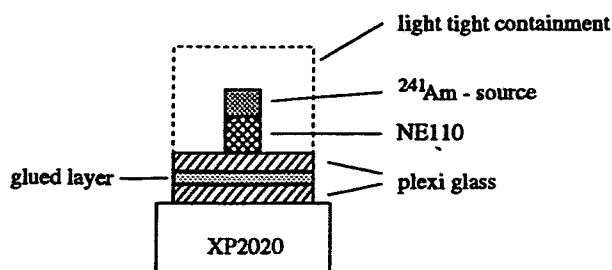


Fig. 1 Sketch of the setup used for determination of the light attenuation length λ

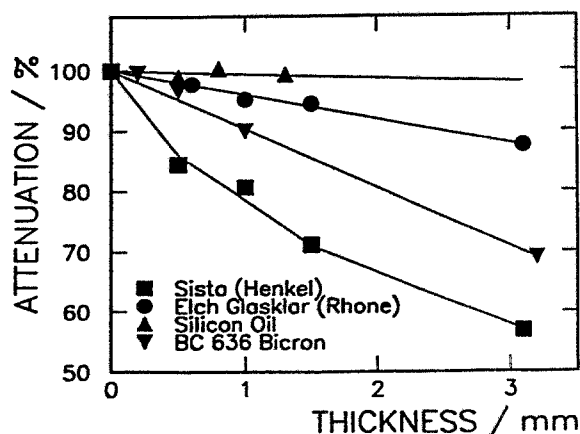


Fig. 2 Light attenuation versus thickness of the layer for different probes of adhesives

Test of a Scintillating-Fiber Calorimeter for Photons with Energies below 1 GeV^{B,K}

B. HÜBNER¹, K.-TH. BRINKMANN¹, H. FREIESLEBEN¹, J. S. LANGE¹,
B. NAUMANN, AND L. NAUMANN

In certain cases, such as the pp-bremsstrahlung experiment at the COSY TOF spectrometer, the detection of photons requires the coverage of large solid angles with good angular resolution, i.e. granularity, and high efficiency. The energy resolution may be less important in this special case. Therefore, a calorimeter of the spaghetti type (consisting of scintillating fibers embedded in a lead matrix) may offer an affordable and efficient alternative to high-resolution calorimeters of e.g. CsI-type. The performance of such a device at low photon energies ($50 \text{ MeV} \leq E_\gamma < 1 \text{ GeV}$) was studied [1] using an early prototype of the SPACAL array [2] which operates at CERN. Its properties were investigated experimentally with real photons from the Mainz microtron MAMI and were verified in extensive Monte-Carlo studies using the computer code GEANT. Experimentally, the detector efficiency was found to equal 100% above the minimum available photon energy of 110 MeV as shown in figure 1. The Monte Carlo studies reveal that the efficiency drops rapidly around $E_\gamma = 40 \text{ MeV}$. The energy resolution is $(\sigma/E) \approx 10\%/(E_\gamma/\text{GeV})^{-1/2}$ over the full energy range as extracted from a fit to the experimental results presented in figure 2. Typical GEANT results are included in the figure. The energy resolution obtained with this array is sufficient for a discrimination of $pp\gamma$ events from π^0 production background. Based on these studies design criteria for future arrays can be matched to experimental requirements. In particular, the average density of the scintillator-lead array is useful in the extrapolation of design parameters for the possible future development of new arrays of this type.

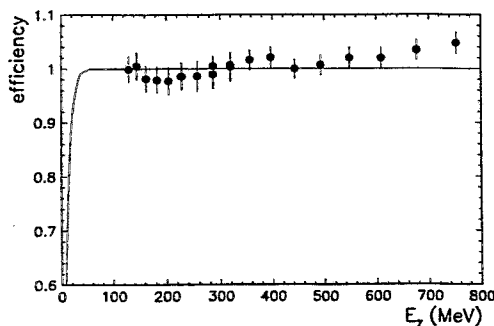


Fig. 1 Efficiency for photon detection as a function of energy. The full line shows the result of calculations using GEANT.

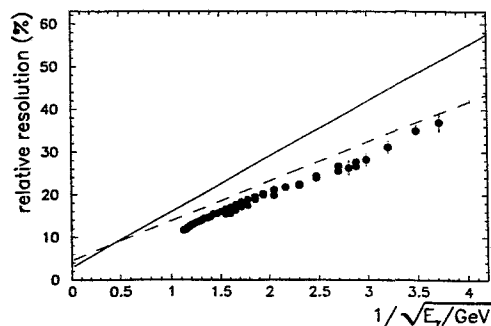


Fig. 2 Photon energy resolution; the full line is a typical GEANT result using a fiber diameter of 1 mm, the dashed line is for $\varnothing = 1.2 \text{ mm}$.

¹ Institut für Kern- und Teilchenphysik, TU Dresden

References

- [1] B. Hübner, diploma thesis, Dresden (1995)
- [2] D. Acosta et al., Nucl. Instr. Meth. **A294**, 193 (1990), and D. Acosta et al., Nucl. Instr. Meth. **A305**, 55 (1991).

Ratio of Kaon- to Pion-Pair Production as a Signature of Enhanced Strangeness Production^B

V.I. KOMAROV¹, H. MÜLLER

The study of strange-particle production in proton-nucleus (pA) and nucleus-nucleus (AA) collisions has become an important research area since Rafelski and Müller [1] and Greiner et al. [2] predicted strangeness enhancement for heated and compressed nuclear matter. In this picture nuclear matter, which consists primarily of u and d quarks at normal density, melts into a "soup" of quarks and gluons at high density and temperature. Under such conditions $s\bar{s}$ creation is no longer suppressed and nearly equal amounts of $s\bar{s}$ as well as $u\bar{u}$ and $d\bar{d}$ pairs are produced.

In the experimental studies on strangeness production in heavy-ion collisions at high energies performed by E802 [3], NA34 [4] and NA35 [5] $s\bar{s}$ creation has been indeed observed to be about three times larger than in free pp collisions. For pBe , pAu and $SiAu$ [3] collisions at 14.6 GeV/u the K^+/π^+ ratio becomes larger if the size of the system increases. Such results support the quark-gluon hypothesis, which, nevertheless, needs further confirmation. In particular, there is no clear definition how to determine the meaning of an *enhanced* production of strangeness. To minimize the influence of trivial kinematical factors we propose to measure the ratio $R_{K\pi} = \sigma_{K+K-}/\sigma_{\pi^+\pi^-}$ of the cross sections for the production of K^\pm and π^\pm pairs having *the same invariant mass*. This is a way to compare the creation of $s\bar{s}$ pairs with that of $u\bar{u}$ ($d\bar{d}$) pairs at comparable conditions. Although quark-gluon plasma is expected to be created in AA collisions at high energies we consider here the subthreshold region for kaon production. Under the assumption that particle production in pA interactions arises from locally heated and compressed pieces of nuclear matter [6] one can imagine the following scenario. For relatively low invariant masses the reaction proceeds above the threshold of a free NN -interaction and the ratio $R_{K\pi}$ should be similar to that observed in NN collisions. If, however, the invariant mass increases then the energy necessary for the pair production becomes larger until the subthreshold regime is reached. While the production of a low-mass pair proceeds predominantly at a single nucleon inside the target nucleus the creation of a high-mass pair requires the interaction with several target nucleons in order to gain the necessary energy. Since the energy-momentum transfer to the participating few-nucleon subsystem is rather high, it can be considered as a locally heated and compressed piece of nuclear matter where enhanced strangeness production might be possible. Therefore, for large invariant masses of the observed pairs the value of the considered ratio will exceed the "normal" one if density and temperature become, at least locally, sufficiently high. The proposed approach makes the search of the phenomenon more definite, because the ratio $R_{K\pi}$ is considered as a function of an observable, the invariant mass, which allows a tuning of the conditions between creation from "normal NN -interactions" and "locally heated few-nucleon groups". The same kind of effect can be expected if not the invariant mass but the incident energy is changed. In case of production at heated pieces of nuclear matter with enhanced strangeness production the ratio $R_{K\pi}$ should decrease more slowly if the energy is decreased below the NN threshold than in the case of "normal" strangeness production.

The ANKE spectrometer [7] being installed at COSY is well suited to carry out the proposed investigations. Kaons emitted at angles $\theta \leq 10^\circ$ will be measured by two similar detection systems at both sides of the deflecting magnet. Due to the smaller mass of the

pions a larger relative momentum of the two pions is needed to get a pair having the same invariant mass as the kaon pair. This can be accomplished by measuring the π^- at forward angles with the same detector as the K^- mesons and the π^+ at angles $\theta \geq 165^\circ$ using the backward detector of ANKE.

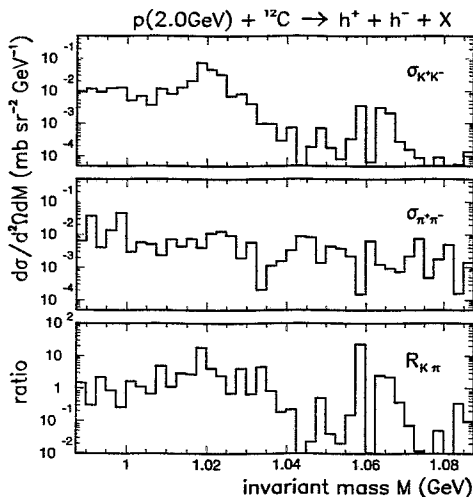


Fig. 1 Calculated invariant mass spectra of kaon ($\sigma_{K^+K^-}$) and pion pairs ($\sigma_{\pi^+\pi^-}$) and the ratio $R_{K\pi} = \sigma_{K^+K^-}/\sigma_{\pi^+\pi^-}$ for $p^{12}C$ interactions at 2.0 GeV

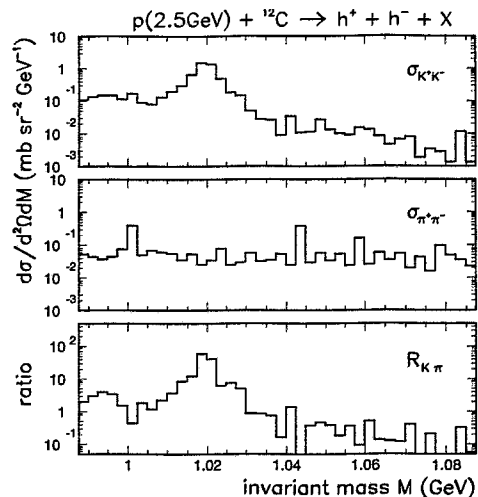


Fig. 2 The same as Fig. 1 for 2.5 GeV

In Figs. 1 and 2 predictions for $p^{12}C$ interactions at 2.0 and 2.5 GeV from the Rossendorf collision model [8, and references therein] for the invariant mass spectra of kaons and pions as well as the ratio $R_{K\pi}$ are plotted. There is a peak around 1.02 GeV in the invariant mass spectra of kaons, which originates from the production of ϕ mesons with subsequent decay into kaon pairs. The calculated cross sections for the production of the kaon and the pion pair are of comparable magnitude under the selected kinematical conditions. They may serve for an estimate of the expected counting rates. The cross sections increase by more than one order of magnitude if the energy is changed from 2.0 to 2.5 GeV, the ratio $R_{K\pi}$, however, is much less affected.

In the calculations a constant ratio $u : d : s = 1 : 1 : 0.15$ for the production of up, down and strange quark pairs is used. No peculiarities concerning the dependence of this ratio on density and temperature are taken into account. Therefore, these calculations may serve as a measure of “normal” $s\bar{s}$ creation. Enhanced strangeness production should then manifest itself in a larger measured ratio at high invariant masses in comparison to the calculated one.

¹ Joint Institute for Nuclear Research Dubna, Russia

References

- [1] J. Rafelski, B. Müller, Phys. Rev. Lett. **48** (1982) 1066
- [2] C. Greiner, P. Koch, H. Stöcker, Phys. Rev. Lett. **58** (1987) 1825
- [3] T. Abbott et al. Phys. Rev. Lett. **66** (1991) 1567
- [4] Helios Collaboration: Nucl. Phys. A**525**(1991) 227c
- [5] J. Bartke et al., Z. Phys. C**48** (1990) 191
- [6] T. Maruyama et al., Nucl. Phys. A**573** (1994) 653
- [7] O.W.B. Schult et al., Nucl. Phys. A**583** (1995) 629
- [8] H. Müller, Z. Phys. A **353** (1995) 237

Test Measurements with the ANKE MWC1^B

CHR. SCHNEIDER, TH. KIRCHNER, L.V. HORN¹ AND V. KRUGLOV²

At the ANKE-spectrometer at COSY-Jülich two multiwire chambers (MWC1, MWC2) will be used to perform the measurement of the particle tracks[1]. These chambers are build in Rossendorf and the first one was completed in 1995.

The precision of measuring the tracks at ANKE is limited through the small angel scattering of the particles going through the detector system. Based on the results of Monte Carlo simulations it was established [1] that a value of $\sigma_{\text{MWC}} = 0.7$ mm for the position resolution of the MWCs is sufficient. The particles leaving the spectrometer pass the MWCs under angles between 0° and 58° . This makes it necessary to investigate the problem of inclined particle tracks.

The MWC1 consists of three anode planes (sensitive area 1300×350 mm²) with wire orientation 0° (vertical) and $\pm 30^\circ$ respectively. The three anode planes have a wire spacing of about 2.5 mm to achieve the needed position resolution. They are stacked within four cathode planes with a gap of 5 mm between each plane. The cathodes are made from mylar foil covered by carbon.

To control the normal chamber operation and to determine chamber parameters like efficiency or position resolution test measurements were performed in the laboratory and under real beam conditions at BIG KARL COSY. In the laboratory the chamber was tested using a ⁹⁰Sr source and szintillators as reference detectors. The set-up of the experiment at the BIG KARL is shown in Fig. 1. As reference detectors the drift chambers DC1 and DC2 and the szintillator hodoskop H2 are used to trigger on the beam protons. This equipment was provided by the GEM collaboration. The position of MWC1 is shown in Fig. 1, too. The momentum of the proton beam was 1 GeV/c.

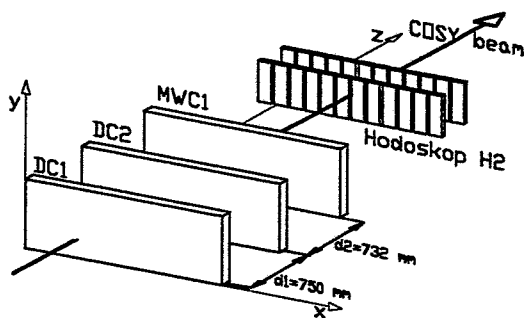


Fig. 1 Scheme of the detector arrangement at BIG KARL

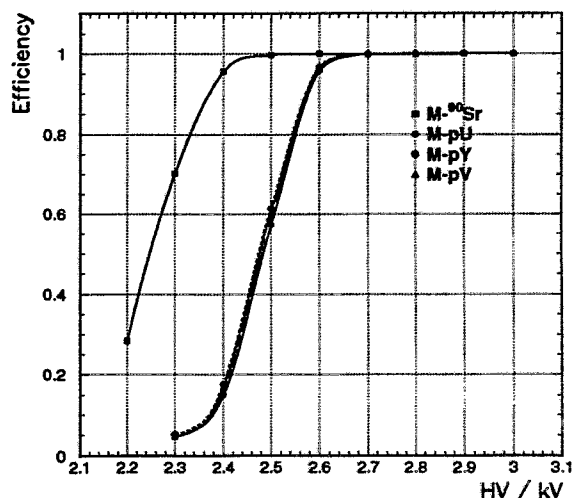


Fig. 2 Efficiency curves from the laboratory and BIG KARL measurements

In Fig. 2 the efficiency curves from the laboratory for the vertical anode plane(M-⁹⁰Sr) and from the BIG KARL measurements for all three anode planes (M-pY, M-pV, M-pU) are shown. All curves were taken with a gas mixture of 70% Argon and 30% CO₂. The

shift between the curve M-⁹⁰Sr and the curves M-pY, M-pV, M-pU is caused by different amplifier thresholds. The shape of the curve and the small differences between the curves from the three anode planes (M-pY, M-pV, M-pU) indicate normal chamber operation.

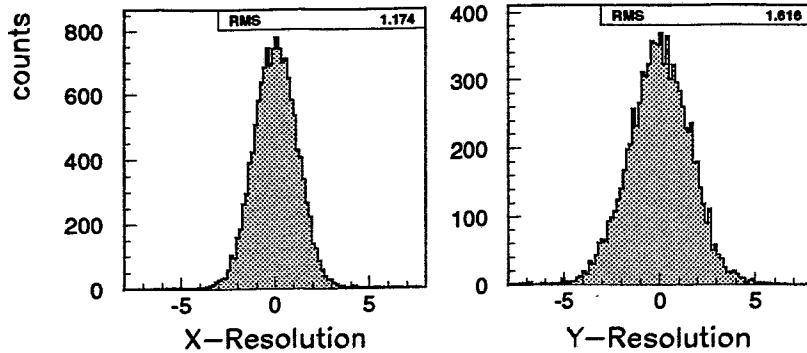


Fig. 3 Deviation of the x- and y-position measured with MWC1 from the particle tracks calculated by DC1 and DC2

The position resolution of MWC1 is determined from the deviation of the measured coordinate of MWC1 against the track calculated from the signals of the drift chambers. The results for x- ($\sigma_{MWC1} = 1.2$) and y-direction ($\sigma_{MWC1} = 1.6$ mm) are plotted in Fig 3. The distributions in Fig. 3 contain the quadratic sum of three contributions, the resolution of the drift chambers, the small angle scattering of the protons in the air between DC2 and MWC1, and the resolution of MWC1 we are interested in. The resolution of one drift chamber in x-direction is about $\sigma_{DC_x} = 0.2$ mm. If we consider the projection of errors of both drift chambers into the plane of MWC1 the contribution is about $\sigma_{DC_x} = 0.8$ mm. The small angle scattering in the air is approximately $\sigma_{Air} = 0.4$ mm. From these values we calculate for the x-resolution $\sigma_{MWC1} = 0.8$ mm. This is in good agreement with the proposed value. The number of wires responding for three different angles of incidence (α) of the beam protons onto MWC1 are plotted in Fig. 4. The curves for $\alpha = 0^\circ, 30^\circ$ and 50° are measured with the same amplifier threshold. From geometrical considerations, i.e. projecting the particle track on the corresponding cathode plane one would expect for 30° 2.3 wires and for 50° 4.7 wires respectively. This agrees with Fig. 4 within the statistical accuracy.

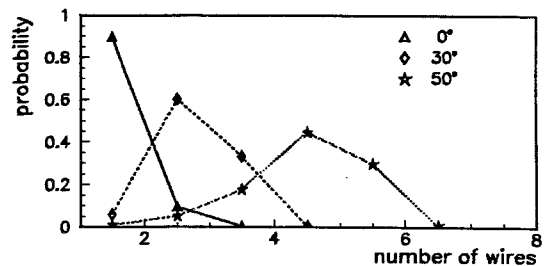


Fig. 4 Distribution of responding wires for three angles of incidence

¹ Institut für Kernphysik KFA Jülich, Germany
² Laboratory of Nuclear Problems, Russia

References

[1] Chr. Schneider et al., Annual Report 1993, FZR-35 (1994) 42

Reconstruction of Particle Coordinates with the Wire Chambers at the ANKE-Facility^{B,K}

T. KIRCHNER, H. MÜLLER, CH. SCHNEIDER AND CHR. SCHNEIDERREIT

At the ANKE-Facility particle trajectories will be reconstructed with the help of two multi-wire chambers MWPC1 and MWPC2 [1] by determining the position and angle of the particle tracks in the detection system. Each chamber has three sensitive anode wire planes. In one plane the wires are inclined by 0° in the two others by $\pm 30^\circ$ with respect to the vertical direction. During experiment the chamber read-out electronics will furnish for each detected event the wire-numbers of the fired wires in each anode plane. In most cases this will not be only one wire per plane, but a cluster of several wires. In order to obtain the position information for the detected particles, the wire-numbers have to be transformed in spatial and angular chamber coordinates. A first procedure for that has been worked out and tested in GEANT simulation calculations. The basic idea will be summarized briefly in the following.

We consider the case where the ejectile has been detected in all six anode planes. This restriction is not necessary, but simplifies the description of the procedure. Later in real data analyzing programs other cases have to be included (e.g. only signals available from two planes in the first and second chamber) in order to increase the overall particle detection efficiency. It is a reasonable assumption to use for each cluster of wires the center of gravity for further calculations. In each plane this center of gravity corresponds to a virtual line parallel to the wires of the corresponding plane. In the following this virtual line will be called X_1 , U_1 and V_1 for the three anode planes in the chamber MWPC1 and X_2 , U_2 and V_2 in the planes of the second chamber MWPC2.

The x-coordinate of the scattered particle in both chambers is automatically determined by the positions of line X_1 and X_2 . Both x-coordinates fix the angle θ of the particle trajectory in the median plane at the exit of the spectrometer. The vertical y-coordinate can be determined separately in both chambers using the other virtual lines. In the MWPC1 V_1 and U_1 are translated along the particle track (along the θ -direction) into the anode plane containing the line X_1 . As a result of this projection there are now three lines in one plane, one vertical and two inclined lines. The point of intersection between two of them gives the y-coordinate. The best accuracy is obtained by crossing the two inclined lines. The y-coordinate in the chamber MWPC2 is determined by the same way. The z-coordinate is equal to the position of the plane to which the virtual lines have been projected (the plane from which x and y coordinates were extracted). The x, y and z information of MWPC1 and MWPC2 allow to determine the vertical angle ϕ of particle track with respect to the median plane.

To calculate particle coordinates different geometrical parameters must be known. A complete measurement of the chamber and its position in the detection system before the beginning of the experiment could be one possibility to obtain them.

The accuracy of the position reconstruction can be tested by comparing the calculated coordinates with the coordinates given by the GEANT simulation. For this test particle tracks have been simulated in the whole momentum and angular acceptance of the spectrometer. In addition physical processes like multiple scattering were included. The difference of the two coordinate values (in mm) is shown in Fig. 1 for the x and y coordinates in the chamber MWPC1 and MWPC2.

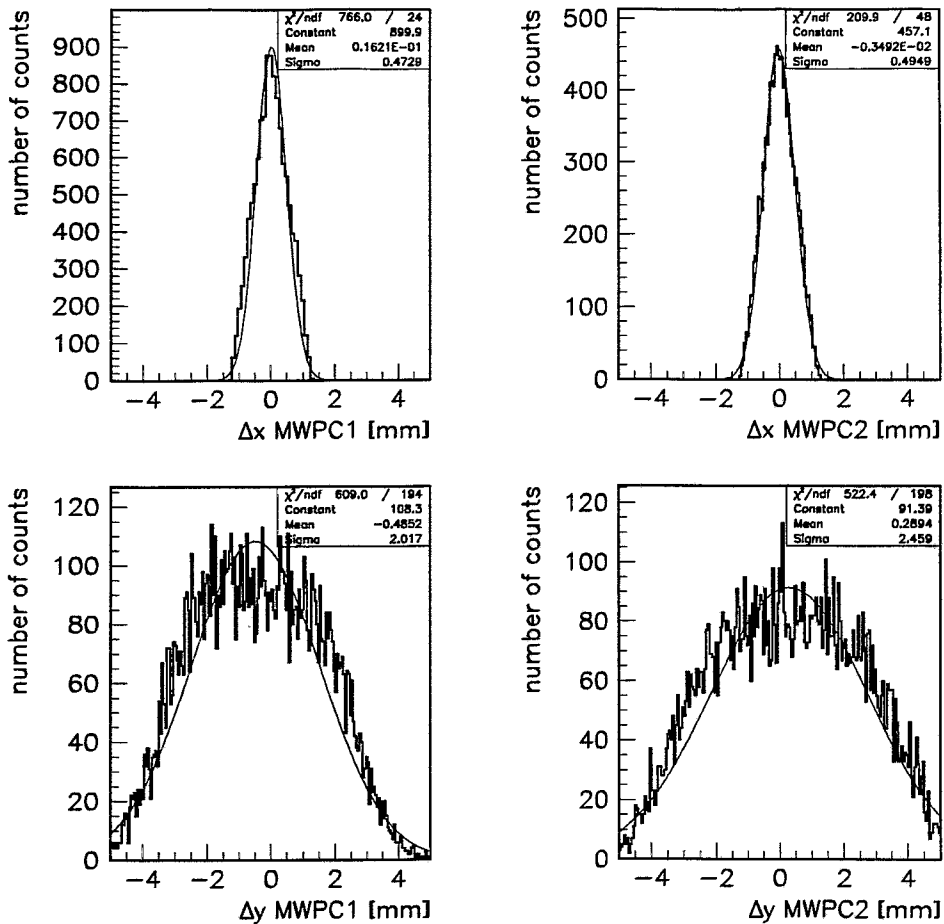


Fig. 1 Difference in mm between simulated and reconstructed x and y coordinates for the chambers MWPC1 and MWPC2.

The x -position resolution is about 1.1 mm FWHM, better than half a wire distance. For the y -coordinate the resolution is lower due to a larger wire distance of about 5.1 mm in the vertical direction. More detailed studies have shown that the obtained position resolutions are independent of the particle momentum and the angle of its trajectory. The discussed procedure for the reconstruction of local track coordinates does not take into account the fringe field of the D2 spectrometer. Tracks are assumed to be straight after the spectrometer exit. Additional investigations have to be done to include events with more than one detected particle and events without complete chamber informations as already mentioned. Further improvements of the program will give more accurate particle track positions and better resolutions, especially for the y -coordinates.

References

- [1] Schult, O.W.B. et al., Nucl. Phys. A **583** (1995) 629.

Hadron production in proton-proton interactions at medium energies
(Z. Phys. A 353 (1995) 103)

Müller, H.

Abstract: Hadron production in proton-proton interactions is described in the framework of a collision model, which aims at describing simultaneously all reaction channels in a wide energy region. An empirical matrix element based on the present knowledge of the partonic structure of hadrons is combined with the concept of intermediate subsystems and the calculation of modified statistical weights of the various final states. It is demonstrated that the energy dependence of total cross sections between threshold and about 50 GeV incident energy can be satisfactorily reproduced. This is the basis for considering theoretical and experimental problems of K^- , η and η' production in more detail.

Hadron production in p Be interactions at 14.6 GeV/c
(Z. Phys. A 353 (1995) 237)

Müller, H.

Abstract: Invariant cross sections for the production of π^\pm , K^\pm , p , and d in p Be interactions at 14.6 GeV/c are well reproduced by calculations carried out in the framework of the Rossendorf collision model.

Plans for investigations of subthreshold K^+ production in $p+A$ collisions
(Nucl. Phys. A 583 (1995) 629)

Schult, O.W.B., K. Sistemich, V. Koptev, H. Müller, W. Cassing, L. Jarczyk, V.I. Komarov, A. Sibirtsev, J. Ernst, R. Santo, M. Nioradze, A.V. Kulikov, A. Hardt, N.S. Amaglobeli, M. Büscher, U. Bechstedt, W. Borgs, B. Childaze, T. Demski, S. Dienel, H. Dombrowski, S.V. Dshemuchadse, R. Eßer, A. Franzen, L. Glonti, D. Gotta, D. Grzonka, F. Hinterberger, L. von Horn, M. Ivanov, A. Kacharava, B. Kamys, W. Klein, W. Klimala, H.R. Koch, M. Köhler, D. Kopyto, S. Kopyto, K.W. Leege, G. Macharashvili, Z. Menteshashvili, G. Müller, W. Oehme, W. Oelert, H. Ohm, B. Prietzsch, A. Puzynin, A. Petrus, B. Rimarzig, Z. Rudy, R. Schleichert, Chr. Schneider, Chr. Schneidereit, H. Seyfarth, U. Sieling, J. Smyrski, H. Stechemesser, A. Strzalkowski, W. Tenten, S.V. Trusov, V. Chernyshev, K.-H. Watzlawik, B.Zh. Zalykhanov, N.I. Zhuravlev, P. Zolnierczuk, K. Zwoell

Abstract: We plan to investigate sub-threshold K^+ production in proton bombardment of atomic nuclei in order to study the reaction mechanism through a measurement of the double differential cross section and of $K^+ p$ and $K^+ d$ coincidences. The status of the theoretical studies is summarized, and the spectrometer to be installed in the COSY ring is briefly described.

K^- -meson production in proton-nucleus collisions
(Z. Phys. A 351 (1995) 333)

Sibirtsev, A., M. Büscher, H. Müller, Ch. Schneidereit

Abstract: K^- -meson production in proton-nucleus interactions at projectile energies up to 15 GeV is studied. As a first step the available data on K^- -meson production in pp interactions are compared with different parametrizations and results of model calculations. Because of considerable uncertainties in the current descriptions of the energy dependence of the elementary K^- cross section a new parametrization is suggested. Experimental data on K^- production in pA collisions are analyzed in the framework of the Rossendorf collision and folding models. Satisfactory descriptions of the momentum spectra at forward angles are achieved. From an analysis of the A dependence it can be concluded that K^- mesons are well suited to investigate final-state interactions for particles interacting strongly with the residual nucleus. Furthermore, we propose experimental studies on K^- production close to threshold. Such measurements are particularly sensitive to contributions from secondary processes or from multi-nucleon interactions.

3 Experimental Nuclear Spectroscopy

Tilted Rotation in Nuclei around $A = 80$

R. SCHWENGER, S. FRAUENDORF, J. REIF AND G. WINTER

An interesting phenomenon found in the odd- Z nuclei $^{77,79,81}\text{Br}$, $^{79,81,83}\text{Rb}$ and in the odd- N nuclei ^{79}Kr , ^{83}Sr is the existence of $\Delta I = 1$ bands that start with $13/2^- \leq I^\pi \leq 17/2^-$ states at about 2.5 – 3 MeV and that have regular energy spacings and little signature splitting. The levels of these bands depopulate via strong M1 transitions with strengths of $B(M1) \approx 0.5$ W.u. while E2 transitions are not observed in most cases. The bands found in $^{77,79,81}\text{Br}$ are shown in figure 1. These bands have been interpreted as 3-qp excitations of the type $\pi g_{9/2} \nu g_{9/2} \nu(fp)$ on the basis of a semiclassical coupling scheme [1-3].

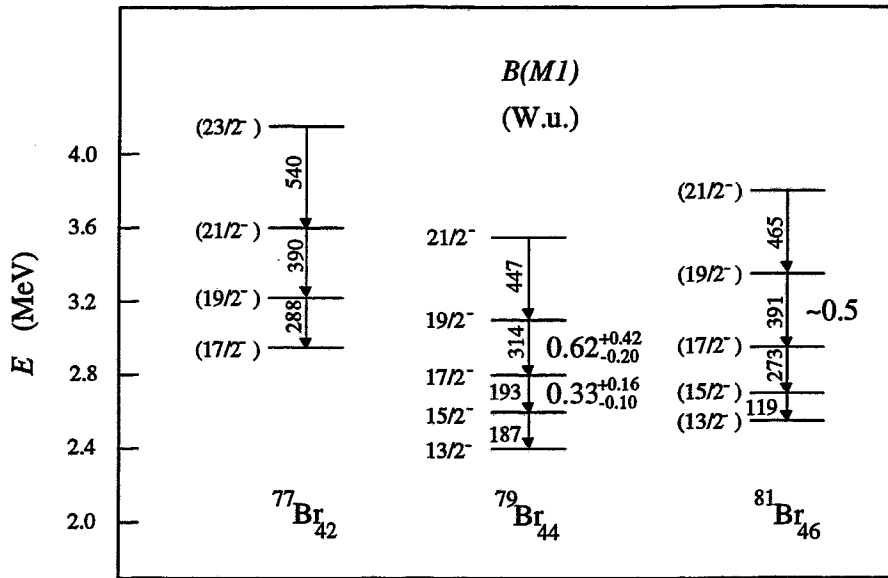


Fig. 1 High-lying $\Delta I = 1$ bands in $^{77,79,81}\text{Br}$. Inter-band transitions to the $3/2^-$ ground state band and to the $9/2^+$ band are omitted. The numbers on the right of the transitions indicate M1 transition strengths in W.u. The data were taken from [1-3].

The recently developed tilted-axis cranking (TAC) model [4] enables the description of rotation about axes different from the principal axes and involves the description of a new rotational mode referred to as magnetic rotation. The characteristics of this mode are compatible with that observed in the $\Delta I = 1$ bands and thus suggest an interpretation of these bands within the framework of the TAC model. In a first step calculations were performed for the $\pi(fp)$ and $\pi g_{9/2}$ 1-qp bands and for all possible 3-qp excitations with negative parity in the nucleus ^{79}Br . For all configurations a quadrupole deformation of $\epsilon_2 = 0.2$ was assumed that agrees roughly with the value deduced from experimental $B(E2)$ values of the 1-qp bands. Calculated excitation energies are compared with experimental ones in figure 2. The experimental $\pi(fp)$ and $\pi g_{9/2}$ 1-qp bands are reproduced with slightly too large gradients that may indicate a larger deformation in these bands than assumed in the calculations. The solutions for both these configurations correspond to an angle of tilting of $\theta_T = 90^\circ$ which means rotation about the principal axis perpendicular to the symmetry axis. Accordingly, M1 transitions are not noticeable while the predicted

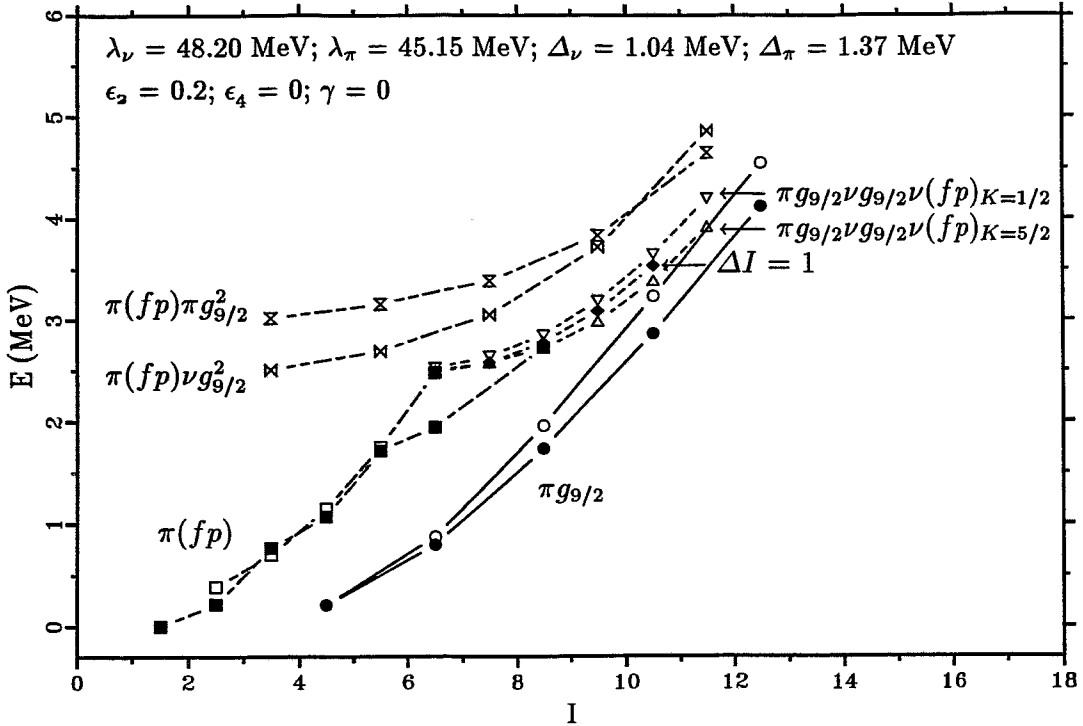


Fig. 2 Comparison of experimental excitation energies (full symbols) with calculated ones (open symbols) of bands in ^{79}Br as a function of spin.

E2 transition strengths have values of $B(E2) \approx 25 - 50$ W.u. which corresponds to the experimental findings. Calculations with the 3-qp configurations $\pi(fp)^3$ and $\pi(fp)\nu(fp)^2$ result in bands lying about 2 MeV above the experimental $\Delta I = 1$ band and are not included in figure 2. The bands based on the configurations $\pi(fp)\pi g_{9/2}^2$ and $\pi(fp)\nu g_{9/2}^2$ are predicted about 0.5 MeV above the $\Delta I = 1$ band and are solutions with $\theta_T = 90^\circ$ involving negligibly small $B(M1)$ values. For configurations of the type $\pi g_{9/2}\nu g_{9/2}\nu(fp)$ real TAC solutions are obtained. Two configurations have been tested where the neutron in the (fp) shell occupies either the lowest orbit with $K = 5/2$ or the second lowest orbit with $K = 1/2$. Both resulting bands lie very close to the experimental $\Delta I = 1$ band (see figure 2). The first one involves an angle of tilting of $\theta_T \approx 50^\circ$ and M1 transition strengths of $B(M1) \approx 0.4$ W.u. while the second one corresponds to values of $\theta_T \approx 65^\circ$ and $B(M1) \approx 0.3$ W.u. These $B(M1)$ values are consistent with the experimental ones of the $\Delta I = 1$ band (cf. figure 1) and are obtained only with these configurations. The calculated $B(E2)$ values are in both cases smaller than the experimental limit of $B(E2) \approx 30$ W.u. derived for the not observed E2 transitions. This accurate description shows that the $\Delta I = 1$ band observed in ^{79}Br is based on a tilted-axis configuration and is an example for rotation with a strong magnetic component (cf. [5]).

References

- [1] J. Döring et al., Phys. Rev. C **48** (1993) 2524
- [2] R. Schwengner et al., Nucl. Phys. A **486** (1988) 43
- [3] L. Funke et al., Z. Phys. A **324** (1986) 127
- [4] S. Frauendorf, Nucl. Phys. A **557** (1992) 259c
- [5] S. Frauendorf, contribution to this report

Experiments on ^{79}Br and ^{72}Kr with EUROBALL CLUSTER detector arrays at the Max-Planck-Institut für Kernphysik in Heidelberg

T. SERVENE, S. SKODA, J. REIF, H. SCHNARE, R. SCHWENGER, H. PRADÉ, G. WINTER, L. KÄUBLER¹, J. EBERTH², H.G. THOMAS², F. BECKER², B. FIEDLER², S. FREUND², S. KASEMANN², T. STEINHARDT², O. THELEN², T. HÄRTLEIN³, CH. ENDER³, F. KÖCK³, P. REITER³, D. SCHWALM³,

In-beam studies of the nuclei ^{79}Br and ^{72}Kr were performed at the Max-Planck-Institut für Kernphysik Heidelberg using two different arrangements of six EUROBALL CLUSTER detectors.

Excited states in ^{79}Br were populated via the $^{76}\text{Ge}(^7\text{Li},4n)$ reaction using the 35 MeV ^7Li beam of the FN tandem accelerator. The six EUROBALL CLUSTER detectors [1] were located at $\pm 40^\circ$, $\pm 90^\circ$ and $\pm 140^\circ$ relative to the beam. While the four detectors at $\pm 40^\circ$ and $\pm 140^\circ$ were placed in a horizontal plane, the two detectors at $\pm 90^\circ$ had to be tilted out of this plane by 52° to achieve a distance of 25 cm between the target and all Ge crystals. This setup is shown in Fig. 1. The CLUSTER detectors were operated in complete form, i.e. together with their BGO shields and lead collimators. Two experiments were performed with different targets: In the first one the target consisted of $0.2 \text{ mg} \cdot \text{cm}^{-2}$ ^{76}Ge on a $0.05 \text{ mg} \cdot \text{cm}^{-2}$ carbon backing, while in the second one the target consisted of $0.6 \text{ mg} \cdot \text{cm}^{-2}$ ^{76}Ge on a $2.5 \text{ mg} \cdot \text{cm}^{-2}$ gold backing. Since the recoil nuclei are completely stopped in the gold backing, the second experiment enables the determination of mean lifetimes using the Doppler-shift-attenuation method. In each of these experiments a total of about 7×10^8 coincidence events of γ -ray multiplicity two or higher were recorded.

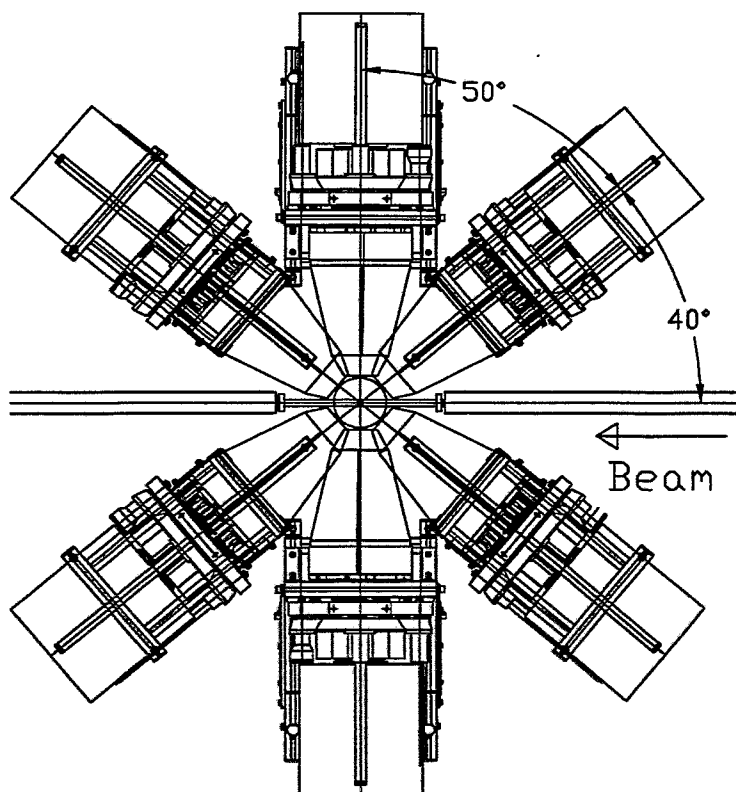


Fig. 1 Top view of the detector setup for the ^{79}Br experiment at the MPIK Heidelberg. The four CLUSTER detectors at $\pm 40^\circ$ and $\pm 140^\circ$ are located in a plane, whereas two CLUSTER detectors at $\pm 90^\circ$ are tilted out of the plane by 52° . Parts of the beamline and the target chamber are also shown. The CLUSTER detectors are fixed on a wooden plate in supports especially designed for this arrangement.

Excited states of the $N=Z$ nucleus ^{72}Kr were populated via the $^{58}\text{Ni}(^{16}\text{O},2n)$ reaction using the 55 MeV ^{16}O beam of the FN tandem accelerator. In this experiment the six CLUSTER detectors were placed on the sides of a cube, with the beam going in through one of the edges. This detector setup is shown in Fig. 2. The CLUSTER cube arrangement, in which the CLUSTER detectors were operated without their BGO shields, allowed us to reduce the distance between the target and the Ge-crystals to 11 cm (24 cm with BGO shield and collimator). The main advantage of the CLUSTER cube is a large detection efficiency because of the enhanced angular acceptance ($\Omega=0.65$ of 4π). In this experiment a total of about 2×10^9 coincidence events of γ -ray multiplicity three or higher were recorded. The analysis of the data of these experiments is in progress.

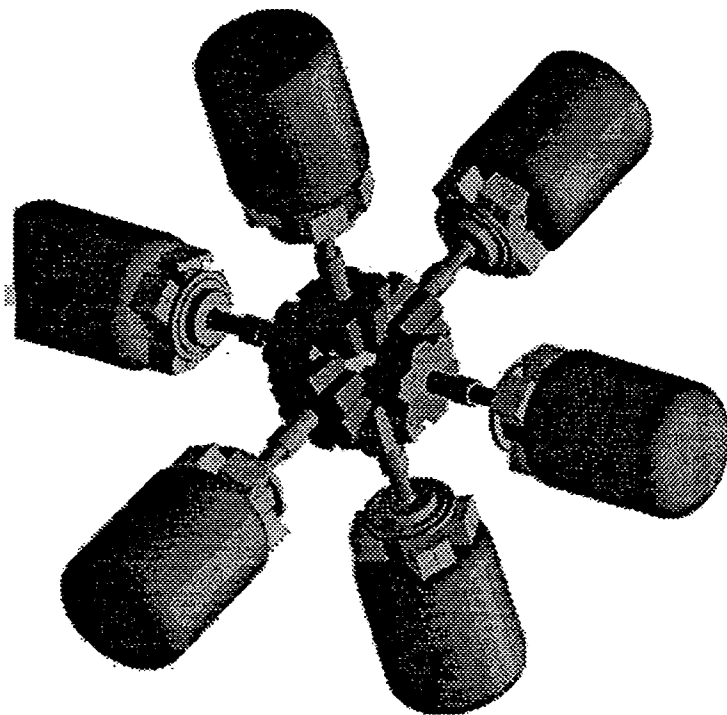


Fig. 2 View of the detector setup for the ^{72}Kr experiment at the MPIK Heidelberg. The CLUSTER cube consists of six CLUSTER detectors placed on the sides of a cube. The beam (not shown) goes in and out through one of the edges. As shown in the picture, the CLUSTER detectors are operated without their BGO shields in order to reduce the distance to the target.

We are grateful to Mr. P Szimkowiak (HMI Berlin) for the preparation of the ^{76}Ge target.

¹ *Institut für Kern- und Teilchenphysik, TU Dresden and Institut für Kern- und Hadronenphysik, FZR*

² *Institut für Kernphysik der Universität zu Köln*

³ *Max-Planck-Institut für Kernphysik, Heidelberg*

References

- [1] J. Eberth, *Prog. Part. Nucl. Phys.*, **28** (1992) 495

Resolution-enhanced Spectroscopy of High-Spin States in ^{81}Y by Kinematic Doppler-Shift Correction^B

H. SCHNARE, J. REIF, R. SCHWENGER, G. WINTER, J. DÖRING¹, G.D. JOHNS¹, S.L. TABOR¹, C.J. GROSS², C. BAKTASH³, Y.A. AKOVALI³, D.W. STRACENER³, F.E. DURHAM⁴, D.G. SARANTITES⁵, M. KOROLIJA⁵, P.F. HUA⁵, D.R. LAFOSSE⁵, A. MACCHIAVELLI⁶, I.Y. LEE⁶, W. RATHBUN⁶, A. VANDER MOLLEN⁷

An experiment was performed at the Lawrence Berkeley Laboratory to investigate high-spin states in nuclei with proton and neutron numbers close to 40.

A ^{32}S beam at an energy of 135 MeV, provided by the 88-Inch cyclotron, was focussed on a thin self-supporting ^{58}Ni target. Emitted γ -rays from the reaction were observed by the Early Implementation phase of GAMMASPHERE consisting of 36 Ge detectors. In addition, evaporated light charged particles (p, d, t and α) were detected with the MICROBALL, a 96-element CsI detector array.

From these data, events belonging to ^{81}Y were enhanced by requiring a coincidence with the charged particle gate for the $2\alpha 1p$ exit channel. These events were sorted into matrices and analyzed with respect to their coincidence and intensity relation [1]. Further analysis was hindered due to a bad energy resolution in γ -lines above 1 MeV. Although the intrinsic energy resolution of the germanium detector is typically 2.5 keV for a 1 MeV γ -line, the observed energy resolution was about 12 keV after correcting for the Doppler-shift in each detector with respect to the beam axis. This effect is due to the opening angle of the germanium detector and the large cone angle of the residual nucleus by α and p emission, resulting in a large Doppler-broadening being observed in a fixed detector. In a conventional Doppler-shift correction the residual nucleus is assumed to follow the beam axis and any recoil momenta of emitted particles are neglected.

A considerable improvement was made by applying a kinematic Doppler-shift correction. From an event-by-event determination of the momenta of all emitted particles the nuclear recoil momentum was deduced with respect to reaction kinematics. In this way a more precise Doppler-shift correction was achieved, thus improving the energy resolution to less than 6 keV for a 1 MeV γ -line [Fig. 1]. It's important to mention that this resolution enhancement by a factor 2 was even obtained without knowing the precise energy calibration of the particle detectors. For all emitted particles an average kinetic energy was assumed, deduced from the value of the Coulomb barrier within the center-of-mass system. This assumption was further improved by analyzing the width of the observed γ -lines in the spectrum as a function of the kinetic energy. The energy at the minimum of this almost parabolic curve was finally taken as the best guess for the kinetic energy of the emitted particles within the center-of-mass system. Because of the low curvature of this function close to the minimum, variations in the kinetic energy only have a small influence on the width of the γ -lines in the corrected spectra. The main effect in kinematic Doppler-shift correction turned out to be the directional correlation of all emitted particles and their effect on the initial momentum of the recoiling nucleus.

It should be noted that the improvement in energy resolution is accompanied by a simultaneous enhancement of the peak-to-background ratio in the observed γ -spectra. Furthermore less contaminated coincidence spectra are created due to the reduced width of the γ -lines which allows a more precise definition of the coincidence gate. The application of this Doppler-shift correction to the further analysis of double and triple coincidences caused a considerable extension of the previously known level scheme [1,2].

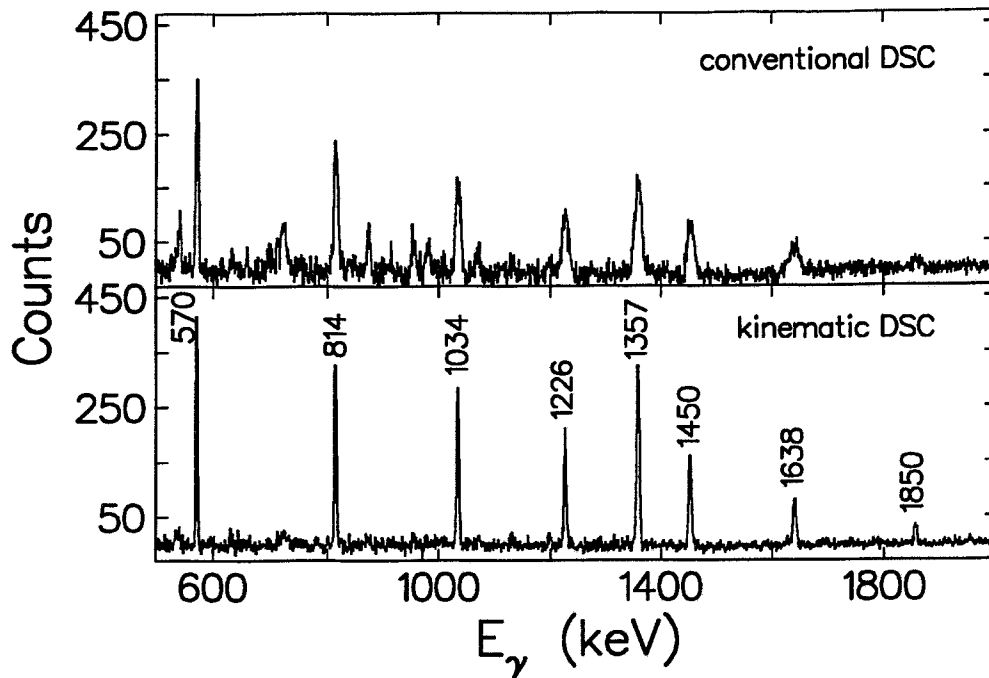


Fig. 1 Comparison of γ -ray coincidence spectra, obtained from a E_γ - E_γ matrix with conventional and kinematic Doppler-shift correction (DSC). The coincidence gate was placed on the 1515 keV transition of the yrast band in ^{81}Y .

¹Physics Department, Florida State University, Tallahassee, USA

²Oak Ridge Institute of Science and Education, Oak Ridge, USA

³Physics Division, Oak Ridge National Laboratory, Oak Ridge, USA

⁴Department of Physics, Tulane University, New Orleans, USA

⁵Chemistry Department, Washington University, St. Louis, USA

⁶Nuclear Science Division, Lawrence Berkeley Laboratory, Berkeley, USA

⁷National Superconducting Cyclotron, Michigan State University, East Lansing, USA

References

- [1] G. Winter et al., Annual Report 1994 **FZR-78** (1995) 60
- [2] T.D. Johnson et al., Z. Phys. **A350** (1994) 189

Photon Scattering Experiment on ^{89}Y ^{B,L}

J. REIF, H. SCHNARE, R. SCHWENGER, T. SERVENE, S. SKODA, H. PRADE, G. WINTER, L. KÄUBLER¹, P. VON BRENTANO², J. EBERTH², R.-D. HERZBERG², N. NICOLAY², N. PIETRALLA², H.G. THOMAS², I. WIEDENHÖVER², A. ZILGES², J. ENDERS³, N. HUXEL³, P. VON NEUMANN-COSEL³, A. RICHTER³, C. SCHLEGEL³ AND V. YU. PONOMAREV⁴

The $^{89}\text{Y}(\gamma, \gamma')$ reaction has been studied at the S-DALINAC accelerator (TH Darmstadt) by using the experimental setup described in Ref. [1]. The endpoint energy of the bremsstrahlung amounted to $E_0=7$ MeV. The scattered photons have been detected with an anti-Compton shielded EUROBALL CLUSTER detector [2] arranged at 130° with respect to the beam axis.

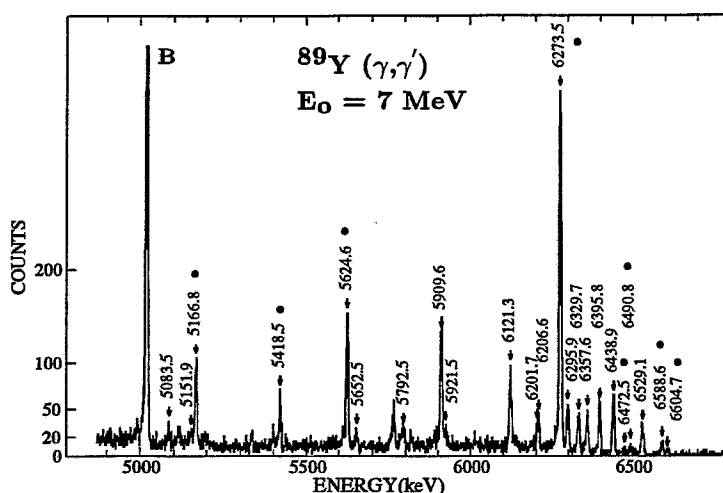


Fig. 1 Photon scattering spectrum of ^{89}Y between 4.9 MeV and 6.7 MeV. Lines assigned to ^{89}Y are marked by their energies in keV. The full circles indicate lines which might be interpreted as E1 ground state transitions on the basis of a comparison with ($^3\text{He},d$) reaction data. The line marked by B belongs to the calibration standard ^{11}B .

Fig. 1 shows the high-energy part of the measured γ -ray spectrum. The lines with $E_\gamma > 5$ MeV are assumed to belong to transitions to the $1/2^-$ ground state. The ground state transitions marked by full circles in Fig. 1 might correspond to levels known from the ($^3\text{He},d$) reaction [3]. Since positive parity is assigned to these levels the corresponding transitions can be assumed to be of E1 type. The very strong electric dipole transition with $B(E1)\uparrow=15(3)\cdot 10^{-3}e^2\text{fm}^2$ observed at 6274 keV is a remarkable feature. This E1 strength is comparable to electric dipole transitions known in the neighboring nuclei ^{88}Sr and ^{90}Zr . For the latter, microscopic calculations within the quasiparticle-phonon model have been performed. The strong E1 transitions were interpreted as a result of the coherent interference between direct excitations of two-phonon configurations and small admixtures of collective GDR phonons.

¹ Institut für Kern- und Teilchenphysik, TU Dresden and Institut für Kern- und Hadronenphysik, FZR

² Institut für Kernphysik der Universität zu Köln

³ Institut für Kernphysik, TH Darmstadt

⁴ Bogoljubov Institute of Theoretical Physics, JINR Dubna, Russia

References

- [1] S. Skoda et al., Annual Report 1994, **FZR-78** (1995) 66
- [2] J. Eberth, Prog. Part. Nucl. Phys., **28** (1992) 495
- [3] H. Sievers, Nucl. Data Sheets, **58** (1989) 351

Spin-Flip Transitions in ^{89}Y

J. REIF, G. WINTER, R. SCHWENGER, S. SKODA, H. PRADE, H. SCHNARE, T. SERVENE AND L. KÄUBLER¹

Recently, the $^{89}\text{Y}(\gamma, \gamma')$ reaction has been investigated [1]. In the energy range between 4 MeV and 6.6 MeV several of the transitions observed have been ascribed to ^{89}Y . By comparison with ($^3\text{He}, d$) data positive parity might be assigned to a part of the excited levels [1]. Since the (γ, γ') reaction is selective to dipole excitations and the ground state has $J^\pi=1/2^-$ (mainly $\pi p_{1/2}$), these levels are likely to be excited by E1 transitions. For the remaining levels positive as well as negative parity can be assumed and $B(\text{E1})\uparrow$ and $B(\text{M1})\uparrow$ values, respectively, might be derived that do not allow to favor one of these assumptions. The $B(\text{M1})\uparrow$ values lie in the range between $0.016 \mu_N^2$ and $0.35 \mu_N^2$. The upper limit of these M1 excitation strengths might be a hint to dominating single-particle transitions. It is well known that spin-flip transitions can be responsible for strong magnetic dipole transitions. In ^{89}Y only the $\pi(p_{3/2} \rightarrow p_{1/2})$ spin-flip transition occurs in the vicinity of the Fermi level and dominates the excitation of the first $3/2^-$ state ($B(\text{M1})\uparrow=1.12\mu_N^2$). Due to the high energy of the considered levels, the excitation of the $N=50$ core and of deep-lying proton orbitals has to be taken into account. In order to estimate the influence of possible spin-flip transitions on the excitation of high-lying $1/2^-$ and $3/2^-$ states, shell-model calculations have been performed considering two configuration spaces. The proton space ($f_{5/2}, p_{3/2}, p_{1/2}, g_{9/2}$) in which the large $B(\text{M1})\uparrow$ values can not be reproduced has been expanded by the $\pi(f_{7/2})$ or the $\nu(g_{9/2}, d_{5/2}, g_{7/2})$ orbitals where the additional configurations are limited to one-particle one-hole excitations ($\pi(f_{7/2})^{-1}$ or $\nu[(g_{9/2})^{-1}(d_{5/2}, g_{7/2})^1]$). In the case of the pure proton space the Hamiltonian based on the surface delta interaction given in Ref. [2] has been used. The difference between the single-particle energies of the proton $f_{7/2}$ and $f_{5/2}$ orbitals has been varied between 2 MeV and 6 MeV. For the space including neutron excitations the Hamiltonian described in Ref. [3] has been applied. The thirty lowest-lying $1/2^-$ and $3/2^-$ states have been calculated. It has been found that the considered proton excitations can not explain the possible large $B(\text{M1})$ values. Due to the dominating $\pi(p_{1/2})$ single-particle character of the ground state only ground state correlations contribute to the spin-flip transition $\pi(f_{7/2} \rightarrow f_{5/2})$. Since these configurations have small amplitudes the resulting influence on the M1 transitions can be neglected in the considered energy range. Contrary to that, the odd $\pi(p_{1/2})$ may play the role of a spectator in the case of the excited neutron core. Therefore the $\nu(g_{9/2} \rightarrow g_{7/2})$ spin-flip transition may contribute almost purely to the M1 transition strength. The calculations predict three $1/2^-$ states around 7.5 MeV excitation energy which are dominated by the $\pi(p_{1/2}) \otimes \nu[(g_{9/2})^{-1}(g_{7/2})^1]$ configuration and which are consequently characterized by large $B(\text{M1})\uparrow$ values. However, the influence of the considered neutron spin-flip transition on states with $E_x < 7$ MeV can not explain large M1 strengths. Therefore the shell-model calculations support the interpretation of the strong dipole excitations as E1 transitions.

¹ *Institut für Kern- und Teilchenphysik, TU Dresden and Institut für Kern- und Hadronenphysik, FZR*

References

- [1] J. Reif et al., contribution to this report
- [2] G. Winter et al., *Phys. Rev.* **C48** (1993) 1010
- [3] J. Reif et al., *Nucl. Phys.* **A587** (1995) 449

Search for Smooth Band Termination in ^{109}Sn ^B

L. KÄUBLER¹, H. SCHNARE, D.B. FOSSAN², W. ANDREJTSCHIEFF³, R. ALLATT⁴, J. DEGRAAF⁵, H. GRAWE⁶, I. HIBBERT⁷, N.O'BRIEN, E. PAUL⁴, H. PRADE, J. REIF, R. SCHUBART⁶, R. SCHWENGER, I. THORSLUND², P. VASKA², R. WADSWORTH⁷
AND G. WINTER

Recently, in ^{109}Sb [1], ^{111}Sb [2] and $^{106,108}\text{Sn}$ [3] smoothly terminating bands have been observed, which are (i) yrast from medium to high spins, (ii) formed by one particular quasiparticle configuration including excitations of the $Z = 50$ core and of the $\pi h_{11/2}$ intruder state and (iii) characterized by a smooth decrease of the dynamical moment of inertia $J^{(2)}$ up to 30 – 40% of the rigid-body value near termination. In a proposal of D.B. Fossan [4] the search for such bands in $^{109,110}\text{Sn}$ was initiated.

Based on the observation of beginning rotational structures in ^{109}Sn [5], an experiment with the Early Implementation of GAMMASPHERE at the LBL Berkeley has been performed. Bombarding a stack of two $440\mu\text{g}/\text{cm}^2$ ^{54}Fe foils with 230 MeV ^{59}Co ions, the reaction $^{54}\text{Fe}(^{59}\text{Co}, 3\text{pn})^{109}\text{Sn}$ has been selected. A total number of 2.33×10^9 $E_\gamma - E_\gamma - E_\gamma$ coincidences were sorted into a cube and analysed with the Radford code [6] giving the ^{109}Sn level scheme shown in Fig. 1.

On top of the $19/2^-$ and $(21/2^+)$ states three rotational-like sequences have been observed evolving to the bands numbered with 1 to 5. The parities of the band levels are uncertain and the spins could be one unit smaller. A DCO-analysis is in progress.

A comparison of experimentally obtained $J^{(2)}$ values and excitation energies (given relative to an average rigid-rotor energy) with first results of calculations using the configuration-dependent shell-correction approach in a cranked Nilsson potential [7], shows especially bands 3b and 5 as candidates for smooth band termination. These bands have quite smooth decreasing $J^{(2)}$ values at high rotational frequencies. The behaviour of the calculated excitation energies of states, e.g. with the configuration

$$\pi[(g_{9/2})_8^{-2}(h_{11/2})_{5.5}^1(g_{7/2})_{3.5}^1]_{17} \otimes \nu[(g_{7/2})_{7.5}^3(d_{5/2})_{4.5}^3(h_{11/2})_{13.5}^3]_{25.5},$$

as a function of the angular momentum fits well with the corresponding experimental behaviour of band 5 and gives nearly the observed terminating spin.

¹ Institut für Kern- und Teilchenphysik, TU Dresden and Institut für Kern- und Hadronenphysik, FZR

² Department of Physics, State University of New York at Stony Brook, USA

³ Institute for Nuclear Research and Nuclear Energy, Bulgarian Academy of Sciences, Bulgaria

⁴ Oliver Lodge Laboratory, University of Liverpool, UK

⁵ Department of Physics, University of Toronto, Canada

⁶ Bereich Festkörperphysik, Hahn-Meitner-Institut Berlin

⁷ Department of Physics, University of York, Heslington, UK

References

- [1] I. Ragnarsson et al., Phys. Rev. Lett. **74** (1995) 3935
- [2] A.V. Afanasjev et al., Nucl. Phys. **A591** (1995) 387
- [3] R. Wadsworth et al., Phys. Rev. **C50** (1994) 483 and TASC-P-95-33 (1995) 1
- [4] D.B. Fossan, private communication
- [5] L. Käubler et al., Phys. Scripta **T56** (1995) 266 and Z. Phys. **A351** (1995) 123
- [6] D. Radford, Nucl. Instr. and Meth. **A361** (1995) 297
- [7] A.V. Afanasjev et al., private communication

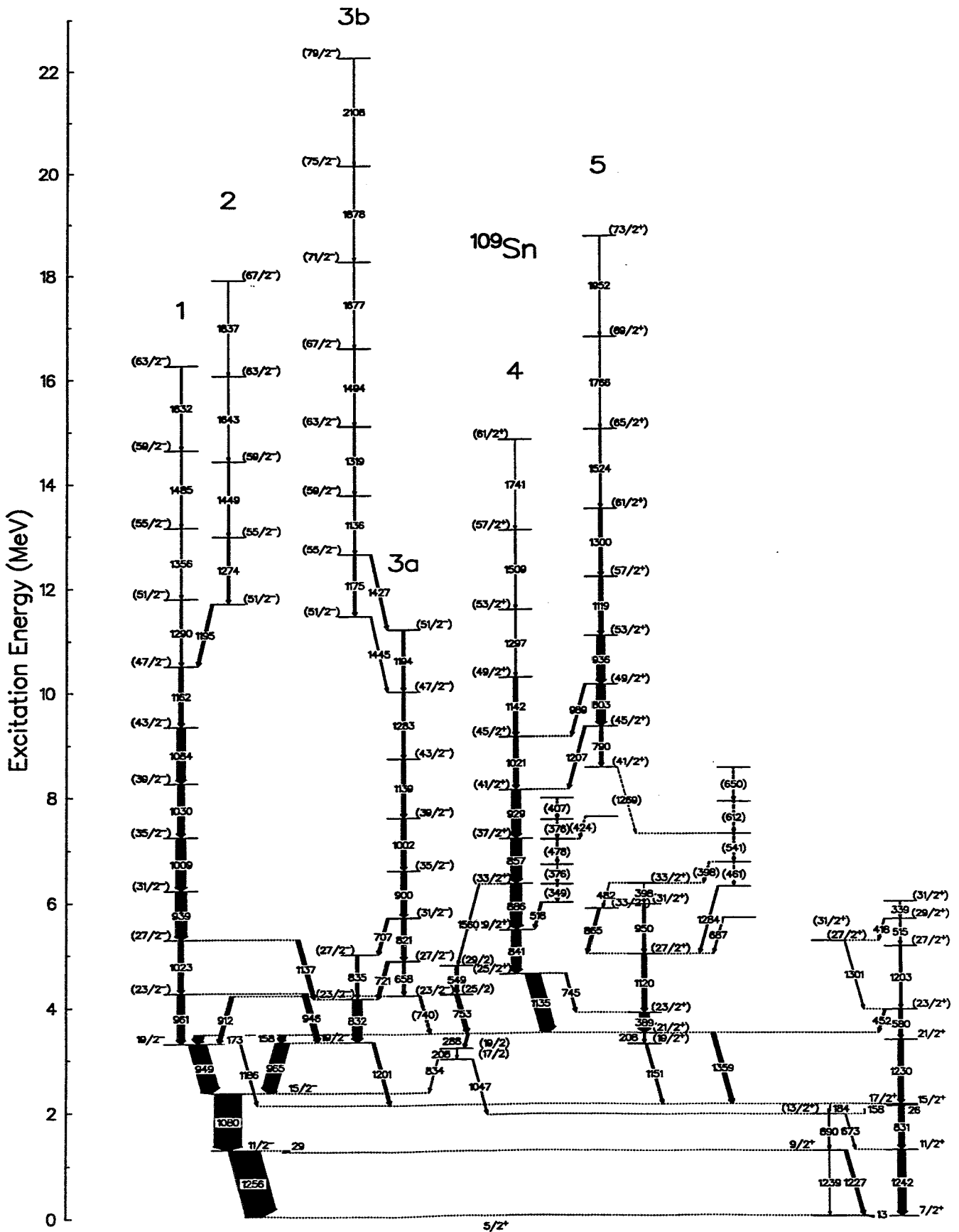


Fig. 1 Preliminary level scheme of ^{109}Sn as obtained in the present experiment

Dipole Excitations in ^{126}Te and ^{130}Te ^B

R. SCHWENGER, G. WINTER, H. PRADE, J. REIF, S. SKODA, H. SCHNARE,
 J. ENDERS¹, N. HUXEL¹, P. VON NEUMANN-COSEL¹, A. RICHTER¹, C. SCHLEGEL¹,
 W. SCHAUER², J. OTT², T. VON EGIDY², P. VON BRENTANO³, J. EBERTH³,
 R.-D. HERZBERG³, N. NICOLAY³, N. PIETRALLA³, H.G. THOMAS³,
 I. WIEDENHÖVER³ AND A. ZILGES³

The nuclei ^{126}Te and ^{130}Te have been investigated in nuclear resonance fluorescence experiments at the superconducting electron accelerator S-DALINAC of the Technische Hochschule Darmstadt with endpoint energies of the bremsstrahlung of 4.5 and 5.5 MeV, respectively. Gamma-ray spectra were measured with an EUROBALL CLUSTER detector [1] positioned at 130° relative to the beam and with an HP-Ge detector of 60% efficiency at 90° . Both detectors were placed inside a lead housing of 30 cm wall thickness to prevent them from background radiation [2].

Part of the γ -ray spectrum measured with the CLUSTER detector during the $^{126}\text{Te}(\gamma, \gamma')$ experiment is shown in figure 1. The multipole orders of some intense γ rays were deduced from the ratios of the intensities observed with the single detector at 90° and the central crystal of the CLUSTER detector at 130° . In both nuclei dipole transitions were identified at energies comparable with the sums of the energies of the lowest 2^+ and 3^- states. The corresponding $J = 1$ states may be interpreted as $2^+ \otimes 3^-$ two-phonon excitations. In this case excitation strengths of $B(E1) \uparrow \approx 2 \cdot 10^{-3} e^2 \text{fm}^2$ can be deduced for these states.

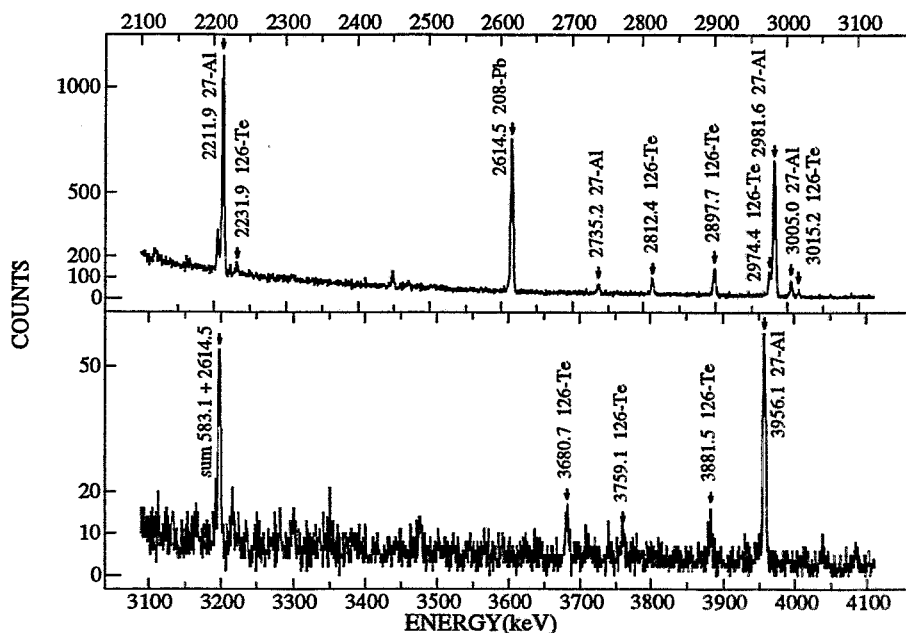


Fig. 1 Gamma-ray spectrum measured with a CLUSTER detector at 130° to the beam in the $^{126}\text{Te}(\gamma, \gamma')$ reaction at an endpoint energy of the bremsstrahlung of $E = 4.5$ MeV.

¹ Institut für Kernphysik, Technische Hochschule Darmstadt, 64289 Darmstadt

² Physik Department, Technische Universität München, 85748 Garching

³ Institut für Kernphysik, Universität zu Köln, 50937 Köln

References

[1] J. Eberth, Prog. Part. Nucl. Phys. **28** (1992) 495

[2] S. Skoda et al., Annual Report 1994, FZR-78 (1995) 66

Dipole Excitations in ^{154}Sm around 6 MeV observed with an EUROBALL CLUSTER Detector ^B

S. SKODA, G. WINTER, H. PRADE, J. REIF, R. SCHWENGER, T. SERVENE
L. KÄUBLER¹, J. ENDERS², N. HUXEL², P. VON NEUMANN-COSEL², A. RICHTER²,
C. SCHLEGEL², P. VON BRENTANO³, J. EBERTH³, R.-D. HERZBERG³, N. NICOLAY³,
N. PIETRALLA³, H.G. THOMAS³, I. WIEDENHÖVER³ AND A. ZILGES³

The nucleus ^{154}Sm was investigated in a nuclear resonance fluorescence experiment at the superconducting electron accelerator S-DALINAC of the Technische Hochschule Darmstadt. The endpoint energy of the bremsstrahlung used in this experiment amounted to 7 MeV. Gamma rays were detected with an anti-Compton shielded EUROBALL CLUSTER detector [1] and a single HP-Ge detector of 60% efficiency arranged at 130° and 90° relative to the beam direction, respectively. Both detectors were placed inside a lead housing of 30 cm wall thickness to shield them against background radiation [2].

The high energy part of the γ -ray spectrum is characterized by a huge number of rather weak lines. After the comparison of spectra from 10 different reactions measured with the same experimental setup 160 lines could be identified as background arising either from the surrounding or from target fixing material. After this exclusion of background lines about 300 transitions were assigned to ^{154}Sm . A part of these are decays into excited levels.

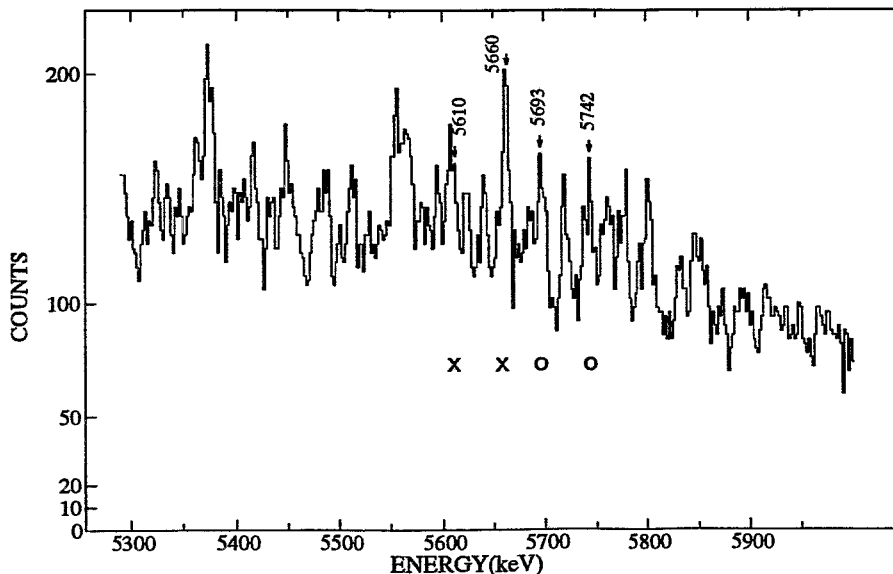


Fig.1 Gamma-ray spectrum measured with a CLUSTER detector at 130° in the $^{154}\text{Sm}(\gamma, \gamma')$ reaction. Two levels of 5693 and 5742 keV carry $0.26 \mu_N^2 B(M1)\uparrow$ strength. The groundstate transitions are marked by an o, and the corresponding transitions to the 2^+ state of ^{154}Sm at 82 keV are marked by an x.

We found 15 low spin levels which cannot be excited from the groundstate but can only be feeded from above. Although the assignment of observed γ -rays to indirect feeding transitions is problematic without a coincidence information the assignment is in progress nevertheless to provide an upper limit estimation of the $B(M1)\uparrow$ excitation strength. The lower limit takes into account only inelastic transitions to the 2_1^+ state of ^{154}Sm at 82 keV. To evaluate the energy dependence of the $B(M1)\uparrow$ excitation strength it is essential to know if an transition is either a groundstate transition or a transition feeding a certain excited level, thus representing a branch deexciting another level identified by a groundstate transition of higher energy.

In figure 1 a small part of the γ -ray spectrum recorded with the CLUSTER detector is shown. For the levels at 5693 and 5742 keV an excitation strength of together $B(M1)\uparrow \approx 0.26\mu_N^2$ was deduced. The value $0.26\mu_N^2$ measured in the (γ, γ') reaction agrees well with the integrated $B(M1)\uparrow$ strength of $0.3\mu_N^2/80$ keV at 5.7 MeV measured in a $^{154}\text{Sm}(p, p')$ experiment [3], which under the kinematics of ref. [3] is sensitive only to the spin part of the M1 excitation. The (γ, γ') reaction is driven by both the orbital and the spin part of the M1 operator while the (p, p') reaction proceeds predominantly through the strong spin-isospin effective nucleon-nucleon interaction [4].

¹ *Institut für Kern- und Teilchenphysik, TU Dresden and Institut für Kern- und Hadronenphysik, FZR*
² *Institut für Kernphysik, Technische Hochschule Darmstadt, 64289 Darmstadt*
³ *Institut für Kernphysik, Universität zu Köln, 50937 Köln*

References

- [1] J. Eberth, Prog. Part. Nucl. Phys. **28** (1992) 495
and S. Skoda et al., Annual Report 1993, **FZR-35** (1994) 88
- [2] S. Skoda et al., Annual Report 1994, **FZR-78** (1995) 66
- [3] D. Frekers et al., Phys. Lett. **B244** (1990) 178
- [4] A. Richter, Nucl. Phys. **A522** (1991) 139c

In-beam investigation and the structure of states in ^{113}Sn
(Preprint FZR-95 (1995))

Käubler, L., J. Döring, L. Funke, P. Kleinwächter, H. Prade, J. Reif, R. Schwengner, G. Winter, I.N. Vishnevski, M.J. Kirichenko, Yu.N. Lobach, I.P. Tkachuk, V.V. Trishin, M.F. Kudojarov, E.V. Kusmin, A.A. Pasternak, J. Blomqvist, L. Kostova

Abstract: The results of in-beam investigations of ^{113}Sn using the (p,n), (p,3n), (α ,n) and (α ,2n) reactions are summarized. Excited states have been identified until $E_x = 4715$ MeV and $J^\pi = (27/2^-)$. For a large number of levels mean lifetimes τ have been determined with the DSA method. For the $J^\pi = 25/2^+$ state at $E_x = 4059$ MeV, $\tau = 1.0(4)$ ns has been measured with the γ -RF method. The experimental results are compared with the predictions of shell-model calculations. Most of the positive-parity states may be considered as one- or three-quasiparticle neutron excitations of the $2d_{5/2}$, $1g_{7/2}$, $3s_{1/2}$ and $2d_{3/2}$ shells, the negative-parity states as the coupling of one $1h_{11/2}$ neutron to the two- or four-quasiparticle neutron excitations in the even-mass ^{112}Sn core. For the $25/2^+$ isomer the three-quasiparticle neutron configuration $\nu(h_{11/2}^2 g_{7/2}^{-1})$ has been proposed on the basis of a shell-model analysis using the mass formula formalism. The experimentally observed yrast states in $^{113}_{50}\text{Sn}_{63}$ are compared with the corresponding states in the valence-mirror nucleus $^{145}_{63}\text{Eu}_{82}$ giving remarkable similarities although the parameters for the shell-model calculations differ considerably. The analysis of nearest-neighbour spacing distributions of $5/2^+$ states in ^{113}Sn does not allow definite conclusions about regularity or chaos.

High-spin states in ^{109}Sn and their decay to the ground state
(Z. Phys. A 351 (1995) 123)

Käubler, L., H. Prade, J. Reif, R. Schwengner, G. Winter, H. Grawe, J. Heese, H. Kluge, K.-H. Maier, R. Schubart, K.-M. Spohr

Abstract: An extended level scheme of ^{109}Sn is presented showing high-spin states up to $E_x \approx 8$ MeV and spins up to $J^\pi = (41/2^+)$. Their decay to the $5/2^+$ ground state has been observed identifying a 12.8 keV $7/2^+ \rightarrow 5/2^+$ transition. A half-life of $T_{1/2} = 7(1)$ ns has been measured for the $17/2^+$ state at $E_x = 2114$ keV. The experimental data are compared with the predictions of shell-model calculations.

In-beam study of ^{109}Sn
(Physica Scripta T56 (1995) 266)

Käubler, L., H. Prade, J. Reif, R. Schwengner, G. Winter, H. Grawe, J. Heese, H. Kluge, K.-H. Maier, R. Schubart, K.-M. Spohr

Abstract: In-beam spectroscopic investigations of ^{109}Sn have been performed using the reactions $^{55}\text{Mn}(^{58}\text{Ni}, 3\text{pn})$ and $^{106}\text{Cd}(\alpha, \text{n})$ with $E_{^{58}\text{Ni}} = 240$ MeV and $E_\alpha = 23$ MeV, respectively. An extended level scheme of ^{109}Sn is presented showing high-spin states up to $E_x \approx 8$ MeV with $J^\pi = (41/2^+)$. The problem of the ^{109}Sn ground state has been solved identifying a 12.8 keV transition deexciting the $7/2^+$ state to the $5/2^+$ g.s. A half-life of $T_{1/2} = 7(1)$ ns has been measured for the $17/2^+$ state at $E_x = 2114$ keV. The experimental data are compared with the predictions of shell-model calculations.

The proton $g_{9/2}$ isomer in the $N = 50$ nucleus ^{87}Rb and M2 transition rates in $^{85,87}\text{Rb}$
(Z. Phys. A 352 (1995) 127)

Käubler, L., Ch. Protophristov, M. Michailova, J. Reif, W. Andrejtscheff, L. Funke, L. Kostova, H. Prade, R. Schwengner, G. Winter

Abstract: Low-lying states of the $N = 50$ nucleus ^{87}Rb have been investigated in the (α, α') reaction measuring $\gamma\gamma$ - and delayed γ -rf-coincidences. A half-life of $T_{1/2} = 6(1)$ ns was obtained for the level at 1578.1 keV. This experimental result confirms the $9/2^+$ assignment and the proton $1g_{9/2}$ single-particle character of this state. Experimental M2 transition strengths in $^{85,87}\text{Rb}$ are compared with predictions of the shell model and the particle-core coupling model.

Break-up of the $N = 50$ core in $^{89}\text{Y}_{50}$
(Nucl. Phys. A 587 (1995) 449)

Reif, J., G. Winter, R. Schwengner, H. Prade, L. Käubler

Abstract: The semi-magic nucleus $^{89}\text{Y}_{50}$ has been studied in the framework of the spherical shell model. Relative to a hypothetical ^{66}Ni core the expanded configuration space $(0f_{5/2}, 1p_{3/2}, 1p_{1/2}, 0g_{9/2})$ and $(1p_{1/2}, 0g_{9/2}, 1d_{5/2}, 0g_{7/2})$ for protons and neutrons, respectively, has been considered. The results, both for the excitation energies and electromagnetic transition probabilities, suggest for the positive-parity states above 4.5 MeV with $17/2 \leq I \leq 23/2$ significant admixtures of the neutron $[(0g_{9/2})^{-1}(1d_{5/2})]$ excitation coupled to the odd proton occupying the $0g_{9/2}$ orbital. The calculations predict that the experimentally observed states above 7.2 MeV with $23/2 \leq I \leq 31/2$ are generated by the additional excitation of one proton to the $0g_{9/2}$ orbital resulting in a parity alteration. The strength of the electric dipole transitions connecting the levels of the two proposed high-spin structures might be explained by small contributions of the neutron $0h_{11/2}$ excitation to the involved wave functions.

Neutron-core excitations in $^{86}\text{Kr}_{50}$
(Physica Scripta T56 (1995) 303)

Reif, J., G. Winter, R. Schwengner, H. Prade, H. Grawe, R. Schubart

Abstract: Shell-model calculations for the $N = 50$ nucleus ^{86}Kr are presented and compared to results of recent in-beam experiments. Two model spaces are considered: a pure proton configuration space containing the $0f_{5/2}$, $1p_{3/2}$, $1p_{1/2}$, $0g_{9/2}$ orbitals and a model space including additionally the particle-hole excitation generated by one neutron lifted from the $0g_{9/2}$ orbital across the shell gap to the $1d_{5/2}$ orbital. The predictions of the shell-model using various sets of residual interactions and based on pure proton excitations are comparable with the experimental findings for the states of positive parity below 4 MeV and for the negative-parity states with spins up to 7. The inclusion of neutron-core excitations causes an improved agreement between experimental and calculated level energies for the positive-parity yrast states with spins $7\hbar$, $9\hbar$ and $10\hbar$. The interpretation of neutron-core excited high-spin states is supported by the comparison of the level structure of $^{86}\text{Kr}_{50}$ to the experimental levels of the valence-mirror nucleus $^{64}\text{Ni}_{36}$.

In-beam spectroscopy and shell model structure of the neutron deficient ^{103}In and $^{100,102}\text{Cd}$

(Physica Scripta T56 (1995) 311)

Schubart, R., H. Grawe, M. Górska, J.B. Fitzgerald, J. Heese, H. Kluge, K.H. Maier, M. Rejmund, M. Schramm, D. Seweryniak, K. Spohr, L. Käubler

Abstract: The γ -decay of the neutron deficient nuclei ^{103}In and $^{100,102}\text{Cd}$ has been studied following the reactions $^{58}\text{Ni} + ^{50}\text{Cr}$ and $^{58}\text{Ni} + ^{46,48}\text{Ti}$ at 250 MeV and 230 MeV bombarding energy of the ^{58}Ni beam, respectively. Evaporation neutrons and charged particles were measured in coincidence with prompt and delayed γ -rays with the multidetector array OSIRIS. To investigate the decay of the $I^\pi = 8^+$ isomers of $^{100,102}\text{Cd}$ a recoil catcher setup inside OSIRIS was used. Six new γ -ray transitions of ^{100}Cd and four of ^{102}Cd with intensities of 1-10 % of the main γ -ray cascades were found. Two new states of ^{100}Cd were established and firm spin-parity assignments were made to all states below the isomer. These new states were identified as the 4^- and the 6^- members of the proton $\pi g_{9/2}^{-2}$ multiplet. The experimental states of ^{103}In and of $^{100,102}\text{Cd}$ are compared to shell model predictions in the $\pi(p_{1/2}, g_{9/2}) \nu(d_{5/2}, g_{7/2}, s_{1/2}, d_{3/2}, h_{11/2})$ configuration space.

Particle excitations and collectivity in the $N=48$ nuclei ^{83}Br and ^{85}Rb
(Nucl. Phys. A 584 (1995) 159)

Schwengner, R., G. Winter, J. Reif, H. Prade, L. Käubler, R. Wirowski, N. Nicolay, S. Albers, S. Eßer, P. von Brentano, W. Andrejtscheff

Abstract: Excited states of the nuclei ^{83}Br and ^{85}Rb were populated in the reactions $^{82}\text{Se}(^7\text{Li}, \alpha 2n)$ and $^{82}\text{Se}(^7\text{Li}, 4n)$, respectively, using the ^7Li beams of the FN tandem accelerator in Cologne ($E = 32$ MeV) and of the 120 cm cyclotron in Rossendorf ($E = 35$ MeV). Gamma-gamma-particle coincidences were measured with six Ge and fourteen Si detectors installed at the detector array Cologne OSIRIS CUBE. This technique enabled a reaction channel selection. Multipole orders of the γ -rays were derived from directional correlations of coincident γ -rays were derived from directional correlations of coincident γ -rays and from angular distributions. Mean lifetimes were deduced for seven levels in ^{83}Br and two levels in ^{85}Rb using the Doppler-shift-attenuation method. The level scheme of ^{83}Br has been extended up to $(21/2^+)$ and $15/2^-$ states. In ^{85}Rb a level sequence built on the ground state has been established up to $15/2^{(-)}$ and a new cascade of fast M1 transitions starting with a $17/2^{(-)}$ state at 3198.2 keV has been found. Furthermore, several medium-spin states have been newly introduced. The level sequences in both nuclei have been interpreted in terms of the shell model. The calculations performed in the model space $\pi(0g_{9/2}, 1p_{1/2}, 1p_{3/2}, 0f_{5/2}) \nu(0g_{9/2}, 1p_{1/2})$ reproduce single-particle characteristics as well as collective properties of the level sequences.

4 Experimental Heavy Ion Physics

Two Modes of IMF Emission Accompanying Fission in the Reaction ${}^7\text{Li}(43\text{A MeV}) + {}^{232}\text{Th}^{\text{B}}$

C.-M. HERBACH, H.-G. ORTLEPP¹, P. GIPPNER¹, K.D. SCHILLING, W. WAGNER¹

Heavy hot nuclei with excitation energies up to 300 MeV have been produced by incomplete fusion in the reaction ${}^7\text{Li}(43\text{A MeV}) + {}^{232}\text{Th}$. The binary fission was identified as the dominating decay channel, which is frequently accompanied by the emission of light charged particles (LCP) and fragments of intermediate masses (IMF) [1]. Our exclusive measurement of LCP and IMF in coincidence with both fission fragments (FF) allowed to determine the linear momentum transfer (LMT) from the projectile to the composite system [2]. Within the frame of the massive transfer approximation, the induced excitation energy can be estimated even for threefold events.

The kinetic energy of the IMF and their angular distribution with respect to the fission axis are observables, which are closely associated with the origin of IMF emission [3]: For example, the velocity of charged particles emitted from a spherical compound nucleus corresponds to the Coulomb repulsion of the total charge. The accelerating Coulomb potential is decreased, if the emission occurs from a strongly deformed fissioning system near the scission point.

In a first step of the event-by-event analysis of the threefold coincidences, from the measured velocity vectors of the three fragments as well as from the IMF mass - derived by means of the time-of-flight versus energy analysis - the velocity of the composite system has been determined considering the momentum conservation. For most of the events, the charge of the IMF (here $Z=3-8$) was measured directly from the Bragg-peak signal. By using an iterative procedure, the energy losses within the target layer and the detector foils have been corrected. The same procedure has been utilized to analyse the measured FF + FF + alpha coincidences.

The velocity spectra relative to the fissioning system are shown in fig. 1. Both spectra can be divided into two groups with relative velocities below and above $v = 2.5$ cm/ns. The component with the higher kinetic energy corresponds to a mean value of about 3.4 cm/ns and is associated with the emission from the compound nucleus. The yields of both groups are displayed in dependence on the LMT (Fig. 2). Within the region from intermediate to large LMT, a strong rise is visible for the faster components. These particles escape at an early stage of the deexcitation cascade and, consequently, their emission probability increases with the larger amount of induced excitation energy. The constant behaviour below the threshold at $E=150$ MeV appears to be generated by a small yield of additional IMF contributions at peripheral collisions. The yields of the events with smaller relative velocities ($v < 2.5$ cm/ns) show a

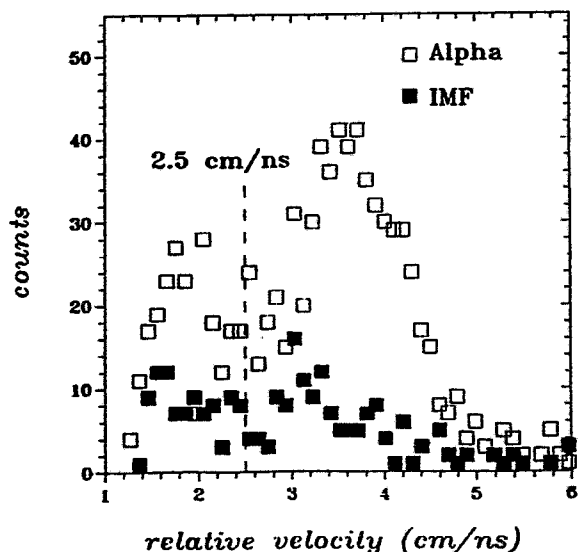


Fig. 1 Relative velocity of the third particle with respect to the fissioning system

lower increase. Taking into account that the temperature at the scission point compared to the induced excitation energy is strongly reduced [4], the assumption about the emission of the lower-energy alphas and IMF from a later stage of the fission process is supported.

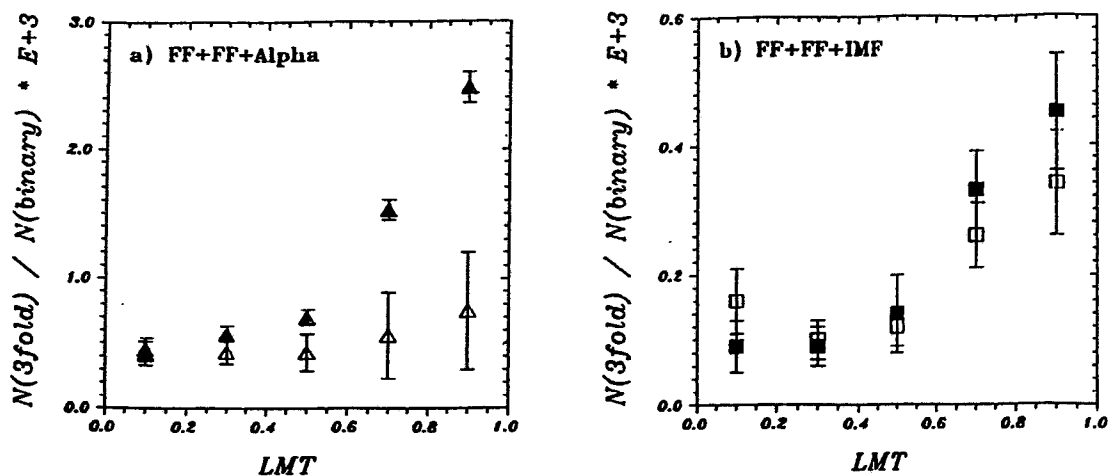


Fig. 2 Yields of threefold events relative to the number of binary fission fragment coincidences. The third particle is an alpha (a) or an IMF (b), the open and closed symbols indicate relative velocities $v < 2.5$ cm/ns and $v > 2.5$ cm/ns, respectively.

It should be expected that the IMF emission before or during the transition from saddle to scission affects the formation of the fragments. Indeed, by comparison with the width of the fission fragment mass distribution $FWHM = 41.5 \pm 1.5$ amu observed for the binary events, the corresponding kinematic analysis results in the smaller values of $FWHM = 34 \pm 3$ and $FWHM = 38 \pm 3$ amu for IMF accompanied fission of the modes with $v > 2.5$ cm/ns and $v < 2.5$ cm/ns, respectively. The more symmetric fission component indicates the formation of the fission fragments at lower temperatures [5].

Further investigations will be based on an amount of experimental data [6], which is increased by a factor of more than 100, and will allow to verify the results in a more detailed analysis that will also include the model-independent mass determination from TOF-E also for the fission fragments.

¹ Institut für Kern- und Hadronenphysik, FZR and Joint Institute for Nuclear Research, Dubna

References

- [1] A.A. Aleksandrov et al., Proc. Fifth Int. Conf. on Nucleus-Nucleus Collisions, Taormina, Italy (1994): Nucl. Phys. A583 (1995) 465c
- [2] C.-M. Herbach et al., Annual Report 1994, FZR-78 (1995) 75
- [3] D.E. Fields et al., Phys. Rev. Lett. 69 (1992) 3713
- [4] D. Hilscher, H. Rossner, Ann. Phys. Fr. 17 (1992) 471
- [5] M.G. Itkis et al., Sov. J. Part. Nucl. 19 (1988) 701
- [6] H.-G. Orltepp et al., contribution to this report

Fragment Masses and Total Kinetic Energies in Two-Body Decays of Hot Heavy Nuclei Produced in the Reaction $^{14}\text{N}(34 \text{ AMeV}) + ^{197}\text{Au}^{\text{B}}$

W. WAGNER¹, H.-G. ORTLEPP¹, C.-M. HERBACH

The decay of hot heavy nuclei produced by the asymmetric reaction $^{14}\text{N}(34 \text{ AMeV}) + ^{197}\text{Au}$ has been measured using the FOBOS array [1].

At nearly maximum linear momentum transfer (LMT) due to incomplete fusion the equilibrated composite nuclear system can reach excitation energies (E^*) up to about 400 MeV corresponding to temperatures of about 4.5 MeV. At such E^* the decay of heavy nuclei is mainly governed by an interplay between the evaporation of light particles (n, $^1,^2,^3\text{H}$, $^3,^4,^6\text{He}$, etc.), the less probable emission of more complex fragments of intermediate mass ($M_{\text{IMF}} \leq 20$) and nuclear fission. Although the E^* are still below the barrier for the multifragmentation, decays into three fragments are already possible. However, the predominant amount of the reaction cross-section is provided by binary decays.

Using the TOF-E-method the masses (M) and momentum vectors (\vec{p}) of both fragments (F) have been determined independently, like earlier for the reaction $^7\text{Li}(43 \text{ AMeV}) + ^{232}\text{Th}$ [2]. By checking the sums ΣM_F and $\Sigma \vec{p}_F$ binary decays with $\text{LMT} \approx 0.8$ were selected. Their M-TKE (total kinetic energy) distribution (fig. 1) extends to very asymmetric mass splits. These M_F fill the gap between fission and evaporation products existing at low E^* .

It is, therefore, an interesting question, in which mass region the presumedly different decay mechanisms of evaporation and fission superimpose or unify [3].

When nuclear fission is treated dynamically as a relatively small [4] overdamped collective motion over a saddle in the landscape of the potential energy to a deformed scission configuration, the evaporation process is characterized by an escape of particles from the surface of the hot nucleus proceeding statistically. The characteristic emission time depends on the level density at $E^* - B_C$, where B_C , in the case of charged particles, denotes the Coulomb barrier.

The TKE is eventually defined by the Coulomb repulsion between the binary fragments in the exit channel. For fission it has been parametrized by Viola [5]. In an evaporation process the TKE of the

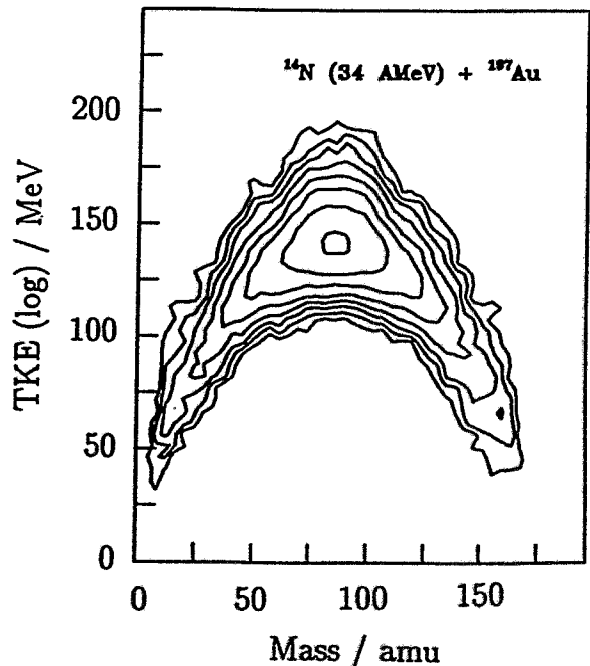


Fig. 1 M-TKE contour plot for the reaction $^{14}\text{N}(34 \text{ AMeV}) + ^{197}\text{Au}$ at $\text{LMT} \approx 0.8$. (in a logarithmic scale)

binary partners, the light charged fragment (IMF) emitted and the remaining evaporation residue (ER), is governed by the B_C , and the energy spectrum of the evaporated particles can be considerably well described by a Maxwell distribution.

In fig. 2 we drew the most probable TKE for 5 amu broad mass bins, as resulting from the distribution given in fig. 1, versus the mass number of the light fragment A_L . The shaded area corresponds to the dispersion (σ) of the TKE. For comparison the TKE according to Viola [5] and the B_C defined by Bass [6] are shown.

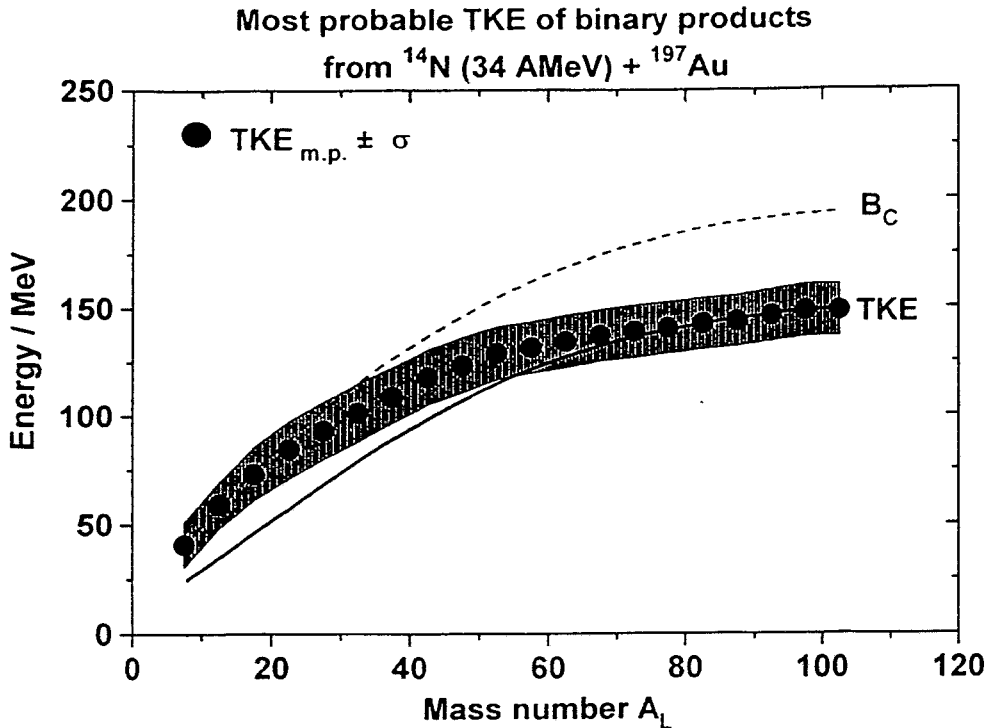


Fig. 2 Most probable TKE versus the mass number of the light fragment (full circles).

One observes a smooth transition from a fission-like to an evaporation-like behaviour. A first conclusion can be made considering energy dissipation. With increasing asymmetry of the fragment mass split the collective motion to scission becomes less damped as has been predicted earlier in ref. [3].

¹ *Institut für Kern- und Hadronenphysik, FZR and Joint Institute for Nuclear Research, Dubna*

References

- [1] A.A. Aleksandrov et al., Annual Report 1994, FZR-78 (1995) 77
- [2] C.-M. Herbach, Proc. of the FOBOS workshop '94, Cracow, Poland, 1994 (Ed. W. Wagner) Report FZR-65 (1995)
- [3] L.G. Moretto and G.J. Wozniak, Prog. in Part. and Nucl. Phys., vol. 21 (Ed. A. Faessler) Pergamon Press (1988) 401
- [4] D. Hilscher and H. Rossner, Ann. Phys. Fr. 17 (1992) 471
- [5] V.E. Viola et al., Phys. Rev. C31 (1985) 1550
- [6] R. Bass, "Nuclear Reactions with Heavy Ions", Springer-Verlag, Berlin, Heidelberg, New York (1980)

Pre- and Post-Scission Components of Light Charged Particles Accompanying Fission in the Reaction $^{14}\text{N}(34 \text{ AMeV}) + ^{197}\text{Au}^{\text{B}}$

H.-G. ORTLEPP¹, P. GIPPNER¹, C.-M. HERBACH, D.V. KAMANIN¹, A. MATTHIES¹,
K.D. SCHILLING, W. WAGNER¹

Experiments presently being carried out at the FOBOS array [1] are directed to get new data about the fission of hot nuclei. The capability of this detector system to determine the mass of both fission fragments (FF) and their total kinetic energy (TKE) without any kinematical assumption [2] as well as the relatively large solid angle covered ($\approx 5 \text{ sr}$ for FF and $\approx 4 \text{ sr}$ for light charged particles (LCP) [3]) make it ideally suited for the study of FF-LCP correlations.

The decomposition of the LCP spectra into the pre- and the post-scission emitted components allows to determine the portion of excitation energy remaining in the FF and to derive the scission time [4, 5, 6]. The latter is a key quantity for the understanding of the dynamics of the fission process. The LCP provide an interesting alternative to neutrons widely used for this purpose [7], if the detector efficiency is large enough to compensate for the smaller LCP yields. To investigate the role of the mass-asymmetry degree of freedom in the collective motion of the hot system from equilibrium to scission, one has to extend this procedure to very asymmetric FF mass splits.

We used the relatively light ^{14}N projectiles to be sure that all binary events observed are due to fission of an equilibrated composite system. Thus, fast fission can be excluded and fragments heavier than ^{14}N cannot be produced from deep inelastic collisions.

Since several hundred parameters are involved, the full data analysis requires a large effort. In this report, only preliminary results based on a small amount of the data are presented.

The spectra of α -particles measured at backward angles are shown in fig. 1.

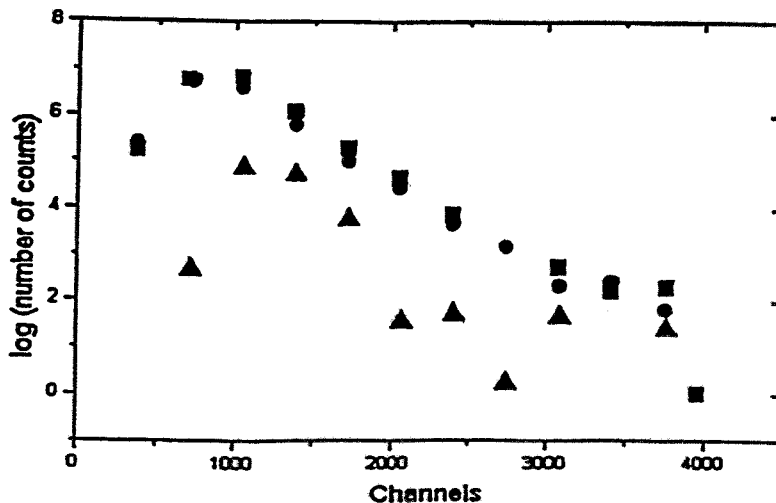


Fig. 1 α -particle spectra and their difference spectrum (for symbols see text)

The first spectrum (squares) contains coincidences with such FF, where one fragment was recorded in nearly the same direction like the α -particles. In the second spectrum (circles), the α -particles were emitted nearly perpendicular to the fission axis. Most particles of both spectra are due to the emission from the hot composite system, but the difference of the spectra (triangles) is consistent with the emission from those fragments moving in the direction of the α -particle detector. The other α -particle components emitted from FF moving in the opposite or perpendicular directions have much lower energies and do not reach the FOBOS scintillator shell, but are stopped within the ionization chambers.

In tab. 1, preliminary α -particle yields derived by use of this simple subtraction procedure are compared with results of ref. [6]. The final analysis presently in progress will be based on a three-source fit considering different FF mass splits.

Table 1 α -particle yields per fission (extrapolated to 4π sr)

$\langle E^* \rangle / \text{MeV}$	α_{pre}	α_{post}	α_{pre} [6]	α_{post} [6]
250	0.36(12)	0.09(4)	0.4	0.08

¹ *Institut für Kern- und Hadronenphysik, FZR and Joint Institute for Nuclear Research, Dubna*

References

- [1] H.-G. Ortlepp et al., Proc. Int. School-Seminar on Heavy-Ion Physics, Dubna, Russia, 1993, Report JINR E7-93-274, vol. 2 (1993) 466
- [2] W. Wagner et al., contribution to this report
- [3] Proc. of the FOBOS workshop '94, Cracow, Poland, 1994 (Ed. W. Wagner) Report FZR-65 (1995)
- [4] K. Siwek-Wilczynska et al., Phys. Rev. C48 (1993) 228
- [5] M. Gui et al., Phys. Rev. C48 (1993) 1791
- [6] Y. Lou et al., Nucl. Phys. A581 (1995) 373
- [7] D. Hilscher, H. Rossner, Ann. Phys. Fr. 17 (1992) 471

Study of the Reaction ^{14}N (53 AMeV) + ^{197}Au by Simultaneous Registration of Charged Products from Protons up to Evaporation Residues with the FOBOS Array^B

A.A. ALEKSANDROV¹, I.A. ALEKSANDROVA¹, L. DIETTERLE², V.N. DORONIN³,
S. DSHEMUCHADSE, P. GIPPNER², C.-M. HERBACH, D.V. KAMANIN²,
A. MATTHIES², H.-G. ORTLEPP², YU.E. PENIONZHKEVICH³, G. RENZ²,
K.D. SCHILLING, D.I. SHISHKIN³, O.V. STREKALOVSKIY³, I.P. TSURIN³,
C. UMLAUF², D.V. VAKATOV³, W. WAGNER², M. WILPERT⁴, V.E. ZHUCHKO³

The investigation of the fission of hot heavy nuclei after incomplete fusion has been continued at the 4π array FOBOS by studying the reaction $^{14}\text{N} + ^{197}\text{Au}$ at the higher beam energy of 53 AMeV (cf. 34 AMeV in [1]).

The measurements were performed at the U-400M cyclotron of the FLNR in Dubna using a $500 \mu\text{g}/\text{cm}^2$ thick self-supporting gold target. Altogether, 23 gas-filled modules of the FOBOS array [2] - each consisting of a position-sensitive double-grid avalanche counter and a Bragg ionization chamber - as well as an additional position-sensitive avalanche counter (area $70 \times 70 \text{ mm}^2$, polar angles $\theta = 9^\circ - 19^\circ$) for the detection of heavy residues were operated. The light charged particles were recorded by 161 CsI(Tl) counters of the FOBOS scintillator shell [3]. Two further transmission avalanche counters near the target supplied the timing reference signals for the TOF measurements.

The goal of the experiment was to measure the correlations between different charged reaction products, such as light charged particles (LCP), intermediate-mass fragments (IMF), fission fragments (FF) and - in particular - heavy residues (HR). For this purpose, coincidences between FF and IMF, FF and LCP, HR and LCP, as well as HR and IMF have been recorded. Composite systems with excitation energies up to $E^* = 600 \text{ MeV}$ could be produced.

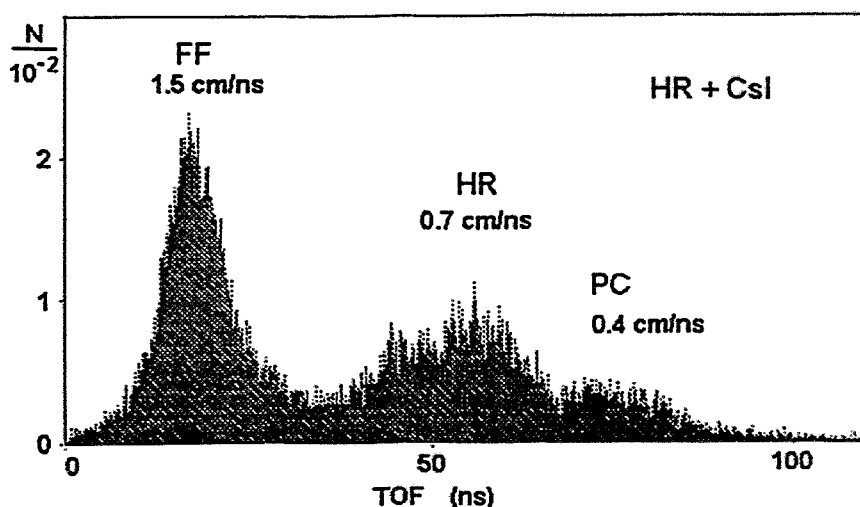


Fig. 1 TOF spectrum of the HR detector in coincidence with evaporated particles (LCP) (for explanation see text)

The de-excitation of a hot heavy nucleus always includes LCP and neutron emission. The higher the E^* , the more complex particles can be evaporated removing a considerable

part of energy and mass - thus definitely changing the subsequent decay probabilities. Finally, a remnant with strongly reduced fissility can survive. As already established in [4], enhanced light particle emission will lower the fission probability and necessarily lead to an enlarged evaporation residue formation. The simultaneous measurement of all above mentioned coincidences is, therefore, needed to draw definite conclusions on the detailed de-excitation mechanism and to enable the comparison with dynamical calculations.

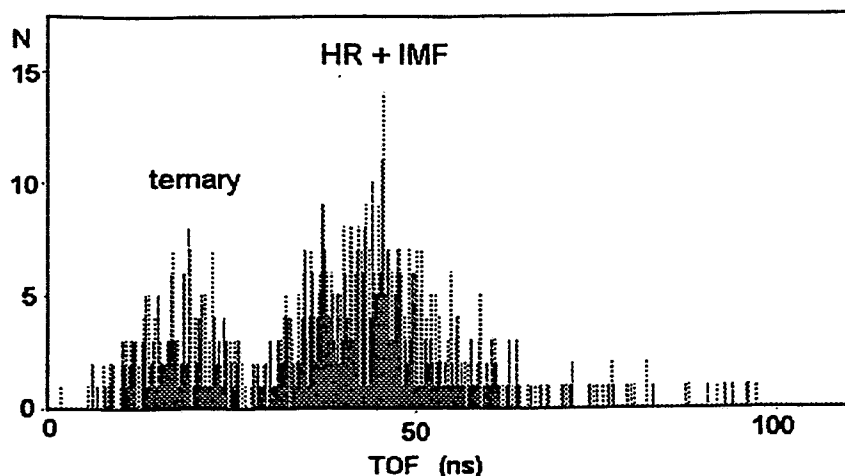


Fig. 2 TOF spectrum of the HR detector in coincidence with an IMF.

According to our preliminary analysis [5], the HR turn out to be mainly produced by a binary decay of the composite system at excitation energies E^* below about 2 AMeV. This is demonstrated in figs. 1 and 2, where coincidences of the HR detector with LCP respective IMF are shown. The typical structure at the velocity $v = 0.7$ cm/ns can be connected with the occurrence of the heavy evaporation residues (HR) and the structure at $v = 0.4$ cm/ns with target-like recoils resulting from peripheral collisions (PC). In this way, the enhanced emission of more complex fragments (IMF) seems to be associated with the production of heavy residues. The further analysis is in progress.

¹ *Moscow Engineering Physics Institute, Moscow, Russia*

² *Institut für Kern- und Hadronenphysik, FZR and Joint Institute for Nuclear Research, Dubna*

³ *Joint Institute for Nuclear Research, Dubna, Russia*

⁴ *Hahn-Meitner-Institut, Berlin, Germany*

References

- [1] A.A. Aleksandrov et al., Annual Report 1994, FZR-78 (1995) 77
- [2] H.-G. Ortlepp et al., Proc. Int. School-Seminar on Heavy Ion Physics, JINR Dubna, Russia, vol. 2 (1993) 466
- [3] W. Wagner et al., Annual Report 1994, FZR-78 (1995) 117
- [4] D. Hilscher, H. Rossner, Ann. Phys. Fr. 17 (1992) 471
- [5] W. Wagner et al., Preprint FZR-104 (1995)

Combined Dynamical Statistical Model Calculations for Hot Fissioning Systems Studied at the 4π -Array FOBOS^B

R.S. KURMANOV¹, L.A. LITNEVSKY¹,
H.-G. ORTLEPP², W. WAGNER²

We performed calculations for symmetric fission of hot nuclei in the framework of the so called Combined Dynamical Statistical Model (CDSM) [1,2]. The dynamics is described by a Langevin equation in the Smoluchowski (overdamped) limit for the deformation coordinate. The calculations have been executed with a strong universal coordinate dependence of the reduced friction parameter proposed in ref. [1].

Using as an example the induced fission of the compound system ^{205}Pb , the following quantities have been investigated:

- the pre-scission γ -, neutron, proton, deuteron and α -particle multiplicities
- the energy spectra of these particles
- the fission and evaporation residue production probabilities
- the multiple-chance fission distributions
- the fission time distributions

Figure (1) shows the calculated average pre-scission proton (p_{pre}) and α -particle (α_{pre}) multiplicities and the fission probabilities (P_f) for ^{205}Pb versus the total excitation energy (E_{tot}^*) and for different angular momenta (L).

Hot nuclei in the mass region of $A \approx 200$ were produced by the reactions ^{14}N (34 and 52.5 AMeV) + ^{197}Au . The coincident emission of light charged particles with binary decays of the equilibrated composite system has been studied at the 4π -array FOBOS [3]. For a first comparison, preliminary values for the total and post-scission emission of protons and α -particles per fission within two bins of the excitation energy ($\langle E^* \rangle$) are given in table (1).

We plan the further development of the CDSM by inclusion of the pre-scission cluster emission and of the post-scission emission of light particles. More difficult, but very interesting, is the investigation of mass-asymmetric fission.

Table 1 Total and post-scission yields per fission of light charged particles measured for the reaction ^{14}N (34 AMeV) + ^{197}Au .

$\langle E^* \rangle / \text{MeV}$	p_{tot}	α_{tot}	p_{post}	α_{post}
80	0.18(4)	0.02(2)	–	–
250	1.01(12)	0.45(8)	0.06(4)	0.09(4)

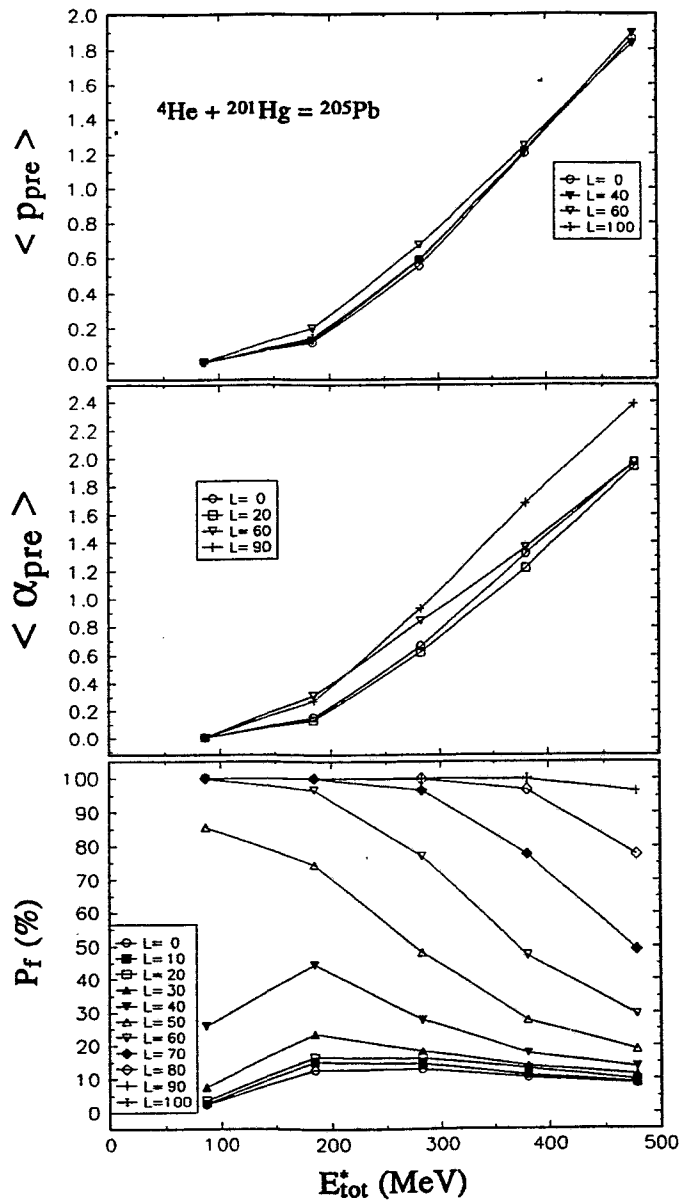


Fig. 1 Average pre-scission proton and α -particle multiplicities and the fission probability P_f versus the excitation energy E_{tot}^* for different angular momenta L .

¹ Omsk State Railway Academy, Omsk, Russia

² Institut für Kern- und Hadronenphysik, FZR and Joint Institute for Nuclear Research, Dubna

References

- [1] P. Fröbrich, I.I. Gontchar and N.D. Mavlitov, Nucl. Phys. **A556** (1993) 281
- [2] I.I. Gontchar, Fiz. El. Chas. At. Yad. **26** (1995) 932
- [3] W. Wagner, H.-G. Ortlepp, C.-M. Herbach et al., **FZR-104** (1995)

Spontaneous Fission of ^{252}Cf Examined at the FOBOS Spectrometer^B

YU.V. PYATKOV¹, A.A. ALEKSANDROV¹, I.A. ALEKSANDROVA¹,
S. DSHEMUCHADSE, P. GIPPNER², C.-M. HERBACH, D.V. KAMANIN²,
A. MATTHIES², H.-G. ORTLEPP², V.V. PASHKEVICH³, YU.E. PENIONZHKEVICH³,
G. RENZ², K.D. SCHILLING, O.V. STREKALOVSKIJ³, V.G. TISHCHENKO¹,
A.V. UNZHAKOVA³, D.V. VAKATOV³, W. WAGNER²

Recent investigations of the spontaneously fissioning ^{252}Cf provide new nontrivial results concerning two extreme situations in nuclear fission : (i) the true cold fission [1] and (ii) the fission out of hyperdeformed states of the fissioning system [2]. The success of these investigations is due to the application of highly efficient experimental set-ups.

The present experiment has been performed with two modules of the FOBOS array [3] each consisting of a position-sensitive double-grid avalanche counter (DGAC) and a Bragg ionization chamber (BIC). The velocity of the fission fragments (ff) has been determined using a microchannel-plate start detector [4] and the DGAC stop signals (TOF paths about 50 cm). The ff energies were measured in the BIC's. From the velocity and energy measurements, the mass and the momentum values have been deduced for both fragments of each correlated pair. The momentum conservation has been verified event-wise within a given interval determined by the resolution and the neutron emission. Events not satisfying the selection rule were rejected. In this way, the peak-to-valley ratio in the mass distributions increased from 34 to 52. Thus, the combined TOF-TOF and TOF-E analysis yields a twice better ratio than the twin-ionization chamber method [1]. A total number of 1.5×10^7 ff pairs satisfied the above selection rule.

The interesting peculiarity of the observed total kinetic energy-mass (TKE-M) distributions consists in a remarkable difference of the fragment mass yields at fixed excitation energies $E^* = Q - \text{TKE}$ (Q : reaction Q value) between the spontaneous fission of ^{252}Cf and the thermal-neutron induced fission of (close by mass) ^{249}Cf . Fig. 1 shows a cut of the two-dimensional TKE-M distributions, which reveal a "bump" for high TKE values near the mass $M=118/132$ amu region for $^{250}\text{Cf}^*$. The availability of two-dimensional TKE-M matrices for these two isotopes extended fundamentally the possibilities of the present analysis in comparison with ref. [5].

The observed peculiarity can - apparently - not be explained by dissipation effects as it is suggested in ref. [6] by a comparative analysis of the $\overline{TK E}(M)$ dependence for spontaneous and induced fission. The difference in the behaviour of this dependence is connected - as mentioned above - with the presence of a two-dimensional "bump" especially in the region of cold fission, where the dissipation cannot be large by definition. The feature just considered might be the manifestation of some fission mode, which is realized in $^{250}\text{Cf}^*$ and suppressed in ^{252}Cf . But, special calculations of the potential energy surfaces for the two isotopes considered do not support such a hypothesis.

The observed difference may be explained within the frame of a two-cluster mechanism for the formation of the fission mode [7] and the phenomenologic scission criterion derived from the well-known $\overline{TK E}(M)$ dependence. The fission fragments in the region of $M=132$ amu (heavy cluster) are preferentially formed at high TKE values, i.e. in compact scission configurations - whereas the fragments in the vicinity of $M=82$ amu (light cluster) originate from elongated configurations. Thus, a "scission wave" [7] moves from

the heavy cluster to the light one according to the elongation of the fissioning nucleus on the descent to scission. In spontaneous fission, consequently, the shape of the nucleus at the barrier-penetration point corresponds to the state of the "scission wave" with a maximum at the $M=140/112$ amu region. That means that the state, where high TKE fragments with M around 132 amu should be generated, turns out to be a "transient" one in the off-shell phase. Quantitative estimates within the scope of the proposed model are in progress.

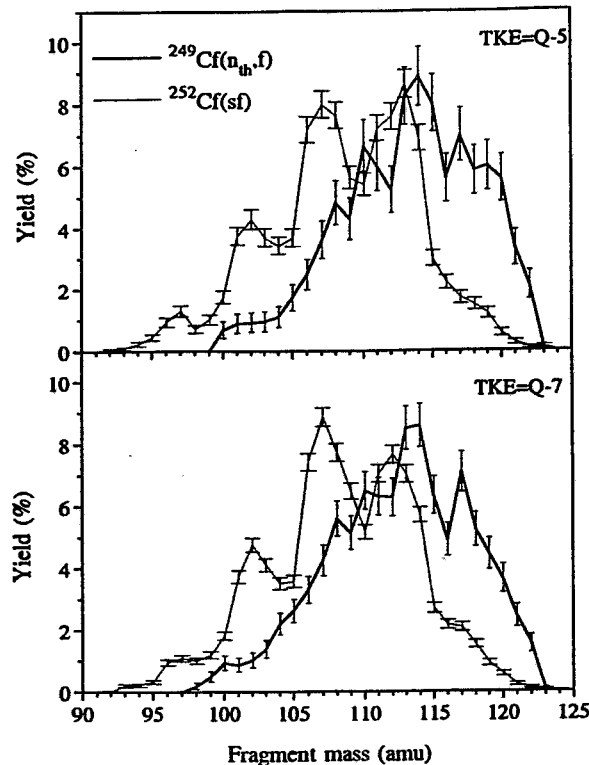


Fig. 1 Comparison of fragment mass spectra at fixed excitation energies for $^{252}\text{Cf}(sf)$ and $^{249}\text{Cf}(n_{th}, f)$

¹ Moscow Engineering Physics Institute, Moscow, Russia

² Institut für Kern- und Hadronenphysik, FZR and Joint Institute for Nuclear Research, Dubna

³ Joint Institute for Nuclear Research, Dubna, Russia

References

- [1] F. Gönnerwein, Proc. XIII Meeting of Nuclear Physics in Memory of Prof. G.N. Smirenkin (in press)
- [2] G.M. Ter-Akopyan, J. Hamilton, Yu.Ts. Oganessian et al., Izv. RAN, ser. fiz. (in press)
- [3] H.G. Ortlepp et al., Proc. Int. School-Seminar on Heavy-Ion Physics, JINR Dubna, Russia, E7-63-274, vol. 2 (1993) 466
- [4] S.A. Podshibyakin, A.I. Slyusarenko, A.N. Shemetov et al., PTE 6 (1988) 78
- [5] Yu.V. Pyatkov, R.A. Shekhmamet'ev, A.I. Slyusarenko, JINR Rapid Comm. N2 (58) (1993) 98
- [6] H. Märten, Proc. Int. Conf. on Dynamical Aspects of Nuclear Fission, Smolenice, Czech. (1991) p. 47
- [7] Yu.V. Pyatkov, R.A. Shekhmamet'ev, Phys. of Atomic Nuclei 57 (1994) 1182

Phase Space Distributions of Charged Particles from Central Collisions of Au+Au between 250 and 1050 MeV per nucleon^B

R. KOTTE, J. BIEGANSKY, J. MÖSNER, W. NEUBERT, AND D. WOHLFARTH

Charged particles produced in central Au + Au collisions between 250 and 1050 A·MeV projectile energy have been measured at the SIS at GSI by the FOPI collaboration using the 4 π detector system. The detector acceptance for these velocity distributions is governed by the polar angle range of the forward time-of-flight wall of $1^\circ < \theta_{lab} < 30^\circ$. Approximately equal impact parameter distributions (following from comparison with IQMD calculations [1] using a hard equation of state and momentum dependent forces) with averaged values $\langle b \rangle / b_{max} \simeq 0.13 - 0.14$ and r.m.s. widths of $\sigma(b)/b_{max} \simeq 0.06 - 0.07$ are selected by cutting on high values ER5 of the ratio $E_{rat} = \sum_i E_{\perp i} / \sum_i E_{\parallel i}$ of total transverse and longitudinal energies [2] in the forward c.m. hemisphere (typically

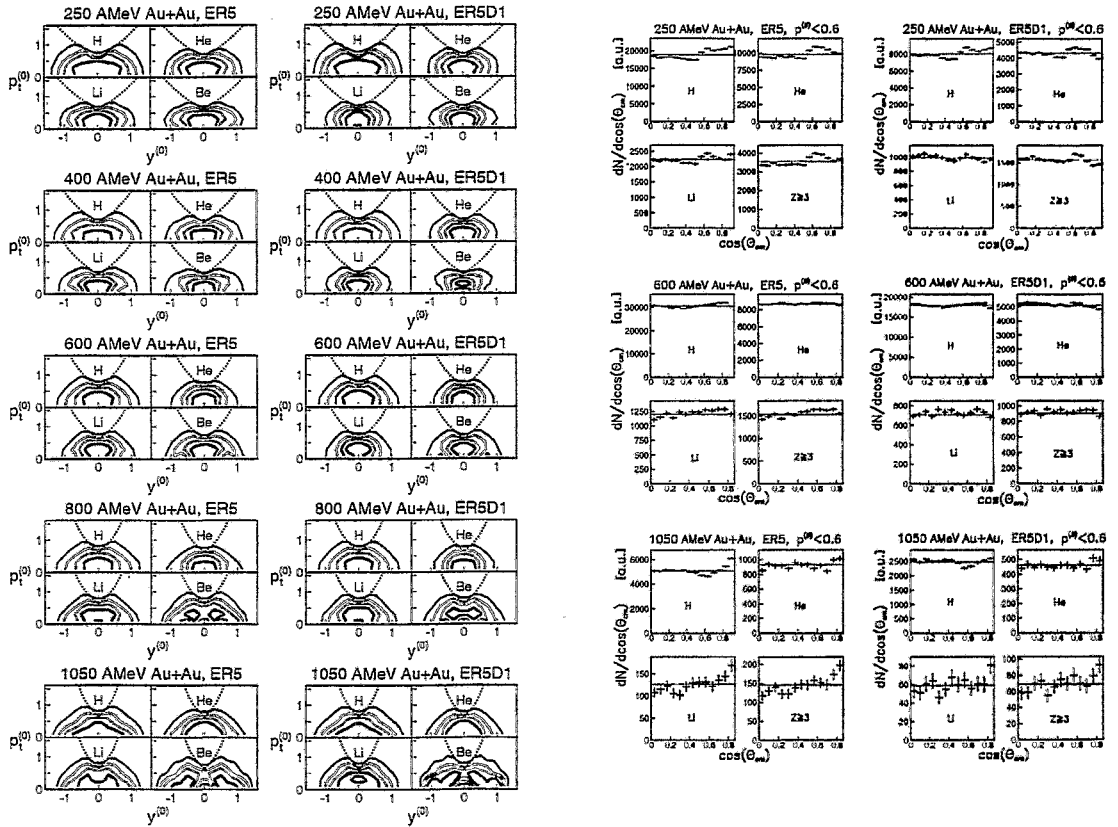


Fig. 1 Left panel: Experimental invariant cross section $d^2N/p_t dp_t dy$ of charged particles with $Z=1-4$ from central collisions selected by ER5 and ER5&D1 for projectile energies of 250 to 1050 A·MeV. The isolines represent equal yields of 20, 40, 60, and 80% of the maximum values. Dashed lines give the detector limit at $\theta_{lab} = 30^\circ$. Right panel: The corresponding c.m. polar angle distributions $dN/d\cos(\Theta_{cm})$ of charged particles with $Z=1, 2, 3$, and $Z \geq 3$ in a phase space region which is not biased by the detector acceptance ($p^0 < 0.6$).

$E_{rat} > ER5 \simeq 0.8$) and (optionally) on small values D1 of the azimuthal directivity [3] $D = |\sum_i \vec{p}_{\perp i}| / \sum_i |\vec{p}_{\perp i}|$ (typically $D < D1 \simeq 0.2$) which correspond to vanishing sideways flow $\langle p_x^{dir} / A \rangle$.

The l.h.s. of Fig. 1 shows distributions of invariant cross section $d^2N/p_t dp_t dy$ in a representation of normalized (to projectile quantities) transverse momentum $p_t^{(0)} = (p_t/A)/(p/A)_{cm}^{proj}$ vs. rapidity $y^{(0)} = (y/y_{proj})_{cm}$. For symmetry reasons the almost unmeasured backward hemisphere is filled by reflection of the forward hemisphere.

The r.h.s. of Fig. 1 displays for 250, 600, and 1050 A·MeV the corresponding polar angle distributions in a phase space region which is not biased by the detector acceptance ($p^0 < 0.6$).

Both the rapidity plots and the almost flat polar angle distributions support the idea of selecting a rather isotropic midrapidity source when applying the very central event selection criterion ER5&D1. (An exception seem to represent only the heavy clusters at the highest energies which are supposed to stem from semicentral collisions mixing into the central bins.) On the other hand, the cut ER5 with about twice the statistics of ER5&D1 and nearly isotropic polar distributions, too, selects slightly elongated flow ellipsoids (with typical axis ratios of the energy flow tensor of about 2) which are rotated off the beam axis thus leading to finite azimuthal anisotropies (see Fig. 2).

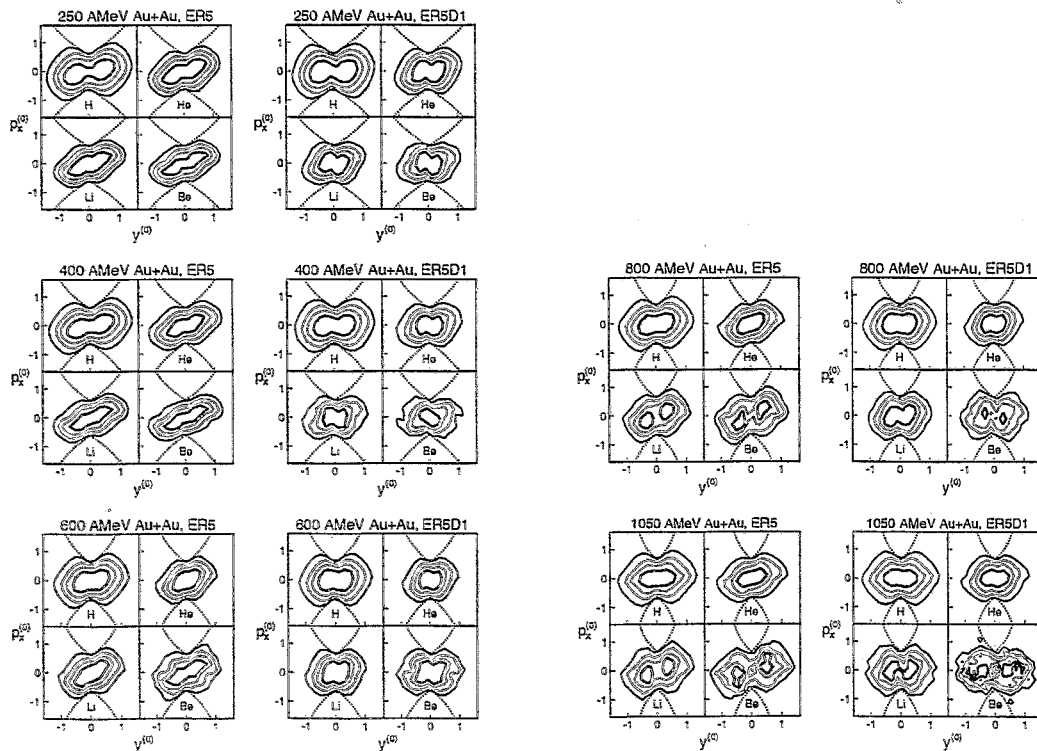


Fig. 2 Experimental distributions $d^2N/dp_x dy$ of charged particles with $Z=1-4$ from central collisions selected by ER5 and ER5&D1 for projectile energies of 250 to 1050 A·MeV. The quantity $p_x^{(0)}$ denotes the projection onto the reaction plane of the normalized transverse momentum $p_t^{(0)}$. The isolines represent equal yields of 20, 40, 60, and 80% of the maximum values. Dashed lines give the detector limit at $\theta_{lab} = 30^\circ$.

References

- [1] J. Aichelin et al., Phys. Rep. **202** (1991) 233
- [2] S.C. Jeong et al., Phys. Rev. Lett. **72** (1994) 3468
- [3] J.P. Alard et al., Phys. Rev. Lett. **69** (1992) 889

Energy Equilibration in Central Au on Au Collisions in the Projectile Energy Range from 150 AMeV to 1050 AMeV ^B

W. NEUBERT, A.S. BOTVINA¹, J. BIEGANSKY, R. KOTTE, J. MÖSNER AND
D. WOHLFARTH

Fragment charge distributions obtained in central Au on Au collisions have been analysed recently with statistical models assuming that the considered system is completely equilibrated [1,2]. This supposition becomes invalid with increasing beam energy as shown by recent investigations based on a blast scenario [3]. Here we report on first results obtained with a statistical model which includes approximately preequilibrium particle emission (code SMMFC). Based on this calculations we established the increasing nonequilibrium character of Au + Au collisions towards higher beam energies. Within this model it is supposed that the part of the c.m. energy and matter of the entire Au + Au system which does not undergo equilibration is removed by fast light particles characterized by an isotropic c.m. distribution.

The following input parameters are essential to the code SMMFC: (1) the thermal excitation energy E_{EXC} , (2) the parameter Y_{REL} which gives the size of the thermalized source as percentage of the full mass of the Au + Au system, (3) the energy of the radial flow and (4) the share S_π of the c.m. energy which is removed by pion production. The radial flow implemented into the code does not influence the process of fragment formation. It changes only the velocity distributions of the fragments. At beam energies above 600 AMeV the value S_π was taken from the measured Δ -resonance population probability in the Au + Au collision [5]. To allow for a comparison with the experimental data a filter routine was implemented into the code which simulates approximately the response of the plastic forward wall of the FOPI detector.

In figs. 1 and 2 we demonstrate how observables related to Intermediate Mass Fragments (IMF) with charges $Z \geq 3$ depend on the parameters of the model. The IMF multiplicity depends on both the size of the thermalized source and its excitation energy thus preventing a definite determination of E_{EXC} . However, the fragment charge distribution (which falls off exponentially $\sim \exp(-\lambda \cdot Z)$) allows to remove this ambiguity if we consider the slope parameter λ of such exponential fits. At higher projectile energies the code SMMFC overestimates the light particle yields compared with the data [4] so that the fit had to be restricted to fragments with $Z \geq 3$. A limitation to $Z \leq 6$ was chosen for a consistent analysis from 150 AMeV to 800 AMeV. The low abundance of heavy fragments at 1050 AMeV required a limitation to $2 \leq Z \leq 4$. The slope parameters of the calculated charge distributions depends only on the thermal excitation energy but not on the source size and the radial flow as shown in fig.2. Based on this feature the thermal excitation energy was determined by comparing with the data [4]. Fig.3 shows that the ratio of the thermal excitation energy and the available c.m. energy falls off with increasing beam energy down to values of about 10% around 1000 AMeV. For the lower beam energies, this behaviour is confirmed by results obtained with a transport model (BUU) coupled to a statistical multifragmentation code [6].

Summarizing, we conclude that the Au+Au collisions are governed by nonequilibrium processes and that only a small part of the c.m. energy undergoes thermalization.

Fig. 1 IMF multiplicity in the forward hemisphere vs. thermal excitation energy for different source size Y_{REL} , the lines are fits to calculated points (dashed - without filter, solid - filtered), the hatched band corresponds to the data of central events [4].

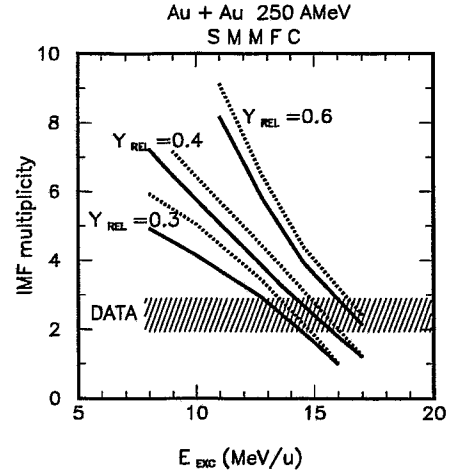


Fig. 2 Slope parameters of exponential fits to the calculated (filtered) different values of the radial flow and the source size as indicated by the symbols. The data are related to [4].

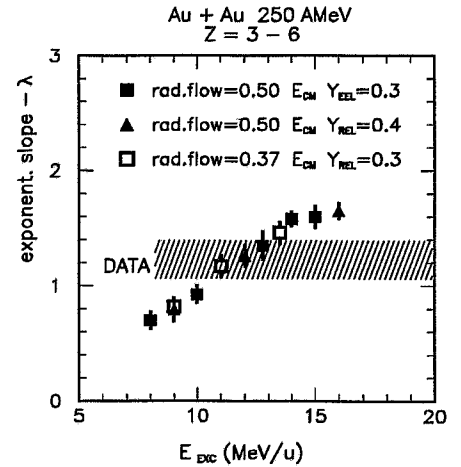
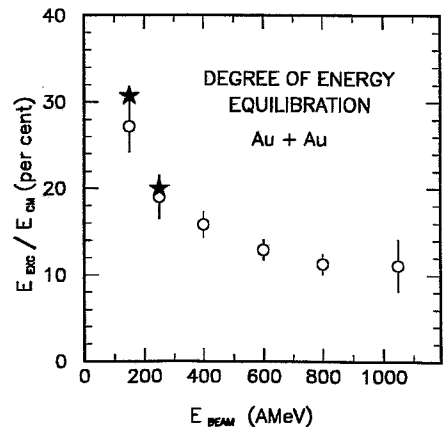


Fig. 3 The ratio of thermal energy to the initial c.m. energy per nucleon as function of the beam energy, the stars show the results of ref. [6].



¹ Hahn-Meitner-Institut Berlin GmbH,
Glienicke Str. 100, 14109 Berlin

References

- [1] C. Kuhn et al., Phys. Rev. **C48** (1993) 1232
- [2] M. Dzelalija et al., Phys. Rev. **C52** (1994) 346
- [3] W. Reisdorf, Acta Phys. Polonica **B25** (1994) 443
- [4] J. Biegansky et al., this report, p.
- [5] R. Averbeck et al., GSI-Nachrichten 10-95
- [6] B. Heide and H.W. Barz, Nucl. Phys. **A588** (1995) 918

Charged Particle Distributions in the Reaction Au + Au at 150 ÷ 1050 A MeV ^B

J. BIEGANSKY, R. KOTTE, J. MÖSNER, W. NEUBERT AND D. WOHLFARTH

Heavy ion collisions in the energy range of 150 ÷ 1050 A MeV were investigated using the Forward Plastic Wall of the 4 π spectrometer FOPI at GSI, Darmstadt. Charged particles could be identified within the polar angles $1^\circ < \vartheta_{lab} < 30^\circ$. The formation of fragments and consequently their relative yields depend on the initial beam energy as well as on the centrality of the event. The more central an event, the more nucleons intensively interact within the region of the geometrical overlap of the colliding nuclei (participant region). Fragment distributions were predicted [1] to show different shapes, depending on whether they contain preferentially participant or spectator matter. The fragments from the spectator region are assumed to follow $dN/dZ \propto Z^{-\tau}$ (left panel of Fig.1) whereas the fragment yields from the participant zone are expected to fall off exponentially $dN/dZ \propto \exp(-\lambda \cdot Z)$ (middle panel).

The ratio of transverse to longitudinal kinetic energy $E_{RAT} = \frac{\sum p_x^2/2m + \sum p_y^2/2m}{\sum p_z^2/2m}$ allows to distinguish central from peripheral events. We chose $E_{RAT} > (0.7 - 0.8)$ to select mostly central events corresponding to impact parameters $b < 2.5$ fm (as calculated with the QMD model [2]). In the distribution of peripheral collisions on the left panel we used a gate around the projectile rapidity $Y^{(0)} \simeq 1$ ($Y^{(0)} = (y_i/y_{pro})_{cm}$) to select the spectator matter. The Z-distributions of central events were generated within the c.m. polar angle range $25^\circ < \Theta_{cm} < 45^\circ$. We analysed the charge distributions applying a multi-Gaussian fit procedure with adjustable background shapes. The corresponding corrections become essential at beam energies above 600 A MeV.

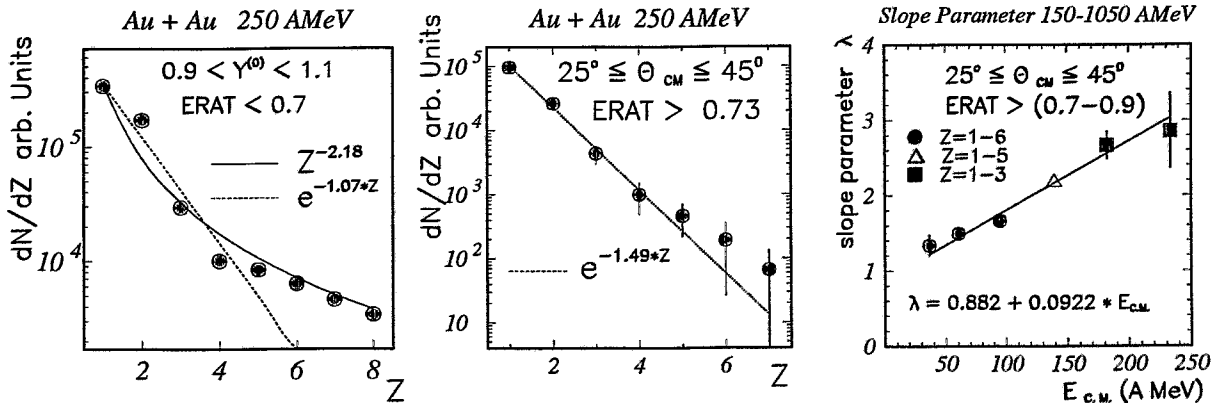


Fig.1: Charge Distributions for peripheral (left panel) and central (middle panel) events selected by a centrality cut ($ERAT$) at $E_{BEAM} = 250$ A MeV. The right panel displays the slope parameter λ vs. the available c.m. energy for distributions at $E_{BEAM} = 150 \div 1050$ A MeV (full line : linear fit).

It is found that the slope parameter λ increases with increasing beam energy reflecting the growing degree of desintegration of the colliding system. As a final result, the right panel shows that λ increases almost linearly with the available center of mass energy.

References

- [1] P.J. Siemens, Nature (London), **305** (1983) 410
- [2] J. Aichelin et al, Phys. Rev. C. **37** (1988) 2451

Bounce Off and Squeeze Out of Charged Particles in the Reaction Au + Au at 1050 AMeV ^B

J. BIEGANSKY, R. KOTTE, J. MÖSNER, W. NEUBERT AND D. WOHLFARTH

The reaction Au + Au at a beam energy $E_{beam} = 1$ AGeV was investigated using the FOPI-Detector at GSI, Darmstadt. The Forward Plastic Wall, a plastic scintillator array covering the polar angles $1^\circ < \vartheta_{lab} < 30^\circ$, is sensitive to charged particles and can be used to study different patterns of collective motion.

The colliding nuclei form a hot and compressed region within their geometrical overlap volume according to the centrality of the reaction. Nucleons inside this volume, where nuclear matter may be compressed up to values twice as high as regular density ρ_0 , are called participants and can be distinguished from those nucleons outside the geometrical overlap of the colliding nuclei (spectators) [1]. The reaction geometry leads to a certain distribution of cold spectator nucleons surrounding the hot participant zone : there are more spectators in direction of the reaction plane (determined according to [2]) compared to the direction perpendicular to it. Due to the smaller amount of matter in this direction there is less resistance against the pressure release from the hot participant zone. As a consequence, some participants are squeezed out, preferentially perpendicular to the reaction plane.

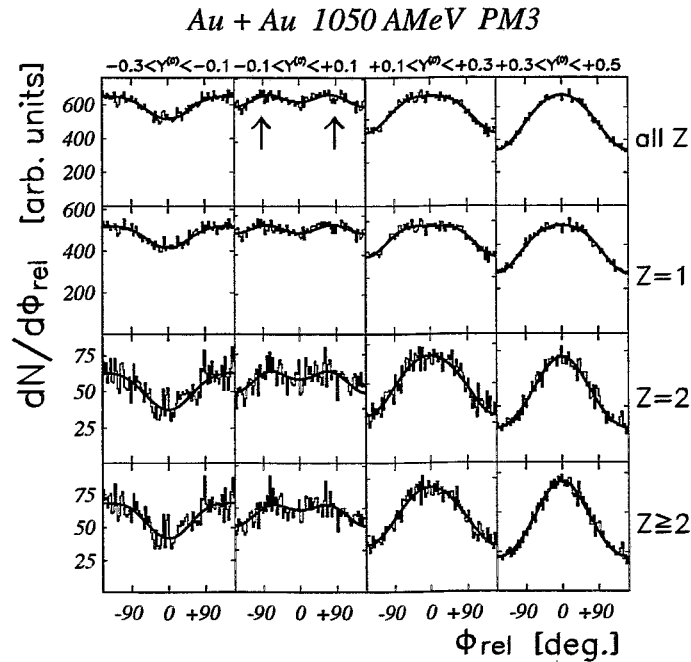


Fig.1: Azimuthal angle distribution relative to the reaction plane as measured in semi-central collisions for different rapidity bins and fragment charges. Squeeze out of hot participant matter is indicated by the enhanced emission perpendicular to the reaction plane for ejectiles with center of mass velocity $Y^{(0)} = 0$. The distributions were parametrized by $\frac{dN}{d\Phi_{rel}} = a_0 \cdot (1 + a_1 \cdot \cos(\Phi) + a_2 \cdot \cos(2\Phi))$, as indicated by the thick lines.

Semicentral events were preselected by requiring a medium multiplicity. The different rapidity bins display the dependence from the particle velocity (see Fig. 1). The particle velocity is quantified using the normalized rapidity $Y^{(0)}$. This quantity amounts -1 for particles moving with target rapidity and $+1$ for projectile rapidity. Thus the rapidity bin $-0.1 < Y^{(0)} < +0.1$ contains stopped fragments from the compressed participant region. The distribution relative to the reaction plane is increased for values of $\Phi_{rel} = \pm 90^\circ$ (arrows), more pronounced for $Z=2$ particles compared to $Z=1$. This indicates an emission of fragments perpendicular to the reaction plane, e.g. the squeeze out of nuclear matter. For the other rapidity bins the peaks are shifting to $\Phi_{rel} \approx 0^\circ$, indicating the in-plane emission of nuclear matter.

To quantify this effect, the magnitude $R_N = \frac{1-a_2}{1+a_2} = \frac{N(\pm 90^\circ)}{N(0^\circ)}$ is derived from the fit coefficients (see Fig.2). It was determined for medium (PM3) and high multiplicities (PM5). The squeeze out ratio R_N is enhanced for PM3 because in semicentral collisions

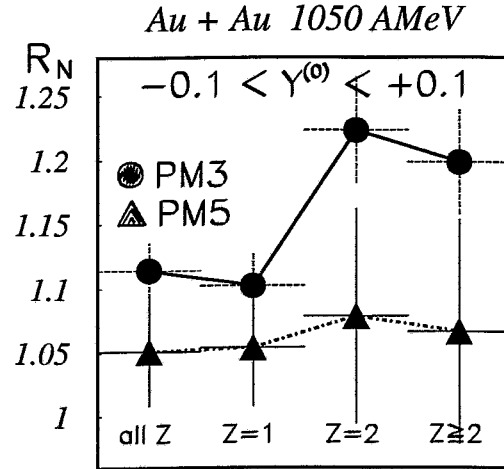


Fig.2: Squeeze out ratio for different multiplicities at midrapidity as measured in the reaction $Au + Au$ at $E_{Beam} = 1 AGeV$.

the reaction plane is well defined. The more central a collision, the more fragments are emitted isotropically and the reaction plane disappears. Thus for central collisions the participant-spectator scenario suggests the absence of both bounce off and squeeze out. $R_N > 1$ for PM5 is caused by semicentral events which cannot be suppressed using the charged particle multiplicity. Similar effects in the same reaction can be found at lower incident energies [3], for neutrons [4], deuterons and tritons as well as for π^\pm mesons [5].

References

- [1] H.H. Gutbrod et al, Phys.Rev.C **42** (1990) 476
- [2] P. Danielewicz and G. Odyniec, Phys. Lett. B **110** (1985) 146
- [3] J.P. Alard et al, GSI Scientific Report 1994 , GSI-94-1 (1995) 59
- [4] Y. Leifels et al, Phys.Rev.Lett. **71** (1993) 963
- [5] Ch. Pinkenburg, Dissertation, Universität Frankfurt/Main (1995)

Nuclear Temperatures from Isotopic Ratios in Proton-Nucleus Interactions ^B

W. NEUBERT

Different production reactions (either proton-nucleus interactions at 1 GeV or heavy ion collisions in the 30-84 AMeV range [2]) lead to nearly the same yield ratios of lithium and boron isotopes [1]. The nuclear temperatures derived from the isotopic yields in ref.[2] are of current interest in connection with the recent study of the calorimetric curve of excited nuclei [3]. With the same aim we reanalysed all data which are available for 1 GeV proton energy (see table 1). The temperatures were determined by using the Albergo formula [4] and they are given also in table 1. The mean excitation energy which corresponds to a certain target nucleus was found by interpolation from the experimental data in ref.[7]. These data were derived from the linear momentum transfer measured at 1 GeV proton energy in the target mass range from $A=27$ to $A=238$.

The results plotted in fig.1 show a surprising agreement of the temperatures derived from very different data. We suggest that in the considered range of excitation energies the fragment formation occurs always in the same equilibrated nucleus although it is reached by different entrance channels. The evaluated temperatures deviate progressively from an evaporative decay of a Fermi liquid (solid curve,[3]) with increasing excitation energy and suggest the onset of multifragmentation. A calculation was performed with the Statistical Multifragmentation Model [8] for a system with $A=190$ and $E^*=2.1$ MeV/u. This parameter choice is predicted by an INC simulation for a central 1 GeV p on Au collision. The temperature derived from the calculated isotopic He and Li yield ratios amounts to $T=3.67$ MeV in good agreement with the experimental value.

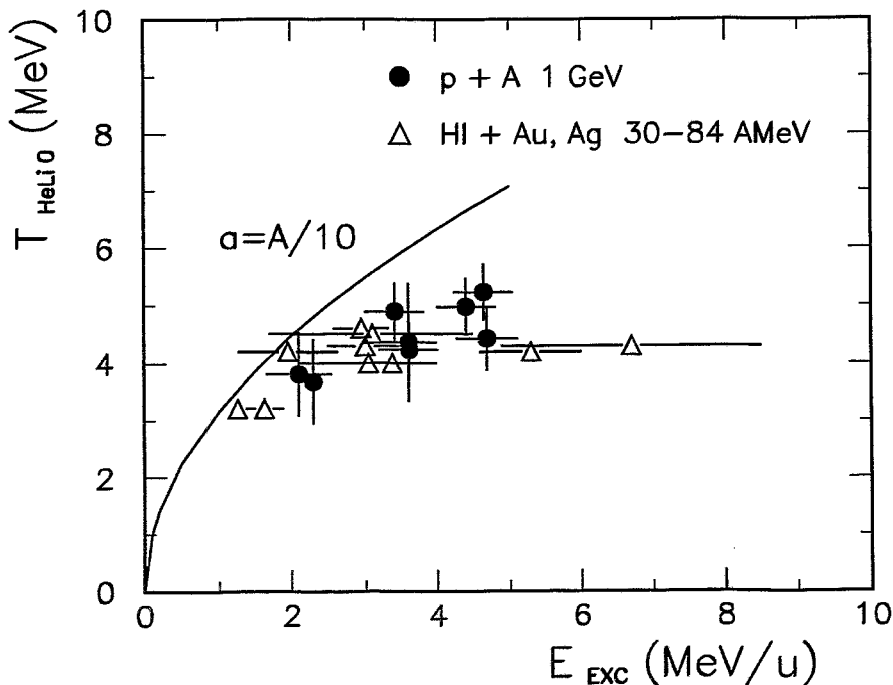


Fig. 1 He/Li temperatures as function of the excitation energy

Table 1 Isotopic ratios from $p + A$ reactions at 1 GeV and associated temperatures, the values in parantheses are the errors

target	$Y(^3\text{He})/Y(^4\text{He})$	$Y(^6\text{Li})/Y(^7\text{Li})$	T_{HeLi} (MeV)	remarks
^{58}Ni	0.132 (0.02)	1.22 (0.27)	4.43 (0.55)	σ_{tot} [5]
^{48}Ti	0.120 (0.02)	0.702	5.23	$\Theta_{lab} = 60^\circ$ [6]
^{64}Ni	0.108 (0.017)	0.720	4.98	$\Theta_{lab} = 60^\circ$ [6]
^{112}Sn	0.086 (0.01)	0.923	4.23	$\Theta_{lab} = 60^\circ$ [6]
Ag	0.088 (0.031)	0.858 (0.316)	4.36 (1.03)	σ_{tot} [5]
^{124}Sn	0.083 (0.010)	0.582	4.89	$\Theta_{lab} = 60^\circ$ [6]
^{197}Au	0.035 (0.013)	0.533 (0.082)	3.81 (0.73)	σ_{tot} [5]
^{238}U	0.025 (0.010)	0.430 (0.090)	3.68 (0.74)	σ_{tot} [5]

target	$Y(^{10}\text{B})/Y(^{11}\text{B})$	T_{HeB} (MeV)	$Y(^9\text{Be})/Y(^{10}\text{Be})$	T_{HeBe} (MeV)	remarks
^{112}Sn	0.538	5.41			$\Theta_{lab} = 60^\circ$ [6]
Ag	0.542	5.47 (2.20)	1.77(0.71)	6.77(2.51)	σ_{tot} [5]
^{124}Sn	0.271	(8.84)			$\Theta_{lab} = 60^\circ$ [6]
^{197}Au	0.371	4.12 (1.28)	1.12(0.34)	5.51(1.47)	σ_{tot} [5]
^{238}U	0.282	4.01 (1.34)	0.92(0.32)	5.22(1.38)	σ_{tot} [5]

target	$Y(^7\text{Li})/Y(^8\text{Li})$	T_{HeLi} (MeV)	remarks
^{112}Sn			$\Theta_{lab} = 60^\circ$ [6]
Ag	6.60 (2.50)	3.71 (0.54)	σ_{tot} [5]
^{124}Sn			$\Theta_{lab} = 60^\circ$ [6]
^{197}Au	4.92 (1.52)	3.29 (0.39)	σ_{tot} [5]
^{238}U	3.93 (1.23)	3.22 (0.40)	σ_{tot} [5]

References

- [1] L.N. Andronenko et al., Z.f.Phys. **A350** (1994) 1
- [2] R. Wada et al., Phys. Rev. Letters **58** (1987) 1829
- [3] J. Pochodzalla et al., Phys. Rev. Let. **75** (1995) 1040 and W.F.J. Müller et al., GSI-Nachrichten 03-95
- [4] S. Albergo et al., Nuovo Cimento 89A (1985) 1
- [5] E.N. Volnin et al., preprint LNPI Nr.101, Gatchina 1974
- [6] E.N. Volnin., thesis, Leningrad 1974 (unpublished)
- [7] A.A. Kotov et al., Nucl. Phys. **A583** (1995) 575C
- [8] A.S. Botvina, code version SMM3

Systematic Study of Emission Temperatures in Projectile Fragmentation ^B

T. MÖHLENKAMP, J. POCHODZALLA,³ A. SCHÜTTAUF,² W. SEIDEL, A. WÖRNER,¹
AND THE ALADIN/LAND-COLLABORATION

A new method to determine emission temperatures in nuclear reactions was recently developed [1]. For a nuclear system at low density and in chemical and thermal equilibrium a measure of the temperature of the system may be obtained via double ratios of two isotope pairs differing by one neutron each [2]. We derived a temperature $T_{HeLi,0}$ in terms of the yield ratios ${}^3He/{}^4He$ and ${}^6Li/{}^7Li$. Calculations indicate that $T_{HeLi,0}$ depends almost linearly on the actual temperature T of the system. In order to account pragmatically for the systematic underprediction of the temperature by the quantity $T_{HeLi,0}$, we define the final isotope temperature via $T_{HeLi} = 1.2 \cdot T_{HeLi,0}$. Thus, T_{HeLi} provides a common temperature scale in the evaporation, fragmentation as well as the vapor regime of nuclear systems. Applying this method to highly excited projectile spectators and by determining their excitation energy through an energy balance [5] we obtained the so-called "caloric curve of nuclei". The S-shape of the curve is reminiscent of a first order liquid gas phase transition in a macroscopic system. A region of constant temperature of $T \approx 5$ MeV separates the liquid and vapour regime for excitation energies in between 2 and 10 MeV per nucleon. If the excitation energy exceeds 10 MeV per nucleon the temperature is increasing again.

The kinematically well separated projectile spectators were investigated with the ALADIN forward spectrometer system. The TP-MUSIC detector equipped with 18 multi-wire proportional counters allowed the measurement of the charges, positions and angles of fragments with $Z \geq 2$. Combining this tracking information with the time-of-flight measurement the masses of light fragments could be determined with a resolution of about $\Delta A_{FWHM} = 0.3$.

Previous experiments have shown that in this range of relativistic energies the decay of excited spectators proceeds independently of the entrance channel dynamics and without indication of radial outward flow [3]. Furthermore, the analysis of dynamical variables has shown an isotropic decay. Therefore, projectile spectators, which are produced over a wide range of excitation energy and mass, are well suited for the investigation of highly excited nuclear systems in thermal equilibrium. The universal behavior of multifragment decays of these systems is apparent in the Z_{bound} scaling of the charge spectra [4]. The mean number of intermediate mass fragments M_{IMF} as a function of Z_{bound} was found to be independent of the target nucleus as well as of the beam energy. But the M_{IMF} versus Z_{bound} correlation depends on the mass of the projectile. More fragments are to be expected from heavier projectiles. This increase of IMF's is linear to the projectile mass Z_{proj} . Therefore M_{IMF} plotted against Z_{bound}/Z_{proj} is again invariant with respect to the projectile mass. This universality is not restricted to M_{IMF} but appears to be a very general feature also of the relative asymmetries and other correlations between the abundancies and the atomic numbers of the fragmentation products.

In order to check how this universal behavior of multifragment decays of projectile spectators corresponds with the emission temperature of these systems, the temperature determination was extended to different combinations of projectile and target nuclei at two different beam energies. Since the determination of the excitation energy is not available yet we have plotted all temperature values as a function of Z_{bound} . Despite the fact that

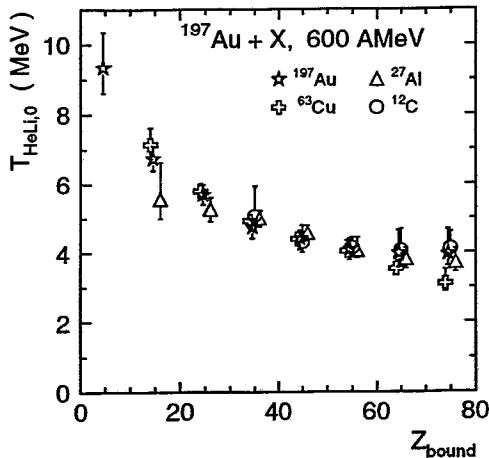


Figure 1: Isotope temperature $T_{HeLi,0}$ vs. Z_{bound} for Au 600 AMeV on different targets.

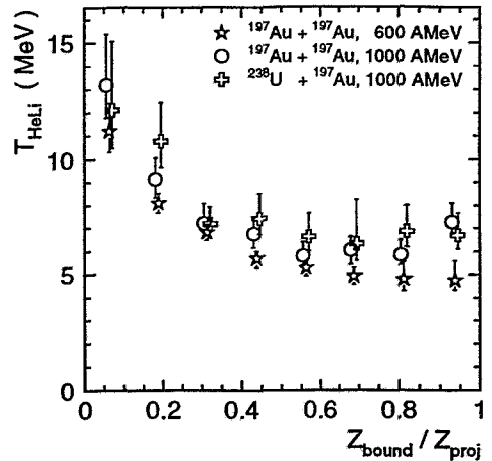


Figure 2: Isotope temperature $T_{HeLi,0}$ vs. Z_{bound}/Z_{proj} for different systems.

Z_{bound} is almost linearly related to the excitation energy [5], the characteristic shape of the caloric curve is expected to be smeared out, due to the summation over different event classes, which otherwise can be separated by Z_{max} .

In figure 1 the uncorrected temperature $T_{HeLi,0}$ is plotted versus Z_{bound} for reactions with the gold projectile at $E/A = 600$ MeV. The temperature shows no dependence on the four different targets ranging from C to Au. This behaviour is in line with the target independence of the charge spectra mentioned above.

In figure 2 three different systems are compared, Au + Au at 600 AMeV, Au + Au at 1000 AMeV and U + Au at 1000 AMeV. The temperatures in Au + Au reactions are slightly increased by increasing the beam energy from 600 AMeV to 1000 AMeV. A rise of the projectile mass from Au to U at 1000 AMeV gives systematically higher temperatures. The opposite behaviour would have been expected, if the increase of the temperature in the caloric curve would only be the result of the decreasing system size [6]. While this observation can not exclude a weak dependence on the beam energy or the projectile size, potential systematic uncertainties might be the reason for slightly larger temperatures. Taking these uncertainties into account the universality of the charge spectra with respect to a variation of the beam energy or the projectile mass corresponds to a constant break-up temperature. The determination of the excitation energy of these different systems, will hopefully give further insight into the global features of the projectile fragmentation.

¹ Gesellschaft für Schwerionenforschung Darmstadt

² Institut für Kernphysik, Universität Frankfurt

³ Heisenberg fellow of DFG

References

- [1] J. Pochodzalla, *et al.*, Phys. Rev. Lett. **75**, 1040 (1995)
- [2] S. Albergo, *et al.*, Il Nuovo Cimento **89A**, 1 (1985)
- [3] G.J. Kunde, *et al.*, Phys. Rev. Lett. **74**, 38 (1995)
- [4] A. Schüttauf, Ph.D. thesis, University of Frankfurt (1996)
- [5] E. Zude, PhD thesis, University of Frankfurt (1995)
- [6] P. Bonche, *et al.*, Nucl. Phys. **A436**, 265 (1985)

Multifragmentation of spectators in relativistic heavy-ion reactions
(Nucl. Phys. A 584 (1995) 737)

Botvina, A.S., I.N. Mishustin, M. Begemann-Blaich, J. Hubele, G. Imme, I. Iori, P. Kreuz, G.J. Kunde, W.D. Kunze, V. Lindenstruth, U. Lynen, A. Moroni, W.F.J. Müller, C.A. Ogilvie, J. Pochodzalla, G. Raciti, Th. Rubehn, H. Sann, A. Schüttauf, W. Seidel, W. Trautmann, A. Wörner

Abstract: Using the ALADIN forward-spectrometer at SIS we have studied multi-fragment decays of ^{197}Au projectiles after collisions with C, Al, Cu and Pb targets at a bombarding energy of $E/A = 600$ MeV. The new data presented in this work comprise the measured cross sections of multifragment processes, the N/Z ratios of the produced fragments, and the differential distributions of fragment multiplicities and of observables built on the charge correlations within the event. The $^{197}\text{Au} + \text{Cu}$ data are analyzed with the statistical multifragmentation model. It is shown that all observables can be simultaneously reproduced on an absolute scale, apart from an overall normalization constant which relates the number of model events to the measured cross section. A continuous distribution of excited residual nuclei, used as input for the calculations, was derived from the criterion of a best fit to the data. It exhibits a correlation between decreasing mass number A and increasing excitation energy E_x/A and a saturation of the excitation energy at $E_x/A \approx 8$ MeV.

Entropy in central Au + Au reactions between 100 and 400 A MeV
(Phys. Rev. C 52 (1995) 346)

Dzelalija, M., N. Cindro, Z. Basrak, R. Caplar, S. Hölbling, M. Bini, P.R. Maurenzig, A. Olmi, G. Pasquali, G. Poggi, N. Taccetti, C. Cerruti, J.P. Coffin, P. Fintz, G. Guillaume, A. Houari, F. Jundt, C. Kuhn, F. Rami, R. Tezkratt, P. Wagner, J.P. Alard, N. Bastid, L. Berger, I.M. Belayev, S. Boussange, A. Buta, P. Dupieux, J. Erö, Z. Fodor, L. Fraysse, A. Gobbi, N. Herrmann, K.D. Hildenbrand, M. Jorio, J. Kecskemeti, P. Koncz, Y. Korchagin, R. Kotte, M. Krämer, A. Lebedev, I. Legrand, V. Manko, G. Mgebrishvili, J. Mösner, D. Moisa, G. Montarou, W. Neubert, D. Pelte, M. Petrovici, W. Reisdorf, D. Schüll, Z. Seres, B. Sikora, V. Simion, S. Smolyankin, U. Sodan, M. Trzaska, M.A. Vasiliev, J.P. Wessels, T. Wienold, D. Wohlfarth and A.V. Zhilin

Abstract: The ratio of the total charge bound in fragments with Z between 2 and 15 to hydrogen production, $(\sum_2^{15} M_i Z_i)/M_H$, and the neutron-to-proton yield ratio n/p have been determined for central Au + Au reactions between 100 and 400 A MeV using the phase I setup of the detector system FOPI at the GSI, Darmstadt. Taking into account charged particles detected in the polar-angle range between 7° and 30° , the entropy per nucleon (S/A) has been deduced for two rapidity regions by comparing these ratios with those predicted by the modified FREESCO code. The values of S/A obtained in the midrapidity region are systematically lower by about 20 % than those in the whole half-sphere, suggesting that global equilibrium is not reached in these collisions. The S/A values are in good agreement with recent hydrodynamic calculations and, in the region of overlap, with entropies obtained in a related study by Kuhn et al.

Interplay of collective flow phenomena and velocity correlations of intermediate-mass fragments in collisions of Au + Au at $E=(100-400) A$ MeV
(Phys. Rev. C 51 (1995) 2686)

Kotte, R., B. Kämpfer, J. Mösner, W. Neubert, D. Wohlfarth, J.P. Alard, V. Amouroux, Z. Basrak, N. Bastid, I.M. Belayev, L. Berger, Th. Blaich, S. Boussange, A. Buta, R. Caplar, C. Cerruti, N. Cindro, J.P. Coffin, R. Donà, P. Dupieux, J. Erö, Z.G. Fan, P. Fintz, Z. Fodor, L. Fraysse, R. Freifelder, S. Frolov, A. Gobbi, Y. Grigorian, G. Guillaume, N. Herrmann, K.D. Hildenbrand, S. Hölbling, O. Houari, M. Ibnouzhahir, S.C. Jeong, F. Jundt, J. Kecskemeti, P. Koncz, Y. Korchagin, M. Krämer, C. Kuhn, I. Legrand, A. Lebedev, V. Manko, T. Matulewicz, G. Mgebrishvili, D. Moisa, G. Montarou, I. Montbel, D. Pelte, M. Petrovici, P. Pras, F. Rami, V. Ramilien, W. Reisdorf, A. Sadchikov, D. Schüll, Z. Seres, B. Sikora, V. Simion, S. Smolyankin, U. Sodan, K. Teh, R. Tezkratt, M. Trzaska, M.A. Vasiliev, P. Wagner, J.P. Wessels, T. Wienold, Z. Wilhelmi, A.V. Zhilin

Abstract: Velocity correlations of intermediate mass fragments (IMF), produced in collisions of Au + Au at 100, 150, 250, and 400 A MeV beam energy, are extracted from measurements with the 4π detector system (FOPI) in construction stage I at Schwerionen-Synchrotron (SIS) at the Gesellschaft für Schwerionenforschung (GSI) in Darmstadt. The IMF correlation functions of peripheral and semicentral events are found to be strongly affected by the collective sideward motion of nuclear matter. The sideflow causes an enhancement of correlations at small relative velocities. This enhancement results from the mixing of differently azimuthally oriented events; it vanishes if the events are rotated into a unique reaction plane. Selecting violent central collisions, the comparison of the data with a Coulomb dominated finale-state interaction model points to a radius of the expanding and multifragmenting source of $R_s \approx 13$ fm for 100 A MeV which appears shrinking by 20 % when increasing the projectile energy to 400 MeV per nucleon. The deduced source radii are found to depend on the radial explosion energy used in the model. The inclusion of such a collective expansion is necessary for a reasonable description of the experimental single-particle spectra of the IMF. The unique Coulomb suppression of small relative IMF velocities, found for the given beam energy range, is attributed to rather constant averaged next-neighbour distances ($d_{\text{IMF}} = 8.6 \pm 0.2$ fm) of the IMF charge centers within the source at breakup time.

Fragment flow and the multifragmentation phase space
(Phys. Rev. Lett. 74 (1995) 38)

Kunde, G.J., W.C. Hsi, W.D. Kunze, A. Schüttauf, A. Wörner, M. Begemann-Blaich, Th. Blaich, D.R. Bowman, R.J. Charity, A. Cosmo, A. Ferrero, C.K. Gelbke, J. Hubele, G. Immé, I. Iori, P. Kreuzt, V. Lindenstruth, M.A. Lisa, W.G. Lynch, U. Lynen, M. Mang, T. Möhlenkamp, A. Moroni, W.F.J. Müller, M. Neumann, B. Ocker, C.A. Ogilvie, G.F. Peaslee, J. Pochodzalla, G. Raciti, T. Rubehn, H. Sann, W. Seidel, V. Serfling, L.G. Sobotka, J. Stroth, L. Stuttge, S. Tomasevic, W. Trautmann, M.B. Tsang, A. Tucholski, G. Verde, C.W. Williams, E. Zude, B. Zwieglinski

Abstract: Fragment distributions have been measured for Au + Au collisions at $E/A = 100$ and 1000 MeV. A high detection efficiency for fragments was obtained by combining the

ALADIN spectrometer and the MSU-Miniball/WU-Miniwall array. At both energies the maximum multiplicity of intermediate mass fragments (IMF) normalized to the size of the decaying system is about one IMF per 30 nucleons but the element distributions show significant differences. Within a coalescence picture the suppression of heavy fragments in central collisions at $E/A = 100$ MeV may be related to a reduction of the density in momentum space which is caused by the collective expansion.

Cluster formation during expansion of hot and compressed nuclear matter produced in central collisions of Au on Au at 250 A MeV

(Phys. Rev. Lett. 74 (1995) 5001)

Petrovici, M., N. Herrmann, I. Legrand, A. Gobbi, K.D. Hildenbrand, W. Reisdorf, A. Buta, R. Freifelder, S.C. Jeong, M. Krämer, D. Moisa, D. Schüll, V. Simion, U. Sodan, K. Teh, J.P. Wessels, T. Wienold, J.P. Alard, V. Amouroux, Z. Basrak, N. Bastid, I.M. Belyaev, L. Berger, Th. Blaich, S. Boussange, R. Caplar, C. Cerruti, N. Cindro, J.P. Coffin, R. Donà, P. Dupieux, J. Erö, P. Fintz, Z. Fodor, L. Fraysse, G. Guillaume, S. Hölbling, A. Houari, F. Jundt, J. Kecskemeti, P. Koncz, Y. Korchagin, R. Kotte, C. Kuhn, M. Ibnouzahir, A. Lebedev, C. Maguire, V. Manko, J. Mösner, G. Montarou, I. Montbel, P. Morel, W. Neubert, D. Pelte, F. Rami, V. Ramillien, A. Sadchikov, Z. Seres, B. Sikora, S. Smolyankin, R. Tezkratt, M. Trzaska, M.A. Vasiliev, P. Wagner, Z. Wilhelmi, D. Wohlfarth, A.V. Zhilin

Abstract: Complete distributions of the light and intermediate mass fragments ($Z = 1$ to 6) produced within the polar angular range $1^\circ \leq \Theta_{\text{lab}} \leq 30^\circ$ in highly central collisions of 250 A MeV Au + Au are presented. The results of this measurement and a model analysis are used to study the expansion and clustering of the hot and compressed transient state formed in central collisions of such a heavy system. The influence of the initial conditions on the final observables is discussed.

Multifragmentation and flow: peripheral vs. central collisions

(Nucl. Phys. A 583 (1995) 553)

Pochodzalla, J., S. Aiello, M. Begemann-Blaich, Th. Blaich, D.R. Bowman, R.J. Charity, A. Cosmo, A. Ferrero, C.K. Gelbke, W.C. Hsi, J. Hubele, G. Immé, I. Iori, J. Kempter, P. Kreuzt, G.J. Kunde, W.D. Kunze, V. Lindenstruth, M.A. Lisa, W.G. Lynch, U. Lynen, M. Mang, L.G. Moretto, A. Moroni, W.F.J. Müller, M. Neumann, B. Ocker, C.A. Ogilvie, V. Pappalardo, G.F. Peaslee, G. Raciti, F. Rosenberger, T. Rubehn, H. Sann, R. Scardaoni, A. Schüttauf, W. Seidel, V. Serfling, L.G. Sobotka, J. Stroth, L. Stuttge, W. Trautmann, M.B. Tsang, A. Tucholski, C.W. Williams, A. Wörner, E. Zude, B. Zwieglinski

Abstract: Multifragment decays of heavy nuclei have been studied at the ALADIN spectrometer system at beam energies between 100 and 1000 MeV per nucleon. The observed fragment distributions signal a universality of spectator decays at bombarding energies $E/A \geq 400$ MeV. The role of the radial flow for the fragmentation process is explored by comparing fragment distributions measured for Au + Au collisions at $E/A = 100$ MeV in central collisions and at $E/A = 1000$ MeV in more peripheral reactions. At both

energies the maximum multiplicity of intermediate mass fragments (IMFs) normalized to the size of the decaying system is about one IMF per 30 nucleons but the element distributions show significant differences. Within a coalescence picture the suppression of heavy fragments in central collisions at $E/A = 100$ MeV may be related to a reduction of the density in momentum space which is caused by a large collective expansion velocity component.

Probing the nuclear liquid-gas phase transition

(Phys. Rev. Lett. 75 (1995) 1040)

Pochodzalla, J., T. Möhlenkamp, T. Rubehn, A. Schüttauf, A. Wörner, E. Zude, M. Begemann-Blaich, Th. Blaich, H. Emling, A. Ferrero, C. Gross, G. Imme, I. Iori, G.J. Kunde, W.D. Kunze, V. Lindenstruth, U. Lynen, A. Moroni, W.F.J. Müller, B. Ocker, G. Raciti, H. Sann, C. Schwarz, W. Seidel, V. Serfling, J. Stroth, W. Trautmann, A. Trzcinski, A. Tucholski, G. Verde, B. Zwieglinski

Abstract: Fragment distributions resulting from Au - Au collisions at an incident energy of $E/A = 600$ MeV are studied. From the measured fragment and neutron distributions the mass and the excitation energy of the decaying prefragments were determined. A temperature scale was derived from observed yield ratios of He and Li isotopes. The relation between this isotope temperature and the excitation energy of the system exhibits a behavior which is expected for a phase transition. The nuclear vapor regime takes over at an excitation energy of 10 MeV per nucleon a temperature of 5 MeV and may be characterized by a density of 0.15-0.3 normal nuclear density.

Evidence for collective expansion in light-particle emission following Au + Au collisions at 100, 150 and 250 A MeV

(Nucl. Phys. A 586 (1995) 755)

Poggi, G., G. Pasquali, M. Bini, P. Maurenzig, A. Olmi, N. Taccetti, J.P. Alard, V. Amouroux, Z. Basrak, N. Bastid, I.M. Belayev, L. Berger, Th. Blaich, S. Boussange, A. Buta, R. Caplar, C. Cerruti, N. Cindro, J.P. Coffin, R. Donà, P. Dupieux, M. Dzelalija, J. Erö, Z.G. Fan, P. Fintz, Z. Fodor, L. Fraysse, R. Freifelder, S. Frolov, A. Gobbi, Y. Grigorian, G. Guillaume, N. Herrmann, K.D. Hildenbrand, S. Hölbling, A. Houari, S.C. Jeong, F. Jundt, J. Kecskemeti, P. Koncz, Y. Korchagin, R. Kotte, M. Krämer, C. Kuhn, M. Ibnouzahir, I. Legrand, A. Lebedev, C. Maguire, V. Manko, G. Mgebrishvili, J. Mösner, D. Moisa, G. Montarou, I. Montbel, P. Morel, W. Neubert, D. Pelte, M. Petrovici, F. Rami, V. Ramillien, W. Reisdorf, A. Sadchikov, D. Schüll, Z. Seres, B. Sikora, V. Simion, S. Smolyankin, U. Sodan, K. The, R. Tezkratt, M. Trzaska, M.A. Vasiliev, P. Wagner, J.P. Wessels, T. Wienold, Z. Wilhelmi, D. Wohlfarth, A.V. Zhilin, P. Danielewicz

Abstract: Light-particle emission from Au + Au collisions has been studied in the bombarding-energy range 100-250 A MeV, using $\Delta E-E_R$ telescopes in coincidence with the FOPI detector in its phase I configuration. Center-of-mass energy spectra have been measured for $Z = 1, 2$ isotopes emitted in central collisions at CM polar angles between 60° and 90° . Evidence for a collective expansion is reported, on the basis of the mean kinetic

energies of hydrogen isotopes. Comparison is presented with statistical calculations (WIX code). For CM kinetic energy spectra, fair agreement is found between data and a recently developed transport model.

Sideward flow in Au + Au collisions at 400 A MeV

(Nucl. Phys. A 587 (1995) 802)

Ramillien, V., P. Dupieux, J.P. Alard, V. Amouroux, N. Bastid, L. Berger, S. Boussange, L. Fraysse, M. Ibnouzhahir, G. Montarou, I. Montbel, P. Pras, Z. Basrak, I.M. Belayev, M. Bini, Th. Blaich, A. Buta, R. Caplar, C. Cerruti, N. Cindro, J.P. Coffin, R. Donà, J. Erö, Z.G. Fan, P. Fintz, Z. Fodor, R. Freifelder, S. Frolov, A. Gobbi, Y. Gregorian, G. Guillaume, C. Hartnack, N. Herrmann, K.D. Hildenbrand, S. Hölbling, A. Houari, S.C. Jeong, F. Jundt, J. Kecskemeti, P. Koncz, Y. Korchagin, R. Kotte, M. Krämer, C. Khun, I. Legrand, A. Lebedev, C. Maguire, V. Manko, P. Maurenzig, G. Mgebrishvili, J. Mösner, D. Moisa, W. Neubert, A. Olmi, G. Pasquali, D. Pelte, M. Petrovici, G. Poggi, F. Rami, W. Reisdorf, A. Sadchikov, D. Schüll, Z. Seres, B. Sikora, V. Simion, S. Smolyankin, U. Sodan, K. Teh, R. Tezkratt, M. Trzaska, M.A. Vasiliev, P. Wagner, J.P. Wessels, T. Wienold, Z. Wilhelmi, D. Wohlfarth, A.V. Zhilin

Abstract: We present new experimental data obtained with the FOPI detector at SIS, for the Au + Au heavy-ion collisions at 400 A MeV incident energy. The sideward flow, determined from a method without reaction-plane reconstruction, and the nuclear stopping are studied as a function of the centrality of the collisions. In order to study the nuclear in-medium effects, which act on the NN cross sections and potential and hence on experimental observables like the nuclear-matter flow and stopping, these results are compared with the predictions of two different QMD versions. The first one offers a fully microscopic calculation of the cross sections and potential in the G-matrix formalism and naturally includes the in-medium effects (this version is for the first time confronted with experiment). The second one uses a standard Skyrme potential plus a momentum-dependent term in order to mimic the in-medium effects.

On the transverse momentum distribution of strange hadrons produced in relativistic heavy ion collisions

(Z. Phys. A 352 (1995) 355)

Ritman, J.L., N. Herrmann, D. Best, J.P. Alard, V. Amouroux, N. Bastid, I. Belyaev, L. Berger, J. Biegansky, A. Buta, R. Caplar, N. Cindro, J.P. Coffin, P. Crochet, R. Dona, P. Dupieux, M. Dzelalija, P. Fintz, Z. Fodor, A. Genoux-Lubain, A. Gobbi, G. Goebels, G. Guillaume, Y. Grigorian, E. Häfele, K.D. Hildenbrand, S. Hölbling, F. Jundt, J. Kecskemeti, M. Kirejczy, Y. Korchagin, R. Kotte, C. Kuhn, D. Lambrecht, A. Lebedev, A. Lebedev, I. Legrand, Y. Leifels, C. Maazouzi, V. Manko, T. Matulewicz, J. Mösner, S. Mohren, D. Moisa, W. Neubert, D. Pelte, M. Petrovici, C. Pinkenburg, F. Rami, V. Ramillien, W. Reisdorf, C. Roy, D. Schüll, Z. Seres, B. Sikora, V. Simion, K. Siwek-Wilczynska, V. Smolyankin, U. Sodan, L. Tizniti, M. Trzaska, M.A. Vasliev, P. Wagner, G.S. Wang, T. Wienold, D. Wohlfarth, A. Zhilin

Abstract: Particles with strange quark content produced in the system 1.93 AGeV ^{58}Ni on

^{58}Ni have been investigated at GSI Darmstadt with the FOPI detector system. The correlation of these produced particles was analyzed with respect to the reaction plane. Λ baryons exhibit a very pronounced sideward flow pattern which is qualitatively similar to the proton flow. However, the kaon (K^+ , K^0) flow patterns are significantly different from that of the protons, and their form may be useful to restrict theoretical models on the form of the kaon potential in the nuclear medium.

The FOPI Detector at SIS/GSI

(Nucl. Phys. B (Proc. Suppl.) 44 (1995) 708)

Ritman, J. for the FOPI Collaboration

Abstract: The FOPI detector system has been assembled at SIS/GSI to study the properties of hot and dense nuclear matter. The program of FOPI was subdivided to permit the start of a specific program from the beginning of SIS operation. Therefore, the completed system which covers nearly the full 4π solid angle has been built in three stages. (1) The forward plastic wall detector was completed in 1990 and has been successfully employed to measure intermediate mass fragment production in reactions of Au on Au at 150 to 1000 A MeV. (2) The superconducting solenoid and Central Drift Chamber were completed in 1992 and have also been successfully employed to study charged pion production in Au on Au at 1050 A MeV. (3) The plastic scintillator/Cherenkov Barrel and forward drift chamber HELITRON are partially installed and the full commissioning is expected at the beginning of 1995. Results from recent test experiments involving all three phases which demonstrate the detector's ability to identify the rare signals from Kaon and Λ particle production will be presented.

Electromagnetic fission of ^{238}U at 600 and 1000 MeV per nucleon

(Z. Phys. A 353 (1995) 197)

Rubehn, Th., W.F.J. Müller, R. Bassini, M. Begemann-Blaich, Th. Blaich, A. Ferrero, C. Groß, G. Imme, I. Iori, G.J. Kunde, W.D. Kunze, V. Lindenstruth, U. Lynen, T. Möhlenkamp, L.G. Moretto, B. Ocker, J. Pochodzalla, G. Raciti, S. Reito, H. Sann, A. Schüttauf, W. Seidel, V. Serfling, W. Trautmann, A. Trzcinski, G. Verde, A. Wörner, E. Zude, B. Zwieglinski

Abstract: Electromagnetic fission of ^{238}U projectiles at $E/A = 600$ and 1000 MeV was studied with the ALADIN spectrometer at the heavy-ion synchrotron SIS. Seven different targets (Be, C, Al, Cu, In, Au and U) were used. By considering only those fission events where the two charges added up to 92, most of the nuclear interactions were excluded. The nuclear contributions to the measured fission cross sections were determined by extrapolating from beryllium to the heavier targets with the concept of factorization. The obtained cross sections for electromagnetic fission are well reproduced by extended Weizsäcker-Williams calculations which include E1 and E2 excitations. The asymmetry of the fission fragments' charge distribution gives evidence for the excitation of the double giant-dipole resonance in uranium.

Multifragmentation study on 30 A MeV $^{32}\text{S} + ^{58}\text{Ni}$
(Z. Phys. A 350 (1995) 327)

Siwek, A., A. Sourell, A. Budzanowski, H. Fuchs, H. Homeyer, G. Pausch, W. Kantor, G. Röscher, C. Schwarz, W. Terlau and A. Tutay

Abstract: In a multidetector experiment on 26 or 30 A MeV $^{32}\text{S} + ^{58}\text{Ni}$, up to four coincident heavier or intermediate-mass fragments were observed. One of these occasionally has the characteristics of a projectile-like fragment, up to three may be attributed to the decay of the heavy reaction product. Taking the velocity of the fragments as a measure of the heavy-product excitation energy, one finds evaporation, fission and multifragmentation to follow one another with rising excitation. Model simulations of sequential decay with up to two binary fissions and, alternatively, of simultaneous statistical multifragmentation were performed for comparison with experimental distributions of mass, velocity and (for events with three slow intermediate-mass fragments) relative azimuthal angle. Though in the three-fragment events indications of simultaneous multifragmentation are present, the sequential binary decay predominates. Evaporated protons and α particles detected in coincidence have a mean multiplicity growing with excitation energy, while the temperature governing the spectra has a plateau with a value of about 5.5 MeV.

Temporal and thermal properties of intermediate-mass fragments from the $^{32}\text{S} + ^{58}\text{Ni}$ reaction at 30 A MeV
(Acta Physica Polonica B 26 (1995) 1413)

Tutay, A., A. Budzanowski, H. Fuchs, H. Homeyer, G. Pausch, C. Schwarz, A. Siwek, A. Taymaz

Abstract: Information on thermal and temporal aspects of intermediate-mass fragment (IMF) formation was obtained by studying correlations between (a) two IMFs, (b) one IMF and one α particle, and (c) one heavy residue and one α particle produced in collisions of 960 MeV ^{32}S projectiles with ^{58}Ni . The fragments and/or light particles were detected in the ARGUS multidetector array at the VICKSI accelerator of the HMI Berlin. The relative-energy distributions are of Maxwellian shape yielding a temperature of 5 MeV for the heavy reaction products, but only of about 3 MeV for the primary IMFs. Thus IMFs seem to be emitted towards the end of the evaporation chain. The relative-velocity correlations between two IMFs (Li, Be, B, C) display longer emission times when one of the IMFs is a lighter one (Li, Be), compatible with the picture that the latter are more likely to result from a multi-step decay.

5 Positron Emission Tomography and Radiation Physics

The Installation of a PET-Scanner for In-Situ Dose Localization at the Heavy Ion Therapy at GSI Darmstadt^B

W. ENGHARDT¹, B.G. HASCH, R. HINZ, K. LAUCKNER, J. PAWELKE, M. SOBIELLA

There has been considerable progress in building up the heavy ion therapy at GSI Darmstadt during the year 1995: The treatment cave with the medical beam line and the technical control room have been finished to a major extent. Furthermore, a new building that houses all the auxiliary facilities for therapy (e.g. the medical control room, the patient waiting and preparation areas) has become available by the end of the year. Patient treatments with ^{12}C -beams are envisaged to start in the second half of 1996.

The installation of the PET-scanner [1] for in-situ therapy control by means of in-beam imaging the spatial distribution of β^+ -emitters produced by the therapy beam via nuclear fragmentation in the target volume has to be synchronized with those activities. Thus, the construction of the PET-gantry that will bear the detector heads has been completed in spring 1995 and the gantry has been mounted at the beam delivery in June (Fig. 1). In November it has been completed by a computer controlled stepping motor driven movement system [2] for a precise positioning of the detectors with respect to the patient. The detectors will be mounted in January 1996. Further activities in preparing the PET application to heavy ion therapy concerning tomographic reconstruction and data evaluation are published elsewhere in this report [3,4,5].

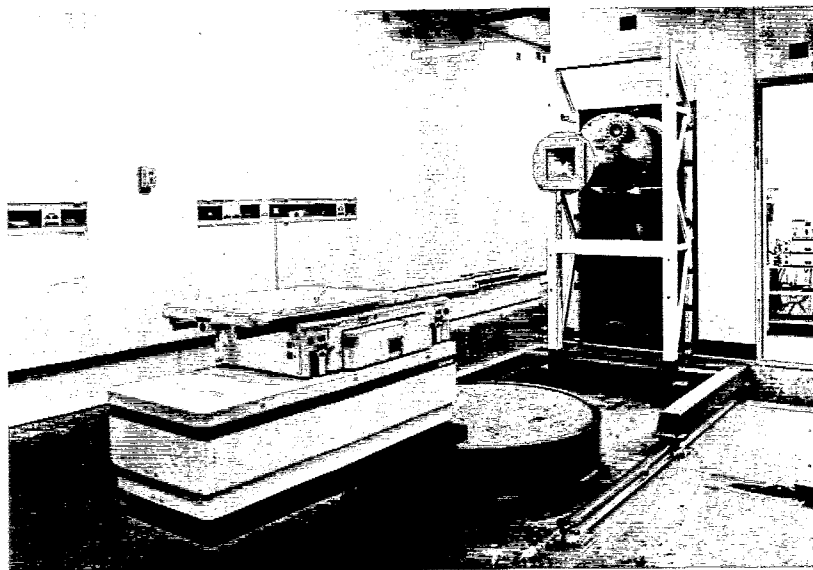


Fig. 1 The medical beam delivery with the PET-gantry. For imaging the gantry will be moved beam-down to the patient couch in the foreground. (Photo: A. Zschau, GSI)

¹ FZR and Uniklinikum der TU Dresden, Fetscherstr. 74, D-01307 Dresden, Germany

References

- [1] W. Enghardt et al., Annual Report 1994, **FZR-78** (1995) 135
- [2] R. Hinz et al., Annual Report 1994, **FZR-78** (1995) 137
- [3] K. Lauckner et al., this Annual Report
- [4] R. Hinz et al., this Annual Report
- [5] B.G. Hasch et al., this Annual Report

The Determination of the Bragg Peak Position from β^+ -Emitters Generated by Nuclear Fragmentation for the Treatment Plan Verification at Heavy Ion Tumour Therapy^B

B.G. HASCH, W. ENGHARDT¹, J. PAWELKE, D. SCHARDT², L. SIHVER²,
M. SOBIELLA, U. WEBER²

The verification of the treatment plan for heavy ion tumour therapy requires the determination of the Bragg peak position since it coincides with the region, where the maximum biological effect is observed. This position can be extracted from the spatial distribution of β^+ -emitters, which are produced by nuclear fragmentation of the stable therapy beam. The technique of positron emission tomography enables the imaging of that distribution. This method of control is founded on the comparison of the measurements performed by a PET-scanner [1,2] and simulations of the heavy ion transport in the irradiated target volume [3]. Depending on the operation mode of the PET-scanner two different situations can be met in the application of this control method to the heavy ion tumour therapy. In the first case, in which β^+ -emitters are produced by primary projectiles of single energy the comparison of simulated and measured spatial distributions of the positron emitting fragments show that the position of the Bragg peak can be determined with an accuracy better than 1 mm (Fig. 1).

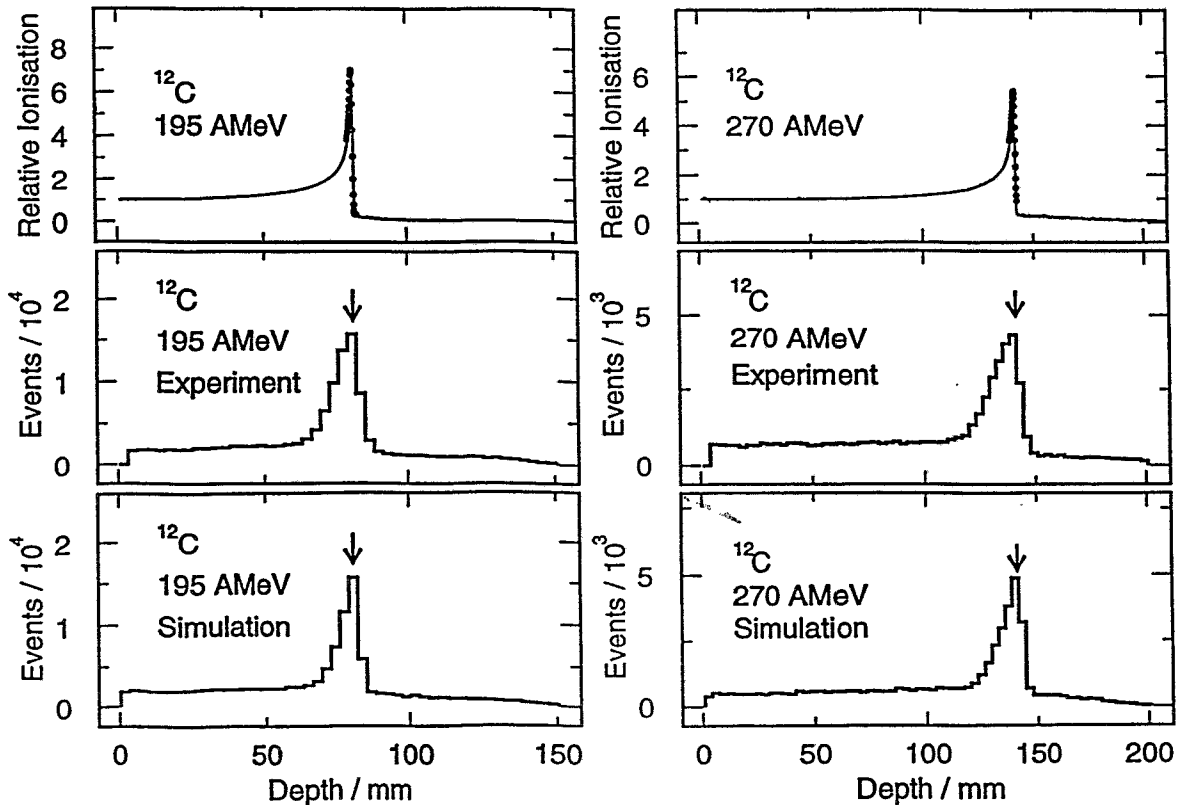


Fig. 1 Comparison between the simulated (solid line) and the measured (dots) depth dose distribution and the depth distributions of the annihilation points corresponding to the depth distribution of the produced β^+ -emitting fragments for a 195 AMeV and 270 AMeV ^{12}C beam in PE (poly-ethylene). The arrows are indicating the Bragg peak position.

These experiments were realized with a small positron camera in combination with a binary range shifter [4] which allowed us to measure the corresponding depth dose distribution in the vicinity of the Bragg peak position.

Tumour conform irradiation requires the variation of particle ranges by the variation of the beam energy. While the first operation mode for one energy could be useful to test the correctness of the treatment plan at critical points of the treatment volume with a relatively low dose before the full dose fraction will be given, in a second operation mode of the PET-scanner a superposition of spatial distributions of β^+ -emitters each corresponding to one beam energy will be measured. Concerning this we simulated the irradiation of a PMMA phantom in such a way that a horizontal oriented disk of 5 cm diameter and a thickness of 1 cm with its centre in a depth of 10 cm would receive a physical isodose of 2 Gy (Fig. 2).

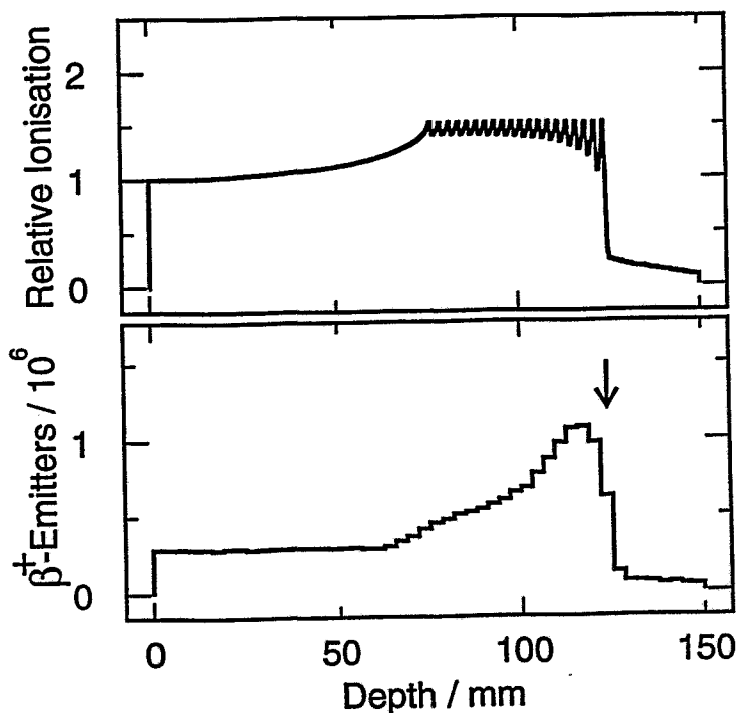


Fig. 2 Simulated depth dose distribution for ^{12}C of 20 energies (202.5-269.5 AMeV) normalized to the dose in the entrance channel (top) and the corresponding superposition of depth distributions of β^+ -emitting fragments in a PMMA target (bottom) for a 1.25 cm broad band along the beam axis. The calculated Bragg peak position for primary projectiles with 269.5 AMeV is marked with an arrow.

¹ FZR and Uniklinikum der TU Dresden, Fetscherstr. 74, D-01307 Dresden, Germany

² Gesellschaft für Schwerionenforschung, Planckstr. 1, D-64291 Darmstadt, Germany

References

- [1] W. Enghardt et al., this Annual Report
- [2] K. Lauckner et al., this Annual Report
- [3] B.G. Hasch et al., Annual Report 1994, FZR-78 (1994) 138
- [4] U. Weber et al., GSI Scientific Report 1994, GSI 94-1 (1995) 217

Parallelization of an Iterative Reconstruction Algorithm for Positron Emission Tomography ^B

R. HINZ, W. ENGHARDT¹

The therapy monitoring and treatment plan verification in the heavy ion tumour therapy at GSI will be performed by PET. Due to the limited angle geometry of the PET scanner and low count rates an iterative algorithm is required to reconstruct the spatial distribution of β^+ -emitters [1]. Its major drawbacks in comparison with conventional filtered backprojection are long computation time and large memory requirements. For a clinical use the time for a complete image reconstruction (approximately 50 iteration steps) must not exceed one hour. Therefore, the program has been accelerated by parallelization of the code and installation of a powerful multiprocessor computer.

The reconstruction algorithm has been parallelized by Single Program Multiple Data (SPMD) programming technique where the same program is executed on each node of the multiprocessor with its local data. Caused by the coarse granularity of the program, i. e. there is much more floating point computation inside a single program thread than communication between these threads, a high speedup - roughly the number of processors - compared with a single processor system is achieved.

A lot of investigations were done to find out a hardware adapted optimally to the specific problem [2]. A benchmark program was extracted from the most time consuming part of the whole reconstruction. It was run on several machines with different processor architectures (Tab. 1).

The Silicon Graphics PowerChallenge parallel computer has become the machine of our choice. It combines an intuitive shared-memory programming model, high floating point uniprocessor performance, expandability up to 18 processors, general-purpose software environment, reliability and compelling price/performance.

Table 1 Measured runtimes of a specific benchmark program on several single processors

Machine	Processor	Time consumed
HP 9000/735	HP PA-7100 (90 MHz)	2:33 min
SUN SPARCstation 10 Modell 50	SuperSPARC (50 MHz)	8:01 min
DEC 4000-710	Alpha 21064 (190 MHz)	3:22 min
DRESSLER GIGAmachine	SuperSPARC (50 MHz)	7:13 min
Parsytec GC/PowerPlus	PowerPC 601 (80 MHz)	6:23 min
PARAMID TTM 220	Intel i860-XP (50 MHz)	5:58 min ^a
SGI PowerChallenge	MIPS R8000 (90 MHz)	1:11 min ^a
Parsys TransAlpha	Alpha 21066 (233 MHz)	1:49 min

^a) processor architecture and compiler supported vectorized intrinsic functions.

¹ FZR and Uniklinikum der TU Dresden, Fetscherstr. 74, D-01307 Dresden, Germany

References

- [1] K. Lauckner et al., this Annual Report
- [2] R. Hinz, Diploma Thesis, TU Chemnitz-Zwickau 1994

Modifications of an Iterative Reconstruction Algorithm for a Spherical Symmetric PET-Scanner^B

K. LAUCKNER, W. ENGHARDT¹, F. HENSEL, R. HINZ

A double head PET-scanner, each head consisting of 8x4 BGO detector blocks, will be used to perform a treatment plan verification of 3D conformal radiation therapy. Due to its spherical geometry modifications of the reconstruction algorithm, which was developed for preceding investigations [1], were necessary. Consequently the modelling of the measurement for computing a 3D backprojection from an iteratively calculated source distribution has been changed substantially.

This involved a determination of solid acceptance angles for each voxel in the image space relating to the camera dimensions. In an effort to avoid repetitive calculations these values were calculated explicitly and stored in look-up tables. In addition the blurring of a considered source voxel has been determined depending on the distance to each voxel that was checked before to lie within the acceptance angle of this source voxel. The consequence of this model to the backprojection of measured data is that the increment of the voxels hit by a coincidence line is dependent on the slope of this line through the voxel.

A reconstruction of two ²²Na point sources of 2 mm diameter in a distance of 25 mm to each other is performed into an image space of 64x32x32 voxels and a voxel size of 3.375 mm. Comparison and updating of the estimated image are executed voxel-by-voxel [2].

The algorithm converges fast. After five iteration steps the spatial resolution (FWHM) of the investigated point sources did not change significantly. Table 1 displays the FWHM determined by a Gaussian fit after backprojection of the measured data (line 1) compared to the FWHM after five iteration steps (line 2). However, further investigations showed that as the number of iterations increased the image became increasingly noisy. In order to reduce the higher spatial frequencies a 3x3x3 lowpass spatial filter, the filter shape modeled by a sampled Gaussian function, is used. In line 3 the FWHM for point sources reconstructed using such smoothing filter show a loss of spatial resolution and a slower convergence. If the camera will be installed at the beam line at GSI Darmstadt, further investigations will follow with measured data.

Table 1 FWHM of two point sources

	left source - 389 kBq			right source - 3.94 MBq		
	x/mm	y/mm	z/mm	x/mm	y/mm	z/mm
exp. backprojection	8.0	7.0	n.a.	9.3	7.5	n.a.
5. Iteration without filter	3.4	4.7	16.8	6.4	6.0	23.1
5. Iteration with filter	5.6	5.6	16.6	7.3	6.9	21.2

¹ Uniklinikum der TU Dresden and Institut für Kern- und Hadronenphysik, FZR

References

- [1] Enghardt W. et al, Phys. Med. Biol., **37** (1992) 791
- [2] Daube-Witherspoon M., Muehllehner G., IEEE Trans. Med. Imaging, **MI-5** (1986) 61

Detector Investigations for Non-Invasive PET Input Function Measurement^B

J. PAWELKE, B. BEUTHIEN-BAUMANN

The quantitation of physiological functions in-vivo by means of PET requires the accurate measurement of the radiotracer concentration in arterial blood (input function). In contrast to the traditional invasive techniques [1] we evaluated the feasibility of using an external detector probe around the arm or wrist for a non-invasive measurement of the arterial blood activity kinetics [2].

For this purpose the detector performance of a positron camera based on different small area multi-crystal BGO detectors [3] was tested in measurements with two ^{22}Na line sources (17.4 kBq/mm, 220 mm long, 3 mm in diameter) placed parallel next to each other (source separation of 4.5 mm) between a detector pair (separation of 830 mm). The influence of a patient arm was simulated by means of surrounding the line sources with a plastic cylinder (60 mm in diameter, 100 mm long). After subtraction of random coincidences and dead time correction tomograms were constructed by backprojection in the midplane of the camera field of view containing the line sources. Fig. 1 shows that an improved spatial resolution of the detectors results to a better separation of the line sources. For quantitative information the tomogram has been corrected with regard to the inhomogeneity of detector efficiency as well as attenuation and scattering caused by the phantom by means of blank and transmission scans with flood and point sources. However, the poor maximum count rate of the detector electronics as well as data acquisition system of about 2000 cps avoid adequate correction in practical use. Thus, the large area double head tomograph described in [3] was used for verifying the correction methods which works adequate as it is shown in Fig. 2.

We plan to use two detectors with an improved maximum count rate in clinical experiments.

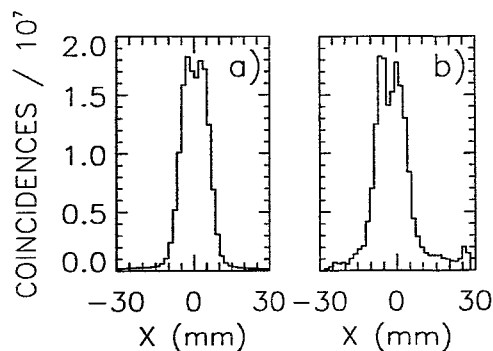


Fig. 1 Projection of the tomogram onto the axis perpendicular to the source line measured with two detectors of 6.75 mm (a) and 3.2 mm (b) intrinsic spatial resolution, respectively.

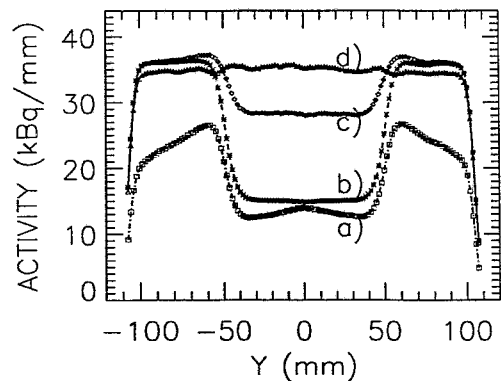


Fig. 2 Projection of the tomogram onto the axis parallel to the line sources after backprojection (a) including efficiency (b), attenuation (c) and scatter correction (d) measured with the tomograph.

References

- [1] L. Eriksson et al., IEEE Trans. Nucl. Sci. NS42 (1995) 1007
- [2] S. Rajeswaran et al., Proc. of the 1990 IEEE Nucl. Sci. Symp. (1990) 1308
- [3] J. Pawelke et al., Proc. of the Int. Conf. SCINT 95, (1996) 21

Experimental Determination of the Linewidth of Parametric X-Ray Radiation at Electron Energies below 10 MeV^{B,D,S}

R. ZAHN, J. FREUDENBERGER¹, M. GALEMANN¹, H. GENZ¹, L. GROENING¹, P. HOFFMANN-STASCHHECK¹, V.L. MOROKHOVSKII², V.V. MOROKHOVSKII¹, U. NETHING, H. PRADE, A. RICHTER¹, J.P.F. SELLSCHOP³

Parametric X-ray radiation (PXR) is created by a mechanism which allows the production of X-rays in the energy region from a few to several tens of keV using electron beams below 10 MeV [1] and is thought of as being a non-conventional source of X-rays [2]. PXR is generated when charged particles, i. e. electrons, are penetrating a crystal. The mechanism may be understood as the Bragg diffraction of virtual photons associated with the relativistic charged particle. In order to get more information about the properties of the radiation and the mechanism of its generation it is helpful to determine the linewidth. By the aid of the linewidth it becomes possible to deduce the spectral density which is of great interest concerning applications. Thus, we have determined the linewidth using an absorber technique [3].

The experiments have been performed behind the injection section of the superconducting linear accelerator S-DALINAC at the TH-Darmstadt [4]. The electron beam of 6.8 MeV kinetic energy hits a (55 ± 2) μm thick diamond crystal target which is mounted on a three axes goniometer. PXR is detected by means of a Si(Li)-detector which is placed at 42.9° with respect to the beam direction. The distance between crystal and detector of 2.307 m and the detector aperture of 7.5 mm diameter resulted in a solid angle of $\Delta\Omega = (8.3 \pm 0.03) \cdot 10^{-6}$ sr. In order to measure the beam current of a few nA the electrons were deflected into a Faraday-cup by a dipole magnet.

Because of the limited energy resolution of the Si(Li)-detector of about 250 eV (FWHM) at 5.9 keV it is impossible to determine the linewidth with this experimental set-up if the linewidth is much smaller than this energy resolution. Therefore, a copper absorption foil of $d_{Cu} = (27.7 \pm 0.9)$ μm thickness has been placed in front of the detector. The energy of the PXR line can be tuned by rotating the crystal with respect to the electron beam direction [5]. Thus, one is able to vary the PXR peak generated at the $(\bar{1}11)$ plane across the K-absorption edge of copper at $E_{K,Cu} = 8.979$ keV [6]. In fig. 1 the transmission $T(E)$ of the photons through the copper foil is plotted. The experimental points have been fitted by the function

$$T(E) = \frac{a}{1 + \exp\left(\frac{E - E_{K,Cu}}{W + s(E - E_{K,Cu})}\right)} \quad (1)$$

Here a , W and s are the attenuation, the linewidth and an asymmetry parameter. Approximating the absorption factor $A = \exp(-\mu d_{Cu})$, where μ is the absorption coefficient, near the K-edge of copper by a step function and assuming that the line shape does not vary in the investigated energy range the line shape is given by the derivative of the transmission. The line shape is plotted in fig. 2. The shaded area represents the range allowed by the experimental errors. The variance of the spectral distribution is $\sigma = (48 \pm 5)$ eV, which is in agreement with a Monte-Carlo-simulation [7]. The experimental accuracy is limited by the width of the K-edge of about 5 eV [8]. The measured linewidth allows us to deduce the spectral density of the peak of $J = (0.95 \pm 0.16) \cdot 10^{-7}$ photons/(electron sr eV). Furthermore, the Monte-Carlo-simulation shows that the main contributions to the linewidth

are caused by multiple scattering of the electrons ($\sigma_{MS} = 43$ eV) and are due to the solid angle of the detector ($\sigma_{\Delta\Omega} = 18$ eV).

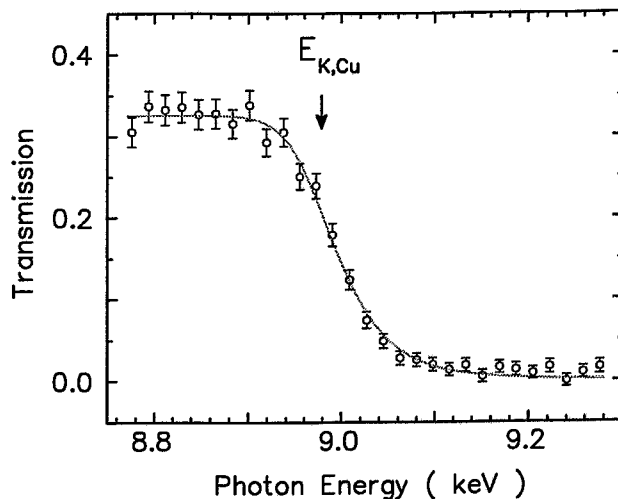


Fig. 1 Transmission of PXR through the absorber foil as a function of the PXR peak energy.

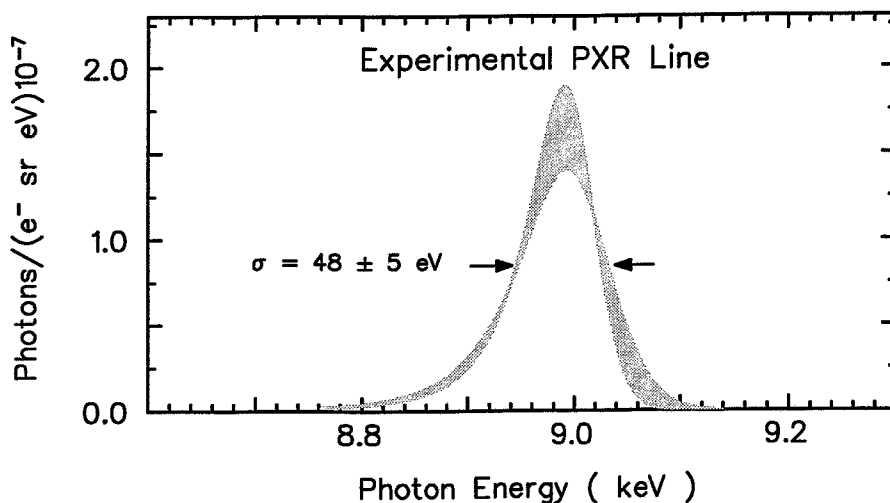


Fig. 2 Experimental shape of the PXR line at the K-edge of copper (8.979 keV).

¹Institut für Kernphysik, Technische Hochschule Darmstadt, Darmstadt, Germany

²Kharkov Institute of Physics and Technology, Kharkov, Ukraine

³University of the Witwatersrand, Johannesburg, South Africa

References

- [1] J. Freudenberger et al., Phys. Rev. Lett. **74** (1995) 2487
- [2] V.G. Baryshevsky, I.D. Feranchuck, Nucl. Instrum. and Meth. **228** (1985) 490
- [3] J. Freudenberger et al, accepted for publication in Nucl. Instrum. and Meth. B
- [4] J. Auerhammer et al., Nucl. Phys. A **553** (1993) 841c
- [5] V.L. Morokhovskii, CSRI atominform, Moscow, **39** (1989)
- [6] WM.J. Veigle, Atomic Data Tables **5** (1973) 51
- [7] J. Freudenberger et al., to be published
- [8] E.B. Saloman et al., Atomic Data and Nuclear Data Tables **38** (1988) 1

Comparison of Channeling Radiation and Parametric X-Ray Radiation Intensities for Diamond Crystals^{B,D,S}

U. NETHING, J. FREUDENBERGER¹, H. GENZ¹, L. GROENING¹,
P. HOFFMANN-STASCHECK¹, W. KNÜPFER³, V.L. MOROKHOVSKII²,
V.V. MOROKHOVSKII¹, A. RICHTER¹, J.P.F. SELLSCHOP⁴, AND R. ZAHN

The intensity of channeling radiation (CR) [1-3] was compared with the intensity of parametric X-ray radiation (PXR) [4-8] originating from the same diamond crystals. The investigations were carried out with relativistic electrons provided by the injector of the S-DALINAC at energies between 3.0 and 9.0 MeV. Both types of radiation were observed by means of Si(Li) detectors placed at 0° and 43° with respect to the electron beam axis for CR and PXR, respectively. A typical channeling spectrum is shown in fig. 1.

The results regarding PXR that are presented here were obtained by bombarding a 55 μm thick diamond crystal by electrons of 8.3 MeV and using the ($\bar{2}20$) plane. The bulk of data at other energies and planes was published elsewhere [4-8]. All experiments were performed in so-called Laue geometry, where electrons and photons leave the crystal through the same surface. An example of a PXR spectrum obtained under the conditions described above is shown in fig. 2.

Under the present experimental conditions the bandwidth of PXR is one order of magnitude smaller than that of channeling radiation. For the investigated electron energies the total number of photons produced by channeling radiation is four orders higher than that obtained by the ($\bar{2}20$) PXR reflex and three orders higher than that obtained by the ($\bar{1}11$) reflex [4].

To compare CR and PXR with synchrotron radiation we selected as an example the photon flux required to perform K-edge subtraction angiography [9]. For noninvasive digital subtraction angiography successful images were obtained with photon fluxes of $3.35 \cdot 10^{11}$ photons/(s mm²) at 33.17 keV with a bandwidth of 300 eV.

Using measured channeling radiation intensity produced in a 55 μm thick natural diamond crystal and scaling to the maximum beam current of the S-DALINAC of 60 μA , one can produce $\Phi = 2 \cdot 10^8$ photons/(s mm²) in an energy window of 300 eV. Assuming a linear increase of CR intensity with crystal thickness, using a 500 μm diamond at a beam current of 6 mA, one should be able to obtain $2 \cdot 10^{11}$ photons/(s mm²). To provide the required photon energy of 33 keV an electron beam energy of 21 MeV is necessary. At this photon energy, however, the linewidth will amount to 4.8 keV. Under these conditions one would need a monochromator which will reduce the CR flux to about 10^{10} photons/(s mm²) which is insufficient to meet the above stated criteria.

Using PXR and the present geometry one would need 100 MeV electrons in order to obtain with a Si crystal of 3.5 mm and a beam current of 6 mA a flux $\Phi = 2 \cdot 10^8$ photons/(s mm²) which is insufficient for the above selected example. For mammography, however, which is asking for photon energies at 16 and 20 keV the PXR fluxes are sufficient.

In conclusion it can be stated that both types of radiation, CR and PXR, can be used as tunable X-ray sources, where PXR is additionally nearly free of background. Furthermore, PXR is several orders of magnitude less intense than CR. Compared to monochromatic X-rays provided by synchrotrons and wigglers, on the basis of the present knowledge

CR does not meet the criteria with respect to the requirements of digital subtraction angiography since the CR spectral line is too wide.

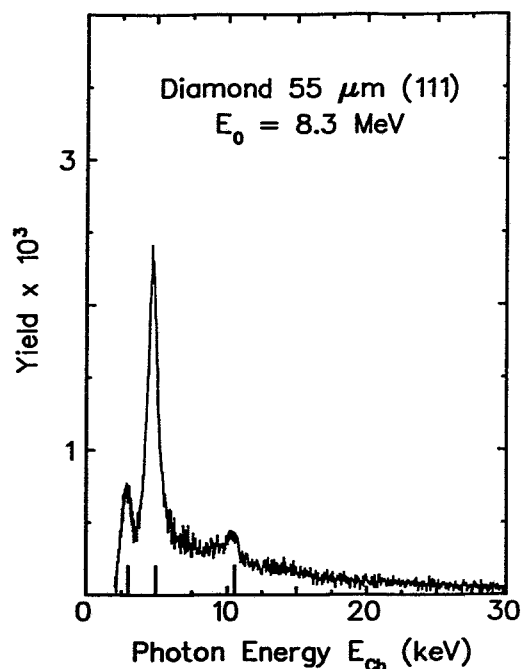


Fig.1 Channeling radiation spectrum for channeling along the (111) plane of diamond crystal obtained with 8.3 MeV electrons. The bremsstrahlung background has been subtracted.

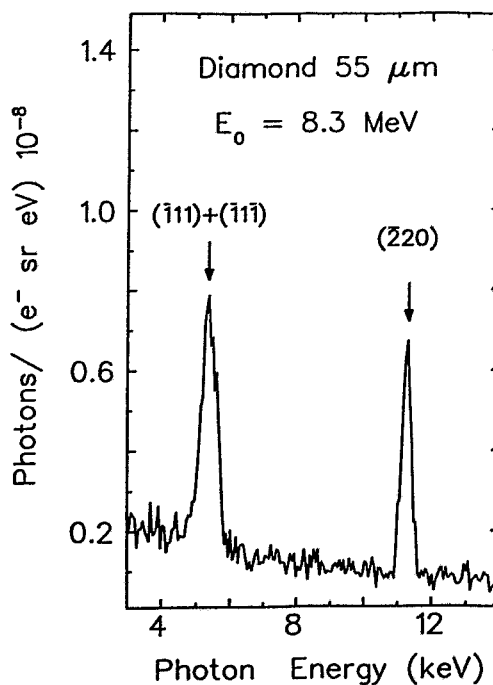


Fig.2 Parametric X-ray radiation spectrum obtained by bombarding a diamond crystal with 8.3 MeV electrons. No Background has been subtracted.

¹Institut für Kernphysik, Technische Hochschule Darmstadt, Darmstadt, Germany

²Kharkov Institute of Physics and Technology, Kharkov, Ukraine

³Siemens AG, Bereich Medizinische Technik, Erlangen, Germany

⁴University of Witwatersrand, Johannesburg, South Africa

References

- [1] U. Nething et al., Phys. Rev. Lett. **72**, 2411 (1994)
- [2] H. Genz et al., accepted for publication in Phys. Rev. B
- [3] U. Nething, PhD thesis, Technische Hochschule Darmstadt, 1995
- [4] J. Freudenberger et al., Phys. Rev. Lett. **74**, 2487 (1995)
- [5] J. Freudenberger et al., in preparation for publication
- [6] J. Freudenberger et al., accepted for publication in Nucl. Instrum. Methods B
- [7] J. Freudenberger et al., submitted for publication in Nucl. Instrum. Methods B
- [8] J. Freudenberger, Diploma Thesis, Technische Hochschule Darmstadt, 1995
- [9] W. Graeff and W.-R. Dix, in Handbook on Synchrotron Radiation, Vol. 4, edited by S. Ebashi, M. Koch and E. Rubenstein, Elsevier Science Publishers, pp. 402 (1991)

6 Technical and Methodic Developments

Status of the Beam Transport System for ELBE*

U. NETHING AND R. ZAHN

The ELBE project concerns a superconducting continuous wave (CW) linear accelerator for electrons with energies up to 20 MeV and a maximum beam current of 1 mA to be built up in Rossendorf. Since the gradient of the accelerator cavities may be higher than now assumed, the beam line is designed for electron energies up to 50 MeV. The research programme of the accelerator facility ELBE includes four kinds of experiments or fields: (a) nuclear resonance fluorescence experiments; (b) neutron experiments; (c) radiation physics (parametric X-rays, channeling radiation, Smith-Purcell radiation, transition radiation) and (d) application of a free electron laser (FEL). Consequently the accelerated beams will be directed into any one of four beam lines. The design of the corresponding beam transport system should be worked out on the basis of using only one kind of dipole and quadrupole magnets. This has the advantages of relatively low cost of the beam line and facilitates replacing defect components. In addition the number of power supplies is reduced. All bending arcs are symmetric and consist of three bending magnets. In order to simplify the beam handling it was tried to separate the bending and focusing functions from each other. Thus, the bending should take place in the arcs only and the focusing in straight sections.

The first optical element, a quadrupole triplet to match the beam into the arcs, is intended to be placed 2.5 m behind the last cavity of the accelerator, to leave space for pumps and diagnostic elements. The transport system to the free electron laser should be isochronous to provide the micro pulse structure of the electron beam which will be delivered by the accelerator [1] itself. Each isochronous arc [2] consists of three bending magnets and two quadrupole triplets. The bending angle of each sector dipole magnet is 30° and thus the total deflection is 90° . In comparison with other total deflection angles this conception guarantees the most effective use of the experimental area. Three arcs of this type has been chosen. The first one guides the beam into the radiation physics hall. The second one deflects the beam to the chamber of radiation physics experiments and the third one to the undulator of the FEL. To focus and match the electron beam into each arc quadrupole triplets are used. The transport system to the nuclear physics cave including the utilization of a tagging facility should be achromatic. It is possible to use a Brown-system [2] consisting of two bending magnets with a quadrupole triplet in between or a Penner-system (Leboutet and Pinel-system) [3] made out of three dipoles. In order to deflect the beam by 30° we decided to design a Penner-system. It is much shorter than the Brown-system and furthermore the Brown-system would need 15° -magnets. It should be possible to place a collimator in the symmetry plane of this arc to get a well defined energy for the tagger. Behind that arc a quadrupole duplet is intended to match the electron beam into the tagger. If the two bending magnets which are placed collinear to the accelerator are degaussed the electron beam will be transported to beam diagnostic elements and afterwards to a neutron production target.

The calculations were performed with the programs TRANSPORT [4] and XBEAM [5]. Furthermore, the transport system will be calculated in higher orders with the program MAD [6]. All these programs are based on matrices. In addition, we will study the space charge effects with the aid of the program TRACE 3-D [7]. This is in particular of great

* a superconducting 20 MeV Electron source with high Brilliance and low Emittance.

interest for the pulsed beam, which is necessary for the FEL. The calculations which have been performed up to now are based on phase space ellipsoids at energies of 2.9, 10.2 and 20.2 MeV for CW operation. The ellipsoids include 90% of the electrons. Figure 1 shows the result for the envelopes of the electron beam at an electron energy of 2.9 MeV in the range from the last cavity of the accelerator ($d=0$) to the end of the first isochronous arc. In figure 2 the resulting envelopes are shown starting again at the last cavity of the accelerator and ending behind the achromatic transfer system for the tagging system. The transport system may still change in the near future, because the ELBE project is still in a developing process. Furthermore, the position of beam monitors and pumping units has not been fixed yet finally. Nevertheless, the above described concept is flexible and should meet the requirements.

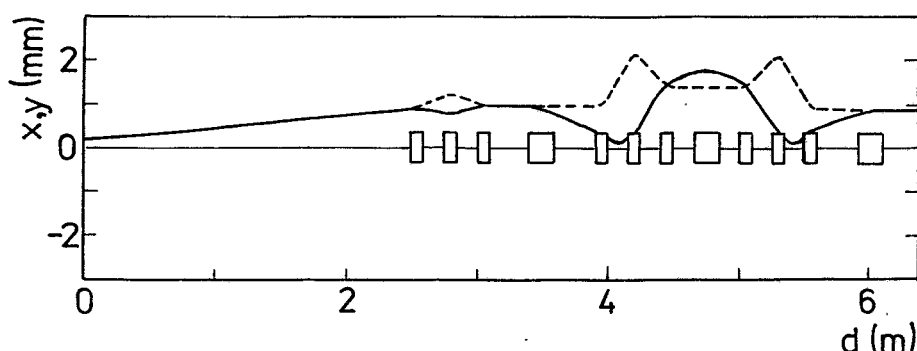


Fig1. Envelopes of the electron beam for the first triplet and the isochronous arc. The horizontal (solid line) and vertical (dashed line) plane are shown. The square boxes are the dipole magnets and the rectangular boxes the quadrupoles.

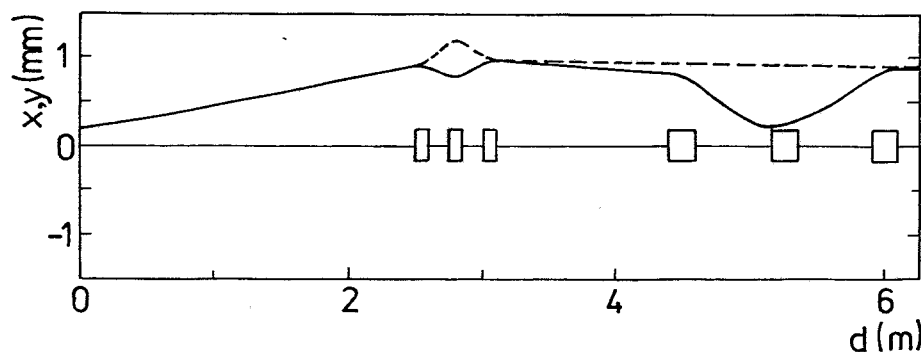


Fig2. Envelopes of the electron beam for the achromatic beam transport system to the tagger. The horizontal (solid line) and vertical (dashed line) plane are shown. The square boxes are the dipole magnets and the rectangular boxes the quadrupoles.

References

- [1] Elbe-Quelle, 20 MeV-Elektronenquelle, interner Projekt-Vorschlag, FZR, 1995
- [2] High Energy Beam Optics, K.G. Steffen, Interscience Publishers, John Wiley Sons, New York, 1965
- [3] S. Penner, Rev. Sci. Instrum., Vol. 32 2, 150, 1961
- [4] Third-Order Transport, D.C. Carey, K.L. Brown and F. Rothacker, SLAC-R-95-462
- [5] XBEAM, Th. Winkler, Diploma thesis, TH-Darmstadt, 1994
- [6] MAD, H. Grote, F.C. Iselin, CERN program library entry T5001, CERN, 1990
- [7] TRACE 3-D, K.R. Crandall and D.P. Rusthoy, LA-UR-90-4146, Los Alamos, 1990

EuroSiB – A 4π Silicon Ball for Detection of Light Charged Particles Inside the γ -Spectrometer EUROBALL

G. PAUSCH, H. PRADE, M. FREITAG, J. HUTSCH, M. SCHEINPFLUG, M. SOBIELLA,
W. BOHNE¹, H. GRAWE¹, K.-H. MAIER¹, M. MOSZYŃSKI², D. WOLSKI²,
J. CEDERKÄLL³, A. JOHNSON³, R. SCHUBART⁴, G. DEANGELIS⁵,
AND THE EUROBALL ANCILLARY DETECTORS GROUP

EuroSiB – a 4π Si ball for charged-particle detection to be used as an ancillary detector for the European γ -spectrometer EUROBALL – is presently under construction at the Research Center Rossendorf and planned to be assembled for first experiments in 1997. The combination of such a 4π detector for light charged particles (LCP) with the highly efficient γ -array EUROBALL opens a wide field of applications, such as exit-channel selection for exotic states and nuclei, charged-particle spectroscopy, and Doppler correction of γ -ray energies [1]. Presently operated ancillary LCP detectors suffer either from relatively large absorption of γ -rays due to the use of high- Z scintillators (CsI arrays), or from poor proton-alpha discrimination at low energies which reduces the total α -counting efficiency (ΔE or $\Delta E-E$ Si-arrays). The design goal of EuroSiB is to overcome these limitations by combining the advantage of a selfsupporting Si ball [2,3] (minimum interference with γ detection because of low mass and low Z) with a new method of LCP identification – the pulse-shape discrimination (PSD) technique which allows p/α discrimination in "reversed" planar Si detectors down to ≈ 2 MeV [4].

EuroSiB is composed of 42 elements, each of them consisting of a Si detector (implanted p^+nn^+ structure, 500 μm thickness, active area ≈ 1300 mm^2) glued onto a thin (630 μm) ceramics backing. These elements are connected to a selfsupporting structure by means of small aluminum connectors. After completing the CAD design [5], three sets of ceramics backings were produced by Radeberger Hybridelektronik GmbH [6] and assembled at the Detector Laboratory Rossendorf. A first "dummy ball", consisting of backings without detectors, was mounted (Fig. 1).

Serious efforts have been made to test the performance of prototype Si detectors with respect to PSD without expensive beam experiments (see contributions in this volume). The first prototype detectors for EuroSiB delivered by Eurisys Mesures [7] turned out to suffer from inhomogeneities of the bulk resistivity, which limit the p/α resolution at low energies. This is in contrary to the results [4] obtained with detectors from the Berlin Si Ball [2,3]. To reach the design goal – a total counting efficiency of $\approx 90\%$ for protons as well as for alpha particles – it is necessary to improve the homogeneity of the detectors. A prototype of the frontend electronics for EuroSiB, based on the principle described in ref. [4], was developed at Swierk (Poland) [8] and successfully tested in a beam experiment at VICKSI. This electronics comprises the complete spectroscopy channel (spectroscopy amplifier with ballistic-deficit correction) and the zero-crossing channel (shaping amplifier, constant-fraction discriminator, zero-crossing discriminator) on half of a standard NIM module. Serial production of the NIM modules will start in 1996.

¹ *Hahn-Meitner-Institut Berlin, Bereich F, Glienicke Str. 100, D-14109 Berlin*

² *Soltan Institute for Nuclear Studies, Dept. of Nuclear Electronics, PL-05-400 Otwock-Świerk, Poland*

³ *Royal Institute of Technology, Physics Department, S-10405 Stockholm, Sweden*

⁴ *GSI Darmstadt, Postfach 11 05 52, D-64220 Darmstadt*

⁵ *INFN, Laboratori Nazionali di Legnaro, Via Romea 4, I-35020 Legnaro (PD), Italy*

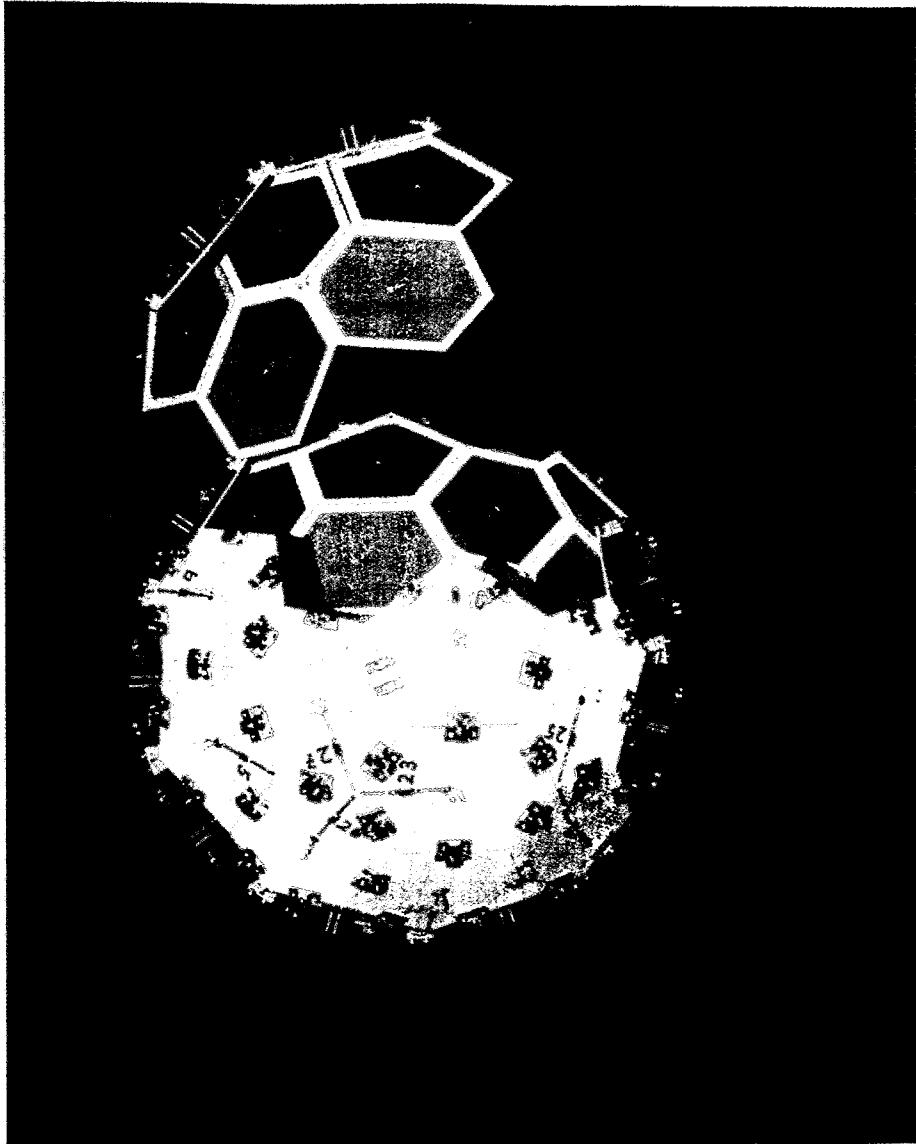


Fig. 1 *The EuroSiB "dummy ball" mounted at the Detector Laboratory*

References

- [1] H. Grawe et al., Proposal for a 4π Si-ball for EUROBALL, HMI Berlin, July 1994
- [2] W. Bohne et al., Annual Report 1991, HMI-B 497 (1992) 92, HMI Berlin
- [3] W. Bohne et al., Annual Report 1992, HMI-B 507 (1993) 79, HMI Berlin
- [4] G. Pausch et al., Nucl. Instr. and Meth. **A365** (1995) 176
- [5] W. Enghardt et al., Annual Report 1994, FZR-78 (1995) 107, FZ Rossendorf
- [6] Radeberger Hybridelektronik GmbH, Heidestraße 70, D-01454 Radeberg, Germany
- [7] Eurisys Meßtechnik GmbH, Nahestraße 2-4, D-55118 Mainz, Germany
- [8] M. Moszyński, D. Wolski, EUROBALL Ancillary Detectors Group Meeting, FZ Rossendorf, May 18-19, 1995

Beam Test of Si Detectors and Electronics for EuroSiB

G. PAUSCH, W. BOHNE¹, J. CEDERKÄLL², H. GRAWE¹, W. KLAMRA²,
M. MOSZYŃSKI³, G. RÖSCHERT¹, R. SCHUBART⁴, D. WOLSKI³

The 4 π Si ball EuroSiB [1,2] – an ancillary charged-particle detector for the γ -spectrometer EUROBALL – will exploit the pulse-shape discrimination (PSD) technique with "reversed" Si-detectors to identify the protons and α particles produced in fusion-evaporation reactions [3]. This technique has never been applied in a multidetector array, and therefore it was necessary to test the performance of prototype detectors delivered by Eurisys [4] and the prototype module of the frontend electronics developed at the SINS Swierk [5] in a beam experiment at the Ion-Beam Laboratory (ISL) Berlin.

We produced protons and alphas by bombarding a 6 mg/cm² Ni target with a 2 pA beam of 150 MeV ³⁶Ar projectiles. The detectors were mounted without any absorber foil at a distance of 15 to 17 cm from the target. To protect the detectors against δ electrons we applied a voltage of +20 kV to the target. The electronics realized in the prototype module corresponds to the usual scheme of signal processing for PSD with reversed Si detectors [3]. The two analogue outputs – zero-crossing time t_{ZC} and energy signal E – were used to generate the particle-identification plots. The results obtained with a "reference" detector (Tab. 1, No. 1) demonstrate a proper work of the frontend electronics (Fig. 1c). However, we observed an unexpected high background of low-energy signals due to the X-rays produced in the target. To optimize the energy resolution under such conditions – which are typical for nuclear-structure experiments – it is necessary to modify the baseline restorer of the spectroscopy amplifier. The performance of the EuroSiB prototype detectors (Tab. 1, No. 2-3) with respect to p/α -discrimination turned out to be insufficient (Fig. 1a,b). Simple measurements with radioactive α sources suggested that this is due to resistivity variations in the bulk silicon on a scale of a few millimeters, which cause the pulse shape to depend on the point of impact [2]. This fact was confirmed in the beam experiment. We applied an aperture in front of the detector, thus selecting a spot of ≈ 2 mm diameter which was exposed to the reaction products. The resulting p/α -discrimination is excellent (Fig. 1d). A disturbance of the discrimination performance due to the large detector capacitance or noise problems is therefore excluded.

In addition to these tests we exposed a telescope – consisting of two reversed, 50 μ m (ΔE) and 500 μ m (E) Si detectors (Tab. 1, No. 4 and 1) – to intermediate-mass fragments produced in reactions of 510 MeV ³⁶Ar projectiles with C, Al, Ni, Ag, and Au nuclei in mixed targets. PSD was applied to both detectors, but for the ΔE detector we used the "stretcher method" [6] instead of the zero-crossing technique. The scatterplot (Fig. 2a) confirms the presumption that the particle-discrimination thresholds are reduced by exploiting thinner detectors of lower resistivity. We identified C, Mg, and Ar ions down to 1.8, 2.5, and 3.0 A MeV, respectively. Elements up to Cr ($Z=24$) were identified. The ΔE - E spectrum (Fig. 2b) can be used to identify most of the ions stopped in the E detector, and to analyze the shape of the $t_{ZC}(E)$ curves in the PSD plot (Fig. 2c) as a function of Z down to energies below the PSD identification thresholds. Information about the physical effects limiting the PSD resolution at low energies is expected from such an analysis.

¹ Hahn-Meitner-Institut Berlin, Bereich F, Glienicker Str. 100, D-14109 Berlin

² Royal Institute of Technology, Physics Department, S-10405 Stockholm, Sweden

³ Soltan Institute for Nuclear Studies, Dept. of Nuclear Electronics, PL-05-400 Otwock-Świerk, Poland

⁴ GSI Darmstadt, Postfach 11 05 52, D-64220 Darmstadt

Table 1 Detectors used in our beam test

No.	Type / Shape	Producer	Technology	d [μm]	A [mm^2]
1	IPH 450-500-20 TM	Eurisys	Implanted p^+nn^+ structure	500	450
2	EuroSiB Hexagon	Eurisys	Implanted p^+nn^+ structure	500	≈ 1300
3	EuroSiB Pentagon	Eurisys	Implanted p^+nn^+ structure	500	≈ 1300
4	TD-15-50-50	Ortec	Surface-barrier detector	50	50

References

- [1] H. Grawe et al., Proposal for a 4π Si-ball for EUROBALL, HMI Berlin, July 1994
- [2] G. Pausch et al., see contribution in this volume
- [3] G. Pausch et al., Nucl. Instr. and Meth. **A365** (1995) 176
- [4] Eurisys Meßtechnik GmbH, Nahestraße 2-4, D-55118 Mainz, Germany
- [5] M. Moszyński, D. Wolski, EUROBALL Ancillary Detectors Group Meeting, FZ Rossendorf, May 18-19, 1995
- [6] W. Bohne et al., Annual Report 1992, HMI-B 507 (1993) 79

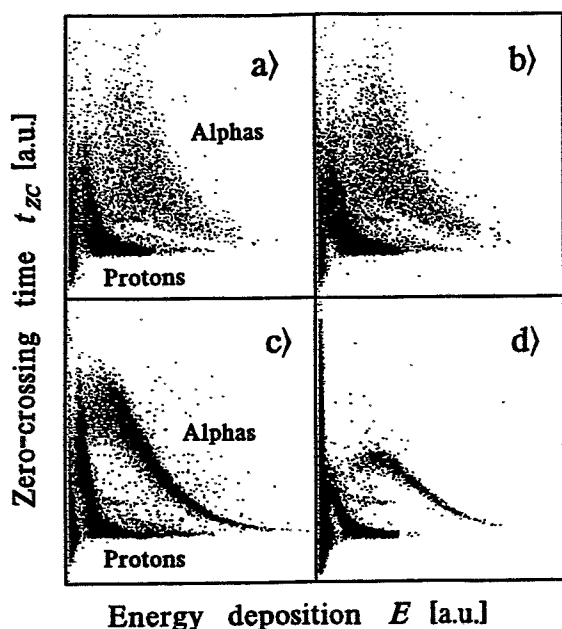
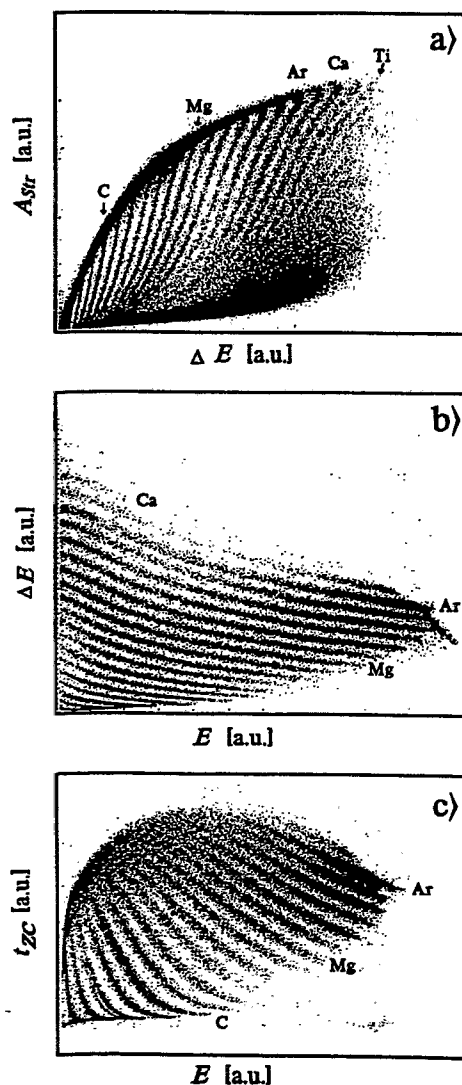


Fig. 1 p/α -discrimination obtained with the prototype electronics and detectors 1-3 of Tab. 1 (see text): a) EuroSiB pentagon; b) EuroSiB hexagon; c) "Reference" detector; d) EuroSiB hexagon (spot irradiation).

Fig. 2 IMF identification with a silicon ΔE - E telescope (see text): a) PSD plot (ΔE det.); b) ΔE - E plot; c) PSD plot (E det.).



A Simple Method to Test the Performance of Si Detectors for Particle Identification Based on PSD

G. PAUSCH, M. MOSZYŃSKI¹, D. WOLSKI¹, J. VON BORANY², J. CEDERKÄLL³,
M. FREITAG, J. HUTSCH, M. SOBIELLA

Recent investigations demonstrated that pulse-shape discrimination (PSD) with Si detectors is an excellent technique for particle identification in the energy range of a few AMeV [1]. However, the particle resolution turned out to depend strongly on individual detector properties. This is due to inhomogeneities of the Si material, like resistivity variations, which cause the pulse shape to depend on the point of impact [2,1]. For applications of this technique it is therefore important to characterize the performance of detectors with respect to PSD without expensive beam experiments.

We exposed the front and the rear sides of $500 \mu\text{m} / \approx 1300 \text{mm}^2$ prototype detectors for our Si ball (see other contribution in this volume) simultaneously to α particles from ^{239}Pu - ^{241}Am - ^{244}Cm mixed-nuclide sources (Fig. 1a), thus producing short ionization tracks in the high-field (front contact) and the low-field (rear contact) regions. With the electronics scheme described in [3] we measured event-by-event the zero-crossing time t_{ZC} of a bipolar signal, which characterizes the charge-collection time, and the energy deposition E . In plots of t_{ZC} versus E , the front-side and rear-side α 's are separated due to the different charge-collection times (Fig. 2). As expected, the charge-collection time for rear-side events turned out to be extremely sensitive to the electric field distribution at the rear side which is (at a given bias voltage) determined by the resistivity of the Si material. The spread of charge-collection times for rear-side α 's is therefore a measure of the homogeneity of the Si material and of the expected performance of a given detector for pulse-shape discrimination (PSD). Figs. 2a-b show $t_{ZC}(E)$ plots for a "reference" detector which has shown excellent particle resolution in previous beam experiments [4], and for a hexagonal prototype detector which is obviously of worse quality. Scanning of the prototype detector with a collimated source (Fig. 1b; spot size $\approx 2 \text{mm}$) demonstrated that the spread of t_{ZC} for the rear-side events is indeed caused by variations of the charge-collection time across the detector face (Figs. 2c-e). On the other hand, excellent resolution is observed for selected spots (e.g. Fig. 2d). This fact indicates that the particle resolution obtained in previous beam experiments [3,4] is – though surprisingly good – still far from the limits and mainly determined by material inhomogeneities at a scale of a few millimeters. A more detailed investigation of the "reference" detector demonstrates that useful information can be extracted from such simple measurements (Fig. 3). We measured the energy deficit, $\epsilon = (E_F - E_R)/E_F$, and the particle resolution, $R = \Delta t_R / (t_R - t_F)$, for different α energies as a function of the detector bias U_D . $E_{F/R}$ and $t_{F/R}$ denote the energies and zero-crossing times measured for front-/rear-side α 's, Δt_R the half-width of the t_{ZC} distribution for rear-side α 's of a certain energy. A depletion voltage of 132 V was extracted from the plot of $1/C_D^2$ versus U_D (C_D - detector capacitance). The figure shows that choosing a bias voltage means making a compromise between particle resolution – which becomes better with decreasing bias – and the energy deficit which is composed of a ballistic deficit and incomplete charge collection, e.g. due to trapping or recombination of the slowly moving holes.

¹ Soltan Institute for Nuclear Studies, Dept. of Nuclear Electronics, PL-05-400 Otwock-Świerk, Poland

² FZ Rossendorf, Institut für Ionenstrahlphysik und Materialforschung

³ Royal Institute of Technology, Physics Department, S-10405 Stockholm, Sweden

References

- [1] G. Pausch et al., IEEE Nucl. Sci. Symp. '95 (subm. to IEEE Transact. Nucl. Sci.)
- [2] F.Z. Henary et al., Nucl. Instr. and Meth. **A288** (1990) 439
- [3] G. Pausch et al., Nucl. Instr. and Meth. **A365** (1995) 176
- [4] G. Pausch et al., Nucl. Instr. and Meth. **A349** (1994) 281

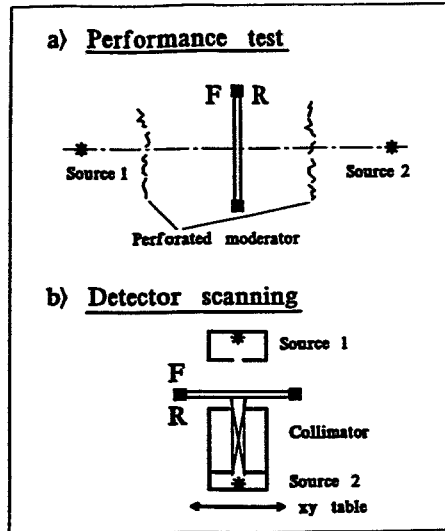


Fig. 1 Principle of our detector test: Front (F) and rear (R) sides are simultaneously exposed to α particles. Thin (crumpled and perforated) moderator foils produce a quasi-continuous low-energy "tail" if necessary.

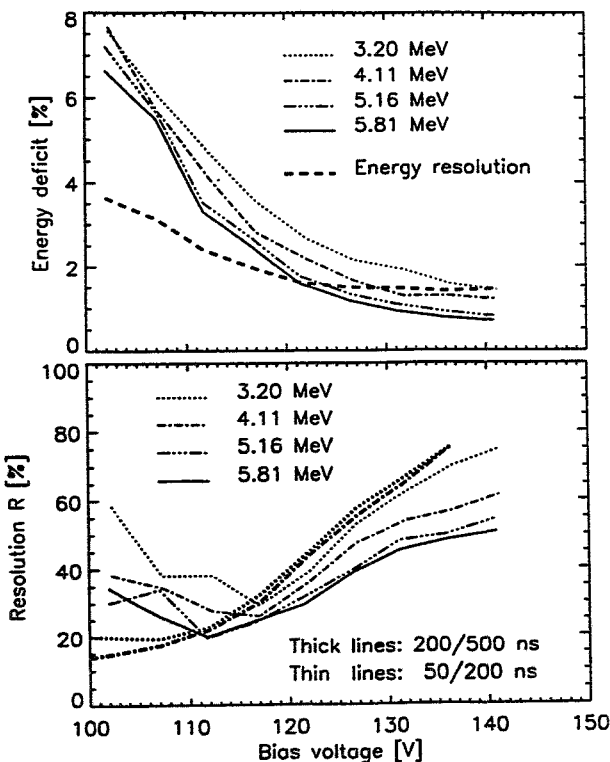
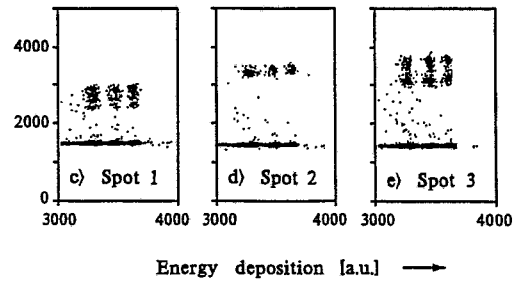
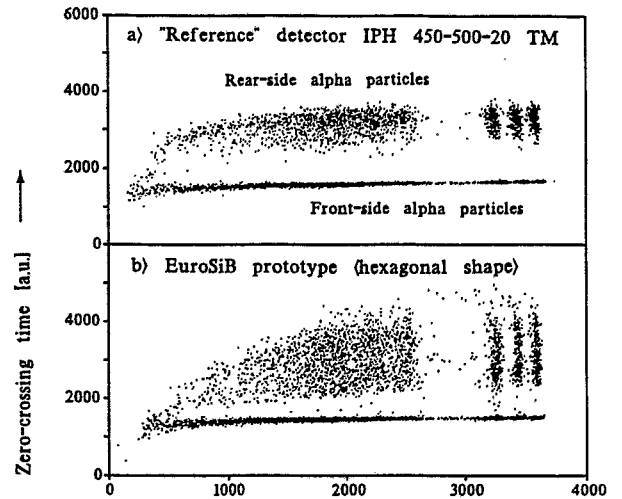


Fig. 2 Plot of t_{zc} versus E (see text):
 a) "Reference" detector (EurisyS, $500\mu\text{m}$, totally exposed)
 b) EuroSiB prototype (EurisyS, $500\mu\text{m}$, totally exposed)
 c)-e) EuroSiB prototype (EurisyS, $500\mu\text{m}$, spots of 2mm diameter exposed)

Fig. 3 Energy deficit and energy resolution for rear-side alphas (upper part), and F/R particle resolution (lower part), as a function of the detector bias and the α energy. The lower alpha energies were produced by moderating source particles with a thin foil. The particle resolution is influenced by the shaping-time constants of the electronics (lower figure).

Detector: EurisyS IPH-450-500-20 TM

A Method to Localize and Characterize Resistivity Fluctuations in Large-Area Si Detectors

G. PAUSCH, W. SEIDEL, M. FREITAG, J. HUTSCH, M. SOBIELLA

Resistivity fluctuations in the bulk material of Si detectors are responsible for a dependence of the charge-collection time on the point of impact of the detected particle [1,2,3]. Inhomogeneities of the bulk silicon are therefore a limiting factor for the attainable time resolution [1] as well as for the performance of detectors with respect to particle identification based on the pulse-shape discrimination (PSD) technique [2,3]. To investigate the influence of the technology for crystal and detector production on such inhomogeneities it is necessary to measure these fluctuations in a non-destructive manner.

In the context of our Si-ball project (see other contributions in this volume) we prepared a test stand which allows to generate "detector maps" characterizing local resistivity variations. Our method is based on a simultaneous measurement of the point of impact (x, y) and the charge-collection time (t_{CC}) for α particles hitting the rear side of the totally depleted (n-type) Si detector. It exploits the high sensitivity of t_{CC} to the bulk resistivity in the case of particle tracks which are located in the low-field region near the rear contact [3].

The principle is shown in Fig. 1. Each α particle has to penetrate a double-grid avalanche counter (DGAC) before it is hitting the Si-detector. The DGAC [4,5] – a position-sensitive, gaseous transmission counter with a common cathode for both the x and y wire planes, thin ($3 \mu\text{m}$) mylar windows, and an active area of $5 \times 5 \text{ cm}^2$ – is operated with pentane at 5-7 Torr. The resulting energy loss for 5-6 MeV α particles is $\approx 800 \text{ keV}$. The wire planes are read out via delay lines, the time difference with respect to the common cathode signal defines the x and y coordinates of a particle hit (Fig. 1). The electronics for the Si detector corresponds to the usual PSD scheme exploited for particle identification [3,6]. The zero-crossing time t_{ZC} of the bipolar signal formed by a shaping amplifier characterizes the charge-collection time t_{CC} . In addition to the usual scheme we measure t_{ZC} also with respect to the DGAC timing signal (Fig. 1). All parameters are digitized and stored event-by-event.

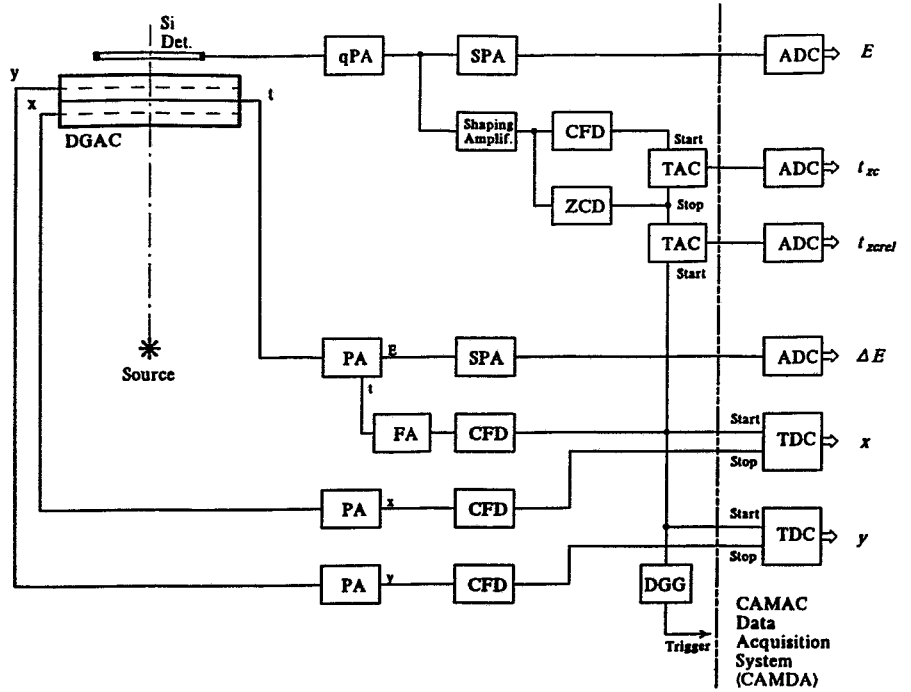
Fig. 2 presents first preliminary results for a hexagonal prototype detector of $500 \mu\text{m}$ thickness and $\approx 1300 \text{ mm}^2$ active area, produced by Eurisys Mesures for the Si ball EuroSiB. The spread of the t_{ZC} distribution for α particles of a given energy indicates considerable inhomogeneities in the bulk material (Fig. 2b). We defined gates in the $t_{ZC}(E)$ plot, corresponding to low, medium, and large charge-collection times t_{CC} (Fig. 2b), and plotted the point of impact (x, y) for the corresponding events (Fig. 2c). In addition to the expected edge effect (slow charge collection due to field distortions) we observed indeed gross structures characterizing regions of different bulk resistivities.

References

- [1] H.A. Rijken, PhD thesis, Technische Universiteit Eindhoven, 1993
- [2] F.Z. Henary et al., Nucl. Instr. and Meth. **A288** (1990) 439
- [3] G. Pausch et al., IEEE Nucl. Sci. Symp. '95 (subm. to IEEE Transact. Nucl. Sci.)
- [4] W. Seidel et al., Annual Report 1988, ZfK-667 (1989) 126
- [5] W. Seidel et al., Nucl. Instr. and Meth. **A273** (1988) 536
- [6] G. Pausch et al., Nucl. Instr. and Meth. **A365** (1995) 176

Fig. 1 Principle and electronics block scheme of the detector mapping:

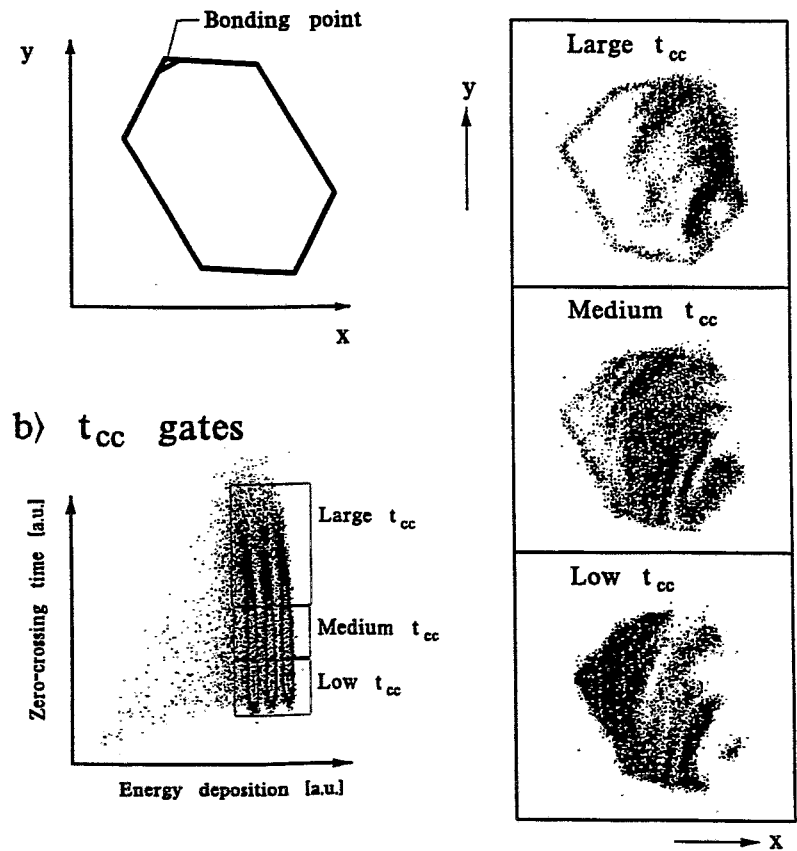
(q)PA: (charge-sensitive) preamplifier; SPA: spectroscopy amplifier; CFD: constant-fraction discriminator; ZCD: zero-crossing discriminator; FA: fast amplifier; TAC: time-to-amplitude converter; DGG: delay and gate generator; ADC: peak-sensing analogue-to-digital converter; TDC: time-to-digital converter



a) Detector location

c) Detector map

Fig. 2 Results obtained for a hexagonal EuroSiB prototype detector (thickness: 500 μm ; active area: 1300 mm^2): Gates for low, medium, and large charge-collection time t_{cc} were defined in the (t_{zc}, E) -plot (b). Corresponding (x, y) -plots show the detector regions with fast, medium, and slow charge collection (c), corresponding to high, medium, and low resistivity of the bulk silicon.



Activities of the Detector Laboratory

W. ENGHARDT¹, M. FREITAG, J. HUTSCH, G. PAUSCH, H. PRADE, M. SOBIELLA

The Detector Laboratory Rossendorf provides experimental groups of the Institute for Nuclear and Hadronic Physics with infrastructure and technical support for development, manufacture and test of detector components.

Most of the technical investments in 1995 were due to the start chamber for ANKE (COSY 0°-Facility [1]). The reconstruction of the cleanroom was completed, and an optical table of 2m × 3m is now available for assembling large-area detectors. A measuring stand for precise wire-distance measurements on large wire planes, a new gas-mixing apparatus, and a test stand to study the performance of the ANKE start-chamber were put into operation.

Besides the activities which are described in separate contributions (PET for the control of the heavy-ion tumour therapy, EuroSiB and ELBE projects), the main activities in 1995 have concerned

- the production of the last 10 double-grid avalanche counters (DGAC's) for the heavy-ion spectrometer FOBOS in Dubna [2],
- the manufacture of one complete start chamber and of the wire planes for a second, identical counter for ANKE (COSY 0°-Facility) [1],
- technical support for the construction of the stop chamber for ANKE,
- the manufacture of one table frame [3] for the EUROBALL cluster detector in Risø (Denmark), and of three support frames for the German cluster experiments which have been performed in Heidelberg and Darmstadt,
- support of the assembly of an electron gun for the ELBE project.

Research groups from the Institute of Ion-Beam Physics and Material Research (FZ Rossendorf) and the LMU Munich have been supported by delivering Frisch grids for ionization chambers used for ERDA experiments.

Since October 1995, a new part of the detector laboratory is being erected. The detector laboratory will be extended by laboratory rooms for radiation physics and semiconductor detectors, and by a storeroom.

¹ *FZR and Uniklinikum der TU Dresden, Fetscherstr. 74, D-01307 Dresden, Germany*

References

- [1] R. Esser et al., Annual Report 1993, FZR-35 (1994) 86.
- [2] H.-G. Ortlepp et al., Report FZR 92-11 (1992).
- [3] J. Stephan and M. Freitag, Annual Report 1993, FZR-35 (1994) 89.

Status of the 2nd Multiwire Proportional Chamber MWPC2 for the ANKE-Facility^{B,K}

T. KIRCHNER, H. MÜLLER, CH. SCHNEIDER, L. V. HORN¹, H. OHM¹ AND V. KRUGLOV²

The reconstruction of particle tracks at the ANKE-Facility will be assured by two multiwire chambers running in proportional mode. The first chamber MWPC1[1] has been constructed and tested with success. The construction of the second chamber MWPC2 will be based on the experience acquired for the first. Although the principle geometrical layout of the 2nd wire chamber is basically unchanged compared to the first chamber, its much larger size demands additional detailed investigations concerning the mechanical tension and diameter of the anode wires, thickness and type of cathod-foils. The following will resume the outcome of these investigations.

The MWPC2 is located close to the focal plane of the spectrometer magnet D2. Using GEANT calculations the position distribution of ejectiles can be simulated at this location. From this distribution (see Fig. 1) the sensitive area of the chamber can be deduced. For our purpose it has to be 600 mm × 1961 mm, in order to detect the particles emitted within the spectrometer acceptance.

The vertical and inclined ($\pm 30^\circ$ with respect to the vertical axis) anode wires must be tensioned by 70 g each in order to withstand the electrostatic forces during the operation of the chamber. In this case the wire tension is a factor of ≈ 1.6 higher than the critical wire tension $T_C = 45$ g necessary for the equilibrium between the mechanical and electrostatic forces under operation conditions. The 20 μm wires used in the first chamber are not strong enough to withstand these 70 g. So the wires in the new chamber will have a diameter of 25 μm . The total number of 768 wires in each anode plane provokes a total force on the corresponding frame of ≈ 45 kg. The size of the frames must be large enough in order to withstand this weight. Frames with a total dimension of 900 mm × 2161 mm will satisfy the needs. Further parameters of the 2nd wire chamber are the gap distance of 5 mm and a wire distance of 2.53 mm, same as for the MWPC1. As operation parameter there are the gas mixture of Argon, CO₂ with a small quantity of Freon ($\approx 2\%$), and the high voltage of the chamber, which is estimated to be ≈ 3.4 kV. This value is higher than in the MWPC1 because it takes into account the larger diameter of the anode wires in order to have the same signal (charge) on the wire surface. This allows to use also the same read-out electronics been developed for the first chamber. The verification of the operation parameters has to be done once the construction of the chamber is finished.

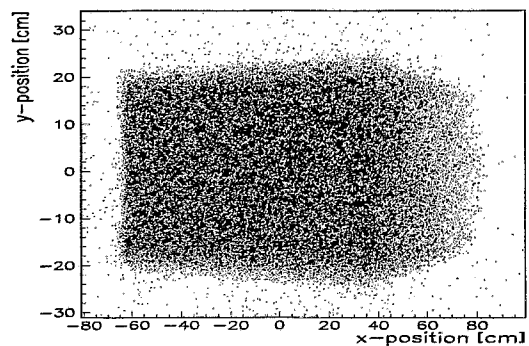


Fig. 1 Position distribution of particles within the momentum range of 150 MeV/c to 600 MeV/c at the location of the 2nd multiwire chamber.

¹ Institut für Kernphysik KFA Jülich, Germany
² Laboratory of Nuclear Problems Dubna, Russia

References

- [1] Ch. Schneider et al., Annual Report 1994, KFA Jülich, Jül-3035 (1995) 60

Apparatus for an Investigation of Long Scintillator Strips through Use of Cosmic Rays^B

P. MICHEL, K. MÖLLER¹, A. SCHAMLOTT AND A. SCHÜLKE
FOR THE COSY-TOF COLLABORATION

In the past two years a vacuum chamber has been built which partially resembled those conditions as given by the COSY-TOF spectrometer [1,2]. With this set up various scintillator configurations were to be tested which will be used in the presently discussed barrel detector. It should be recalled that a new version consisting of one-layer scintillator elements with up to 3 m long strips has been developed, since larger problems with the original version were found.

A sketch of the test set up consisting of scintillator strip, reflector and light guide is shown in Fig. 1. The 90° read out light guide as well as the vacuum-tight seal at the outlet are identical to those as will be used for the TOF-spectrometer. Test measurements with respect to position and time resolution were performed with cosmic rays. To identify the position of impact of the traversing myons three pairs of additional 5 mm thick scintillator sheets (area 30 × 100 mm²) were used which could be moved along the long axis of the strip.

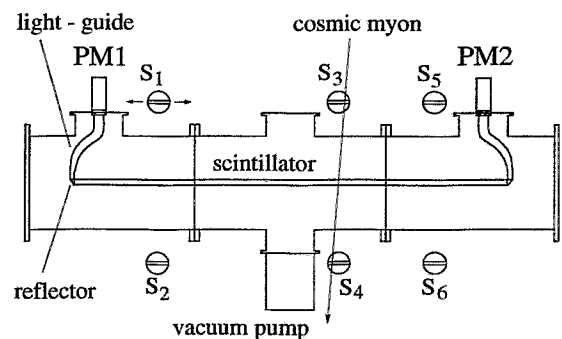


Fig. 1 Set up for the investigation of the prototype scintillator module

These scintillator pairs called "master pairs" were mounted outside of the chamber 30 cm above and below the central axis, thus limiting the angular spread of the traversing myons to $90^\circ \pm 5^\circ$. With an observed coincidence rate of approximately 10 events/h reasonable statistics could be obtained within 24 h.

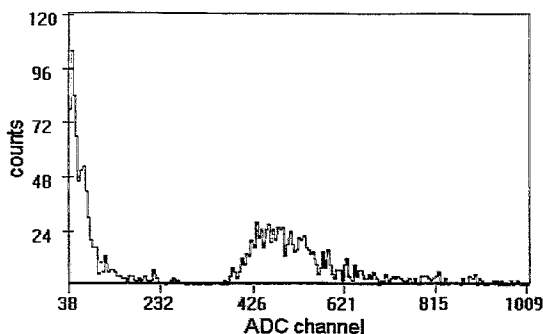


Fig. 2a Typical spectra of master pairs energy spectrum

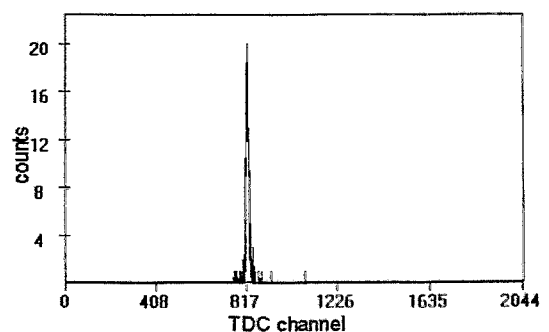


Fig. 2b Typical spectra of master pairs time spectrum

In Fig. 2a is shown an energy spectrum obtained with one such master in coincidence with its upper unit. A strong peak corresponding to about 80 photoelectrons is clearly visible, the low energy continuum is due to Cerenkov light. The latter stems from reactions of the

traversing myons with the long light guide made from plexi glass (length 100 mm, ϕ 43 mm). A suitably set threshold allows elimination of those events in the off-line analysis. The time spectrum as obtained for such a master pair is shown in Fig. 2b; the resolution was found to be 520 ps (FWHM). A sketch of the electronics used for these test measurements is shown in Fig. 3.

CAMAC units were employed with read-out via a suitably chosen adapter by means of PC; the CAMDA-software was used for data-acquisition-analysis. As a valid trigger coincidence between signals of any pair and one observed at either side of the long strip was chosen which in turn started the read out procedure. The common start signal is taken from the left side of the long strip, various stop signals are generated from the right end as well as the coincident master pairs. If this coincidence condition is fulfilled the TDC is started by the time signal from the long strip.

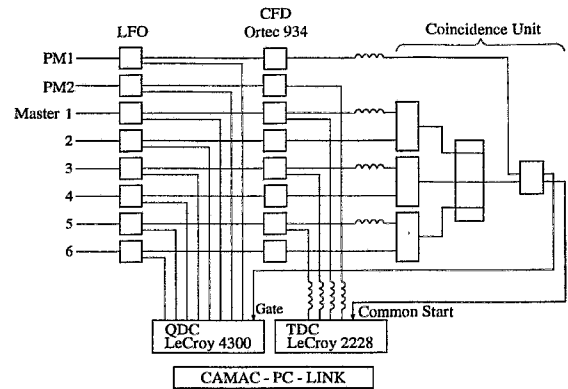


Fig. 3 *Electronical set up for the test measurements*

The right side of the scintillator strip as well as the upper scintillators of each master pair generate corresponding stop signals leading to peaks at different positions in TDC-spectra. Thus the position of myon hits on the scintillator strip can be measured and the spatial resolution determined (time difference spectrum of signals from COMMON START and the right side of the long strip). The time resolution of the long strip for read out at either side can be extracted from the measured time difference between COMMON START and the corresponding master pair. The two-sided read out of the long strips results in an improvement of the time of flight resolution of the TOF spectrometer compared to one-sided read out.

¹ *Institut für Kern- und Teilchenphysik, TU Dresden and Institut für Kern- und Hadronenphysik, FZR*

References

- [1] P. Michel et al., Annual Report 1994, KFA Jülich, Jül-3035 (1995) 11
- [2] E. Kuhlmann et al., Physica Scripta **48** (1993) 226
- [3] P. Michel et al., this Annual Report

A LED-Based Monitoring System for Scintillation and Čerenkov Counters at ANKE^B

B. PRIETZSCHK, B. RIMARZIG, A. SCHNEIDER¹, R. SCHLEICHERT¹, R. ESSER¹ AND H. OHM¹

The gain and timing stability of scintillation and Čerenkov counters at ANKE will be monitored with pulsed light emitting diodes (LED). The decision in q of LEDs over laser-based systems has been made since the LED system is more flexible. Delays can easily be changed which is very useful for adjusting the time-of-flight based trigger of ANKE [1]. It is known that LEDs show some systematic variations of the light output which, however, can be kept under control. Therefore, a detailed investigation of the LED performance was carried out.

There is a temperature dependence of the light output with a typical magnitude of -1% K^{-1} , see fig. 1. This value varies even between different LEDs of the same type. Consequently, the temperature dependence has to be known for each LED separately. The temperature will be measured by several temperature sensors in various places of the detector system. Furthermore there are aging effects increasing with the LED current. This effect is of minor importance only when the number of pulses applied to the LED is relatively low [2]. A constant DC current was sent through the LED while the light intensity was measured with a PIN photo diode directly coupled to the LED. Even at low currents (5 mA) the drop of intensity is about 40 % within several hours.

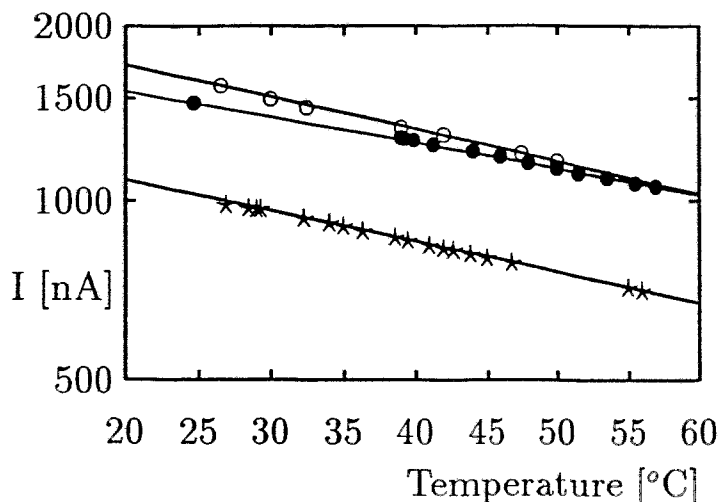


Fig. 1 Variation of the light output of three red LEDs of the same type (HP HLMP 3301) with the temperature.

The intensity flattens off until almost constant light output is reached. In addition to this effect the temperature coefficient changes. However, it reaches a constant value after some burn-in. Therefore we have decided to subject all the LEDs to an aging procedure before they are installed in the counters.

On each scintillator paddle or Čerenkov counter one LED will be mounted in the center of the surface parallel to the particle trajectory. New 'ultrabright' LEDs which became

available recently [3] deliver enough light so as to illuminate each photomultiplier tube (PMT) at the ends of the paddle with sufficient intensity. With this position of the LED it is possible to monitor not only the gain of the individual PMTs but also the quality of the optical joints between scintillators, light guides and PMTs.

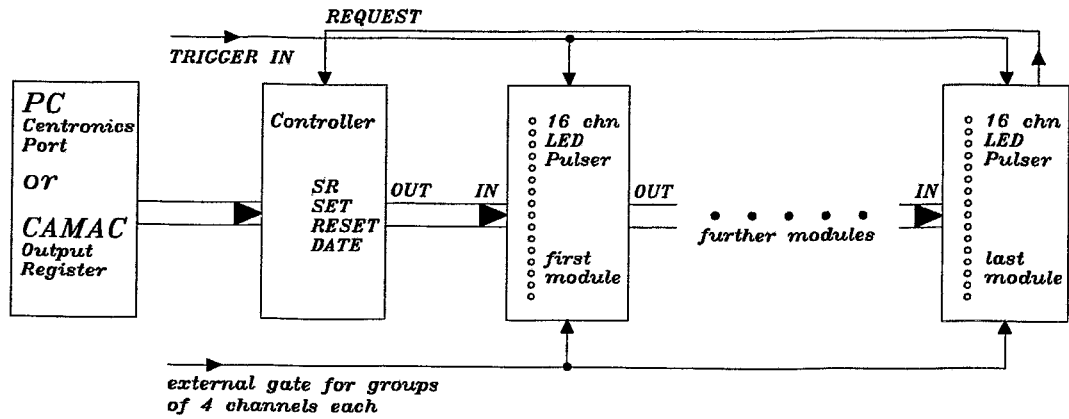


Fig. 2 Schematic diagram of the control unit and the LED pulsers.

A pulse generator has been developed which delivers fast pulses with adjustable amplitudes up to 12 V. The timing resolution of a scintillation counter obtained with LED pulses is approximately the same as with minimum ionizing particles traversing the counter. This generator is triggered with logical signals delivered by a commercial device allowing to select a precise delay between a reference signal and the LED pulse. In that way the time of flight of the particles to be considered can be simulated. The pattern of the LEDs which fire will be determined under computer control either directly from a PC or via a CAMAC output register, see fig. 2. The pattern information is sent to a controller which feeds it into the appropriate number of subsequent LED pulser units. For each LED output to be fired a bit is set which opens a gate for the trigger signal. In addition it is possible to select individual LED pulser channels manually for applications of the pulse generators in small laboratory experiments.

¹ *Institut für Kernphysik KFA Jülich, Germany*

References

- [1] R. Schleichert, Annual Report 1995, KFA Jülich
- [2] G. Anton et al., NIM A274 (1989) 222
- [3] HEWLETT PACKARD, Optoelectronics Designer's Catalog 1993, p. 3-3

Commissioning of three EUROBALL CLUSTER Detectors ^B

W. SCHULZE, A. UHLMANN, T. MYLAEUS, H. PRADE, J. REIF, H. SCHNARE,
R. SCHWENGER, T. SERVENE, S. SKODA, G. WINTER, L. KÄUBLER¹,
H.G. THOMAS², P. VON BRENTANO² AND J. EBERTH²

In the framework of the EUROBALL project three of seven German EUROBALL CLUSTER detectors [1] funded by the BMBF were awarded to the Spectroscopy group of the FZ Rossendorf. The first and second one of these detectors were assembled and tested in collaboration with the Spectroscopy group at the University of Cologne. The first detector was used in nuclear resonance fluorescence experiments at the accelerator S-DALINAC of the TH Darmstadt [2]. The first and the second detector were in operation as part of a six-CLUSTER-detector array at the tandem accelerator of the MPI Heidelberg [3] for seven months. During these measuring periods a continuous effort to maintain a good performance of the detectors was necessary. The third detector was assembled in Rossendorf. After tests for proper vacuum and cooling conditions measurements with standard sources are being carried out. The properties of the encapsulated HPGe crystals of these three CLUSTER detectors are given in table 1.

Table 1 Characteristics of the encapsulated crystals of the three CLUSTER detectors

	Crystal Serial No.	mass (g)	efficiency ^a (%)	P/C ^b	FWHM (keV) at 122 keV	FWHM (keV) at 1332 keV
<u>CLUSTER 1:</u>	72005	1547	55.2	59.5	1.28	2.24
	72106	1589	59.7	55.4	1.04	2.27
	72158	1584	57.5	65.5	1.12	2.06
	72187	1632	57.4	59.2	1.30	2.22
	72200	1621	58.8	64.8	1.09	2.09
	7928	1554	53.8	60.2	1.06	1.92
	72355	1628	63.6	74.7	0.92	1.90
<u>CLUSTER 2:</u>	72101	1598	57.9	54.9	0.93	2.32
	72176	1632	59.8	63.7	1.04	2.07
	72367	1593	60.8	69.4	1.11	1.94
	72369	1620	61.8	68.8	1.15	2.04
	72368	1616	60.9	69.0	0.97	2.02
	72417	1616	62.7	59.8	1.21	2.23
	72519	1609	62.3	67.7	1.20	2.03
<u>CLUSTER 3:</u>	72276	1591	62.2	61.9	1.18	2.14
	72510	1626	61.9	62.2	1.07	2.09
	72497	1614	61.4	67.4	1.12	1.92
	72474	1626	60.9	66.6	1.14	2.03
	72520	1574	60.9	61.5	1.16	2.13
	72511	1596	60.0	60.3	1.15	2.10
	72552	1588	58.2	60.2	1.18	1.97

^a Relative to a 3" × 3" NaI crystal

^b Ratio of intensities of the peak at 1332 keV and of the corresponding Compton background

¹ Institut für Kern- und Teilchenphysik, TU Dresden, and Institut für Kern- und Hadronenphysik, FZR
² Institut für Kernphysik, Universität zu Köln, 50937 Köln

References

- [1] H.G. Thomas, Thesis, Köster, Berlin 1995
- [2] J. Reif et al., R. Schwengner et al., S. Skoda et al., contributions to this report
- [3] T. Servene et al., contribution to this report

Analysis and Calibration of the Response of the FOBOS CsI(Tl) Scintillator Shell for Light Charged Particles^B

W. WAGNER¹, D.V. KAMANIN¹

Light charged particles (LCP) penetrating the gas detectors of the 4 π -array FOBOS [1] are registered by a scintillator shell of 210 CsI(Tl) crystals. The charge (Z) and mass (A) separation up to $Z \leq 3$ is performed by application of the pulse-shape analysis method (PSA) [2]. Integration gates for the fast and slow light components of $t_1 = 0 - 400$ ns and $t_2 = 1600 - 3600$ ns respectively effect an efficient LCP separation (fig.1).

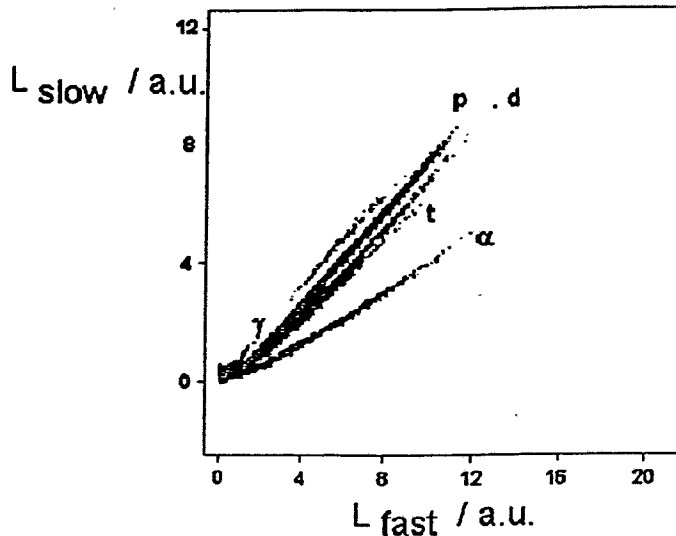


Fig.1 Pulse-shape analysis matrix measured for the reaction ^{14}N (52.5 A MeV) + ^{197}Au at an angle $\vartheta = 79^\circ \pm 6^\circ$ relative to the beam axis.

Since the total integrals of the light pulses corresponding to the nonlinear response function of CsI(Tl) scintillators [3]

$$L(E, Z, A) = S [E - a(Z, A) \cdot \ln(E/a(Z, A) + 1)] \quad (1)$$

(E - energy, $a(Z, A)$ - quenching constant, S - scintillation efficiency) are not available in the PSA variant used, the energy calibration is not straight forward.

We simulated the PSA matrix approximating the light pulse-shape by the expression

$$L(t) = \frac{h_{fast}}{\tau_{fast}} \cdot e^{-\frac{t}{\tau_{fast}}} + \frac{h_{slow}}{\tau_{slow}} \cdot e^{-\frac{t}{\tau_{slow}}} - \left[\frac{h_{fast}}{\tau_{fast}} + \frac{h_{slow}}{\tau_{slow}} \right] \cdot e^{-\frac{t}{\tau_{front}}} \quad (2)$$

(τ , - rise and decay time constants, h_i - magnitudes of the light components).

The ratio $R = \frac{h_{slow}}{h_{fast}}$ and the time constant of the fast light component τ_{fast} are known to be decreasing functions of the specific stopping power $\frac{dE}{dx}$. Their experimentally ascertained dependence on E , Z and A [4] has been fitted by appropriate empirical functions

$R(E, Z, A)$ and $\tau_{fast}(E, Z, A)$.

Setting $L(E; Z, A) = \int_0^\infty L(t, E, Z, A) dt$ and fixing the constants in the eq. (1) and (2) one can simulate a PSA matrix

$$L_{slow}(E, Z, A) = \mathcal{F}\{L_{fast}(E, Z, A)\}, \quad (3)$$

where L_{slow} and L_{fast} are the integrals of $L(t, E, Z, A)$ within the time intervals t_1 and t_2 respectively (fig.2).

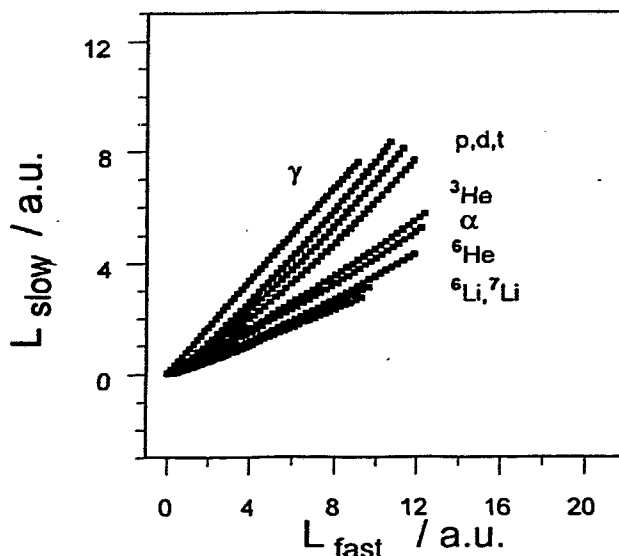


Fig.2 Simulated pulse-shape analysis matrix corresponding to the measured one of fig.1.

The factor S in eq. (1) allows an absolute energy scaling and, therefore, an intrinsic calibration using for normalization of the simulated PSA matrix the well defined punch-through of high-energetic protons (fig.1).

Due to the nonlinearity of the particle-dependent functions $L(E, Z, A)$ (1), $R(E, Z, A)$ and $\tau_{fast}(E, Z, A)$ the integrals $L_{fast}(E, Z, A)$ and $L_{slow}(E, Z, A)$ are in general nonlinear functions of E too. The presented procedure delivers the different energy scales for all particle branches simultaneously.

¹ Institut für Kern- und Hadronenphysik, FZR and Joint Institute for Nuclear Research, Dubna

References

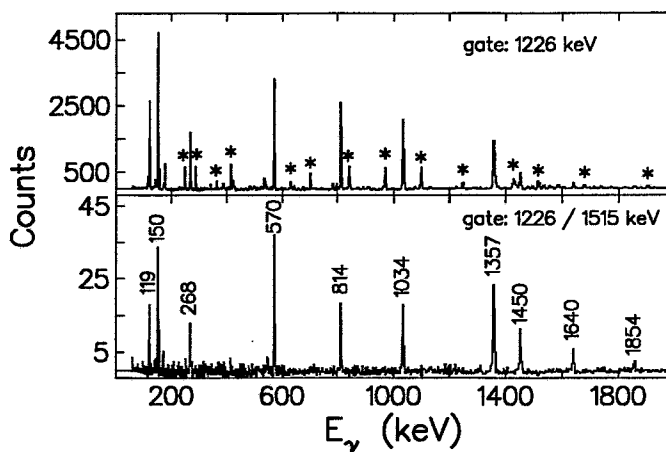
- [1] Proc. FOBOS workshop '94, Cracow, Poland, 1994, FZR-65, Rossendorf, 1995
- [2] W. Wagner et al., Annual Report 1992, FZR-93-10 (1993) 93
- [3] -D. Horn et al., Nucl. Instr. and Meth. A320 (1992) 273
- [4] F. Benrachi et al., Nucl. Instr. and Meth. A281 (1989) 137

Installation of RADWARE, Programs for the Analysis of High-Spin Spectroscopy Experiments

H. SCHNARE, R. SCHWENGNER

Recently experiments with the GAMMASPHERE array and Euroball CLUSTER detectors generated large amounts of high-fold coincidences in nuclear spectroscopy experiments. Compared to the conventional analyzing techniques such as "simple gating" in a 2D coincidence matrices, these large data-sets require more sophisticated software tools of extracting information in an easy and reliable way. Especially from the large amount of triple coincidences a 3D coincidence cube can be created. By setting 2 gates in such a cube, spectra with less contaminating γ -lines are produced.

Fig. 1 Comparison of γ -ray spectra of the nucleus ^{81}Y , obtained from a coincidence matrix (single-gated spectrum) and a coincidence cube (double-gated spectrum). Note the absence of contaminating γ -lines (indicated by *) in the double-gated spectrum.



To perform the analysis of high-fold data, the software package RADWARE [1] was installed on our computer system. These programs allow the inspection of high-fold coincidence data in an interactive graphical way. In addition to the observed coincidence spectrum a "simulated" spectrum calculated on the basis of a proposed level scheme is displayed. In this way the user can easily find discrepancies between both spectra and modify the proposed level scheme accordingly. Furthermore the book-keeping of the analysis is simplified. All information, including the level scheme, is displayed simultaneously on the screen and quick gating and editing tasks can be performed by mouse and keyboard commands. The calculation of the expected spectrum is based on least-squares fits directly to the 2D and 3D data and takes into account γ -ray energy calibrations and detection efficiencies as well as electron conversion coefficients. In order to use these analysis tools, new programs were written in C and FORTRAN to perform the necessary sorting procedure of high-fold data into the required data format, such as coincidence matrices and cubes. Up to now this software was successfully applied to two data sets from the GAMMASPHERE array (^{109}Sn [2] and ^{81}Y [3]) and will be used for the analysis of the recent CLUSTER experiments at the MPI Heidelberg and upcoming EUROBALL experiments.

References

- [1] D.C. Radford, Nucl. Inst. and Meth., **A361** (1995) 297
- [2] L. Käubler et al., contribution to this report
- [3] H. Schnare et. al., contribution to this report

Application of the pulse-shape technique to proton-alpha discrimination in Si-detector arrays

(Nucl. Instr. and Meth. in Phys. Research A 365 (1995) 176)

Pausch, G., M. Moszynski, D. Wolski, W. Bohne, H. Grawe, D. Hilscher, R. Schubart, G. de Angelis, M. de Poli

Abstract: The capability of the pulse-shape technique with reversed n-type Si detectors for discrimination of protons and alphas produced in fusion-evaporation reactions was tested at the VICKSI cyclotron in Berlin. We applied a zero-crossing technique which does not need any external time reference, and which can therefore be exploited at DC accelerators. Excellent proton-alpha discrimination in the full energy range of the evaporation spectra, but also charge and even isotope resolution for heavier ions produced in projectile fragmentation, was obtained with detectors of an existing Si ball. There is no doubt that the pulse-shape discrimination works well with detectors from serial production and under experimental conditions which are typical for nuclear structure studies. An application of this technique in Si detector arrays is obvious, but some special features must be considered in the design of the electronics. The particle discrimination depends strongly on the electric field distribution inside the detector. Stabilization of the bias voltage at the detector is therefore recommended. A consequence of the rear-side injection mode is a strong variation of the charge-collection time with energy, charge, and mass number of the detected ion. To obtain a precise energy signal it is indispensable to correct for the ballistic deficit.

II Publications and Talks

1 Publications

Baldsiefen, G., P. Maagh, H. Hübel, W. Korten, S. Chmel, M. Neffgen, W. Pohler, H. Grawe, K.H. Maier, K. Spohr, R. Schubart, S. Frauendorf, H.J. Maier:
Shears bands in ^{201}Pb and ^{202}Pb ;
Nucl. Phys. A 592 (1995) 365

Botvina, A.S., I.N. Mishustin, M. Begemann-Blaich, J. Hubele, G. Imme, I. Iori, P. Kreutz, G.J. Kunde, W.D. Kunze, V. Lindenstruth, U. Lynen, A. Moroni, W.F.J. Müller, C.A. Ogilvie, J. Pochodzalla, G. Raciti, Th. Rubehn, H. Sann, A. Schüttauf, W. Seidel, W. Trautmann, A. Wörner:
Multifragmentation of spectators in relativistic heavy-ion reactions;
Nucl. Phys. A 584 (1995) 737

Deleplanque, M.A., S. Frauendorf, R.M. Clark, R.M. Diamond, F.S. Stephens, J.A. Becker, M.J. Brinkman, B. Cederwall, P. Fallon, L.P. Farris, E.A. Henry, H. Hubel, J.R. Hughes, W. Korten, I.Y. Lee, A.O. Macchiavelli, M.A. Stoyer, P. Willsau, J.E. Draper, C. Duyar, E. Rubel:
Low-spin termination of the superdeformed band in ^{135}Nd ;
Phys. Rev. C 52 (1995) R2302

Dzelalija, M., N. Cindro, Z. Basrak, R. Caplar, S. Hölbling, M. Bini, P.R. Maurenzig, A. Olmi, G. Pasquali, G. Poggi, N. Taccetti, C. Cerruti, J.P. Coffin, P. Fintz, G. Guillaume, A. Houari, F. Jundt, C. Kuhn, F. Rami, R. Tezkratt, P. Wagner, J.P. Alard, N. Bastid, L. Berger, I.M. Belayev, S. Boussange, A. Buta, P. Dupieux, J. Erö, Z. Fodor, L. Fraysse, A. Gobbi, N. Herrmann, K.D. Hildenbrand, M. Jorio, J. Kecskemeti, P. Koncz, Y. Korchagin, R. Kotte, M. Krämer, A. Lebedev, I. Legrand, V. Manko, G. Mgebrishvili, J. Mösner, D. Moisa, G. Montarou, W. Neubert, D. Pelte, M. Petrovici, W. Reisdorf, D. Schüll, Z. Seres, B. Sikora, V. Simion, S. Smolyankin, U. Sodan, M. Trzaska, M.A. Vasiliev, J.P. Wessels, T. Wienold, D. Wohlfarth, A.V. Zhilin:
Entropy in central Au + Au reactions between 100 and 400 A MeV;
Phys. Rev. C 52 (1995) 346

Dönau, F., S. Frauendorf, O. Vogel, A. Gelberg, P. von Brentano:
Tilted four-quasiparticle bands in even-even Xe- and Ba-nuclei;
Nucl. Phys. A 584 (1995) 241

Frauendorf, S.:
Evaporation rates for liquid clusters;
Z. Phys. D 35 (1995) 191

Gorelik, G., H. Rotter:
Matweij Bronstein und die Anfänge der Quantengravitation;
Phys. Bl. 51 (1995) 423

Heide, B.:
Ein Hybrid-Modell zur Untersuchung von Stößen schwerer Ionen bei mittleren Energien;
Dissertation, TU Dresden, 1995
FZR-108 (1995)

Heide, B., H.W. Barz:

Collective effects and multifragmentation in heavy-ion collisions at intermediate energies within a hybrid model;

Nucl. Phys. A 588 (1995) 918

Hinz, R.:

Parallelisierung eines iterativen Rekonstruktionsalgorithmus für die Positronen-Emissions-Tomographie;

Diplomarbeit, TU Chemnitz-Zwickau, Fakultät für Elektrotechnik und Informationstechnik, Sep. 1995

Iskra, W., M. Müller, I. Rotter:

Radial pattern of nuclear decay processes;

Phys. Rev. C 51 (1995) 1842

Kämpfer, B., O.P. Pavlenko, M.I. Gorenstein, A. Peshier, G. Soff:

Rapidity dependence of thermal dileptons resulting from hadronizing quark-gluon matter with finite baryon charge;

Z. Phys. A 353 (1995) 71

Kämpfer, B., O.P. Pavlenko, A. Peshier, G. Soff:

Dilepton production in a chemically equilibrating, expanding and hadronizing quark-gluon plasma;

Phys. Rev. C 52 (1995) 2704

Kaptari, L.P., A.Yu. Umnikov, F.C. Khanna, B. Kämpfer:

The tensor analyzing power T_{20} in deuteron break-up reactions within the Bethe-Salpeter formalism;

Phys. Lett. B 351 (1995) 400

Käubler, L., H. Prade, J. Reif, R. Schwengner, G. Winter, H. Grawe, J. Heese, H. Kluge, K.-H. Maier, R. Schubart, K.-M. Spohr:

High-spin states in ^{109}Sn and their decay to the ground state;

Z. Phys. A 351 (1995) 123

Käubler, L., Ch. Protochristov, M. Michailova, J. Reif, W. Andrejtscheff, L. Funke, L. Kostova, H. Prade, R. Schwengner, G. Winter:

The proton $g_{9/2}$ isomer in the $N = 50$ nucleus ^{87}Rb and M2 transition rates in $^{85,87}\text{Rb}$;

Z. Phys. A 352 (1995) 127

Käubler, L., H. Prade, J. Reif, R. Schwengner, G. Winter, H. Grawe, J. Heese, H. Kluge, K.-H. Maier, R. Schubart, K.-M. Spohr:

In-beam study of ^{109}Sn ;

Physica Scripta T56 (1995) 266

Käubler, L., J. Döring, L. Funke, P. Kleinwächter, H. Prade, J. Reif, R. Schwengner, G. Winter, I.N. Vishnevski, M.J. Kirichenko, Yu.N. Lobach, I.P. Tkachuk, V.V. Trishin, M.F. Kudojarov, E.V. Kusmin, A.A. Pasternak, J. Blomqvist, L. Kostova:
In-beam investigation and the structure of states in ^{113}Sn ;
FZR-95 (1995)

Kolomeizev, E.E., D.N. Voskresensky, B. Kämpfer:
Kaon polarization in nuclear matter;
Nucl. Phys. A 588 (1995) 889

Korten, W., G. Baldisiefen, M. Neffgen, H. Hübel, S. Chmel, W. Pohler, U.J. van Severen, P. Willsau, S. Frauendorf, J. Meng, H. Grawe, J. Heese, H. Kluge, K.H. Maier, R. Schubart, K. Spohr:
"Shears Bands" in Pb nuclei - a new nuclear structure effect;
Physica Scripta T56 (1995) 44

Kotte, R., B. Kämpfer, J. Mösner, W. Neubert, D. Wohlfarth, J.P. Alard, V. Amouroux, Z. Basrak, N. Bastid, I.M. Belayev, L. Berger, Th. Blaich, S. Boussange, A. Buta, R. Caplar, C. Cerruti, N. Cindro, J.P. Coffin, R. Donà, P. Dupieux, J. Erö, Z.G. Fan, P. Fintz, Z. Fodor, L. Fraysse, R. Freifelder, S. Frolov, A. Gobbi, Y. Grigorian, G. Guillaume, N. Herrmann, K.D. Hildenbrand, S. Hölbling, O.Houari, M. Ibnouzahir, S.C. Jeong, F. Jundt, J. Kecskemeti, P. Koncz, Y. Korchagin, M. Krämer, C. Kuhn, I. Legrand, A. Lebedev, V. Manko, T. Matulewicz, G. Mgebrishvili, D. Moisa, G. Montarou, I. Montbel, D. Pelte, M. Petrovici, P. Pras, F. Rami, V. Ramillien, W. Reisdorf, A. Sadchikov, D. Schüll, Z. Seres, B. Sikora, V. Simion, S. Smolyankin, U. Sodan, K. Teh, R. Tezkratt, M. Trzaska, M.A. Vasiliev, P. Wagner, J.P. Wessels, T. Wienold, Z. Wilhelmi, A.V. Zhilin:
Interplay of collective flow phenomena and velocity correlations of intermediate-mass fragments in collisions of Au + Au at $E = (100-400)$ A MeV;
Phys. Rev. C 51 (1995) 2686

Kunde, G.J., W.C. Hsi, W.D. Kunze, A. Schüttauf, A. Wörner, M. Begemann-Blaich, Th. Blaich, D.R. Bowman, R.J. Charity, A. Cosmo, A. Ferrero, C.K. Gelbke, J. Hubele, G. Immé, I. Iori, P. Kreuz, V. Lindenstruth, M.A. Lisa, W.G. Lynch, U. Lynen, M. Mang, T. Möhlenkamp, A. Moroni, W.F.J. Müller, M. Neumann, B. Ocker, C.A. Ogilvie, G.F. Peaslee, J. Pochodzalla, G. Raciti, T. Rubehn, H. Sann, W. Seidel, V. Serfling, L.G. Sobotka, J. Stroth, L. Stuttge, S. Tomasevic, W. Trautmann, M.B. Tsang, A. Tucholski, G. Verde, C.W. Williams, E. Zude, B. Zwieglinski:
Fragment flow and the multifragmentation phase space;
Phys. Rev. Lett. 74 (1995) 38

Kutasarova, T., R.M. Lieder, H. Schnare, G. Hebbinghaus, D. Balabanski, W. Gast, A. Krämer-Flecken, M.A. Bentley, P. Fallon, D. Howe, A.R. Mokhtar, J.F. Sharpey-Schafer, P. Walker, P. Chowdhury, B. Fabricius, G. Sletten, S. Frauendorf:
Study of high-spin states in $^{181,182}\text{Os}$;
Nucl. Phys. A 587 (1995) 111

Müller, H.:

Hadron production in proton-proton interactions at medium energies;
Z. Phys. A 353 (1995) 103

Müller, H.:

Hadron production in p Be interactions at 14.6 GeV/c;
Z. Phys. A 353 (1995) 237

Müller, M.:

Zur Herausbildung verschiedener Zeitskalen beim Zerfall von Compoundkern-Resonanzen
als Folge des Trapping-Effekts;
Dissertation, TU Dresden, 1995
FZR-79 (1995)

Müller, M., F.-M. Dittes, W. Iskra, I. Rotter:

Level repulsion in the complex plane;
Phys. Rev. E 52 (1995) 5961

**Pausch, G., M. Moszynski, D. Wolski, W. Bohne, H. Grawe, D. Hilscher, R. Schubart,
G. de Angelis, M. de Poli:**

Application of the pulse-shape technique to proton-alpha discrimination in Si-detector arrays;
Nucl. Instr. and Meth. A 365 (1995) 176

Pawelke, J.:

Methodische Untersuchungen zum Einsatz der Positronen-Emissions-Tomographie in der
Leichtionen-Tumorthherapie;
Dissertation, TU Dresden, 1995
FZR-97 (1995)

Person, E.:

Threshold phenomena in an open quantum mechanical system;
Master Work an der Universität Stockholm, May 1995
FZR-83 (1995)

Peshier, A., B. Kämpfer, O.P. Pavlenko, G. Soff:

A new effective model of the quark-gluon plasma with thermal parton masses;
in "Hot Hadronic Matter: Theory and experiment", Eds. J. Letessier, H.H. Gutbrod, J.
Rafelski, Plenum Press, New York and London 1994, NATO ASI series B, 346 (1995) 139

**Petrovici, M., N. Herrmann, I. Legrand, A. Gobbi, K.D. Hildenbrand, W. Reisdorf, A.
Buta, R. Freifelder, S.C. Jeong, M. Krämer, D. Moisa, D. Schüll, V. Simion, U. Sodan,
K. Teh, J.P. Wessels, T. Wienold, J.P. Alard, V. Amouroux, Z. Basrak, N. Bastid, I.M.
Belyaev, L. Berger, Th. Blaich, S. Boussange, R. Caplar, C. Cerruti, N. Cindro, J.P.
Coffin, R. Donà, P. Dupieux, J. Erö, P. Fintz, Z. Fodor, L. Fraysse, G. Guillaume, S.
Hölbling, A. Houari, F. Jundt, J. Kecskemeti, P. Koncz, Y. Korchagin, R. Kotte, C. Kuhn,
M. Ibnouzhahir, A. Lebedev, C. Maguire, V. Manko, J. Mösner, G. Montarou, I. Montbel,
P. Morel, W. Neubert, D. Pelte, F. Rami, V. Ramilien, A. Sadchikov, Z. Seres, B. Sikora,
S. Smolyankin, R. Tezkratt, M. Trzaska, M.A. Vasiliev, P. Wagner, Z. Wilhelmi, D.
Wohlfarth, A.V. Zhilin:**

Cluster formation during expansion of hot and compressed nuclear matter produced in central collisions of Au on Au at 250 A MeV;

Phys. Rev. Lett. 74 (1995) 5001

Pochodzalla, J., S. Aiello, M. Begemann-Blaich, Th. Blaich, D.R. Bowman, R.J. Charity, A. Cosmo, A. Ferrero, C.K. Gelbke, W.C. Hsi, J. Hubele, G. Immé, I. Iori, J. Kempter, P. Kreutz, G.J. Kunde, W.D. Kunze, V. Lindenstruth, M.A. Lisa, W.G. Lynch, U. Lynen, M. Mang, L.G. Moretto, A. Moroni, W.F.J. Müller, M. Neumann, B. Ocker, C.A. Ogilvie, V. Pappardo, G.F. Peaslee, G. Raciti, F. Rosenberger, T. Rubehn, H. Sann, R. Scardaoni, A. Schüttauf, W. Seidel, V. Serfling, L.G. Sobotka, J. Stroth, L. Stuttge, W. Trautmann, M.B. Tsang, A. Tucholski, C.W. Williams, A. Wörner, E. Zude, B. Zwieglinski:

Multifragmentation and flow: peripheral vs. central collisions;

Nucl. Phys. A 583 (1995) 553

Pochodzalla, J., T. Möhlenkamp, T. Rubehn, A. Schüttauf, A. Wörner, E. Zude, M. Begemann-Blaich, Th. Blaich, H. Emling, A. Ferrero, C. Gross, G. Imme, I. Iori, G.J. Kunde, W.D. Kunze, V. Lindenstruth, U. Lynen, A. Moroni, W.F.J. Müller, B. Ocker, G. Raciti, H. Sann, C. Schwarz, W. Seidel, V. Serfling, J. Stroth, W. Trautmann, A. Trzcinski, A. Tucholski, G. Verde, B. Zwieglinski:

Probing the nuclear liquid-gas phase transition;

Phys. Rev. 75 (1995) 1040

Poggi, G., G. Pasquali, M. Bini, P. Maurenzig, A. Olmi, N. Taccetti, J.P. Alard, V. Amouroux, Z. Basrak, N. Bastid, I.M. Belayev, L. Berger, Th. Blaich, S. Boussange, A. Buta, R. Caplar, C. Cerruti, N. Cindro, J.P. Coffin, R. Donà, P. Dupieux, M. Dzelalija, J. Erö, Z.G. Fan, P. Fintz, Z. Fodor, L. Fraysse, R. Freifelder, S. Frolov, A. Gobbi, Y. Grigorian, G. Guillaume, N. Herrmann, K.D. Hildenbrand, S. Hölbling, A. Houari, S.C. Jeong, F. Jundt, J. Kecskemeti, P. Koncz, Y. Korchagin, R. Kotte, M. Krämer, C. Kuhn, M. Ibnouzhahir, I. Legrand, A. Lebedev, C. Maguire, V. Manko, G. Mgebrishvili, J. Mösner, D. Moisa, G. Montarou, I. Montbel, P. Morel, W. Neubert, D. Pelte, M. Petrovici, F. Rami, V. Ramillien, W. Reisdorf, A. Sadchikov, D. Schüll, Z. Seres, B. Sikora, V. Simon, S. Smolyankin, U. Sodan, K. Teh, R. Tezkratt, M. Trzaska, M.A. Vasiliev, P. Wagner, J.P. Wessels, T. Wienold, Z. Wilhelmi, D. Wohlfarth, A.V. Zhilin, P. Danielewicz:

Evidence for collective expansion in light-particle emission following Au + Au collisions at 100, 150 and 250 A MeV;

Nucl. Phys. A 586 (1995) 755

Pyatkov, Yu.V., A.A. Aleksandrov, B.I. Andreev, P. Gippner, C.-M. Herbach, H.-G. Ortlepp, Yu.E. Penionzhkevich, R.A. Shekhmamet'ev, W. Wagner:

Evidence for a supershort fission mode in the reaction $^{242}\text{Am}(n_{th}, f)$ and $^{244}\text{Cm}(sf)$;

Report FZR-98 (1995)

Ramillien, V., P. Dupieux, J.P. Alard, V. Amouroux, N. Bastid, L. Berger, S. Boussange, L. Fraysse, M. Ibnouzahir, G. Montarou, I. Montbel, P. Pras, Z. Basrak, I.M. Belayev, M. Bini, Th. Blaich, A. Buta, R. Caplar, C. Cerruti, N. Cindro, J.P. Coffin, R. Donà, J. Erö, Z.G. Fan, P. Fintz, Z. Fodor, R. Freifelder, S. Frolov, A. Gobbi, Y. Gregorian, G. Guillaume, C. Hartnack, N. Herrmann, K.D. Hildenbrand, S. Hölbling, A. Houari, S.C. Jeong, F. Jundt, J. Kecskemeti, P. Koncz, Y. Korchagin, R. Kotte, M. Krämer, C. Khun, I. Legrand, A. Lebedev, C. Maguire, V. Manko, P. Maurenzig, G. Mgebrishvili, J. Mösner, D. Moisa, W. Neubert, A. Olmi, G. Pasquali, D. Pelte, M. Petrovici, G. Poggi, F. Rami, W. Reisdorf, A. Sadchikov, D. Schüll, Z. Seres, B. Sikora, V. Simion, S. Smolyankin, U. Sodan, K. Teh, R. Tezkraat, M. Trzaska, M.A. Vasiliev, P. Wagner, J.P. Wessels, T. Wienold, Z. Wilhelmi, D. Wohlfarth, A.V. Zhilin:

Sideward flow in Au + Au collisions at 400 A MeV;

Nucl. Phys. A 587 (1995) 802

Reif, J., G. Winter, R. Schwengner, H. Prade, H. Grawe, R. Schubart:

Neutron-core excitations in $^{86}_{36}\text{Kr}_{50}$;

Physica Scripta T56 (1995) 303

Reif, J., G. Winter, R. Schwengner, H. Prade, L. Käubler:

Break-up of the $N=50$ core in $^{89}_{39}\text{Y}_{50}$;

Nucl. Phys. A 587 (1995) 449

Reimann, S.M., S. Frauendorf, M. Brack:

Triaxial shapes of sodium clusters;

Z. Phys. D 34 (1995) 125

Ritman, J.L., N. Herrmann, D. Best, J.P. Alard, V. Amouroux, N. Bastid, I. Belyaev, L. Berger, J. Biegansky, A. Buta, R. Caplar, N. Cindro, J.P. Coffin, P. Crochet, R. Dona, P. Dupieux, M. Dzelalija, P. Fintz, Z. Fodor, A. Genoux-Lubain, A. Gobbi, G. Goebels, G. Guillaume, Y. Grigorian, E. Häfele, K.D. Hildenbrand, S. Hölbling, F. Jundt, J. Kecskemeti, M. Kirejczyk, Y. Korchagin, R. Kotte, C. Kuhn, D. Lambrecht, A. Lebedev, A. Lebedev, I. Legrand, Y. Leifels, C. Maazouzi, V. Manko, T. Matulewicz, J. Mösner, S. Mohren, D. Moisa, W. Neubert, D. Pelte, M. Petrovici, C. Pinkenburg, F. Rami, V. Ramillien, W. Reisdorf, C. Roy, D. Schüll, Z. Seres, B. Sikora, V. Simion, K. Siwek-Wilczynska, V. Smolyankin, U. Sodan, L. Tizniti, M. Trzaska, M.A. Vasiliev, P. Wagner, G.S. Wang, T. Wienold, D. Wohlfarth, A. Zhilin:

On the transverse momentum distribution of strange hadrons produced in relativistic heavy ion collisions;

Z. Phys. A 352 (1995) 355

Ritman, J. for the FOPI Collaboration:

The FOPI Detector at SIS/GSI;

Nucl. Phys. B - Proc. Suppl. 44 (1995) 708

Rubehn, Th., W.F.J. Müller, R. Bassini, M. Begemann-Blaich, Th. Blaich, A. Ferrero, C. Groß, G. Imme, I. Iori, G.J. Kunde, W.D. Kunze, V. Lindenstruth, U. Lynen, T. Möhlenkamp, L.G. Moretto, B. Ocker, J. Pochodzalla, G. Raciti, S. Reito, H. Sann, A. Schüttauf, W. Seidel, V. Serfling, W. Trautmann, A. Trzcinski, G. Verde, A. Wörner, E. Zude, B. Zwieglinski:

Electromagnetic fission of ^{238}U at 600 and 1000 MeV per nucleon;
Z. Phys. A 353 (1995) 197

Schubart, R., H. Grawe, M. Górska, J.B. Fitzgerald, J. Heese, H. Kluge, K.H. Maier, M. Rejmund, M. Schramm, D. Seweryniak, K. Spohr and L. Käubler:

In-beam spectroscopy and shell model structure of the neutron deficient ^{103}In and $^{100,102}\text{Cd}$;
Physica Scripta T56 (1995) 311

Schülke, A.:

Methodische Untersuchungen und Testmessungen für das pp-Bremsstrahlungsexperiment am COSY-TOF-Spektrometer;

Dissertation, TU Dresden, 1995

FZR-120 (1995)

Schult, O.W.B., K. Sistemich, V. Koptev, H. Müller, W. Cassing, L. Jarczyk, V.I. Komarov, A. Sibirtsev, J. Ernst, R. Santo, M. Nioradze, A.V. Kulikov, A. Hardt, N.S. Amaglobeli, M. Büscher, U. Bechstedt, W. Borgs, B. Chiladze, T. Demski, S. Dienel, H. Dombrowski, S.V. Dshemuchadze, R. Eßer, A. Franzen, L. Glonti, D. Gotta, D. Grzonka, F. Hinterberger, L. von Horn, M. Ivanov, A. Kacharava, B. Kamys, W. Klein, W. Klimala, H.R. Koch, M. Köhler, D. Kopyto, S. Kopyto, K.W. Leege, G. Macharashvili, Z. Menteshashvili, G. Müller, W. Oehme, W. Oelert, H. Ohm, B. Prietzschk, A. Puzynin, A. Petrus, B. Rimarzig, Z. Rudy, R. Schleichert, C. Schneider, C. Schneiderei, H. Seyfarth, U. Sieling, J. Smyrski, H. Stechemesser, A. Strzalkowski, W. Tenten, S.V. Trusov, V. Chernyshev, K.-H. Watzlawik, B.Zh. Zalykhanov, N.I. Zhuravlev, P. Zolnierczuk and K. Zwoll:

Plans for investigations of subthreshold K^+ production in p+A collisions;

Nucl. Phys. A 583 (1995) 629

Schwengner, R., G. Winter, J. Reif, H. Prade, L. Käubler, R. Wirowski, N. Nicolay, S. Albers, S. Eßer, P. von Brentano, W. Andrejtscheff:

Shell-model states and collectivity in $^{83}\text{Br}_{48}$ and $^{85}\text{Rb}_{48}$;

Physica Scripta T56 (1995) 126

Schwengner, R., G. Winter, J. Reif, H. Prade, L. Käubler, R. Wirowski, N. Nicolay, S. Albers, S. Eßer, P. von Brentano, W. Andrejtscheff:

Particle excitations and collectivity in the $N = 48$ nuclei ^{83}Br and ^{85}Rb ;

Nucl. Phys. A 584 (1995) 159

Sibirtsev, A., M. Büscher, H. Müller, Chr. Schneiderei:

\bar{K} -meson production in proton-nucleus collisions;

Z. Phys. A 351 (1995) 333

Siwek, A., A. Sourell, A. Budzanowski, H. Fuchs, H. Homeyer, G. Pausch, W. Kantor, G. Röscher, C. Schwarz, W. Terlau, A. Tutay:
Multifragmentation study on 30 A MeV $^{32}\text{S} + ^{58}\text{Ni}$;
Z. Phys. A 350 (1995) 327

Sobeslavsky, E., F.M. Dittes, I. Rotter:
Resonance phenomena at high level density;
J. Phys. A 28 (1995) 2963

Titov, A.I., B. Kämpfer, E.L. Bratkovskaya:
Dielectron production in proton-proton and proton-deuteron collisions at 1-2 GeV;
Phys. Rev. C 51 (1995) 227

Tutay, A., A. Budzanowski, H. Fuchs, H. Homeyer, G. Pausch, C. Schwarz, A. Siwek, A. Taymaz:
Temporal and thermal properties of intermediate-mass fragments from the $^{32}\text{S} + ^{58}\text{Ni}$ reaction at 30 A MeV;
Acta Physica Polonica B 26 (1995) 1413

2 Conference Contributions and Research Reports

Akindinov, A., M. Büscher, M. Chumakov, V. Demechin, R. Esser, A. Franzen, A. Gerasimov, V. Goryachev, L. v. Horn, Y. Kiselev, V. Koptev, D. Kopyto, V. Kostromin, V. Kruglov, S. Mikirtychants, H. Ohm, B. Prietzschk, B. Rimarzig, C. Schneider, O. Schult, A. Sibirtsev, K. Sistemich, V. Sopov, V. Tchernyshev:

Measurement of the cross-section ratio $\sigma(K^+):\sigma(p)$ in p-Be interactions at $T_p = 2.5$ GeV;
Verhandl. DPG (VI), 30 (1995) 686

Aleksandrov, A.A., I.A. Aleksandrova, M. Andrassy, L. Dietterle, V.N. Doronin, P. Gippner, C.-M. Herbach, D. Hilscher, S.I. Ivanovskij, A. Matthies, D. May, H.-G. Ortlepp, G. Pausch, Yu.E. Penionzhkevich, V.N. Pokrovskij, G. Renz, K.D. Schilling, D.I. Shishkin, V.E. Shuchko, O.V. Strelalovskij, V.V. Trofimov, C. Umlauf, D.V. Vakotov, V. M. Vasko, W. Wagner:

First Experiments with FOBOS;
Nucl. Phys. A 583 (1995) 465 c

Aleksandrov, A.A., I.A. Aleksandrova, M. Andrassy, L. Dietterle, V.N. Doronin, P. Gippner, C.-M. Herbach, D. Hilscher, S.I. Ivanovsky, A. Matthies, D. May, H.-G. Ortlepp, G. Pausch, Yu.E. Penionzhkevich, V.N. Pokrovsky, G. Renz, K.D. Schilling, D.I. Shishkin, V.E. Shuchko, O.V. Strelalovsky, V.V. Trofimov, C. Umlauf, D.V. Vakotov, V.M. Vasko, W. Wagner:

Correlations between intermediate mass and fission fragments in the reaction
 ${}^7\text{Li}(43 \text{ AMeV})$ on ${}^{232}\text{Th}$ studied at FOBOS;

Proc. FOBOS Workshop '94, Cracow, Poland, Jun. 1994, FRZ-65 (1995) 85

Aleksandrov, A.A., I.A. Aleksandrova, L. Dietterle, V.N. Doronin, S. Dshemuchadse, P. Gippner, C.-M. Herbach, S.I. Ivanovsky, D.V. Kamanin, A. Matthies, D. May, H.-G. Ortlepp, G. Pausch, Yu.E. Penionzhkevich, G. Renz, K.D. Schilling, D.I. Shishkin, O.V. Strelalovsky, V.V. Trofimov, C. Umlauf, D.V. Vakotov, V.M. Vasko, W. Wagner, V.E. Zhuchko, I.P. Zurin:

Study of fission and IMF emission in the reaction ${}^{14}\text{Li}$ (34 AMeV) on ${}^{197}\text{Au}$ at FOBOS;
Proc. FOBOS Workshop '94, Cracow, Poland, Jun. 1994, FZR-65 (1995) 104

Aleksandrov, A.A., I.A. Aleksandrova, B.I. Andreev, P. Gippner, C.-M. Herbach, E.M. Kozulin, A. Matthies, Yu.Ts. Oganessian, H.-G. Ortlepp, Yu.E. Penionzhkevich, Yu.V. Pyatkov, G. Renz, K.D. Schilling, O.V. Strelalovsky, V.M. Vasko, W. Wagner:

Spontaneous fission of ${}^{244}\text{Cm}$ studied by the two-velocities method at the FOBOS spectrometer;

Report FZR-99 (1995)

Alheit, H., W. Enghardt, C. Geipel, P. Geyer, P. Henzel, T. Herrmann, J. Kulig, R. Kumpf, M. Reimann, H. Röthig, L. Voigtmann, R. Weise, T. Zacharias, R. Hinz, M. Sobiella, W. Becher, T. Haberer, G. Kraft, M. Krämer, G. Lenz, D. Schardt, M. Scholz, U. Weber, J.G. Festag, R. Künkel, D. Wendt, K. Poppensieker, K. Reimers:

The response of pig skin and lung to single exposures with ${}^{12}\text{C}$ -beams and X-rays: Pilot experiment and preliminary results;

Poster, Fifth Workshop on Heavy Charged Particles in Biology and Medicine, Darmstadt, Aug. 1995, Book of Abstracts, GSI-Report 95-10, p. 160

Andrassy, M., A.A.Aleksandrov, I.A. Aleksandrova, A. Budzanowski, M. Danziger, L. Dietterle, V.N. Doronin, S. Dshemuchadse, A.S. Fomichev, P. Gippner, M. Gebhardt, K. Heidel, S. Heinitz, C.-M. Herbach, D. Hilscher, J. Holik, H. Homeyer, A.I. Ivanenko, S.A. Ivanovsky, W. Janczur, D.V. Kamanin, I.V. Kolesov, A. Matthies, D. May, S.I. Merzlyakov, W. von Oertzen, Yu.Ts. Oganessian, H.-G. Ortlepp, Yu.E. Penionzhkevich, G. Pausch, V.N. Pokrovsky, Yu.V. Pyatkov, S.V. Radnev, G. Renz, L.A. Rubinskaya, I.D. Sandrev, K.D. Schilling, W. Seidel, D.I. Shishkin, H. Sodan, O.V. Strelakovsky, V.V. Trofimov, I.P. Tsurin, C. Umlauf, D.V. Vakarov, V.M. Vasko, W. Wagner, V.E. Zhuchko, P. Ziem, L. Zrodowski:
The FOBOS 4π -detector of charged particles at the FLNR of the JINR Dubna;
Dubna-Report E7-95-148 (1995)

Barz, H.W., B. Heide:
Flow and multifragmentation in heavy-ion collisions at intermediate energies;
Proc. FOBOS Workshop '94, Cracow, Poland, Jun. 1994, FZR-65 (1995) p. 165

Barz, H.W., B. Kämpfer, Gy. Wolf and W. Bauer:
Analysis of hard two-photon correlations measured in heavy-ion reactions at intermediate energies;
FZR-111 (1995)

Biegansky, J., R. Kotte, J. Mösner, W. Neubert, D. Wohlfarth:
Some Experimental Results from the Reaction Au+Au at 1 GeV/u;
GSI-Report 95-1, p. 60

Biegansky, J., R. Kotte, J. Mösner, W. Neubert, D. Wohlfarth:
Investigation of One-Particle-Observables and Flow Values in the Reaction Au+Au at 1.05 GeV/u;
Verhandl. DPG (VI), 30 (1995) 739

Bilger, R., H.Brand, S. Brand, H. Clement, M. Dahmen, P. Cloth, W. Dutz, V. Drücke, W. Eyrich, H. Freiesleben, D. Filges, R. Geyer, P. Hermanowski, V. Jaeckle, P. Jahn, K. Kilian, M. Kirsch, H. Koch, R. Kraft, J. Krug, S. Lange, E. Kuhlmann, H. Machner, H. Matthäy, W. Meyer, P. Michel, K. Möller, H.P. Morsch, C. Nake, H. Nann, B. Naumann, L. Naumann, P. Ringe, E. Roderburg, K. Röhrich, M. Rogge, A. Schamlott, A. Schülke, O. Schult, M. Schmidt, T. Seifzick, M. Steinke, F. Stinzig, V. Renken, R. Stratmann, P. Turek, G. Wagner, S. Wirth:
The TOF - Facility at COSY;
Proc. Int. Conf. on Physics with GeV - Particle Beams, Jülich, Aug. 1994
World Scientific Publishing Co. Pte. Ltd. 1995, p. 564

Brinkmann, K.-Th., H. Freiesleben, P. Hermanowski, H. Koch, J. Krug, E. Kuhlmann, H. Matthäy, P. Michel, K. Möller, A. Schamlott, A. Schülke, M. Steinke, U. Zielinski:
The barrel scintillator hodoscope for the COSY-TOF-Spectrometer;
Review-Meeting, Nov. 1995

Büscher, M., O.E. Gorchakov, V.I. Komarov, H. Müller, A.Yu. Petrus, A.I. Puzynin, M.G. Sapozhnikov, H. Seyfarth, K. Sistemich:
Expected missing-mass resolution in the deuteron-fragmentation experiment at the ZDF and conditions for studies of the $\bar{p}p \rightarrow pp\phi$ process;
Annual Report 1994, IKP Jül-3035 (1995) 63

Büscher, M., H. Müller:
Conceptual studies for a K^- -detection system at the 0° -Facility;
Annual Report 1994, IKP Jül-3035 (1995) 72

Chmel, S., G. Balzsiefen, H. Hübel, W. Korten, P. Maagh, D. Metha, M. Neffgen, N. Nenoff, W. Pohler, M. Schönhofer, U.J. van Severen, N. Singh, B.U. Thirumala Rao, P. Willsau, S. Frauendorf, H. Grawe, J. Hesse, H. Kluge, K.H. Maier, R. Schubart, K. Spohr, A. Korichi, M. Piiparinen, G. Sletten, H.J. Maier:
Shears Bands in Pb Isotopes;
Verhandl. DPG (VI), 30 (1995) 752

Crochet, P., R. Dona, F. Rami, R. Kotte, C. Cerruti, J.P. Coffin, P. Fintz, G. Guillaume, F. Jundt, C. Maazouzi, C. Roy, L. Tizniti, P. Wagner and the FOPI-Collaboration:
Flow angle determination from IMF measurement for Au+Au collisions;
GSI-Report 95-1, p. 51

Debowski, M., W. Ahner, R. Barth, M. Boivin, Y. Le Bornec, M. Cieslak, M.P. Comets, P. Courat, R. Gacougnolle, E. Grosse, T. Kirchner, D. Miskowicz, C. Müntz, E. Schwab, P. Senger, C. Sturm, B. Tatischeff, J. Yonnet, W. Walus, N. Willis, R. Wurzinger, A. Zghiche:
Subthreshold K^+ production in proton-nucleus collisions;
Verhandl. DPG (VI), 30 (1995) 575

Dittes, F.M.:
Optimization on rugged landscapes: A democratic approach;
Preprint FZR-92 (1995)

Doll, P., U. Brandt, K. Daumiller, H. Hucker, H.O. Klages, P. Kleinwächter, G. Kolb, J. Lang, L. Pentchev:
Streamerröhren als KASCADE Myon Detektor;
Verhandl. DPG (VI), 30 (1995) 653

Enghardt, W., L. Byars, H. Geissel, B.G. Hasch, K. Lauckner, J. Pawelke, D. Schardt, M. Sobiella:
Die Anwendung der Positronen-Emissions-Tomographie für das Monitoring der Schwerionentumorthherapie;
76. Deutscher Röntgenkongress, Wiesbaden, May 1995; Der Radiologe 35 (1995) 165

Enghardt, W., L. Byars, B.G. Hasch, R. Hinz, K. Lauckner, J. Pawelke, D. Schardt, M. Sobiella, U. Weber:
A positron emission tomograph for the on-line control of heavy ion tumour treatment;
Fifth Workshop on Heavy Charged Particles in Biology and Medicine, Darmstadt, Aug. 1995, Book of Abstracts, GSI-Report 95-10, p. 181

Enghardt, W., B.G. Hasch, K. Lauckner, J. Pawelke, D. Schardt, M. Sobiella:
PET zum Monitoring der Schwerionen-Tumorthherapie;
Poster, 1. Deutscher Kongreß für Radioonkologie, Strahlenbiologie und Medizinische
Physik, Baden-Baden, Nov. 1995; Strahlenther. Onkol. 171 (1995) Sonderheft I, p. 85

Eßer, R., L. v. Horn, D. Kopyto, H. Ohm, M. Büscher, A. Franzen, M. Chumakov, A.
Gerasimov, V. Sorov, V. Tchernyshev, V. Kostromin, S. Mikirtychants, V. Koptev, B.
Prietzschk, B. Rimarzig, C. Schneider, V. Kruglov:
The detector setup for K^+ -production studies at the 0° Facility of COSY Jülich:
Test measurements at ITEP Moscow;
Verhandl. DPG (VI), 30 (1995) 676

Eßer, R., L. v. Horn, D. Kopyto, H. Ohm, A. Franzen, M. Büscher, B. Prietzschk, B.
Rimarzig, Chr. Schneider, V. Chernyshev, M. Chumakov, V. Koptev, S. Mikirtichyants,
V. Kruglov:
Test at the ITEP synchrotron of a prototype telescope for the K^+ measurements with the 0°
Facility;
Annual Report 1994, IKP Jül-3035 (1995) 52

Fodor, Z., J. Kecskemeti, Z. Seres, K.H. Hermann, J. Mösner, W. Neubert, D. Wohl-
farth, G. Augustinski, H.W. Daues, A. Gobbi, Y. Leifels, M. Marquardt, C. Schröder, D.
Schüll, J. Weinert, Y. Yatsounenko, N. Herrmann, S. Mohren, D. Pelte and the FOPI-
Collaboration:
First results from the HELITRON drift chamber at FOPI;
GSI-Report 95-1, p. 266

Franzen, A., M. Büscher, R. Eßer, L. v. Horn, D. Kopyto, H. Ohm, B. Prietzschk, B.
Rimarzig, Chr. Schneider, V. Kurglov, A. Akindinov, M. Chumakov, V. Demechin, A.
Gerasimov, V. Goryachev, V. Kostromin, V. Sopov, V. Tchernyshev, V. Koptev, S.
Mikirtychants:
Test at the ITEP synchrotron of a prototype telescope for the K^+ measurements with the 0° -
Facility: Particle identification and verification of GEANT simulations;
Annual Report 1994, IKP Jül-3035 (1995) 54

Frauendorf, S., J. Reif, G. Winter:
Shell-model study of shears bands in Pb nuclei;
Verhandl. DPG (VI), 30 (1995) 587
FZR-107 (1995)

Freudenberger, J., V.B. Gavrikov, M. Galemann, H. Genz, L. Groening, V.L. Morok-
hovskii, V.V. Morokhovskii, U. Nething, A. Richter, J.P.F. Sellschop, N.F. Shul'ga:
First observation of parametric x-rays at electron energies below 10 MeV;
Verhandl. DPG (VI), 30 (1995) 388

Freudenberger, J., M. Galemann, H. Genz, L. Groening, V.V. Morokhovskii, P. Hoffmann-Stascheck, A. Richter, V.L. Morokhovskii, U. Nething, R. Zahn, K. Runkel, J.P.F. Sellschop:

Parametric x-ray radiation observed in diamond at low electron energies;

Int. Workshop on Radiation Physics at Electron Accelerators, Bad Honnef, Germany, Jun. 1995, Book of Abstracts

Freudenberger, J., V.B. Gavrikov, M. Galemann, H. Genz, L. Groening, V.L. Morokhovskii, V.V. Morokhovskii, U. Nething, H. Prade, A. Richter, J.P.F. Sellschop, N.F. Shul'ga, R. Zahn:

First observation of parametric x-ray radiation at electron energies below 10 MeV;

16th Int. Conference on Atomic Collisions in Solids, ICACS 16, Johannes-Kepler-Universität, Linz, Austria, Jul. 1995, Book of Abstracts B 39

Freund, S., F. Becker, T. Burkhardt, J. Eberth, U. Hermkens, M.K. Kabadiyski, T. Mylaeus, S. Skoda, W. Teichert, H.-G. Thomas, A. von der Werth, A. Dewald, P. Petkov:

DSA lifetimes in ^{73}Br and ^{73}Kr ;

Verhandl. DPG (VI), 30 (1995) 633

Gebhardt, M., V.N. Doronin, P. Gippner, H.-G. Ortlepp, G. Renz, D.I. Shishkin, W. Wagner:

Test measurements performed with a bragg ionization chamber;

Proc. FOBOS Workshop '94, Cracow, Poland, Jun. 1994, FZR-65 (1995) p. 43

Goldenbaum, F., W. Bohne, J. Eades, T. von Egidy, P. Figuera, H. Fuchs, J. Galin, Ye.S. Golubeva, K. Gulda, F.J. Hartmann, D. Hilscher, A.S. Iijinov, U. Jahnke, J. Jastrzebski, W. Kurcewicz, B. Lott, M. Morean, G. Pausch, A. Peghaire, L. Pienkowski, D. Polster, S. Proschitzki, B. Quednau, H. Rossner, S. Schmid, W. Schmid, P. Ziem:

Decay of hot nuclei produced in antiproton annihilation at rest and in flight on light and heavy nuclei;

Verhandl. DPG (VI), 30 (1995) 648

Groening, L., J. Freudenberger, M. Galemann, H. Genz, P. Hoffman-Staschek, U. Nething, A. Richter, M. Höfer, J. Hormes, M. Weber, C. Toepffer, J.P.F. Sellschop:

Channeling radiation from diamond and ruby crystals: intensities, occupation and coherence lengths;

Verhandl. DPG (VI), 30 (1995) 688

Groening, L., J. Freudenberger, H. Genz, P. Hoffman-Staschek, A. Richter, U. Nething, R. Zahn, V.L. Morokhovskii, K. Runkel, J.P.F. Sellschop:

Latest results on channeling radiation observed at the S-DALINAC;

Poster, Int. Workshop on Radiation Physics at Electron Accelerators, Bad Honnef, Jun. 1995 Book of Abstracts

Gumalov, T.I., A.I. Titov, B. Kämpfer:

Rho meson self-energy and dielectron emissivity in an isospin-asymmetric pion medium;

FZR-90 (1995)

Gulamov, T.I., A.I. Titov, B. Kämpfer:

Asymmetry of the dielectron emission rate in an isospin-asymmetric pion medium;
FZR-113 (1995)

Hasch, B.G., W. Enghardt, L. Sihver:

The determination of particle ranges from β^+ -emitters generated by nuclear fragmentation for the treatment plan verification at heavy ion tumour therapy;
Poster, Third International Symposium on Swift Heavy Ions in Matter, Caen, France, May 1995, Proceedings, p. P33

Hasch, B.G., W. Enghardt, J. Pawelke, D. Scharadt, L. Sihver, M. Sobiella, U. Weber:
The determination of particle ranges from β^+ -emitters generated by nuclear fragmentation for the treatment plan verification at heavy ion tumour therapy;
Poster, Fifth Workshop on Heavy Charged Particles in Biology and Medicine, Darmstadt, Aug. 1995, Book of Abstracts, GSI-Report 95-10, p. 185

Heide, B., H.W. Barz:

Collective effects and multifragmentation in heavy-ion-collisions at intermediate energies within a hybrid-modell;
FZR-71 (1995)

Heide, B., H.W. Barz:

Effects of flow on multifragmentation processes in intermediate energy heavy ion collisions;
Verhandl. DPG (VI), 30 (1995) 738

Herbach, C.-M., A.A. Aleksandrov, I.A. Aleksandrova, L. Dietterle, V.N. Doronin, S. Dshemuchadse, P. Gippner, S.I. Ivanovsky, D.V. Kamanin, J. Krüger, A. Matthies, D. May, H.-G. Ortlepp, G. Pausch, Yu.E. Penionzhkevich, G. Renz, K.D. Schilling, D.I. Shishkin, O.V. Strelakovsky, V.V. Trofimov, C. Umlauf, D.V. Vakarov, V.M. Vasko, W. Wagner, V.N. Zhuchko:

Coincidence measurements of light (LCP) and intermediate (IMF) charged particles with fission fragments (FF) produced by ^{14}N (34 A MeV) + ^{197}Au ;
Verhandl. DPG (VI), 30 (1995) 775

Herbach, C.-M., D.V. Vakarov:

Upgrade of the FOBOS data analysis software;
Proc. FOBOS Workshop '94, Cracow, Poland, Jun. 1994, FZR-65 (1995) 56

Herbach, C.-M.:

Analysis of the fission fragment distribution observed in the reaction $^7\text{Li} + ^{232}\text{Th}$ at 43 A MeV bombarding energy;
Proc. FOBOS Workshop '94, Cracow, Poland, Jun. 1994, FZR-65 (1995) p. 87

Hermanowski, B., J. Krug, R. Loke, B. Naumann, L. Naumann:

A UV-laser based test system for the COSY-TOF-spectrometer;
Annual Report 1994, IKP Jül-3035 (1995) 10

Hilscher, D., W. Bohne, P. Figuera, H. Fuchs, F. Goldenbaum, U. Jahnke, D. Polster, H. Rossner, P. Ziem, J. Galin, B. Lott, M. Morjean, A. Peghaire, B. Quednau, T. von Egidy, F.J. Hartmann, S. Schmid, W. Schmid, K. Gulda, J. Jastrzebski, W. Kurcewicz, L. Pienkowski, G. Pausch, S. Proschitzki, J. Eades, S. Neumaier, Ye.S. Golubeva, A.S. Iljinov, D.I. Ivanov, V.G. Nedorezov, I.A. Pshenichov, A.S. Sudov:

First results on the decay of hot nuclei at low spin (PS 208);

Proceedings of the Third Biennial Conference on Low Energy Antiproton Physics, Bled, Slovenia, Sep. 1994

World Scientific, Singapore, New Jersey, London, Hong Kong (1995)

Horn, L. v., D. Gotta, H. Ohm, H. Wyrwich, Th. Kirchner, H. Müller, Chr. Schneider:
Design of a multiwire proportional chamber for the 0°-facility;

Annual Report 1994, IKP Jül-3035 (1995) 59

Hutsch, J., M. Sobiella, K. Heidel, G. Pausch:

Activities of the detector lab Rossendorf for FOBOS;

Proc. FOBOS Workshop '94, Cracow, Poland, Jun. 1994, FZR-65 (1995) 62

Iskra, W., H. Lenske, M. Müller, I. Rotter:

Core polarization and chaotic motion in nuclei;

Verhandl. DPG (VI), 30 (1995) 590

Iskra, W., M. Müller, E. Persson, I. Rotter:

Radial and time pattern of nuclear decay processes;

in: Low Energy Nuclear Dynamics, ed. by Yu. Oganessian, R. Kalpakchieva and W. von Oertzen, World Scientific 1995, pp. 569-577

Iskra, W., M. Müller, I. Rotter:

Radial pattern of nuclear decay processes;

Poster, International Nuclear Physics Conference, Beijing, China, Aug. 1995

Jahn, P., M. Moosburger, B. Naumann, M. Rogge, M. Steinke, R. Toelle:

Ion optical investigations in the extraction beam line;

Annual Report 1994, IKP Jül-3035 (1995) 18

Kamanin, D., H. Fuchs, J. Krüger, G. Pausch:

Analysis of light charged particle multiplicities in the reaction ^{32}S (960 MeV) + ^{197}Au ;

Proc. FOBOS Workshop '94, Cracow, Poland, Jun. 1994, FZR-65 (1995) 110

Kämpfer, B., O.P. Pavlenko, A. Peshier, G. Soff:

Dilepton production in a chemically equilibrating, expanding and hadronizing quark-gluon plasma;

FZR-89 (1995)

Kämpfer, B., O.P. Pavlenko, A. Peshier, G. Soff:

Parton kinetics for strangeness and charm production;

Preprint FZR-72 (1995), in Proc. "Strangeness '95", (Eds.) G. Oldenycz, J. Rafelski, American Institute of Physics (1995)

Kämpfer, B., O.P. Pavlenko, A. Peshier, G. Soff:
Parton kinetics for strangeness and charm production;
AIP Conference Proceedings 340, Strangeness in Hadronic Matter, Tucson, AZ 1995,
Editor: Johann Rafelski, p. 355

Käubler, L., H. Prade, J. Reif, R. Schwengner, G. Winter, H. Grawe, K.-H. Maier, R.
Schubart, K.-M. Spohr:
A new level scheme of ^{109}Sn ;
Verhandl. DPG (VI), 30 (1995) 611

Kirchner, T.:
 K^+ production described by the Rossendorf collision model;
Verhandl. DPG (VI), 30 (1995) 686

Klein, R., P. Michel, K. Möller, Ch. Nake, B. Naumann, L. Naumann, A. Schamlott, A.
Schülke for the COSY-TOF-collaboration:
Computer controlled vacuum system for the COSY-TOF-spectrometer;
Annual Report 1994, IKP Jül-3035 (1995) 15

Klein, R., Ch. Nake, B. Naumann, L. Naumann, A. Schamlott, P. Turek for the COSY-
TOF collaboration:
Residual gas analysis of the liquid hydrogen target in the start detector device of the COSY-
TOF-spectrometer;
Annual Report 1994, IKP Jül-3035 (1995) 17

Kolomeitsev, E.E., D.N. Voskresensky, B. Kämpfer:
Kaon polarization in dense nuclear matter;
Verhandl. DPG (VI), 30 (1995) 577

Kolomeitsev, E.E., D.N. Voskresensky, B. Kämpfer:
Kaon polarization in nuclear matter;
Proc. Int. Workshop on Gross Properties of Nuclei and Nuclear Excitations, Hirschegg
XXIII (1995), (Eds.) H. Feldmeier, W. Nörenberg, p. 320

Kolomeitsev, E.E., D.N. Voskresensky, B. Kämpfer:
The impact of kaon polarization in nuclear matter on the K^- production in heavy-ion collisions;
FZR-91 (1995)

Komarov, V.I., A.V. Kulikov, A.Yu. Petrus, V.V. Sidorkin, B.Zh. Zalikhanov, H. Ohm,
R. Schleichert, H. Seyfarth, H. Müller, S. Abdulazizov, S.V. Trusov:
The preparation of the backward detector system for the 0° -facility;
Annual Report 1994, IKP Jül-3035 (1995) 64

Kotte, R., B. Kämpfer, J. Mösner, W. Neubert, D. Wohlfarth:
Interplay of collective flow phenomena and velocity correlations of intermediate mass fragments in collisions of $\text{Au}+\text{Au}$ at $E/A = 100\text{-}400$ MeV;
Verhandl. DPG (VI), 30 (1995) 738

Kotte, R. B. Kämpfer, J. Mösner, W. Neubert, D. Wohlfarth:
Radial blast scenario for single-particle spectra in central Au+Au collisions at 100 MeV/u measured by FOPI and miniball/wall;
GSI-Report 95-1, p. 52

Kraft, G., U. Arndt, W. Becher, D. Böhne, H. Eickoff, Th. Haberer, J. Heilmann, J. Hoffmann, M. Krämer, W. Kraft-Weyrather, B. Langenbeck, G. Lenz, K. Poppensieker, M. Richter, S. Ritter, D. Dhardt, M. Scholz, R. Steiner, P. Strehl, H. Stelzer, U. Weber, J. Debus, M. Wannemacher, F. Wenz, G. Gademann, G. Hartmann, C. Jacob, O. Jäckel, W. Schlegel, W. Enghardt, B.G. Hasch, J. Pawelke, M. Sobiella:
Heavy ion therapy at GSI;
Fifth Workshop on Heavy Charged Particles in Biology and Medicine, Darmstadt, Aug. 1995, Book of Abstracts, GSI-Report 95-10, p. 171

Krüger, J., A. Budzanowski, H. Fuchs, C.-M. Herbach, H. Homeyer, D. Kamanin, A. Matthies, H.-G. Ortlepp, G. Pausch, W. Seidel, V. Shuchko, A. Siwek, V. Trofimov, A. Tutay, W. Wagner, L. Zrodowski:
IMF emission and projectile fragmentation in the system $^{32}\text{S} + ^{197}\text{Au}$ at 30 MeV/u;
Proc. FOBOS Workshop '94, Cracow, Poland, Jun. 1994, FZR-65 (1995) 106

Krüger, J., H. Fuchs, D. Kamanin, G. Pausch and Collaboration FOBOS:
Study of IMF production in the reaction ^{32}S (30 AMeV) + ^{197}Au ;
Verhandl. DPG (VI), 30 (1995) 775

Kuhlmann, E., H. Müller, B. Naumann, L. Naumann for the COSY-TOF collaboration:
Estimate of the total cross section of the proton-proton-bremsstrahlung near pion threshold;
Annual Report 1994, IKP Jül-3035 (1995) 7

Lauckner, K., W. Enghardt, J. Pawelke, M. Sobiella:
The implementation of an iterative reconstruction scheme to limited angle positron cameras;
Poster, 1995 International Meeting on Fully Three-Dimensional Image Reconstruction in Radiology and Nuclear Medicine, Aix-les-Bains, France, Jul. 1995, Proceedings, p. 355

Leifels, Y. for the FOPI-Collaboration:
First results of the HELITRON drift chamber;
GSI-Nachrichten, GSI 08-95, p. 4

Michel, P., K. Möller, A. Schamlott, A. Schülke for the COSY-TOF collaboration:
Test facility for methodical investigations of long scintillator strips for use in the COSY-TOF-Spectrometer;
Annual Report 1994, IKP Jül-3035 (1995) 11

Möhlenkamp, T. and the ALADIN/LAND-Collaboration:
Isotope ratios as thermometers in fragmentation reactions;
Proc. of the XXXIII International Winter Meeting on Nuclear Physics, Bormio, Italy, Jan. 1995

Möhlenkamp, T. for the ALADIN/LAND-Collaboration:
Probing the nuclear liquid-gas phase transition;
GSI-Report 95-1, p. 46

Möhlenkamp, T. and the ALADIN/LAND-Collaboration:
Isotope ratios as thermometers in fragmentation reactions;
Verhandl. DPG (VI), 30 (1995) 626

Mohren, S. and the FOPI-Kollaboration:
Isotopenidentifizierung mit der HELITRON Driftkammer des FOPI-Detektors;
Verhandl. DPG (VI), 30 (1995) 770

Morokhovskii, V.V., J. Freudenberger, M. Galemann, H. Genz, L. Groening, P. Hoffmann-Stascheck, A. Richter, V.L. Morokhovskii, U. Nething, R. Zahn, J.P.F. Sellshop:
Monte-Carlo simulation of the line shape and spectral density of PXR-radiation;
Int. Workshop on Radiation Physics at Electron Accelerators, Bad Honnef, Germany, Jun. 1995, Book of Abstracts

Müller, H., T. Kirchner, C. Schneider, C. Schneiderei, M. Büscher, K. Sistemich, V.I. Komarov, A. Sibirtsev:
Subthreshold production of K^- mesons at the 0° -facility;
Annual Report 1994, IKP Jül-3035 (1995) 47

Müller, M., F.-M. Dittes, W. Iskra and I. Rotter:
Level repulsion in the complex plane;
FZR-70 (1995)

Müller, M.:
Zur Herausbildung verschiedener Zeitskalen beim Zerfall von Compoundkern-Resonanzen als Folge des Trapping-Effektes;
Preprint FZR-79 (1995)

Müller, M., F.-M. Dittes, W. Iskra and I. Rotter:
Level repulsion in the complex plane;
Verhandl. DPG (VI), 30 (1995) 641

Müller, M., E. Persson, I. Rotter, W. Iskra:
Investigation of an ensemble near the elastic threshold;
Poster, Workshop on Nonequilibrium Physics at Short Time Scales, 114. WE-Heraeus-Seminar, Rostock, Jan. 1995

Müller, M., E. Persson, I. Rotter and W. Iskra:
Spectroscopic investigations near particle decay thresholds;
Verhandl. DPG (VI), 30 (1995) 641

Müller, M., E. Persson, I. Rotter, W. Iskra:
Spectroscopic investigations near particle decay thresholds;
Poster, International Nuclear Physics Conference, Beijing, China, Aug. 1995

Müller, W.F.J., J. Pochodzalla, W. Trautmann, M. Begemann-Blaich, Th. Blaich, C. Groß, H. Emling, A. Ferrero, G. Immé, I. Iori, G.J. Kunde, W.D. Kunze, V. Lindenstruth, U. Lynen, T. Möhlenkamp, A. Moroni, B. Ocker, G. Raciti, T. Rubehn, H. Sann, A. Schüttauf, C. Schwarz, W. Seidel, V. Serfling, J. Stroth, A. Trzcinski, A. Tucholski, G. Verde, A. Wörner, E. Zude, B. Zwieglinski:
Boiling nuclei;
GSI-Nachrichten, GSI 03-95, p. 3

Naumann, B., M. Rogge, P. Jahn, A. Hassan:
Phase space measurements by the imaging method at COSY;
Verhandl. DPG (VI), 30 (1995) 662

Nothing, U., J. Freudenberger, H. Genz, L. Groening, P. Hoffmann-Stascheck, M. Höfer, J. Hormes, W. Knüpfer, H. Prade, A. Richter, K. Runkel, J.P.F. Sellshop, C. Toepffer, M. Weber, R. Zahn:
Channeling radiation of diamond and ruby crystals;
Int. Workshop on Radiation Physics at Electron Accelerators, Bad Honnef, Germany, Jun. 1995, Book of Abstracts

Nothing, U., J. Freudenberger, V.B. Gavrikov, H. Genz, L. Groening, P. Hoffman-Staschek, M. Höfer, J. Hormes, W. Knüpfer, V.L. Morokhovskii, V.V. Morokhovskii, H. Prade, A. Richter, K. Runkel, J.P.F. Sellschop, N.F. Shul'ga, C. Toepffer, M. Weber, R. Zahn:
Channeling radiation and parametric x-ray radiation at electron energies less than 10 MeV;
Workshop on Channeling and other coherent crystal effects at relativistic Energie, University of Aarhus, Jul. 1995, Book of Abstracts

Neubert, W., M.N. Andronenko, A.S. Botwina:
Production on Intermediate Mass Fragments in Proton-Nucleus Collisions at 1 GeV;
Verhandl. DPG (VI), 30 (1995) 685

Ortlepp, H.-G., M. Andrassy, G.G. Chubarian, M. Danziger, L. Dietterle, A.S. Fomichev, P. Gippner, C.-M. Herbach, A.I. Ivanenko, I.V. Kolesov, A. Matthies, D. May, Yu.Ts. Oganessian, Yu.E. Penionzhkevich, V.N. Pokrovskij, G. Renz, L.A. Rubinskaja, V.E. Shuchko, O.V. Strelakovsky, V.V. Trofimov, V.M. Vasko, W. Wagner, K. Heidel, K.D. Schilling, W. Seidel, H. Sodan, H. Fuchs, D. Hilscher, H. Homeyer, W. von Oertzen, P. Ziem, G. Pausch, B.A. Burova, S.V. Radnev, I.D. Sandrev:
The 4π -fragment spectrometer FOBOS - status and first preliminary results;
Proc. FOBOS Workshop '94, Cracow, Poland, Jun. 1994, FZR-65 (1995) 29

Ortlepp, H.-G., W. Wagner, A.A. Aleksandrov, I.A. Aleksandrova, L. Dietterle, V.N. Doronin, S. Dshemuchadse, P. Gippner, C.-M. Herbach, D. Hilscher, S.A. Ivanovsky, A. Matthies, Yu.Ts. Oganessian, G. Pausch, Yu.E. Penionzhkevich, G. Renz, K.D. Schilling, D.I. Shishkin, O.V. Strelakovsky, V.V. Trofimov, C. Umlauf, D.V. Vakotov, V.M. Vasko, V.E. Zhuchko, A.G. Artukh, G.F. Gridnev, M. Grushezki, J. Szmider, Yu.G. Teterev, M.G. Nagaenko, Yu.M. Sereda, I.N. Vishnevski, S.G. Genchev:

The COMBAS fragment separator of radioactive nuclei and the FOBOS 4π -detector for charged particles;

Proc. Int. Workshop on Physics with Recoil Separators and Detector Arrays, New Delhi, India, Jan./Feb.1995; Preprint FZR-103 (1995)

Ortlepp, H.-G., W. Wagner, A.A. Aleksandrov, I.A. Aleksandrova, L. Dietterle, V.N. Doronin, S. Dshemuchadse, P. Gippner, C.-M. Herbach, S.I. Ivanovsky, D.V. Kamanin, A. Matthies, G. Pausch, Yu.E. Penionzhkevich, G. Renz, K.-D. Schilling, D.I. Shishkin, O.V. Strelakovsky, V.V. Trofimov, I.P. Tsurin, C. Umlauf, D.V. Vakotov, V.M. Vasko, V.E. Zhuchko:

Spectroscopy of correlated fragments from the fission of hot nuclei performed at the FOBOS 4π -array;

Proc. Int. Conf. on Low Energy Nuclear Dynamics (LEND '95), St. Petersburg, Russia, Apr. 1995; Preprint FZR-102 (1995)

Öschler, H., V. Lips, R. Barth, S.P. Avdeyev, W. Karcz, V.A. Karnaukhov, W.D. Kuznezov, L.A. Petrov, O.V. Bochkarev, L.V. Chulkov, E.A. Kuzmin, W. Neubert, E. Norbeck:

Breakup condition in multifragmentation;

Verhandl. DPG (VI), 30 (1995) 625

Pausch, G., W. Bohne, A. Buscemi, G. DeAngelis, G. DePoli, H. Grawe, D. Hilscher, M. Moszynski, G. Roeschert, R. Schubart, D. Wolski, R. Zanon:

Pulse-shape discrimination for particle identification in 4π silicon balls;

Verhandl. DPG (VI), 30 (1995) 584

Pausch, G., M. Moszynski, D. Wolski, W. Bohne, H. Grawe, D. Hilscher, R. Schubart, G. de Angelis and M. de Poli:

Application of the pulse-shape technique to proton-alpha discrimination in Si-detector arrays; Preprint FZR-85 (1995)

Pausch, G., H.-G. Ortlepp, W. Wagner:

Possible ancillary detectors for FOBOS exploiting pulse-shape discrimination for silicon detectors;

Proc. FOBOS Workshop '94, Cracow, Poland, Jun. 1994, FZR-65 (1995) 69

Pausch, G., H. Prade, M. Sobiella, M. Freitag, H. Grawe, K.-H. Maier, M. Moszynski, D. Wolski, R. Schubart, A. Johnson, G. de Angelis:

A 4π Si-Ball with charged-particle discrimination based on the pulse-shape technique;

Poster, International Nuclear Physics Conference, Beijing, China, Aug. 1995

Pawelke, J., L. Byars, W. Enghardt, H. Geissel, B.G. Hasch, K. Lauckner, P. Manfraß, D. Schardt, M. Sobiella:
A BGO based positron camera for heavy ion tumour therapy control;
Int. Conference on Inorganic Scintillators and their Applications, Delft, Niederlande, Aug./Sep. 1995, Book of Abstracts, p. 98

Persson, E., M. Müller, I. Rotter:
Resonance phenomena near thresholds;
Preprint FZR-119 (1995)

Peshier, A., B. Kämpfer, O.P. Pavlenko, G. Soff:
Quark-Gluon-Plasma with thermal parton masses;
Poster, Quark-Matter 1995, Monterey, USA, Jan. 1995

Peshier, A.:
Das Quark-Gluon-Plasma mit thermischen Partonenmassen und Konsequenzen des Modells für die thermische Dileptonenemission;
FZR-75 (1995)

Peshier, A., B. Kämpfer, O.P. Pavlenko, G. Soff:
A massive quasi-particle model of the SU(3) gluon plasma;
FZR-106 (1995)

Pfeiffer, A., B. Köhler, B. Hasch, W. Enghardt:
Sound radiation caused by heavy ions stopping in water and its possibilities for dose distribution monitoring in modern cancer therapy;
1995 World Congress on Ultrasonics, Berlin, Sep. 1995

Pochodzalla, J., T. Möhlenkamp, T. Rubehn, A. Schüttauf, A. Wörner, E. Zude, M. Begemann-Blaich, Th. Blaich, C. Gross, H. Emling, A. Ferrero, G. Imme, I. Iori, G.J. Kunde, W.D. Kunze, V. Lindenstruth, U. Lynen, A. Moroni, W.F.J. Müller, B. Ocker, G. Raciti, H. Sann, C. Schwarz, W. Seidel, V. Serfling, J. Stroth, A. Trzcinski, W. Trautmann, A. Tucholski, G. Verde, B. Zwieglinski:
Probing the nuclear liquid-gas phase transition;
Preprint GSI-95-13 (1995)

Prade, H., F. Dönau:
ELBE ein supraleitender 250 MeV Elektronenbeschleuniger für das FZR (Interne Projektstudie);
FZR-74 (1995)

Pyatkov, Yu.V., A.A. Aleksandrov, I.A. Aleksandrova, B.I. Andreev, P. Gippner, C.-M. Herbach, E.M. Kozulin, A. Matthies, Yu.Ts. Oganessian, H.-G. Ortlepp, Yu.E. Penionzhkevich, G. Renz, K.D. Schilling, O.V. Strelakovsky, V.M. Vasko, W. Wagner:
A ^{244}Cm cold spontaneous fission study at the FOBOS-spectrometer;
Proc. FOBOS Workshop '94, Cracow, Poland, Jun. 1994, FZR-65 (1995) 74

Rademacher, E., M. Wilhelm, J. Eberth, M. Eschenauer, N. Nicolay, R. Schwengner, S. Skoda, H.G. Thomas, H. Tiesler, P. von Brentano:
The γ -decay of particle-hole states in ^{208}Pb using the EUROBALL-CLUSTER-detector;
Verhandl. DPG (VI), 30 (1995) 753

Renz, G., V.M. Vasko, P. Gippner, A. Matthies, V.N. Doronin, D.I. Shishkin, C. Umlauf, M. Gebhardt:
Status of the evacuation and gas supply system of FOBOS;
Proc. FOBOS Workshop '94, Cracow, Poland, Jun. 1994, FZR-65 (1995) p. 46

Rotter, I.:
Selforganization and chaos in the nuclear system;
in: Dynamical Systems and Chaos, Volume 2 (Physics), ed. by Y. Aizawa, S. Saito and K. Shiraiwa, World Scientific 1995, pp. 550-553

Rotter, I., W. Iskra and M. Müller:
Investigation of an open quantum mechanical system;
Verhandl. DPG (VI), 30 (1995) 1109

Rotter, I., W. Iskra and M. Müller:
Trappingeffekt, Zeitskalen und Chaos in quantenmechanischen Vielteilchensystemen;
Verhandl. DPG (VI), 30 (1995) 1961

Rubehn, Th., W.F.J. Müller, R. Bassini, M. Begemann-Blaich, Th. Blaich, A. Ferrero, C. Gross, G. Imme, I. Iori, G.J. Kunde, W.D. Kunze, V. Lindenstruth, U. Lynen, T. Möhlenkamp, L.G. Moretto, B. Ockere, J. Pochodzalla, G. Raciti, S. Reito, H. Sann, A. Schüttauf, W. Seidel, V. Serfling, W. Trautmann, A. Trzcinski, G. Verde, A. Wörner, E. Zude, B. Zwieglinski:
Electromagnetic fission of ^{238}U at 600 and 1000 MeV per nucleon;
Preprint, GSI-95-28 (1995)

Rubehn, Th., et al., T. Möhlenkamp, W. Seidel:
Charge-pickup of ^{238}U at relativistic energies;
Preprint, GSI-95-60 (1995)

Schilling, K.D., Yu.V. Pyatkov, A.A. Aleksandrov, I.A. Aleksandrova, B.I. Andreev, P. Gippner, C.-M. Herbach, E.M. Kozulin, A. Matthies, Yu.Ts. Oganessian, H.-G. Ortlepp, Yu.E. Penionzhkevich, G. Renz, O.V. Strekalovsky, V.M. Vasko, W. Wagner:
A ^{244}Cm cold spontaneous fission study at the FOBOS-spectrometer;
Verhandl. DPG (VI), 30 (1995) 723

Schleif, M., R. Wunsch:
Pushing and cranking corrections to the meson fields of the bosonized Nambu & Jona-Lasinio model;
Verhandl. DPG (VI), 30 (1995) 741

Schneider, C., Th. Kirchner, H. Müller, L. v. Horn, H. Ohm, V. Kruglov:
The multiwire chamber MWC 1 for the 0° -facility;
Annual Report 1994, IKP Jül-3035 (1995) 60

Schülke, A., E. Kuhlmann, K. Möller, P. Michel, B. Naumann, L. Naumann, A. Schamlott
and the COSY-TOF-Collaboration:

First measurements at the COSY-TOF-spectrometer;
Verhandl. DPG (VI), 30 (1995) 628

Schülke, A., E. Kuhlmann, P. Michel, K. Möller, B. Naumann, L. Naumann, A. Schamlott
for the COSY-TOF collaboration:

Test of the COSY-TOF-start-detector MARS at the COSY beam;
Annual Report 1994, IKP Jül-3035 (1995) 13

Sistemich, K., R. Maier, U. Bechstedt, W. Borgs, W. Bräutigam, N. Brummund, M. Büscher, J. Dietrich, R. Eßer, A. Franzen, D. Gotta, D. Grzonka, U. Hacker, A. Hardt, M. Hartmann, L. von Horn, H.R. Koch, D. Kopyto, S. Kopyto, R. Krause, S. Martin, K. Meyer, P. Munhofen, W. Oelert, H. Ohm, D. Prasuhn, H.J. Probst, M. Sauer, R. Schleichert, A. Schneider, O.W.B. Schult, H. Seyfarth, V. Vau, K.-H. Watzlawik, J. Ernst, F. Hinterberger, L. Jarczyk, B. Kamys, St. Kistryn, R. Kulesa, Z. Rudy, J. Smyrski, A. Strzalkowski, M. Wende, S. Diemel, T. Kirchner, H. Langenhagen, K.W. Leege, H. Müller, W. Oehme, B. Prietzsch, B. Rimarzig, C. Schneider, C. Schneiderei, V. Grebenjuk, V.V. Ivanov, V. Karpukhin, V.I. Komarov, V.I. Komissarov, V. Kruglov, A. Yu. Petrus, A.I. Puzynin, A.I. Rudenko, V.V. Sidorkin, B.Zh. Zalikhanov, S. Belostotsky, O. Grebenyuk, V. Koptev, S. Mikirtichyants, V. Nelubin, W. Cassing, H. Dombrowski, R. Santo, W. Klein, F. Klehr, H. Stechemesser, M. Köhler, G. Müller, U. Sieling, W. Tenten, K. Zwoell, A. Sibirtsev, V. Tchernyshev, N. Amaglobeli, B. Chiladze, L. Glonti, A. Kacharava, G. Macharashvili, Z. Menteshashvili, M. Nioradze, S. Abdulazizov, A. Kulikov, A. Selikov, S. Trusov, V. Yazkov, W. Bothe, U. Schwarz, I. Zychor:

Status of the 0° -facility;
Annual Report 1994, IKP Jül-3035 (1995) 41

Strekalovsky, O.V., K. Heidel, S.I. Ivanovsky, D. May, H.-G. Ortlepp, G. Pausch, G. Renz, V.V. Trofimov, I.P. Tsurin, W. Wagner, V.E. Zhuchko:

The front-end electronics and the data acquisition system of the FOBOS 4π -array;
Proc. FOBOS Workshop '94, Cracow, Poland, Jun. 1994, FZR-65 (1995) 49

Titov, A.I., B. Kämpfer, B.L. Reznik, V. Shklyar:

The reaction $NN \rightarrow NN\gamma$ in the 1 GeV region within an effective one-boson exchange model;
FZR-118 (1995)

Tsang, M.B., et al., W. Seidel:

Squeeze-out of Nuclear Matter in Au + Au Collisions;
MSU Preprint, MSUCL-983, Nov. 95

Tutay, A., A. Budzanowski, H. Fuchs, H. Homeyer, G. Pausch, C. Schwarz, A. Siwek:
Aspects of sequential intermediate-mass fragment formation in 30 A MeV $^{32}\text{S} + ^{58}\text{Ni}$;

Verhandl. DPG (VI), 30 (1995) 648

Voskresensky, D.N., E.E. Kolomeitsev, B. Kämpfer:

The role of the massive photon decay channel for the neutrino cooling of neutron stars;
FZR-117 (1995)

Wagner, W., H.-G. Ortlepp, D.V. Kamanin, A. Matthies, O.V. Strekalovsky, V.E. Zhuchko:

Status of the FOBOS scintillator shell;

Proc. FOBOS Workshop '94, Cracow, Poland, Jun. 1994, FZR-65 (1995) 40

Wagner, W., A. Budzanowski, B. Czech, D. Hilscher, J. Holik, H. Homeyer, W. Janczur, H.-G. Ortlepp, G. Pausch, O.V. Strekalovsky, L. Zrodowski:

The FOBOS forward array;

Proc. FOBOS Workshop '94, Cracow, Poland, Jun. 1994, FZR-65 (1995) 42

Wagner, W., P. Gippner, C.-M. Herbach, H.-G. Ortlepp:

Ternary spontaneous fission of ^{244}Cm ;

Proc. FOBOS Workshop '94, Cracow, Poland, Jun. 1994, FZR-65 (1995) 83

Wagner, W., H.-G. Ortlepp, C.-M. Herbach, P. Gippner, D.V. Kamanin, A. Matthies, Yu.E. Penionzhkevich, G. Renz, K.D. Schilling, O.V. Strekalovsky, D.V. Vakotov, V.E. Zhuchko:

Fission of hot heavy nuclei investigated at the FOBOS 4π -array;

Contr. Int. Symp. on Heavy Ion Physics and its Applications (II SHIPA), Lanzhou, China, Aug./Sep. 1995; Preprint FZR-104 (1995)

Wagner, W., H.-G. Ortlepp, C.-M. Herbach, P. Gippner, A. Matthies, Yu.E. Penionzhkevich, G. Renz, K.D. Schilling, O.V. Strekalovsky, V.E. Zhuchko:

Fission and emission of intermediate mass fragments in asymmetric heavy-ion collisions investigated at the FOBOS 4π -array;

Contr. Int. Nucl. Phys. Conf. (INPC '95), Beijing, China, Aug. 1995; Preprint FZR-105 (1995)

Weber, M., C. Toepffer, H. Genz, P. Hoffmann-Stascheck, U. Nething, A. Richter:

Population dynamics of planar channeling electrons in thick crystals, Book of Abstracts;

146. WE-Heraeus-Seminar: International Workshop on Radiation Physics at Electron Accelerators, Bad Honnef, Germany, Jun. 1995, Book of Abstracts

Wagner, W. (Ed.):

Proc. of the FOBOS Workshop '94, Cracow, Poland, Jun. 1994, FZR-65 (1995)

Wagner, W., H.-G. Ortlepp, D.V. Kamanin, A. Matthies, O.V. Strelakovsky, V.E. Zhuchko:

Status of the FOBOS scintillator shell;

Proc. FOBOS Workshop '94, Cracow, Poland, Jun. 1994, FZR-65 (1995) 40

Wagner, W., A. Budzanowski, B. Czech, D. Hilscher, J. Holik, H. Homeyer, W. Janczur, H.-G. Ortlepp, G. Pausch, O.V. Strelakovsky, L. Zrodowski:

The FOBOS forward array;

Proc. FOBOS Workshop '94, Cracow, Poland, Jun. 1994, FZR-65 (1995) 42

Wagner, W., P. Gippner, C.-M. Herbach, H.-G. Ortlepp:

Ternary spontaneous fission of ^{244}Cm ;

Proc. FOBOS Workshop '94, Cracow, Poland, Jun. 1994, FZR-65 (1995) 83

Wagner, W., H.-G. Ortlepp, C.-M. Herbach, P. Gippner, D.V. Kamanin, A. Matthies, Yu.E. Penionzhkevich, G. Renz, K.D. Schilling, O.V. Strelakovsky, D.V. Vakarov, V.E. Zhuchko:

Fission of hot heavy nuclei investigated at the FOBOS 4π -array;

Contr. Int. Symp. on Heavy Ion Physics and its Applications (II SHIPA), Lanzhou, China, Aug./Sep. 1995; Preprint FZR-104 (1995)

Wagner, W., H.-G. Ortlepp, C.-M. Herbach, P. Gippner, A. Matthies, Yu.E. Penionzhkevich, G. Renz, K.D. Schilling, O.V. Strelakovsky, V.E. Zhuchko:

Fission and emission of intermediate mass fragments in asymmetric heavy-ion collisions investigated at the FOBOS 4π -array;

Contr. Int. Nucl. Phys. Conf. (INPC '95), Beijing, China, Aug. 1995; Preprint FZR-105 (1995)

Weber, M., C. Toepffer, H. Genz, P. Hoffmann-Stascheck, U. Nething, A. Richter:

Population dynamics of planar channeling electrons in thick crystals, Book of Abstracts;

146. WE-Heraeus-Seminar: International Workshop on Radiation Physics at Electron Accelerators, Bad Honnef, Germany, Jun. 1995, Book of Abstracts

3 Lectures and Seminars

Barz, H.W.:

Flow in central and semicentral Au on Au collisions at 150 and 250 AMeV;
CHIC Annual Meeting 1995 and Workshop on Clusterization in Heavy Ion Collisions, NBI
Copenhagen, Denmark, May 1995

Barz, H.W.:

Flow and fragmentation in central and semicentral gold on gold collisions at intermediate
energies;
8th Nordic Meeting on Nuclear Physics, Ronneby Brunn, Sweden, Jun. 1995

Barz, H.W.:

Theoretische Kernphysik;
Lecture course, TU Dresden SS 1995

Biegansky, J.:

Zentrale Stöße schwerer Ionen bei 150 - 1050 AMeV;
Seminar, IKH/FZ Rossendorf, Sep. 1995

Dittes, F.M.:

Selbstorganisierte Kritizität in Quantensystemen;
DFG-Kolloquium, Universität Kaiserslautern, Feb. 1995

Dittes, F.M.:

Optimization on rugged landscapes - new tools and results;
Max-Planck-Institut für Physik komplexer Systeme, Dresden, Sep. 1995

Dittes, F.M.:

How egoism helps to solve global problems;
Int. Conference "Self-Organization of Complex Structures: From Individual to Collective
Dynamics", Berlin, Sep. 1995

Dittes, F.M.:

Optimierung auf "rauhem" Oberflächen;
Seminar, IKH/FZ Rossendorf, Oct. 1995

Dittes, F.M.:

"Freiheit und Zwang - Physikalische Prinzipien zur Optimierung komplexer Systeme";
FZR-Zentrumskolloquium, Nov. 1995

Dittes, F.M.:

Optimierungsansätze für Systeme mit Frustration - ein demokratischer Zugang;
TU Dresden, Dec. 1995

Enghardt, W.:

PET zum Strahlmonitoring bei der Schwerionentherapie;
33. Int. Jahrestagung der Deutschen Gesellschaft für Nuklearmedizin, Dresden, Mar. 1995

Enghardt, W.:

Die Bestrahlung von Minischweinen mit ^{12}C -Ionen und Röntgenstrahlen bei der GSI Darmstadt;

TU Dresden, Medizinische Fakultät, Klinik für Strahlentherapie, May 1995

Enghardt, W.:

Tomographische Rekonstruktion für PET;

TU Dresden, Medizinische Fakultät, Klinik für Nuklearmedizin, May 1995

Enghardt, W.:

Tumorthherapie mit Strahlen schwerer Ionen;

TU Dresden, Fakultät für Elektrotechnik, Institut für Biomedizinische Technik, May 1995

Enghardt, W.:

Die Anwendung der Positronen-Emissions-Tomographie für das Monitoring der Schwerionen-Tumorthherapie;

76. Deutscher Röntgenkongreß, Wiesbaden, May 1995

Enghardt, W.:

A positron emission tomograph for the on-line control of heavy ion tumour treatment;

Fifth Workshop on Heavy Charged Particles in Biology and Medicine, Darmstadt, Aug. 1995

Enghardt, W.:

Premedical studies with minipigs;

2nd Meeting of the International Advisory Board for the Heavy Ion Therapy at GSI, Darmstadt, Aug. 1995

Frauendorf, S.:

Magnetic rotations;

Department of Physics, University of Padua, Italy, Feb. 1995

Frauendorf, S.:

Nuclei and clusters - a prolific union;

The Institute of Physics Annual Congress, Telford, Great Britain, Mar. 1995

Frauendorf, S.:

Tilted axis cranking;

Department of Physics, University of Surrey, Great Britain, Mar. 1995

Frauendorf, S.:

The nucleus - a mesoscopic system;

Nuclear Science Division Colloquium, Lawrence Berkeley Laboratory, Berkeley, USA, May 1995

Frauendorf, S.:

Thermodynamics and decay of liquid alkali clusters;

The NATO Advanced Study Institute, International School of Solid State Physics, 6th Course: Large Clusters of Atoms and Molecules, Erice, Italy, Jun. 1995

Frauendorf, S.:

Magnetische Rotationen;
Seminar, IKH/FZ Rossendorf, Oct. 1995

Frauendorf, S.:

Magnetic rotation;
Workshop nuclear structure under extreme conditions, University of Washington, Seattle, USA, Nov. 1995

Frauendorf, S.:

Residual interaction and spin orientation in rotating nuclei;
Workshop on Gammasphere Physics, Berkeley, USA, Dec. 1995

Hasch, B.G.:

Die physikalischen Grundlagen für ein Verfahren der Kontrolle der Schwerionen-Tumotherapie mit PET;
Seminar, IKH/FZ Rossendorf, Sep. 1995

Heide, B.:

Effects of flow on multifragmentation processes;
DPG-Frühjahrstagung "Physik der Hadronen und Kerne", Köln, Mar. 1995

Herbach, C.-M.:

Coincidence measurements of light (LCP) and intermediate (IMF) charged particles with fission fragments (FF) produced by ^{14}N (34 AMeV) + ^{197}Au ;
DPG-Frühjahrstagung "Physik der Hadronen und Kerne", Köln, Mar. 1995

Iskra, W., M. Müller, E. Persson, I. Rotter:

Radial and time pattern of nuclear decay processes;
Int. Conference on Low Energy Nuclear Dynamics (LEND '95), St. Petersburg, Russia, Apr. 1995

Kamanin, D.:

Aufbau und Test der Szintillatorschale für FOBOS;
Seminar, IKH/FZ Rossendorf, Oct. 1995

Kämpfer, B.:

Eichfeldtheorie der schwachen Wechselwirkung;
Lecture course, TU Dresden, SS 1995

Kämpfer, B.:

Quantenelektrodynamik;
Lecture course, TU Dresden, WS 1995

Kämpfer, B.:

Parton kinetics of strangeness and charm production;
Workshop strangeness '95, Tuscon, USA, Jan. 1995

Kämpfer, B.:

Massive gluon model of the quark-gluon plasma;
QCD-Workshop, Trento, Italy, Jun. 1995

Kämpfer, B.:

Lepton pairs from preequilibrium plasma;
QCD-Workshop, Trento, Italy, Jun. 1995

Kämpfer, B.:

Quasi-Particle interpretation of QCD lattice data;
VIIth Max Born Symposium on Critical Phenomena in Strongly Interacting Matter, Karpacz,
Poland, Oct. 1995

Kolomeitsev, E.:

The kaon propagator in nuclear matter;
Hirschegg '95: Hadrons in nuclear matter, Hirschegg, Austria, Jan. 1995

Kolomeitsev, E.:

Kaonenpolarisation in Kernmaterie;
Seminar, IKH/FZ Rossendorf, Feb. 1995

Kolomeitsev, E.:

The kaon propagator in dense nuclear matter;
DPG-Frühjahrstagung "Physik der Hadronen und Kerne", Köln, Mar. 1995

Kolomeitsev, E.:

Kaon production in HIC: the impact of in-medium effects;
FOPI-Treffen, FZ Rossendorf, Apr. 1995

Kolomeitsev, E.:

Kaonerzeugung in HICs;
GSI-Theorie-Treffen, Stolpen, Jul. 1995

Kolomeitsev, E.:

Kaon polarization in nuclear matter: Neutron stars and kaon production in HICs;
Int. Summer School for Students on Development in Nuclear Theory and Particle Physics,
Dubna, Russia, Aug./Sep. 1995

Kolomeitsev, E.:

Fireball model of heavy ion collision: Inclusion in-medium effects;
Seminar, TU Dresden, Nov. 1995

Kolomeitsev, E.E.;

K^- -Erzeugung in Schwerionenstößen;
Seminar, IKH/FZ Rossendorf, Nov. 1995

Kolomeitsev, E.:

Kaon polarization in nuclear matter: Kaon condensation and kaon production in HICs;
Seminar, Dubna, Russia, Dec. 1995

Krüger, J.:

Study of IMF production in the reaction ^{32}S (30 AMeV) + ^{197}Au ;
DPG-Frühjahrstagung "Physik der Hadronen und Kerne", Köln, Mar. 1995

Krüger, J.:

Untersuchung der Reaktion S (960 MeV) + Au mit einer FOBOS/ARGUS-Komponente;
Seminar, IKH/FZ Rossendorf, Sep. 1995

Lauckner, K.:

Ein iteratives Rekonstruktionsverfahren in der PET;
Seminar, IKH/FZ Rossendorf, Sep. 1995

Möhlenkamp, T.:

Fragmentverteilungen in Schwerionenstößen;
Seminar, IKH/FZ Rossendorf, Sep. 1995

Möller, K.:

Einführung in die Mittelenergiephysik Teil II;
Lecture course, TU Dresden, WS 1995

Müller, M.:

Niveauabstoßung in der komplexen Ebene;
Seminar, TU Dresden, Institut für Theoretische Physik, Feb. 1995

Müller, M.:

Level repulsion in the complex plane;
Gruppenbericht, DPG-Frühjahrstagung "Physik der Hadronen und Kerne", Köln, Mar. 1995

Müller, M.:

Spectroscopic investigations near particle decay thresholds;
DPG-Frühjahrstagung "Physik der Hadronen und Kerne", Köln, Mar. 1995

Müller, M.:

Properties of an open quantum system;
Seminar, Max-Planck-Institut für Physik komplexer Systeme, Dresden, May 1995

Nething, U.:

Channelingstrahlung in Diamant- und Rubinkristallen sowie Untersuchungen zur
parametrischen Röntgenstrahlung am S-DALINAC;
Seminar, IKH/FZ Rossendorf, Feb. 1995

Nething, U.:

Channeling radiation of diamond and ruby crystals;
146. WE-Heraeus-Seminar, Int. Workshop on Radiation Physics at Electron Accelerators,
Bad Honnef, Jun. 1995

Nething, U.:

Channeling radiation and parametric x-ray radiation at electron energies less than 10 MeV;
Workshop on channeling and other coherent crystal effects at relativistic energy, University
of Aarhus, Jul. 1995

Ortlepp, H.-G.:

The FOBOS 4π -detector for charged particles;
Int. Workshop on Physics with Recoil Separators and Detector Arrays, New Delhi, India,
Jan./Feb. 1995

Ortlepp, H.-G.:

Spectroscopy of correlated fragments from the fission of hot nuclei performed at the FOBOS
 4π -array;
Int. Conference on Low Energy Nuclear Dynamics (LEND '95), St. Petersburg, Russia,
Apr. 1995

Ortlepp, H.-G.:

Fission investigations of actinides with the FOBOS array;
13th Meeting on Physics of Nuclear Fission, Obninsk, Russia, Oct. 1995

Ortlepp, H.-G.:

Multifragmentation studies at FOBOS;
Coordination Meeting on Nuclear Physics, Sandanski, Bulgaria, Oct. 1995

Ortlepp, H.-G.:

Experiments with the 4π -fragment spectrometer FOBOS at the JINR Dubna;
KVI Groningen, The Netherlands, Oct. 1995

Ortlepp, H.-G.:

Experiments with the 4π -fragment spectrometer FOBOS at the JINR Dubna;
GANIL, France, Nov. 1995

Ortlepp, H.-G.:

Investigation of fission and three-body decay of hot nuclei in the reactions ${}^7\text{Li}$ (43 AMeV)
+ ${}^{232}\text{Th}$ and ${}^{14}\text{N}$ (43 and 53 AMeV) + ${}^{197}\text{Au}$ at the FOBOS set-up (in Russian);
Seminar on Intermediate Energy Nuclear Collisions, FLNR Dubna, Russia, Dec. 1995

Pausch, G.:

Pulse-shape discrimination with planar Si detectors - simulations and experimental results;
CHICKSI Group Meeting, The Svedberg Laboratory, Uppsala, Sweden, Feb. 1995

Pausch, G.:

Pulse-shape discrimination with planar Si detectors - An excellent method for identification
of charged particles in Si-detector arrays;
Seminar, Heavy Ion Laboratory of the Warsaw University, Feb. 1995

Pausch, G.:

Pulse-shape discrimination for particle identification in 4π silicon balls;
DPG-Frühjahrstagung "Physik der Hadronen und Kerne", Köln, Mar. 1995

Pausch, G.:

Pulse-shape discrimination with planar Si detectors - an excellent method for identification of charged particles in Si-detector arrays;
Seminar, University of Lund, Sweden, Department of Physics, Apr. 1995

Pausch, G.:

Impulsformdiskriminierung in Halbleiterdetektoren und ihre Anwendung im Euroball;
Seminar, IKH/FZ Rossendorf, May 1995

Pausch, G.:

Status and design of the Si-ball (EuroSiB);
Meeting of Inner Charged-Particle Balls and Neutron Detectors for EUROBALL,
Rossendorf, May 1995

Pausch, G.:

Identification of light charged particles and heavy ions in silicon detectors by means of pulse-shape discrimination;
IEEE Nuclear Science Symposium, San Francisco, California, Oct. 1995

Pawelke, J.:

A BGO based positron camera for heavy ion tumour therapy control;
Int. Conference on Inorganic Scintillators and their Applications, Delft, The Netherlands,
Aug./Sep. 1995

Peshier, A.:

Elektromagnetische Signale vom Quark-Gluon-Plasma mit thermischen Partonenmassen;
Seminar, IKH/FZ Rossendorf, Feb. 1995

Peshier, A.:

A massive quasi-particle model of the SU(3)-gluon plasma;
GSI-Theorie-Treffen, Stolpen, Jul. 1995

Peshier, A.:

Chirale Störungstheorie;
Seminar, IKH/FZ Rossendorf, Nov. 1995

Persson, E.:

Threshold phenomena in an open quantum mechanical system;
Seminar, IKH/FZ Rossendorf, Apr. 1995

Persson, E.:

Threshold phenomena in open quantum systems;
Workshop "Parity and time reversal violation in compound nuclear states and related topics". European Centre for Theoretical Studies in Nuclear Physics and Related Areas,
Trento, Italy, Oct. 1995

Persson, E.:

Threshold phenomena in an open quantum mechanical system;
Seminar, TU Dresden, Institut für Theoretische Physik, Dec. 1995

Pfitzner, A.:

Dynamik von Zweiteilchenkorrelationen im Kern;
Seminar, TU Dresden, Institut für Theoretische Physik, Jun. 1995

Richter, H.:

Magnetische Wirbel- und Coulombphase einer Ladung;
Seminar, IKH/FZ Rossendorf, Jun. 1995

Rotter, I.:

Investigation of an open quantum mechanical system;
Workshop on Nonequilibrium Physics at Short-Time Scales (144. WE-Heraeus-Seminar),
Rostock, Jan. 1995

Rotter, I.:

Investigation of an open quantum mechanical system;
59. Physikertagung, Berlin, Mar. 1995

Rotter, I.:

Trappingeffekt, Zeitskalen und Chaos in quantenmechanischen Vielteilchensystemen;
59. Physikertagung, Berlin, Mar. 1995

Rotter, I.:

Resonance states at high level density;
Workshop "Parity and time reversal violation in compound nuclear states and related topics". European Centre for Theoretical Studies in Nuclear Physics and Related Areas,
Trento, Italy, Oct. 1995

Schleif, M.:

Pushing and cranking corrections to the meson fields of the bosonized Nambu & Jona-Lasinio model;
DPG-Frühjahrstagung "Physik der Hadronen und Kerne", Köln, Mar. 1995

Schleif, M.:

$SU(2)_f$ -NJL-Modell bei endlichen Temperaturen und Dichten;
Seminar, TU Dresden, May 1995

Schleif, M.:

Nukleoneneigenschaften im NJL-Modell bei endlichem T;
GSI-Theorie-Treffen, Stolpen, Jul. 1995

Schleif, M.:

$SU(2)$ -NJL Hedgehog Soliton im Wärmebad;
Seminar, TU Dresden, Nov. 1995

Schleif, M.:

Hedgehog im Wärmebad;
Seminar, IKH/FZ Rossendorf, Nov. 1995

Schleif, M.:

Das NJL Soliton im Medium;

Seminar, MPG AG "Theoretische Vielteilchenphysik", Rostock, Dec. 1995

Schneider, C.:

Entwicklung einer Drahtkammer für die Messung von Kaonen am ANKE-Spektrometer;

Seminar, IKH/FZ Rossendorf, Sep. 1995

Schülke, A.:

Methodische Untersuchungen und Testmessungen für das pp-Bremsstrahlungsexperiment am COSY-TOF-Spektrometer;

Seminar, TU Dresden, Nov. 1995

Servene, T.:

Messung von Hochspinzuständen in ^{79}Br mit Euroball-Clusterdetektoren;

Seminar, IKH/FZ Rossendorf, Nov. 1995

Wagner, W.:

Fission and emission of intermediate-mass fragments in asymmetric heavy-ion collisions investigated at the FOBOS 4π -array;

Int. Nuclear Physics Conference, Beijing, China, Aug. 1995

Wagner, W.:

Fission of hot heavy nuclei investigated at the FOBOS 4π -array;

Int. Symposium on Heavy Ion Physics and its Applications (II SHIPA), Lanzhou, China, Aug. 1995

Wünsch, R.:

The rotationally improved NJL soliton;

Universität Bochum, Apr. 1995

Wünsch, R.:

Fakultative Vorlesung Struktur der Hadronen;

Lecture course, TU Dresden, WS 1994/95

Zahn, R.:

Messungen von Übergangsstrahlung am MAMI;

Seminar, IKH/FZ Rossendorf, Feb. 1995

4 Talks of Visitors

G. Wolf, Darmstadt:

Particle production in heavy-ion collisions;

Jan. 23, 1995

V.F. Dmitriev, Novosibirsk:

Nuclear response and spin observables in the Δ region in charge exchange reactions;

Jan. 30, 1995

K.P. Lieb, Göttingen:

Spektroskopie im Massendreieck $^{76}\text{Sr} - ^{88}\text{Sr} - ^{100}\text{Sn}$;

Jan. 31, 1995

P. Geltenbort, Grenoble:

Neue Entwicklungen bei Mikrostreifen- und Mikro"gap"-Gaszählern - ein Überblick;

Mar. 6, 1995

A. Sibirtsev, Dubna:

ϕ and η production in pp and pA collisions;

Mar. 8, 1995

G. Gorelik, Boston:

How Sacharow invented the Soviet H-bomb;

Mar. 27, 1995

K. Sistemich, Jülich:

Status der 0° -Facility "ANKE" bei COSY;

Apr. 3, 1995

S. Drozd, Krakau:

On the fractal structure of compound nuclei;

Apr. 4, 1995

H. Grawe, Berlin:

Gamma-Spektroskopie von $N \approx Z$ - Kernen um ^{100}Sn ;

Apr. 24, 1995

D. Hilscher, Berlin:

Untersuchungen der Produktion und des Zerfalls heißer Kerne mit Antiprotonen;

May 22, 1995

M. Moszynski, Cracow:

New inorganic scintillators for physics and nuclear medicine;

May 24, 1995

H.J. Krappe, Berlin:

Ist die Λ -begleitete Spaltung eine Uhr oder ein Thermometer?

May 29, 1995

V. Nesterenko, Dubna:

Giant resonances in nuclei and metal clusters;

May 31, 1995

V. V. Balashov, Moskau:

Methods and concepts of nuclear reaction theory in modern atomic physics;

Jun. 12, 1995

J. Auerhammer, Rijnuizen:

Freier-Elektronen-Laser und die Anwendungen seiner Strahlung;

Jun. 26, 1995

V.E. Bunakov, Petersburg:

Fundamental symmetry breaking in nuclear resonance reactions;

Jul. 3, 1995

U. Heinz, Regensburg:

Hanbury-Brown-Twiss Interferometrie in Schwerionenstößen;

Jul. 10, 1995

J.A. Sheikh, Bombay:

pn correlations in high-spin nuclear phenomena;

Sep. 18, 1995

R. Kamys, Cracow:

Subthreshold K production in pA collisions;

Sep. 19, 1995

R. Alkofer, Tübingen:

Axiale Anomalie und deren Anwendung in der Hadronenphysik;

Oct. 9, 1995

C.R. Hofmann, Dresden:

Innere Paarkonversion als sensitives Instrument für die Kernspektroskopie;

Nov. 6, 1995

R. Nazmitdimov, Dubna:

Shell structures and quadrupole deformations in terms of classical periodic orbits;

Nov. 13, 1995

S. Popow, Nowosibirsk:

Electromagnetic structure of the deuteron and experiments with internal targets

Nov. 17, 1995

S. Drozd, Cracow:

Signatures of chaos in nuclear decays;

Nov. 20, 1995

W. Cassing, Gießen:

Dynamische Modelle zur Analyse des Dileptonen-Überschusses in den CERES-Messungen;
Dec. 4, 1995

B. Spaan, Dresden:

BABAR: Suche nach TP-Verletzungen in B^0 -Zerfällen;
Dec. 11, 1995

III Personnel

Director

Dr. H. Prade

Administrative Staff

E. Kluge

H. Römer

Scientific Staff

Dr. H.W. Barz ¹
L. Dietterle ^{2,4}
Dr. F.M. Dittes
Dr. F. Dönau
Dr. S. Dshemuchadse ²
Dr. W. Enghardt ¹
Dr. S. Frauendorf
Dr. P. Gippner ⁴
Dr. C.-M. Herbach
Dr. B. Kämpfer ¹
Dr. L. Käubler ¹
Dr. Th. Kirchner ²
Dr. R. Kotte
Dr. A. Matthies ^{2,4}

Dr. P. Michel
Dr. K. Möller ¹
Dr. J. Mösner
Dr. H. Müller
Dr. B. Naumann ²
Dr. L. Naumann
Dr. U. Nething
Dr. W. Neubert
Dr. H.-G. Ortlepp ⁴
Dr. G. Pausch
Dr. J. Pawelke
Dr. A. Pfitzner ³
Dr. J. Reif
G. Renz ^{2,4}

H. Richter ³
Dr. H. Rotter ³
Prof. I. Rotter ¹
A. Schamlott ²
Dr. K.D. Schilling
Dr. M. Schlett
Dr. R. Schwengner
Dr. W. Seidel
Dr. W. Wagner ⁴
Dr. G. Winter
D. Wohlfarth
Dr. R. Wünsch
Dr. R. Zahn

Technical Staff

M. Altus
H. Angermann
U. Baumann
J.U. Berlin
M. Boeck
M. Böse
J. Fiedler
R. Förster
M. Freitag

L. Göbel
K. Heidel
K.H. Hermann
J. Hutsch
J. Kerber
M. Langer
B. Meier
B. Prietzschk

I. Probst
B. Rimarzig
M. Scheinpflug
Chr. Schneidereit
W. Schulze
M. Sobiella
A. Uhlmann
C. Umlauf ^{2,4}

Postgraduate Students

J. Biegansky ²
T. Gorin ²
B.-G. Hasch ²
Dr. B. Heide ²
R. Hinz ²
D. Kamanin ²

J. Kolomeizew
J. Krüger
K. Lauckner
T. Möhlenkamp
Dr. M. Müller ³
E. Persson ²

A. Peshier
M. Schleif ²
Chr. Schneider
Dr. A. Schülke ²
Th. Servene ²

Post Doc

Dr. S. Skoda

Dr. H. Schnare

Guest Scientists

Dr. A.A. Aleksandrov, VIK Dubna / Russian Federation
Dr. I. Aleksandrova, VIK Dubna / Russian Federation
Prof. W. Andrejtscheff, INRE Sofia / Bulgaria
Prof. V. Bunakov, Universität Petersburg/Gatchina /Russian Federation
J. Cederkall, Inst. of. Techn. Stockholm / Sweden
Dr. D. Idiev, NBI Kopenhagen / Denmark
Dr. L. Kaptari, VIK Dubna / Russian Federation
Prof. V. Komarov, VIK Dubna / Russian Federation
Dr. V.V. Kruglov, VIK Dubna / Russian Federation
Dr. N. Kusmenko, Radiuminstitut St. Petersburg / Russian Federation
Prof. M. Moszynski, Soltan Institute Swierk / Poland
Dr. V. Pashkevich, VIK Dubna / Russian Federation
Dr. O.P. Pavlenko, ITF Kiew / Ukraine
Dr. A. Sanshur, Inst. of Nucl. Res. Kiew / Ukraine
Dr. J. Sheik, Tata Inst. Bombay / India
Dr. V. Shilov, VIK Dubna / Russian Federation
Dr. A. Sibirtsev, VIK Dubna / Russian Federation
Prof. V.V. Sokolov, Inst. f. Kernphysik Novosibirsk / Russian Federation
Prof. S. Strakhova, Universität Moskau / Russian Federation
Dr. A. Titov, VIK Dubna / Russian Federation
D.V. Vakotov, VIK Dubna / Russian Federation

¹ WIP/TU Dresden

² Project

³ Free coworker

⁴ at present JINR Dubna